

MODELLING, SIMULATION AND OPTIMIZATION OF A SOLAR/BATTE
HYBRID RENEWABLE ENERGY SYSTEM WITH MAXIMUM POWER PO
TRACKING CONTROL STRATEGY

By

Musong Louis Katche

A Thesis Submitted to the Department of Mechanical, Production, and Energy
Engineering, in Partial Fulfilment of the Requirements for the Award of the Degree of
Doctor of Philosophy in Energy Studies

Moi University

2023

DECLARATION

Declaration By Candidate

This thesis is my original work and has not been presented for a degree in any other University. No part of this thesis may be reproduced without the prior written permission of the author and/or Moi University.


Signature:  _____ Date: 22/11/2023

Musong Louis Katche

PHD/ES/5550/21

Declaration by the Supervisors

This thesis has been submitted for examination with our approval as University Supervisors.

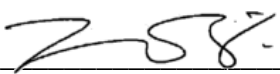
Signature:  _____ Date: 22/11/2023

Prof. Augustine B. Makokha

School of Engineering

Moi University, Eldoret, Kenya.

x


Signature:  _____ Date: 23/11/2023

Prof. Zachary O. Siagi

Department of Mechanical, Production & Energy Engineering,

School of Engineering,

Moi University, Kenya.

Signature:  _____ Date: 23/11/2023

Prof. Muyiwa S. Adaramola

Faculty of Environmental Sciences and Natural Resource Management

Norwegian University of Life Sciences, Ås, Norway

DEDICATION

This work is dedicated to my wife, parents, and entire family.

ACKNOWLEDGMENT

I acknowledge the European Union (EU) and the African Union (AU) for awarding me a scholarship through the project Mobility for Innovative Renewable Energy Technologies (MIRET) to study for a PhD in Energy Studies at Moi University in Kenya.

I also acknowledge the Norwegian Ministry of Education and Research and the Norwegian Ministry of Foreign Affairs for the financial support through the project “Strengthening education, research and innovation capacity in sustainable energy for economic development”, a partnership project between Norwegian University of Life Sciences, As, Norway and Moi University, Kenya.

I thank my supervisors Prof. Augustine B. Makokha, Prof. Zachary O. Siagi, and Prof. Muiyiwa S. Adaramola for directing this research work which enabled me to complete on time.

I also thank Dr. Stephen Talai and Dr. Stephen Kimutai for their words of encouragement throughout this research process.

I thank the Mrs Maureen Nasike for her words of encouragement during this research.

I thank my lovely wife Nji Eunette for standing by me during this research period and providing me with necessary support which kept me motivated till the completion of this research work.

I thank my family for supporting me either directly or indirectly to complete this research work.

I also thank the staff in the school of Engineering for their scientific contributions towards the betterment of this work.

ABSTRACT

Solar energy is abundantly available and it is a choice to drive the energy transition in sub-Saharan Africa. However, harvesting the maximum power from the sun is challenging since it is not always available at all times. Also, the most commonly used perturb and observe technique for harvesting maximum power suffers from slow response time and oscillations around the maximum power point. In addition to that, batteries which are a popular option for energy storage for use in times of no sunshine are costly and have short life-cycle. Hence, they need to be effectively managed to extend their useful life. The main objective of this research was to model and simulate a solar/battery hybrid energy system with a Maximum Power Point Tracking (MPPT) control strategy and to optimize the battery charging/discharging cycle life. The specific objectives were to: analyse the daily energy supply (solar radiation levels) and energy consumption at the study site; model and simulate a solar/battery hybrid system; design and simulate a Maximum Power Point Tracking (MPPT) control strategy; and optimize the solar system performance and the battery charging/discharging cycle life. The research was based at Moi University. The solar radiation and temperature data were collected from the Moi University Meteorological Weather Station. The power consumption was measured using the PCE360 power analyzer. The solar battery hybrid systems were modelled and simulated using HOMER Pro version 3.10.3. The MPPT was designed and simulated in MATLAB/Simulink using Perturb and Observe (P&O) technique, which incorporated a Proportional Integral Derivative (PID) controller, tuned using metaheuristic GA. The efficiency of the tracker was calculated using the EN5030 European standard for converter efficiencies. The charging/discharging of the batteries was done using a bidirectional converter integrated with a GA tuned PID controller. The battery state of charge was steadily monitored and maintained at 30% minimum. The measured average solar radiation and temperature were 4.9 kWh/m²/day and 18°C, respectively. The daily peak power consumption for the Administration building and Library were 86 kW and 93 kW respectively. From the HOMER Pro simulations, the results obtained gave an optimal system size of 90 kW for the Administration Building and 100 kW for the Margaret Thatcher Library. Also, the net present costs were Ksh27,000,000 (\$191,314) for the Administration building and Ksh32,000,000 (\$226,743) for the Margaret Thatcher Library while the payback period in both cases was 6 years. The MPPT had a settling time of 0.025 seconds and a tracking efficiency of 99.5%. The study concluded that maximum power point tracking significantly enhances solar energy harvesting. It is recommended that the strategy for tracking the maximum power point be utilized to boost the output power from solar PV system in Moi university's Administration and Library Buildings and any other similar institution.

TABLE OF CONTENTS

DECLARATION	ii
DEDICATION	iii
ACKNOWLEDGMENT	iv
ABSTRACT	v
TABLE OF CONTENTS	vi
LIST OF TABLES	xi
LIST OF FIGURES	xii
NOMENCLATURE	xv
CHAPTER ONE: INTRODUCTION	1
1.1 Background	1
1.2 Problem Statement	6
1.3 General Objective	7
1.4 Specific Objectives	7
1.5 Justification of the Study	7
1.6 Structure of the Thesis	9
CHAPTER TWO: LITERATURE REVIEW	11
2.1 Introduction	11
2.2 Solar PV Energy	12
2.3 Solar Cell and Model	12
2.4 Factors Affecting Energy Harvesting from PV Systems	14
2.4.1 Environmental factors	14
2.4.1.1 Irradiance	14
2.4.1.2 Temperature	15
2.4.1.3 Dust and soiling	16
2.4.1.4 Shading	18
2.4.1.5 Wind	19
2.5 Maximum Power Harvesting from PV Systems	19
2.5.1 Classical MPPT control techniques	23
2.5.1.1 Perturb and Observe (P&O) MPPT Techniques	23
2.5.1.2 Conventional P&O Algorithms	24
2.5.1.3 Improved (Modified) P&O (IP&O) Method	26
2.5.1.4 Hill Climbing (HC) Method	29

2.5.1.5 Constant Voltage (CV)	30
2.5.1.6 Ripple Correlation Control (RCC)	32
2.5.1.7 Open Circuit Voltage (OCV).....	33
2.5.1.8 Short Circuit Current (SCC).....	33
2.5.1.9 Adaptive Reference Voltage (ARV).....	34
2.5.1.10 Incremental Conductance (InC).....	34
2.5.1.11 Look-Up Table Based (LTB) Method	35
2.5.2 Intelligent MPPT control techniques	36
2.5.2.1 Artificial Neural Network (ANN)	36
2.5.2.2 Fuzzy Logic Controller (FLC).....	37
2.5.2.3 Sliding Mode Control (SMC).....	39
2.5.2.4 Fibonacci Series Based (FSB) Method.....	40
2.5.2.5 Gauss Newton Technique (GNT).....	40
2.5.3 Optimization techniques.....	41
2.5.3.1 Particle Swarm Optimization (PSO).....	42
2.5.3.2 Cuckoo Search (CS)	44
2.5.3.3 Artificial Bee Colony (ABC).....	45
2.5.3.4 Ant Colony Optimization (ACO)	46
2.5.3.5 Genetic Algorithm (GA).....	47
2.5.3.6 Grey Wolf Optimization (GWO).....	48
2.5.4 Hybrid techniques	49
2.5.4.1 Adaptive Neuro Fuzzy Inference System (ANFIS).....	49
2.5.4.2 Fuzzy Particle Swarm Optimization (FPSO).....	49
2.5.4.3 Grey Wolf Optimization Perturb and Observe (GWO-P&O)	50
2.5.4.4 Particle Swarm Optimization Perturb and Observe (PSO-P&O)	50
2.5.4.5 Hill Climbing Adaptive Neuro Fuzzy Inference System (HC-ANFIS) ...	51
2.6 Summary of related works done on the different MPPT techniques	52
2.7 Criteria for comparing different MPPT techniques	55
2.8 Comparative analysis of different MPPT techniques	55
2.9 Power Converters Used in PV Systems	57
2.9.1 DC-DC Converters	58
2.9.1.1 Buck Converter.....	58
2.9.1.2 Boost Converter	59
2.9.1.3 Buck-Boost Converter	61

2.9.1.4 Cuk Converter.....	62
2.9.2 DC-AC Converters.....	64
2.9.3 AC-DC Converters.....	64
2.9.4 Bidirectional Converters	65
2.10 Energy Storage Systems	67
2.10.1 Introduction	67
2.10.2 Types of Energy Storage Systems.....	68
2.10.3 Mechanical storage systems	69
2.10.4 Electrical storage systems	73
2.10.5 Chemical storage systems	75
2.10.6 Thermal storage systems	77
2.11 Battery Storage systems and types of Batteries	79
2.11.1 Terms used in battery storage systems.....	80
2.12 Types of Secondary Batteries	84
2.12.1 Lead Acid (PbA) Battery.....	84
2.12.2 Lithium-ion (Li-ion) batteries	87
2.12.3 Nickel cadmium (NiCd) batteries	90
2.12.4 Nickel-metal hydride (NiMH) batteries	90
2.12.5 Sodium Sulfur (NaS) Batteries.....	91
2.12.6 Flow batteries	92
2.13 Summary of Different Battery Characteristics	94
2.14 Battery States and Their Effects on Lead Acid Batteries	95
2.14.1 State of Charge (SOC).....	96
2.14.1.1 Open-Circuit Voltage Method.....	97
2.14.1.2 Coulomb Counting	97
2.14.1.3 Model-Based Methods.....	97
2.14.1.4 Kalman Filtering (KF)	98
2.14.1.5 Extended Kalman Filtering (EKF)	98
2.14.1.6 Artificial Intelligence (AI) Techniques	98
2.14.2 State of Health (SOH)	99
2.14.2.1 Capacity-Based Methods.....	99
2.14.2.2 Coulomb Counting	99
2.14.2.3 Impedance Spectroscopy	100
2.14.2.4 Voltage-Based Methods	100

2.14.2.5 Model-Based Methods.....	100
2.14.2.6 Machine Learning and Data-Driven Approaches.....	100
2.14.2.7 Aging Models and Estimation Algorithms.....	101
2.14.3 State of Temperature (SOT).....	101
2.15 Software tools used for HRES designs.....	102
2.15.1 HOMER.....	102
2.15.2 MATLAB.....	113
2.15.3 iHOGA.....	117
2.15.4 RETScreen.....	117
2.16 Conclusion.....	124
CHAPTER THREE: METHODOLOGY.....	125
3.1 Introduction.....	125
3.2 Study Site.....	125
3.3 Data Collection.....	126
3.4 Solar PV-Battery Optimization Using HOMER Pro Software.....	128
3.4.1 Grid.....	130
3.4.2 Solar PV.....	130
3.4.3 Battery Storage.....	131
3.4.4 Inverter.....	132
3.4.5 Charge controller.....	132
3.4.6 Economic parameters.....	134
3.5 MPPT Technique Used.....	135
3.6 Tuning of the PID controllers Using Genetic Algorithms.....	137
3.7 Modelling of the Solar/Battery Hybrid System in MATLAB.....	139
3.8 Conclusion.....	141
CHAPTER FOUR: RESULTS AND DISCUSSION.....	142
4.1 Daily Solar Radiation.....	142
4.2 Daily Temperature Variation.....	143
4.3 Load Profile for the Administrative Building.....	144
4.4 Load profile for the Margaret Thatcher Library.....	145
4.5 Results for the simulation of a solar PV/Battery system using HOMER Pro.....	147
4.6 Fitness Curves for the Tuning of the PID controllers Using Genetic Algorithms.....	149
4.6 Results for the MPPT Tracking using MATLAB/Simulink.....	150

4.7 Results for the Optimization of the solar system performance and the battery charging/ discharging	151
4.9 Output Three Phase Voltage Waveforms from The Inverter.....	153
4.10 Conclusion for Chapter 4	154
CHAPTER FIVE: CONCLUSION, RECOMMENDATIONS, AND FUTURE PERSPECTIVES.....	155
5.1 Conclusion	155
5.2 Recommendations.....	157
5.3 Contributions.....	158
5.4 Further Research	159
REFERENCES	160
APPENDICES	182
Appendix A: Solar radiation Data for Moi University.....	182
Appendix B: Temperature Data for Moi University	183
Appendix C: Power Demand data for Administration building.....	184
Appendix D: Power Demand data for Margaret Thatcher Library	185
Appendix E: Loads and Energy Consumption Inventory for Administration Building and Margaret Thatcher Library	186
Appendix F: Simulink model for the power inverter	198
Appendix G: Simulink model for the battery controller	199
Appendix H: Ropp Test.....	200
Appendix I: Research Outputs	202
Appendix J: Plagiarism Certificate	203

LIST OF TABLES

Table 2.1: Classification of MPPT techniques	22
Table 2.2: Contrasting traditional P&O algorithms	26
Table 2.3: Comparison of modified P&O algorithms.....	28
Table 2.4: Fuzzy Logic Rule Table.....	39
Table 2.5: Summary of related works for different MPPT methods	53
Table 2.6: Criteria for determining MPPT rankings.....	55
Table 2.7: Comparison of different MPPT techniques	56
Table 2.8: Float life of different lead acid batteries at different temperatures	83
Table 2.9: Summary of battery characteristics.	94
Table 3.1: Some quantities measured by the PCE-360 power analyzer	128
Table 3.2: Choice of Components for the PV system.....	133
Table 4.1: Technical summary of the solar PV/Battery system.....	148
Table 4.2: Economic summary of the solar PV/Battery systems.....	149

LIST OF FIGURES

Figure 1.1: Characteristics of a solar module (I-V and P-V) under varying temperature	4
Figure 1.2: Characteristics (I-V and P-V c) of a solar module under varying solar radiation.....	5
Figure 1.3: PV module characteristics under partial shading and uniform sunshine conditions	6
Figure 2.1: Types of solar cells.....	13
Figure 2.2: Equivalent circuit of a PV cell	13
Figure 2.3: Single and Double Axis Trackers.....	20
Figure 2.4: Classification of P&O Algorithms	24
Figure 2.5: Block diagram of the P&O method.....	24
Figure 2.6: Block diagram of conventional P&O with (a) adaptive perturbation (b) fixed step pertubation	26
Figure 2.7: Block diagram of modified P&O with (a) adaptive perturbation (b) fixed step size and.....	27
Figure 2.8: Flowchart of the CV method	31
Figure 2.9: Layers of Artificial Neural Network (ANN).....	37
Figure 2.10: Flow diagram of the HC-ANFIS MPPT technique.....	52
Figure 2.11: Reported efficiencies obtained from different MPPT techniques.....	57
Figure 2.12: Buck converter	58
Figure 2.13: Boost converter.....	60
Figure 2.14: Buck-Boost converter.....	61
Figure 2.15: Cuk converter	62
Figure 2.16: Generalized structure for a bidirectional DC-DC converter	67
Figure 2.17: Classification of energy storage systems.....	69
Figure 2.18: Pumped Hydro Storage System.....	70
Figure 2.19: Flywheel energy storage system with hydrostatic transmission	71
Figure 2.20: CAES system.....	72
Figure 2.21: Double layer capacitor storage system.....	74
Figure 2.22: SMES System.....	75
Figure 2.23: Schematic diagram of a fuel cell	76
Figure 2.24: Battery technologies for different purposes	79

Figure 2.25: Effects of temperature on Lead Acid battery capacity	81
Figure 2.26: Relationship between cycle life and DOD for lead acid batteries.....	82
Figure 2.27: Self-discharge rate of lead acid batteries at different temperatures.	83
Figure 2.28: Image a Lead Acid Battery.....	85
Figure 2.29: Image of a Li-ion Battery	89
Figure 2.30: Comparison of different battery storage technologies by source.....	95
Figure 2.31: Proposed HRES for Golbo II village in Ethiopia.....	103
Figure 2.32: Configuration of the proposed HRES used	105
Figure 2.33: Setup of the PV-diesel-battery HES	105
Figure 2.34: PV-hydro-diesel-battery HRES	107
Figure 2.35: HRES for the area.....	108
Figure 2.36: Schematic diagram of the hybrid system	110
Figure 2.37: HRES schematic diagram.....	111
Figure 2.38: Investigated HRES	114
Figure 2.39: Proposed IRES.	115
Figure 2.40: HRES proposed diagram	116
Figure 2.41: Solar PV-battery-diesel generator hybrid standalone system.....	118
Figure 2.42: PV-wind-diesel-battery HRES	119
Figure 2.43: PV-wind-biomass-battery HRES	120
Figure 2.44: Hybrid power system flow diagram	121
Figure 3.1: System Block Diagram.....	125
Figure 3.2: View of Moi University Main Campus' Administration Building	126
Figure 3.3: Power Consumption Data Collection Using the PCE-360 Power Analyser	127
Figure 3.4: Input and Output Parameters Used by HOMER Pro.....	129
Figure 3.5: Schematic Diagram Designed with HOMER Pro for Simulation: (a) Margaret Thatcher Library and (b) Administration Building	134
Figure 3.6: Flow chart of the P&O method	136
Figure 3.7: Flowchart for optimization using GA	137
Figure 3.8: MATLAB simulation block diagram	140
Figure 3.9: MATLAB/Simulink model for MPPT control strategy	141
Figure 4.1: Solar radiation	143
Figure 4.2: Average monthly temperature variation in the study site.....	144
Figure 4.3: Load Profile for the Administration Block.....	145

Figure 4.4: Load Demand Profile for Library.....	146
Figure 4.5: Yearly load profile for the Margaret Thatcher Library	147
Figure 4.6: Battery State of Charge for the Margaret Thatcher Library	147
Figure 4.7: Battery state of charge for the Administration building.....	147
Figure 4.8: Fitness curve for MPPT PID controller.....	150
Figure 4.9: Fitness curve for Batter charging/Discharging PID controller.....	150
Figure 4.10: Tracking of Maximum Power Point.....	151
Figure 4.11: Power output of the solar PV system with and without the Maximum Power Point Tracker	152
Figure 4.12: Battery State of Charge (SOC) Control.....	153
Figure 4.13: Three phase voltage waveforms from the inverter	154

NOMENCLATURE

Abbreviations

ABC	Artificial Bee Colony
AC	Alternating Current
ACO	Ant Colony Optimization
AGM	Absorbent Glass Mat
Ah	Ampere Hour
AI	Artificial Intelligence
ANFIS	Adaptive Neuro Fuzzy Inference System
ANN	Artificial Neural Network
ARV	Adaptive Reference Voltage
BEV	Battery Electric Vehicle
BMS	Battery Management System
CAES	Compressed Air Energy Storage
CeBES	Centralized Battery Energy Storage
COE	Cost of Energy
CS	Cuckoo Search
CV	Constant Voltage
DC	Direct Current
DeBES	Decentralized Battery Energy Storage
DOD	Depth of Discharge
ECM	Equivalent Circuit Model
EKF	Extended Kalman Filter
EMF	Electromotive Force
FESS	Flywheel Energy Storage System

FF	Fill Factor
FFBPA	First Fit Bin Packing Algorithm
FLC	Fuzzy Logic Controller
FPSO	Fuzzy Particle Swarm Optimization
FSB MPPT	Fibonacci Series Based Maximum Power Point Tracking
GA	Genetic Algorithms
GA	Genetic Algorithm
GMPP	Global Maximum Power Point
GNT	Gauss Newton Technique
GWO	Grey Wolf Optimization
GWO-P&O	Grey Wolf Optimization Perturb and Observe
HC	Hill Climbing
HC-ANFIS	Hill Climbing Adaptive Neuro Fuzzy Inference System
HEV	Hybrid Electric Vehicle
HOMER	Hybrid Optimization Model for Electric Renewables
HRES	Hybrid Renewable Energy System
IGBT	Insulated Gate Bipolar Transistor
iHOGA	Improved Hybrid Optimization Model by Genetic Algorithms
InC	Incremental Conductance
IP&O	Improved Perturb and Observe
IRES	Integrated Renewable Energy System
KF	Kalman Filter
LCOE	Levelized Cost of Energy
LDR	Light Dependent Resistor
$\text{Li}_4\text{Ti}_5\text{O}_{12}$	Lithium Titanate

LiCoO_2	Lithium Cobalt Oxide
LiFePO_4	Lithium Iron Phosphate
Li-ion	Lithium ion
LiMn_2O_4	Lithium Manganese Oxide
LiNiMnCoO_2	Lithium Nickel Manganese Cobalt Oxide
LTB MPPT	Look-Up Table Based Maximum Power Point Tracking
LV	Low Voltage
MATLAB	Matrix Laboratory
MESS	Mechanical Energy Storage System
MPC	Model Predictive Control
MPP	Maximum Power Point
MPPT	Maximum Power Point Tracking
MV	Medium Voltage
NASA	National Aeronautics and Space Administration
NiCd	Nickel Cadmium
NiMH	Nickel Metal Hydride
NPC	Net Present Cost
O&M	Operation and Maintenance
OCV	Open Circuit Voltage
OCV	Open Circuit Voltage
P&O	Perturb and observe
PbA	Lead Acid
PbO	Lead Peroxide
PbO_2	Lead Dioxide
PBP	Payback Period

PbSO ₄	Lead Sulphate
PF	Power Factor
PHES	Pumped Hydro Energy Storage
PID	Proportional Integral Derivative
PMS	Power Management Strategy
PS	Partial Shading
PSO	Particle Swarm Optimization
PSO-P&O	Particle Swarm Optimization Perturb and Observe
PV	Photovoltaic
PWN	Pulse Width Modulation
RCC	Ripple Correlation Control
RE	Renewable Energy
RF	Renewable Fraction
SCC	Short Circuit Current
SHS	Sensible Heat Storage
SLA	Sealed Lead Acid
SMC	Sliding Mode Control
SMES	Superconducting Magnetic Energy Storage
SOC	State of Charge
SOH	State of Health
SOP	State of Power
SOT	State of Temperature
SPA	Shortest-Path Algorithm
THD	Total Harmonic Distortion
UPS	Uninterruptible Power Supply

V2G	Vehicle to Grid
V2H	Vehicle to Home
VRLA	Valve Regulated Lead Acid
ZnBr ₂	Zinc Bromide

Symbols

C	Capacitance (F)
f	Frequency (f)
G	Solar Radiation (W/m ²)
I	Current (A)
I _d	Diode Current (A)
I _{pv}	Photovoltaic module current (A)
I _{sc}	Short Circuit Current (A)
L	Inductance (H)
P	Active Power (W)
R _s	Series Resistance (Ω)
R _{sh}	Shunt Resistance (Ω)
T	Temperature (°C)
V	Voltage (V)
V _d	Diode Voltage (V)
V _{oc}	Open Circuit Voltage (V)
V _{pv}	Photovoltaic module voltage (V)

CHAPTER ONE: INTRODUCTION

1.1 Background

The need for universal access to electricity has sparked a passionate global search among researchers. This urgent issue has driven them to investigate cutting-edge, eco-friendly methods for producing electrical power, while also improving present techniques to increase both cost-efficiency and energy sustainability. Researchers are devoting their efforts to the twin goals of cleaner energy production and the optimization of present generation methods as the globe struggles with the ever-increasing demand for electricity. This complex project aims to pave the road for a more sustainable and environmentally conscious future in addition to meeting society's present energy demands (Bose, 2010; Odou et al., 2020; Park et al., 2014) (Chauhan & Saini, 2014). Fossil fuel with its limited nature and utilized in conventional energy generation plants has also driven the shift toward cleaner power generation (Prasad et al., 2006). Clean energy technologies are thought to be safer routes to drive the energy transition in the power sector because of the adverse environmental effects coming from thermal and coal power plants (J. Ahmad et al., 2018; Alshammari & Asumadu, 2020; Aziz et al., 2018, 2019; Bentouba & Bourouis, 2016; Bhandari et al., 2014; Corbus & Bergey, 1997; Cristóbal-Monreal & Dufo-López, 2016; Fazelpour et al., 2014a; Gebrehiwot et al., 2019; H. U. R. Habib et al., 2019; Kazem & Khatib, 2013; Landi D, Castorani V, 2019; Mokhtara et al., 2020, 2021; Murugaperumal et al., 2020; Murugaperumal & Ajay D Vimal Raj, 2019; Patel & Singal, 2018; Ramesh & Saini, 2020; Vai et al., 2020).

Energy plays an important role in the development of every nation (Yimen et al., 2018). Access to electricity is still very limited especially in most rural communities in Africa because of their geographical locations making grid extension difficult. This has led to

millions of people with a majority from rural communities going without electricity. According to the energy progress joint report 2023 by the International Renewable Energy Agency (IRENA), World Bank (WB), International Energy agency (IEA), United Nations Statistics Division (UNSD) and the World Health Organisation (WHO), over 675 million people in the world as at 2021 still lack access to electricity and over 80% of this population live in sub-Saharan Africa (IEA et al., 2023). A majority of this population is in sub-Saharan Africa with a greater percentage coming from the rural communities. Furthermore, according to the 2030 agenda for sustainable development by the United Nations on its sustainable development goal number 7 which seeks to ensure access to affordable, reliable, sustainable and modern energy for all, effort needs to be made in the line of renewable energy for this goal to be achieved (UN, 2015). At the time when technology and industrialization are growing at a fast rate, the means of providing clean electrical energy in a relatively cheap cost to all remains a problem (Rehman, 2021). For this reason, alternative ways for local power generation must be sought so as to provide sustainable energy to all especially to those people who are not connected to the grid and have no hopes for grid extension reaching them in the near future.

Sustainable and cost-effective electricity can be provided to all, no matter their geographical locations by using renewable energy sources such as solar photovoltaic (PV), wind, biomass and mini hydro (Naveen et al., 2020; Rehman, 2021). These are all sources of energy which can be replenish over time making them clean and renewable energy sources (Rehman, 2021). It should also be noted that most, if not all, these sources of energy are readily available in all rural communities in sub-Saharan Africa. They can therefore be harnessed to provide electricity to the communities that have been left in darkness due to the lack or inadequate supply from the traditional grid.

Different approaches can be used in the process of harnessing these sources of energy such as the construction of standalone power systems with or without battery backup, construction of hybrid renewable energy system (HRES) and the construction of grid connected hybrid systems in areas where the grid network is available but not sufficient to supply electricity to all the population available. Therefore, utilizing solar/battery hybrid systems can become a major solution to the energy problem in Africa.

Resources for RE are variable. Due to the constant variation in solar radiation and wind speed, respectively, solar and wind, for instance, are not stable. Additionally, solar photovoltaic (PV) systems use solar modules to capture solar energy, but due to the poor conversion efficiency of these modules, there are limitations on the amount of solar energy that can be harvested to its full potential (Alex, 2005; Fazelpour et al., 2014b; Ludin et al., 2021; Rehman, 2021; Van Beuzekom et al., 2015; Zahraee et al., 2016), (Bounechba et al., 2014; Ngan & Tan, 2011). These factors have led to the current employment of various control strategies to monitor the maximum power from these energy systems.

The Maximum Power Point (MPP) in PV systems is where output power reaches its peak, and its location is continuously affected by temperature and solar radiation. An operating point should thus be at MPP, which is a point on the PV curve displaying the maximum power that can be harvested from a certain PV module at a given time as shown on Figure 2 below, in order to track the maximum power of the PV generator. Consequently, MPPT (Maximum Power Point Tracking) algorithms must continuously track the MPP (Gebrehiwot et al., 2019; Giallanza et al., 2018; Kazem & Khatib, 2013; Murphy & McDonnell, 2017; Murugaperumal et al., 2020; Park et al., 2014), (Jalal & Mehdi, 2021). MPPT is a technique used to maximize energy extraction from PV modules. Utilizing solar tracking techniques increase the overall efficiency of PV

systems especially in partial shading conditions and reduce the overall system cost of PV systems (Hohm & Ropp, 2003). The difficulty with MPPT systems is capturing the maximum output power from the PV system by tracking voltage prediction and appropriately varying duty cycle (Bendib et al., 2015a, 2015b; P.-C. Chen et al., 2015; da Rocha et al., 2020; Mao et al., 2020; Ram et al., 2017; Seyedmahmoudian et al., 2016; Subudhi & Pradhan, 2012). Figures 1.1 and 1.2 show the variation of current, voltage, and power for a typical solar module during temperature and solar radiation variations.

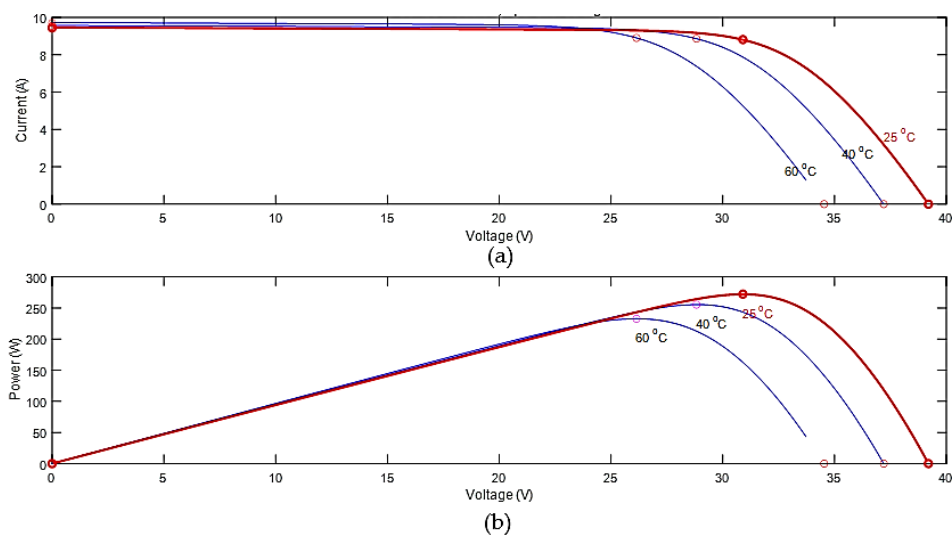


Figure 1.1: Characteristics of a solar module (I-V and P-V) under varying temperature (Bounechba et al., 2014)(Ngan & Tan, 2011).

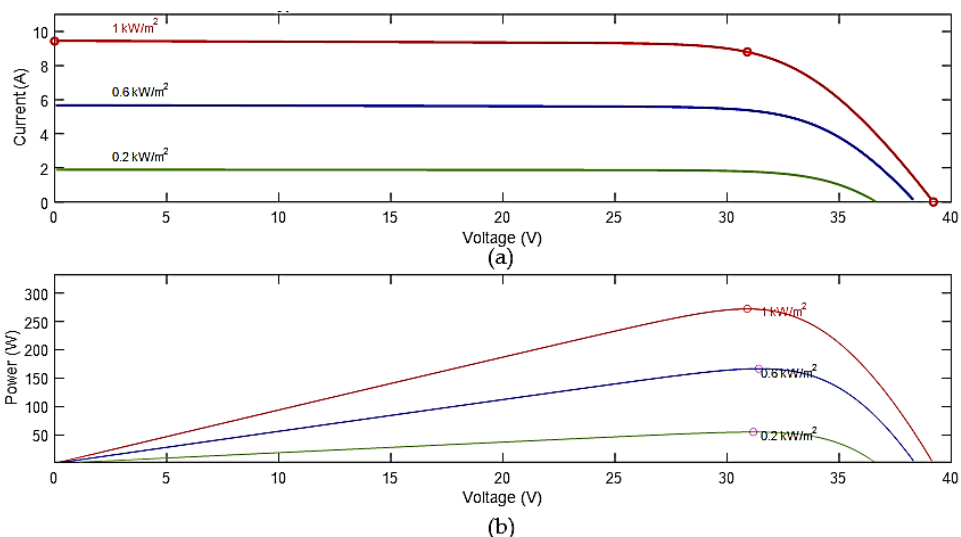


Figure 1.2: Characteristics (I-V and P-V) of a solar module under varying solar radiation (Bounechba et al., 2014)(Ngan & Tan, 2011)

The statistics show that temperature change has a greater impact on a solar module's output voltage than it does on its output current. In contrast, the module's current is significantly more affected by variations in solar radiation than its output voltage is. The solar module's overall output power changes in both situations. The solar module's overall output power changes in both situations (Salas et al., 2006). Additionally, when a PV module is exposed to full sunlight conditions and when partial shading occurs, its I-V and P-V properties are never the same. While the I-V and P-V curves are homogeneous under full sunlight with only one maximum power point, local maxima are seen under partial shade, making it challenging to track the global maximum. These conditions are illustrated in Figure 1.3.

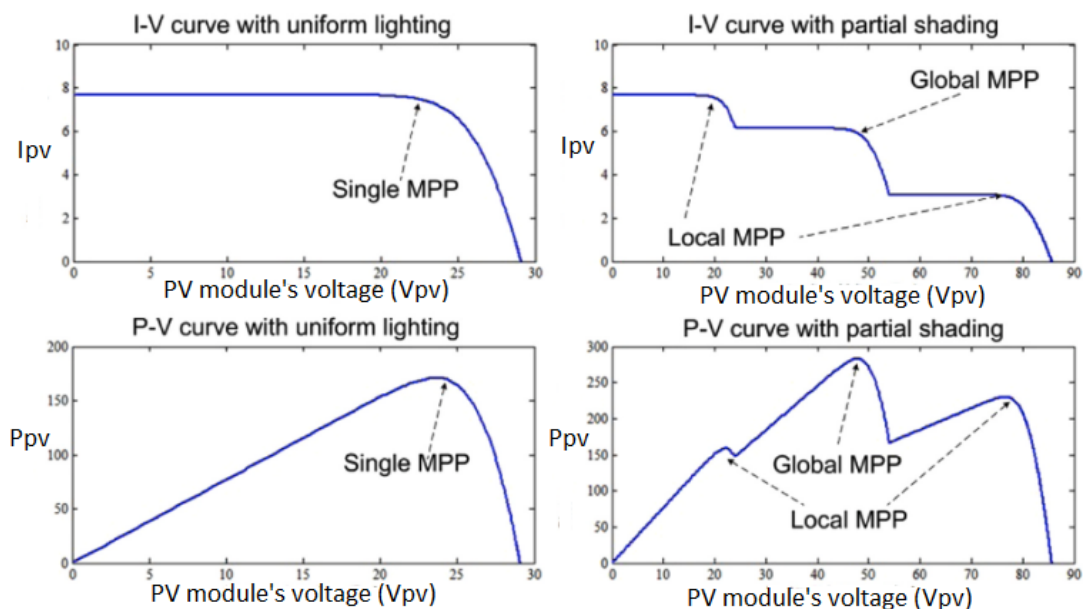


Figure 1.3: PV module characteristics under partial shading and uniform sunshine conditions (R. Ahmad et al., 2019a)

1.2 Problem Statement

Optimal design and control of solar/battery hybrid renewable energy systems still remain a problem. The solar resource is variable and intermittent and the conversion efficiency for solar modules is still very low, ranging between 13% and 22%. Therefore, maximum power should be harvested from the sun when available to supply the loads and charge the batteries. To harvest this maximum power, tracking systems are required. Currently, the tracking is done using Maximum Power Point Trackers (MPPTs). Different control strategies have been developed for these trackers. One of the most used control strategies in most commercial MPPTs is the Perturb and Observe (P&O) which is cost effective. Though the P&O strategy is widely used, it has limitations as it suffers from oscillations around the Maximum Power Point (MPP) during the tracking process and has a slow response time. Lead acid batteries on the other hand which are frequently used for storage have a short life span ranging from 3-6 years. This poses a problem because it increases the long run maintenance cost of the

PV system. Therefore, developing suitable control strategies to harness maximum power from the sun with minimal oscillations and improved tracking time and also to effectively control the charging and discharging of batteries to enhance their performance and increase their life span becomes necessary. This will improve the overall efficiency of solar/battery systems.

1.3 General Objective

The main objective of this work is to model and simulate a solar/battery hybrid renewable energy system with Maximum Power Point Tracking (MPPT) control strategy and optimize the battery charging/discharging cycle life.

1.4 Specific Objectives

The specific objectives of this work are to:

- i) Analyse the daily energy supply (solar radiation levels) and energy consumption at the study site;
- ii) Model and simulate a solar/battery hybrid system;
- iii) Design and simulate a Maximum Power Point Tracking (MPPT) control strategy;
- iv) Optimize the solar system performance and the battery charging/discharging cycle life.

1.5 Justification of the Study

Growing usage of renewable energy sources, like solar energy, is essential for tackling the world's energy problems and cutting greenhouse gas emissions. Researching solar/battery hybrid renewable energy systems aids in the creation of ecologically responsible and sustainable energy solutions.

Solar PV energy is harvested from the sun and it is influenced by environmental factors such as temperature and solar radiation. The power output from PV systems is however variable. Because of this, the energy efficiency of the system can be improved by integrating batteries and using MPPT control techniques, allowing for greater solar energy harvesting and raising the overall system performance. As a result, effective energy management is made possible by modelling, simulating, and optimizing a solar/battery hybrid system with MPPT control technique. Through this, researchers and system designers can pinpoint the best operating points, boost power generation, and efficiently control battery charging and discharging by correctly modelling the system's constituent parts and putting cutting-edge control algorithms to work.

Also, they can find the most dependable and cost-efficient system topologies, component size, and control strategies through simulation and optimization. With the use of this knowledge, practical solar/battery hybrid systems may be designed and put into operation, which will lower installation costs, improve system performance, and boost the affordability of renewable energy sources.

In addition to that, the advancements in control methods, algorithms, and techniques are continually being implemented to improve MPPT control techniques. The development of renewable energy technologies is facilitated by studying and analysing the performance of various MPPT algorithms in a solar/battery hybrid system. This allows for the identification of the most appropriate and effective control technique.

Potential for real-world applications such as off-grid systems, rural electrification initiatives, and remote area power delivery are a few examples of real-world scenarios that could benefit directly from the research's conclusions and insights. Researchers can

support the use and uptake of renewable energy solutions in a variety of contexts by improving the design and control of solar/battery hybrid systems.

Furthermore, promoting the use of solar energy and improving renewable energy systems is consistent with efforts to combat climate change and advance global energy sustainability. Research on solar/battery hybrid systems will help lessen dependency on fossil fuels, reduce carbon emissions, and promote a more sustainable and environmentally friendly energy future.

In conclusion, it is justified to carry out research on the modelling, simulation, and optimization of a solar/battery hybrid renewable energy system with MPPT control strategy given its potential to increase energy efficiency, improve system reliability, lower costs, and support the creation of sustainable energy solutions.

1.6 Structure of the Thesis

In order to better understand the research work, this thesis has been divided in to five chapters as follows.

Chapter 1 which is the first and current chapter is the introductory chapter which talks about the background of the work, the problem statement, the objectives, the justification, and the general structure of the thesis.

Chapter 2 is dedicated for literature review. It gives the generalities of photovoltaic systems, maximum power point tracking techniques, battery storage systems, and related works that have been carried out on this topic.

Chapter 3 is the methodology chapter. It lays emphasis on the study site, the methods and tools used for data collection, and the software tools and simulation techniques used.

Chapter 4 is the result and discussion chapter which presents the results obtained from the findings and also discusses the significance of the results.

Chapter 5 is the general conclusion which concludes the on the overall outcomes of this research. Also, the contributions, recommendations and perspectives of this work are also outline in this chapter.

CHAPTER TWO: LITERATURE REVIEW

2.1 Introduction

Reduction of carbon emissions, safeguarding the environment and the health of the population, influence climate and sea level changes, are the push factors towards the constant drive for renewable energy alternatives. Due to the free and abundant irradiance and bright weather in different parts of the world, solar energy has drawn attention recently (Sibai, 2014). Currently, it is regarded as a noble mission to develop PV solar energy as a clean and environmentally beneficial energy source. In this mission, the sun is purposefully given a new purpose in addition to the one it has always served: to supply energy for Earthly life. The sun will also serve the additional purpose of providing solar electricity, which will supply the Earth with energy for human comfort and wellbeing.

Photovoltaic (PV) panels have been around for a while, but recently they have become more affordable and popular. Due to the solar energy industry's explosive growth, PV systems are now a common alternative energy source in most parts of the world. To satisfy consumers demands, many solar panels must be connected together. Either the solar panels are connected in parallel or series to boost the system voltage or the load current respectively. The best performance from connecting these solar panels in series or parallel is only possible if they are similar and share the same properties. Because it relies on the photovoltaic effect, the direct conversion of solar radiation into electricity is frequently referred to as a photovoltaic (PV) energy conversion. The development of a potential difference at the intersection of two distinct materials in response to visible or other radiation is generally referred to as the photovoltaic effect. Therefore, "photovoltaic" refers to the entire field of solar energy conversion into electricity. Literally, "light-electricity" is what photovoltaic means.

2.2 Solar PV Energy

Photovoltaic is a method to convert solar radiation into electricity using semiconductors that exhibit the photovoltaic effect. Photovoltaic (PV) technologies are based on the use of solar cells. These cells can be interconnected in series (to increase the voltage) and parallel (to increase the current to give a PV module or panel (Villalva et al., 2009). A combination of these modules forms an array (Bagher et al., 2015). The sun's radiation hits the semiconductor material within the PV cell and excites electrons resulting in electric power. These electrons are carried through the PV cell to an electrical circuit. Each PV solar cell is protected by a layer of plastic or glass. A collection of solar panels is called an array. Each array is designed to produce a certain voltage and current. Each is then attached to an inverter that converts the Direct Current (DC) of the array to Alternating Current (AC) (Behl et al., 2012).

Photovoltaic generation of power is caused by electromagnetic radiation separating positive and negative charge carriers in absorbing material. If an electric field is present, these charges can produce a current for use in an external circuit. Such fields exist permanently at junctions or inhomogeneities in photovoltaic (PV) cells as 'built-in' electrostatic fields and provide the electromotive force (EMF) for useful power production. The cell itself provides the source of EMF. It is important to appreciate that photovoltaic devices are electrical current sources driven by a flux of radiation. Efficient power utilization depends not only on efficient generation in the cell, but also on dynamic load matching in the external circuit (Twidell, 2021).

2.3 Solar Cell and Model

There exist different types of solar cells, among which are monocrystalline, polycrystalline, amorphous, and thin film as shown in Figure 2.1 (Bagher et al., 2015).

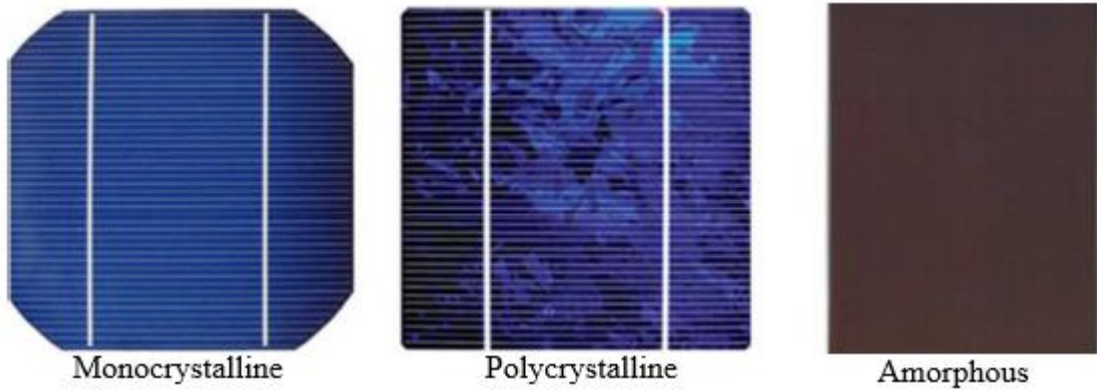


Figure 2.1: Types of solar cells (Eteiba et al., 2013)

A solar cell can be modelled by a light source (represented by a photo-current I_{ph}) in parallel with a junction diode and shunt resistance (R_{sh}), then in series with a series resistance (R_s). The model of a solar cell is shown below (Eteiba et al., 2013).

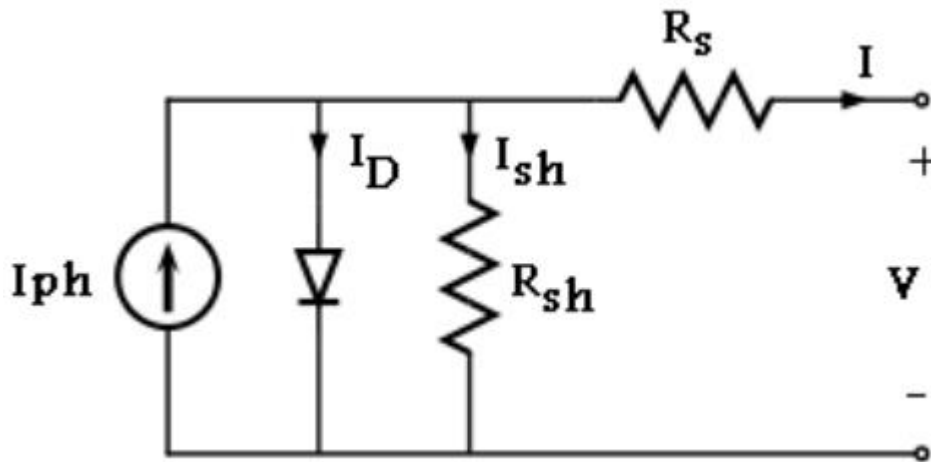


Figure 2.2: Equivalent circuit of a PV cell (Eteiba et al., 2013)

The equations governing the operation of this solar cell as presented by (Villalva et al., 2009) and (Eteiba et al., 2013) are:

$$I = I_{ph} - I_d - I_{sh} \dots\dots\dots 2.1$$

$$I_d = I_o * \exp\left[\left(\frac{qV_d}{AKT_c}\right) - 1\right] \dots\dots\dots 2.2$$

$$I_{sh} = \frac{V+IR_s}{R_{sh}} \dots\dots\dots 2.3$$

$$V_d = V + IR_s \dots\dots\dots 2.4$$

$$I = I_{ph} - I_o * \exp\left[\left(\frac{q(V+IR_s)}{AKT_c}\right) - 1\right] - \frac{V+IR_s}{R_{sh}} \dots\dots\dots 2.5$$

$$V_T = \frac{KT_c}{q} \dots\dots\dots 2.6$$

$$I = I_{ph} - I_o * \exp\left[\left(\frac{V+IR_s}{AV_T}\right) - 1\right] - \frac{V+IR_s}{R_{sh}} \dots\dots\dots 2.7$$

Where I_o is the diode saturation current, V_d is the diode voltage, V is the terminal voltage of the solar cell, V_T is the thermal voltage, K is the Boltzmann constant, q is the electronic charge, T_c is the temperature, and A is the diode ideality constant.

2.4 Factors Affecting Energy Harvesting from PV Systems

Though solar modules are used to harvest energy from the sun, several factors hinder the proper performance of these modules. These factors can be grouped into four main categories which are: environmental, installation, constructional, and maintenance factors.

2.4.1 Environmental factors

Installing solar modules outdoors, where they can bask in direct sunlight, is crucial if you want to maximize their power output capacity. These PV modules' effectiveness and overall performance are closely correlated with a variety of environmental factors. Their efficiency is greatly influenced by variables like irradiance, temperature, dust buildup, soiling, wind exposure, shade, and humidity levels.

2.4.1.1 Irradiance

The intrinsic fluctuation of solar resources has a substantial impact on solar power generation, which is frequently achieved by photovoltaic (PV) panels. This fluctuation is influenced by a number of variables, each of which has a significant impact on how

well PV panels perform. The temporal feature of this variability is particularly important since it has a complex relationship between its level and the resolution of time measurements; as time resolution rises, variability increases. The dynamic character of solar irradiance is caused by a number of factors, making it difficult to fully understand. These variables include the sun's position in the sky, time of day, geographical location, seasonal variations, and meteorological conditions. The sun's position changes during the day, changing its height, which in turn affects the irradiance levels that PV panels get. The amount of sunlight that reaches the solar modules can be greatly reduced by cloud cover, which is one of the most important factors influencing irradiance changes. It's interesting to note that incident irradiance—the amount of light that reaches PV modules—is not exclusively dependent on light from the sun; it is also influenced by reflected light from the environment and nearby objects. Although both direct and reflected solar irradiation play important roles, direct solar irradiation often has a more noticeable impact on PV panel performance. Nevertheless, it becomes more difficult to precisely estimate incident irradiance when neighbouring objects cast shadows or reflect sunlight onto the panels. It is essential to arrange solar panels optimally in order to maximize the absorption of solar radiation. This requires tilting the panels toward the sun, with the tilt angle depending on the location's latitude. PV module output increases as irradiance levels do, while a decrease in irradiance causes a decrease in output. So, in order to fully utilize solar power generation, it is crucial to comprehend and manage the complex nature of solar irradiance (Bounechba et al., 2014)(Ngan & Tan, 2011).

2.4.1.2 Temperature

The overall power generation efficiency of a photovoltaic (PV) panel is significantly influenced by the operational temperature of the PV panel. The PV module's electrical

performance suffers as its temperature rises, which reduces the efficiency with which it can turn sunshine into energy. This issue happens as a result of the fact that PV modules are made to convert just a small portion of solar energy, usually around 20% into electricity, with the remaining 80% being absorbed as heat. As a result, it becomes crucial to maintain and regulate module temperature in order to increase solar installations' overall effectiveness and electrical production. Effective temperature control techniques not only increase energy output but also extend the life of PV panels, making them an important factor in the design and upkeep of solar systems. The bandgap energy of the PV cell material and module temperature have a significant relationship. At high working temperatures, bandgap energy often declines. It affects the cell's ability to absorb photons of longer wavelengths and often lengthens the lifespan of minority carriers. The open-circuit voltage (V_{oc}) is decreased as a result of these components' minor increases in the light-generated current (I_{sc}), which lowers the cell Fill Factor overall (FF). The number of series and shunt resistances in a solar cell and its circuit are determined by the fill factor. The PV module's ability to generate electricity relies on the I_{sc} and V_{oc} .

Every 1°C increase in solar cell temperature results in a 0.03%–0.05% reduction in electrical efficiency in the absence of cooling. The PV performance is influenced by the encapsulating or cover materials' thermal dissipation and absorption characteristics (Bounechba et al., 2014)(Ngan & Tan, 2011).

2.4.1.3 Dust and soiling

It becomes clear that a complex interplay of atmospheric variables can have a considerable impact on photovoltaic (PV) panel performance when evaluating the effect of environmental factors on photovoltaic (PV) panel efficiency. The difficulty of increasing solar energy conversion is exacerbated by airborne pollutants, water vapor,

dust particles, and air molecules. These components create a barrier that prevents sunlight from reaching the PV panels directly, reducing their effectiveness. Airborne dust particles are a major factor in these obstacles. These particles serve as light-scattering agents and are frequently larger than the wavelength of incoming solar beams, decreasing the quantity of solar radiation that reaches the PV surface. If these particles are not removed, they may build up and eventually cover the surface of the PV module with a thick coating. It's interesting to note that this dust layer can change optically, changing its properties. This modification increases light reflection and absorption while reducing surface transmissibility, increasing the output of the PV module as a whole. Several meteorological factors might affect the amount of dust that collects on PV modules. This buildup is affected by a number of variables, including wind speed, humidity levels, the likelihood of rain, the origin and kind of dust particles, the quantity of PV module surface covering, and technological considerations. The problem gets worse in dry, desert areas where there is a lot of dust and little rain. Without routine upkeep, output power generation might decline and occasionally fall to just 50% of its maximum capability. Dust particles gather on the surface of the module mostly as a result of gravity. These particles can collect water vapor in areas with higher relative humidity, resulting in "soiling," a sticky, adhering substance resembling mud. The performance of the PV module is severely impacted by this occurrence. Said et al.'s research shows that a mere 45-day period of dust deposition can significantly lower the overall glass cover transmittance by 20%. PV panels are shaded by soil in both soft and hard ways, which reduces their ability to produce energy. Smog and other environmental conditions can cause soft shading, whereas the presence of a significant soil mass or muck on the panel might cause hard shading. Interestingly, strong shading does not affect current flow since the cells that are not shaded continue

to receive solar irradiance even while it lowers module voltage on some PV module cells. Additionally, the characteristics of dust vary geographically, and various types of dust have various impacts on light transmission. Since the patterns of dust buildup are geographically diverse, so is the loss of PV power caused by soiling. It is important to note that the tilt angle of PV panels also has a significant impact on the buildup of soiling and how it affects output power. The need for careful maintenance and cleaning procedures in the pursuit of the best possible solar energy conversion is further underscored by the fact that panels with flatter orientations or lower tilt angles are particularly vulnerable to the negative effects of soiling.

2.4.1.4 Shading

Shading refers to the obstruction of the light's path to the PV panel. Self-shading, soft shading, and hard shading are a few examples of the various shading kinds. The accumulation of waste, such as leaves, bird droppings, snow, and dust, leads to the development of hard shading. Additionally, poles, trees, and structures also prevent sunlight from forming a distinct and definitive shape. On the other side, air particles like dust, fog, and smoke lessen the strength of the sun's rays and provide the PV module a soft shade. Due to improper spacing, previous rows of solar modules can self-shade. Depending on the shading scenario, array arrangement, and module position, the output of a PV module is significantly reduced by partial or total shade. Partial shadowing has a substantial impact on a PV module's output since no current can flow through the shaded cells. Therefore, cells that are shaded work in a zone of negative voltage and lose energy instead of creating it because the current created in cells that are not shaded flows into those that are. Less energy is produced because the Maximum Power Point Tracker (MPPT) in gloomy areas deviates from the global Maximum Power Point.

2.4.1.5 Wind

A photovoltaic module's ability to generate power is influenced by the wind's properties, such as wind speed and direction. The performance of PV is affected by a variety of factors, including wind, module temperature, surface structure, and dust deposition. The most affordable cooling method is to use convective heat transfer by natural wind flow as much as possible. Rather than wind direction, wind speed has a much greater impact on how much the temperature of PV cells rise. Surface form and structure have a clear impact on convection cooling of PV panels. It may be possible for glass cover surfaces with structure and grooves to perform in colder weather and at higher wind speeds. However, the cooling effect is substantially stronger for the flat surface at low wind speeds. Furthermore, the wind removes dust from the PV module surface and prevents dust accumulation.

2.5 Maximum Power Harvesting from PV Systems

The variability of the solar resource coupled with the daily movement of the sun has led to the design of solar trackers and Maximum Power Point Trackers (MPPTs) to enable maximum power to be harvested from the available solar radiations. Most often, solar trackers are mechanically designed to follow the movement of the sun on daily basis. In this category of trackers, we have single axis and double axis trackers. On the other hand, MPPTs are designed based on the converter technology using soft computing techniques.

A single axis tracker follows the sun every day as it moves from East to West. In a single axis solar tracking system, the sun is tracked using a single pivot point. Tilted, vertical, and horizontal single axis tracking systems are the three primary variants of this technology. The face of the system module is aligned parallel to the axis of rotation in a horizontal single axis tracking system, and the axis of rotation is horizontal with

respect to the ground. Tropical regions frequently use this kind of construction. In a vertical single axis tracking system, which is typically used in high latitude settings, the face of the system module is positioned at an angle with respect to the axis of rotation when the axis of rotation is vertical with regard to the ground. At the tilted single axis tracking system, where the axis of rotation is positioned between the horizontal and vertical axes, the face of the system module is positioned parallel to the axis of rotation (Wang et al., 2016). The primary drawback of a single axis tracking system is that it can only follow the sun's daily motion, not its yearly motion. Additionally, because the tracking device rotates around just one axis, its efficacy is greatly diminished during cloudy days (Tanaka & Nakatake, 2009). Figure 2.3 below shows the schematic diagram for single and double axis solar trackers.

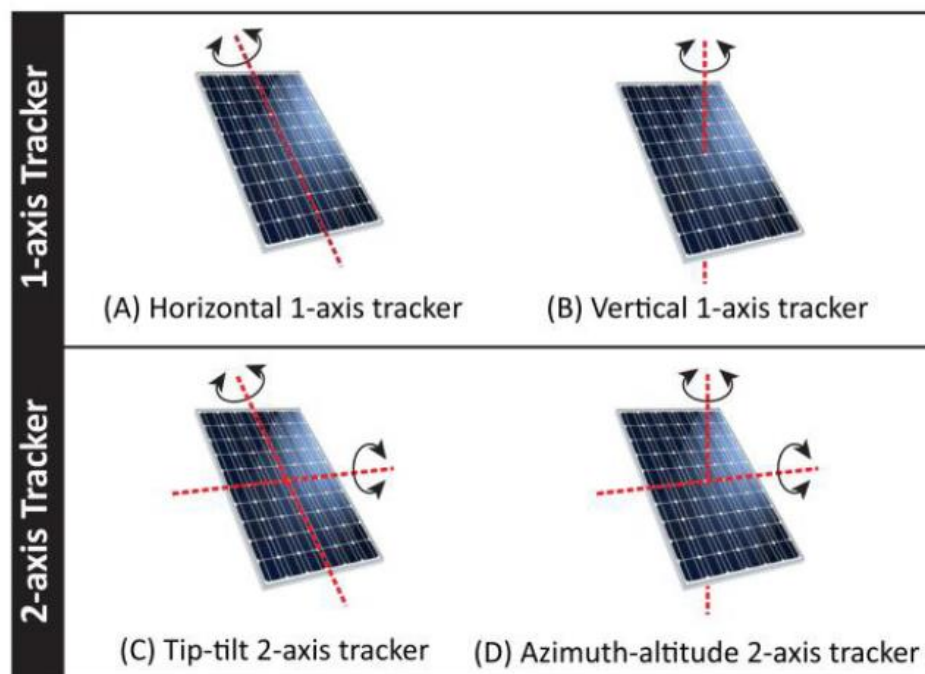


Figure 2.3: Single and Double Axis Trackers (Hong et al., 2016)

A dual axis solar tracking device rotates around two pivot points and tracks the sun along two separate axes. It is divided into azimuth-altitude tracker and tip-tilt dual axis tracker, and it tracks the sun in both north-south motion and east-west motion. The tip-

tilt dual axis tracker provides solar tracking that is concentrated on the panel's slope's rotational axis as well as its horizontal axis. The azimuth-altitude dual axis tracker provides solar tracking that is concentrated on the slope of the panel's vertical and rotational axes. These types of solar trackers often have both horizontal and vertical axes. With dual axis tracking in active systems, four Light Dependent Resistors (LDRs), a controller, and two motors are used typically. When the signal is detected by the controller from the four LDRs, each motor turns the system in one axis. The four LDRs are positioned in separate rotational directions (Fathabadi, 2016; Hafez et al., 2018; Hong et al., 2016).

Single and dual axis tracking, the two main types of tracking, have differing qualities from one another. Despite the fact that dual axis tracking is more sophisticated, more expensive, and requires more instruments and equipment, almost the same energy has been put in by researchers in developing the techniques (Hafez et al., 2018). The key benefit why the dual axis tracker is used over a single axis tracker is its ability in tracking the sun's movement throughout the year, including changes in its altitude from season to season, in addition to its movement throughout the day, as with single axis tracking. When compared to a single tracking system, this advantage makes dual tracking more effective and has a larger solar energy gain.

On the other hand, MPPTs use soft computing techniques to harvest maximum power.

In this category, based on their tracking strategies, MPPT techniques can be divided into four groups: the classical methods, the intelligent methods, the optimization methods, and the hybrid methods. based on their tracking strategies, MPPT techniques can be divided into four groups: the optimization methods, the classical methods, the hybrid methods, and the intelligent methods (Bollipo et al., 2020), (R. Ahmad et al.,

2019a; De Brito et al., 2013; Eltawil & Zhao, 2013; Jalal & Mehdi, 2021; Jayalalitha & Kavya, 2020; Karami et al., 2017; Mohamed & Elbarbary, 2021; Motahhir et al., 2019; Rezk & Eltamaly, 2015; Subudhi et al., 2013a; Verma et al., 2016; Yadav et al., 2020; Zainudin, 2010). Also, each tracking method's effectiveness varies depending on its ability to track maximum power as the weather condition changes (R. Ahmad et al., 2019b; Bollipo et al., 2020; Subudhi et al., 2013b). The different MPPT techniques are shown Table 2.1.

Table 2.1: Classification of MPPT techniques (Bollipo et al., 2020)

Class	Sub-class	Acronym
Classical MPPT control techniques	Perturb and observe	P&O
	Constant Voltage	CV
	Ripple Correlation Control	RCC
	Hill Climbing	HC
	Improved Perturb and Observe	IP&O
	Short Circuit Current	SCC
	Open Circuit Voltage	OCV
	Adaptive Reference Voltage	ARV
	Incremental Conductance	InC
	Look-Up Table Based MPPT	LTB MPPT
Intelligent MPPT control techniques	Artificial Neural Network	ANN
	Fuzzy Logic Controller	FLC
	Sliding Mode Control	SMC
	Fibonacci Series Based MPPT	FSB MPPT
	Gauss Newton Technique	GNT
Optimization techniques	Particle Swarm Optimization	PSO
	Cuckoo Search	CS
	Artificial Bee Colony	ABC
	Ant Colony Optimization	ACO
	Grey Wolf Optimization	GWO
	Genetic Algorithms	GA
Hybrid techniques	Adaptive Neuro Fuzzy Inference System	ANFIS
	Fuzzy Particle Swarm Optimization	FPSO
	Grey Wolf Optimization Perturb and Observe	GWO-P&O
	Particle Swarm Optimization Perturb and Observe	PSO-P&O
	Hill Climbing Adaptive Neuro Fuzzy Inference System	HC-ANFIS

2.5.1 Classical MPPT control techniques

These techniques are easy to implement because of their reduced algorithmic complexity. Under steady irradiance conditions, they are most efficient since the PV module only produces a maximum power point which is global. However, during tracking, these approaches show quick oscillations around the MPP, which reduces their effectiveness. Additionally, the real MPP cannot be tracked because these traditional methodologies ignore the impact of partial shading (R. Ahmad et al., 2019b; De Brito et al., 2013).

2.5.1.1 Perturb and Observe (P&O) MPPT Techniques

It is among the most used control techniques in commercial MPPT controllers (Mousa et al., 2021), (Bollipo et al., 2020). In essence, this approach monitors the variance in PV module power (dP). At this point, the PV module voltage's sign (dV) is also confirmed in order to modify the duty cycle (D) for upcoming updates and corrections. The power and voltage (P - V) curve data of the PV module is typically used to monitor the progression of the operational point of the module's output power (J. Jiang et al., 2016). The actual point is located on the left of the MPP if the gradient (dP/dV) is positive. The real point is located at the right side of the MPP if the change is negative. Till the moment where dP/dV is zero, the process is repeatedly repeated. Therefore, this point is the PV module's tracked MPP. The perturbation frequency, also referred to as the MPPT frequency, is defined as the number of perturbations made each second (Elgendy et al., 2012)(Alik et al., 2015).

The P&O methods for voltage perturbation use the general equations (2.8, 2.9, 2.10) below. When the step size for duty cycle control is either fixed or variable, there is a difference (adaptive control). A duty ratio that regulates the converter to either increase the voltage $V(t)$ by ΔV or lower the voltage by ΔV is created when the power $P(t)$ is

measured and compared to the previous maximum value $P(t-1)$. This difference, or Delta, is then utilized to form the duty ratio.

$$P(t) = V(t) * I(t) \dots\dots\dots 2.8$$

$$\Delta P = P(t) - P(t - 1) \dots\dots\dots 1.9$$

$$V(t) = V(t - 1) \pm \Delta V \dots\dots\dots 2.10$$

Figure 2.4 below shows the classification of different P&O MPPT methods while Figure 2.5 shows the flowchart followed by this method.

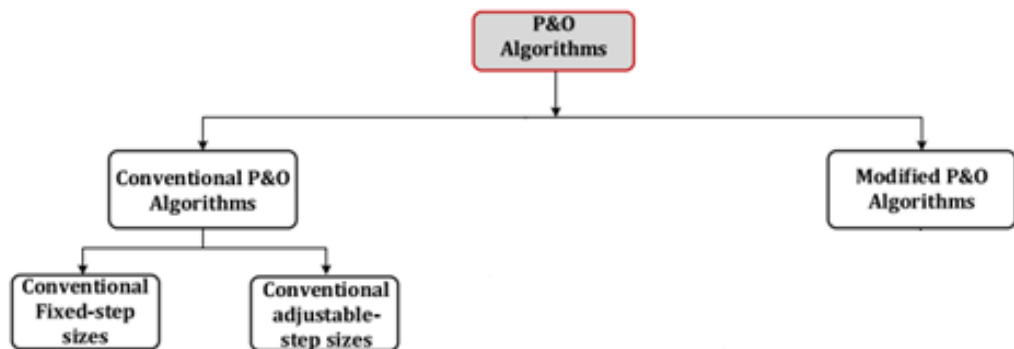


Figure 2.4: Classification of P&O Algorithms (Mousa et al., 2021)

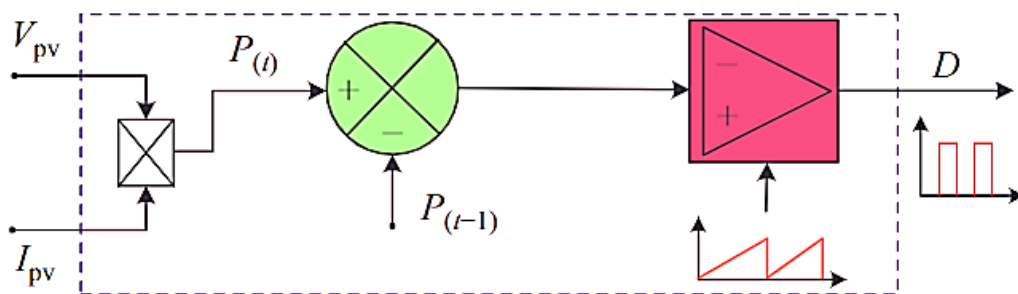


Figure 2.5: Block diagram of the P&O method (Bollipo et al., 2020)

2.5.1.2 Conventional P&O Algorithms

System designers must decide on a certain step size to use in the monitoring process when using the traditional P&O (Perturb and Observe) method with a fixed perturbation

strategy. Tracking speed and perturbation step size are two crucial elements of this tracking system. When using fixed perturbation levels, the magnitude of steady-state oscillations is inversely proportional to the step size. Larger step sizes typically result in larger oscillations, but regrettably they also slow down the system's reaction. This leads to a well-known trade-off between increasing responsiveness more quickly and reducing steady-state oscillations, which is a problem with the traditional method. Furthermore, MPPT (Maximum Power Point Tracking) with a set step size is intrinsically dependent on the particular features of the system to which it is applied. As a result, more complexity and restrictions are created because the perturbation step size is not maintained constant and may change depending on the system setup. The block diagram of this common method is shown in Figure 2.6b. In contrast, the classic P&O method's hill-climbing strategy can be improved by using an adaptive perturbation approach, where the perturbation value in this case is voltage. 10% of the open-circuit voltage is the initial setting for the voltage perturbation step. The perturbation value of each succeeding step is decreased to 0.5% of the open-circuit voltage as the algorithm advances, thereby halving the step size at each iteration. Although this adaptive strategy has produced encouraging results, it has some drawbacks. The established steps of the method continue to limit its adaptability, and much of its success depends on the open-circuit voltage, a variable subject to variations as a result of shifting environmental factors. As a result, the approach does not attain full adaptability since it continues to be influenced by outside circumstances that are outside its control. (Karami et al., 2017).

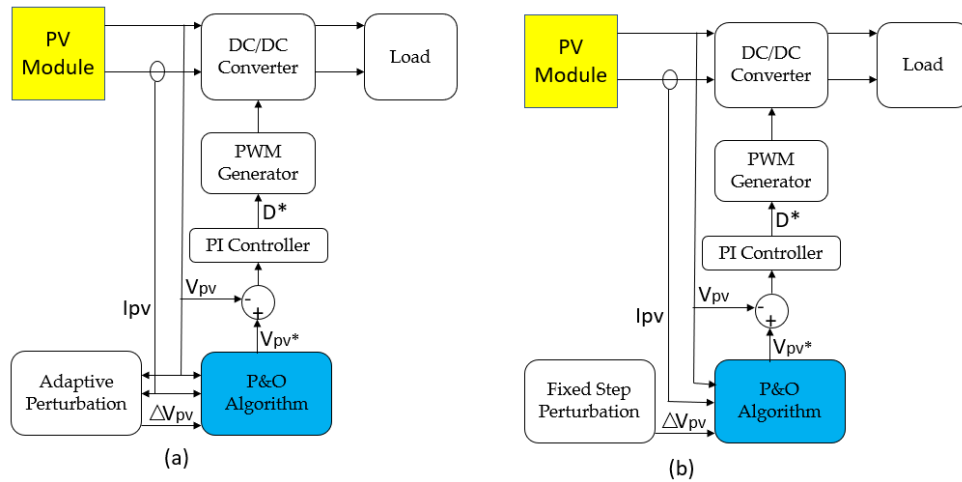


Figure 2.6: Block diagram of conventional P&O with (a) adaptive perturbation (b) fixed step perturbation (Karami et al., 2017)

Table 2.2 compares these different conventional P&O MPPT algorithms. It is noted that these methods are less complex making them cost effective. Also, the time of response for the adaptive step size is better than that of the fixed step size

Table 2.2: Contrasting traditional P&O algorithms

SN	Parameter for Comparison	Fixed step size	Adaptive step size
1	Time of response	Not fast	Fast
2	Complexity	Easy	Simple
3	How it performs under varying temperature and solar radiation?	Moderate	Good
4	Does it oscillate at MPP?	Yes	Yes but minimal
5	Cost	Moderate	Moderate
6	Efficiency	Low	High
7	Memory requirement	No	Depends

2.5.1.3 Improved (Modified) P&O (IP&O) Method

The standard P&O approach has been improved by the improved P&O method. In this method, the tracking reference voltage is scaled by a factor of 0.8 of the open circuit voltage of the PV module in order to avoid using extra power to follow the global MPP. There are two types of modified P&O: one with a fixed perturbation step and the other with an adaptive perturbation.

Instead of using the module voltage as the perturbed signal in the modified P&O with fixed perturbation step, this method uses the converter duty ratio. The removal of the PI/hysteresis controller after the MPPT block, which enables direct control of the converter duty-cycle, simplifies the control technique. The trade-off conundrum that was previously mentioned still exists because the perturbation step is fixed and designer dependent. Figure 2.7b displays the modified P&O with fixed perturbation step. To enhance the effectiveness of P&O procedures, the adaptive calculation of the perturbation value is used in place of the fixed values used in the conventional P & O approach.

Because it employs a variable duty ratio, the modified P&O with adaptive step size is more sophisticated. This method has some drawbacks despite its good performance, such as a high computational burden against accuracy trade-off and a reliance on predetermined constants. The block diagram of a modified P&O with an adaptive perturbation step is shown in Figure 2.7a (Karami et al., 2017).

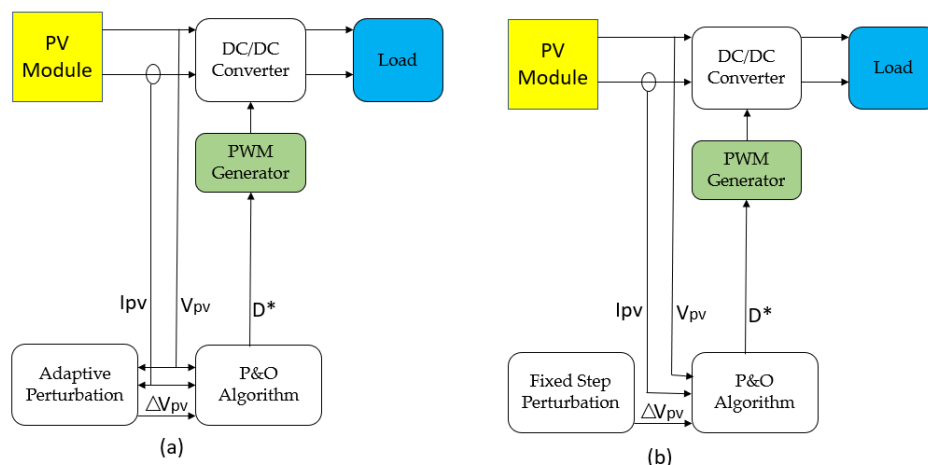


Figure 2.7: Block diagram of modified P&O with (a) adaptive perturbation (b) fixed step size and (Karami et al., 2017)

The comparison of the modified P&O methods in Table 2.3 also reveals an improvement in the fixed step size method's reaction time metrics. These comparisons

show that the P&O systems are typically less sophisticated, which lowers their cost and increases their adoption in various industries.

Table 2.3: Comparison of modified P&O algorithms

SN	Parameter for Comparison	Fixed step size	Adaptive step size
1	Time of Response	Fast	Fast
2	Difficulty	Moderate	Moderate
3	How it performs under varying temperature and solar radiation?	Good	Very good
4	Does it oscillate at MPP?	Minimal	Minimal
5	Cost	Moderate	High
6	Efficiency	High	High
7	Memory requirement	Yes	Yes

In the work of Kolluru et al. (2018), a new P&O MPPT controller with a 0.05s settling time and the ability to measure 10% more power from the PV source was designed. In MATLAB Simulink, their model was simulated. According to their research, utilizing their controller will increase the amount of power that can be harvested from the PV system compared to not using the tracker (Kolluru et al., 2018). Sera et al. (2013), presented a detailed analysis of the two most popular hill-climbing Maximum Power Point Tracking (MPPT) algorithms which were InC and P&O. The two methods were analyzed from both a mathematical and a practical implementation perspective. Their mathematical analysis revealed that there is no difference between the two. Experimental proof of this was provided in accordance with European Standard EN 50530. Efficiency deviations of 0.13% under dynamic and even 0.02% under static conditions were achieved (Sera et al., 2013). Pandey et al. (2019), suggested a P&O method for capturing peak power from solar panels. By combining this method with an MPPT controller, their system was able to match the output power provided by the Panels to the variable load power required. SIMULINK in MATLAB was used to simulate their work (Pandey & Srivastava, 2019). The direct duty ratio perturbation and

the reference voltage perturbation approaches employed for the P&O MPPT algorithm implementation were thoroughly analyzed, along with experimental results by (Elgendy et al., 2012). Using a 1080-Wp experimental set-up, they investigated the impacts of the perturbation rate and step size on system behavior, the selection criteria for these parameters, and the calculated energy usage at slow and fast changing weather conditions. Irradiance and temperature transients were responded to more quickly using the reference voltage perturbation technique. Its flaw was that if a high perturbation rate was utilized, or if low-pass filters were used to remove noise from the array current and voltage feedback signals, it would lose stability. For solar irradiation that changes slowly, their experimental system's energy usage efficiency was calculated to be 97.2%. Due to energy loss during the perturbation and recovery phases when irradiance varies, the efficiency was somewhat lower at 97% for quickly changing irradiance. Direct duty ratio control, on the other hand, had a worse performance at fast changing irradiance and higher utilization of energy and stability characteristics at a slower transient response. They discovered that the experimental system's energy usage efficiency was 99% for the slowly changing irradiance and 97.9% for the rapidly changing irradiance, respectively. They came to the conclusion that direct duty ratio perturbation permits high perturbation rates up to the rate of pulse width modulation (PWM) without a general loss of system stability.

2.5.1.4 Hill Climbing (HC) Method

This method consists of perturbing the duty ratio of the power converter (Rizzo & Piegari, 2010). It is not directly the same as P&O, though they have a similar core premise. To execute MPPT, P&O requires a perturbation in terminal voltage, whereas the hill climbing approach requires a perturbation in duty ratio (Verma et al., 2016)(Jately et al., 2021). This means that the duty ratio used to control the converter is keeps changing

as the PV power deviates from the maximum value at any given instant. The disturbance on the duty ratio determines the tracking direction on the PV power curve. Equation (2.11) is the governing equation for the duty ratio.

$$D(i) = D(i - 1) \pm S \dots\dots\dots 2.11$$

$D(i - 1)$ is the duty at $(i - 1)^{th}$ iteration, $D(i)$ is the duty ratio at i^{th} iteration which goes to control the converter and S is the step size. Depending on the algorithm employed, the step size S may be fixed. The calculation for the variable step is in (Jatly et al., 2021).

The step size can either be positive or negative depending on the direction where the power point is being located on the curve. If the change in power and voltage are both positive or negative, then S will be negative. If the change in power and voltage have different signs, then S will be positive.

2.5.1.5 Constant Voltage (CV)

The set voltage value for MPP assumed by the constant voltage MPPT algorithm is the same as the value actually observed under the manufacturer's Standard Test Conditions (STCs). This set voltage is thought to be in the range of 72% to 88% of the open circuit voltage (Leedy et al., 2012; Ngan & Tan, 2011; Noh et al., 2002). A feedback control loop is then used to modify the duty ratio of a MPPT converter using this fixed value as a reference. This method is easy to implement since the only requirement for building the MPPT control is to measure the array voltage. Both analog and digital circuits can be used (Elgendy et al., 2010). The relationship between the voltage at MPP (V_{mpp}) and the open circuit voltage (V_{oc}) is given by equation (2.12).

$$V_{mpp} = k * V_{oc} \dots\dots\dots 2.12$$

where k is a constant which lies between $0.72 \leq k \leq 0.8$. The flowchart of the CV method is depicted in Figure 2.8.

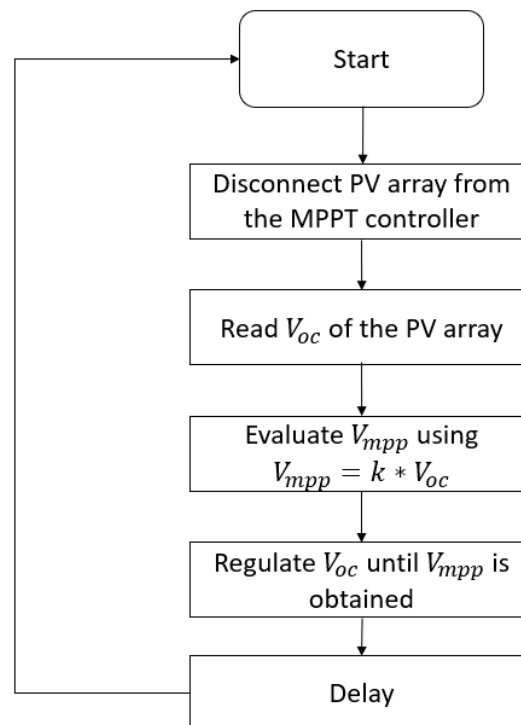


Figure 2.8: Flowchart of the CV method (Ngan & Tan, 2011)

The solar module is temporarily isolated from the Maximum Power Point Tracker (MPPT) during the voltage comparison process. The measurement of VOC, or the open-circuit voltage, is made possible by this significant step. The optimal operating point is then established by the MPPT using equation (2.12) and a predefined value of k , with the goal of achieving the estimated V_{mpp} (maximum power point voltage). To ensure optimal power extraction, the MPPT repeatedly adjusts the module's voltage until it precisely lines up with the V_{mpp} . The MPPT continues this iterative process until it is able to accurately identify the Maximum Power Point (MPP), optimizing the solar system's overall efficiency. To fully utilize solar energy, this practice of constant adjusting and tracking is necessary. Leedy et al. (2012), presented a CV MPP algorithm

that adjusts the reference voltage automatically to account for varying environmental conditions (Leedy et al., 2012).

2.5.1.6 Ripple Correlation Control (RCC)

When a power converter is connected to a solar photovoltaic (PV) array, it causes current and voltage variations known as ripples to appear. These oscillations, which are a natural result of the power converter's switching mechanism, spread across the PV array and have a significant impact on how well it performs as a whole. As a result, these ripples are crucial in determining how much power the PV array produces. A cutting-edge tracking technique called Ripple Correlation Control (RCC) has been created in order to make use of any potential advantages offered by these ripples. RCC makes use of the correlation between the derivatives of PV voltage or current fluctuations and those of PV power variations. The goal is to control the power gradient towards zero using this correlation in order to reach the PV array's maximum power point (MPP). In light of the operational dynamics, the operating point of the PV array is located below the MPP when the voltage or current grows simultaneously with the power production. The operational point, however, surpasses the MPP when the voltage or current rises while the power output falls. The secret to increasing solar energy harvesting and solar PV system efficiency lies in this complex dance of ripples and control mechanisms (Karami et al., 2017). The advantage with RCC is that it does not introduce any external disturbance into the system, rather it makes use of the current or voltage ripple already present in the system. Without the aid of any module parameters or measurements, the method converges asymptotically at maximum speed to the MPP (Ho et al., 2004; Kimball & Krein, 2007; Leedy et al., 2012). Equation (2.13) below is made use of by this method (Verma et al., 2016).

$$\frac{dP}{dt} * \frac{dV}{dt} = 0 \text{ or } \frac{dP}{dt} * \frac{dI}{dt} = 0 \dots\dots\dots 2.13$$

2.5.1.7 Open Circuit Voltage (OCV)

This is a tracking technique which assumes that the voltage at MPP is the open circuit voltage of the solar module multiplied by a constant coefficient ranging from 0.7 to 0.8 (Salman et al., 2018). Due to its straightforward process, this approach is simple to use. Although straightforward, it has the drawback of requiring the load to be disconnected each time the open circuit voltage needs to be monitored. This causes supply disruptions and, as a result, lowers system efficiency (Sarvi & Azadian, 2021). It is therefore not a recommended technique to use in areas where continuity of supply to the load is of ultimate importance.

2.5.1.8 Short Circuit Current (SCC)

Similar to the open-circuit voltage tracking technique, this tracking method is based on the well-established linear connection between the photovoltaic (PV) current at the Maximum Power Point (MPP) and the short-circuit current. Equation (2.14) uses a proportionality constant indicated as K_1 to show how it works. K_1 is a characteristic that is mostly influenced by the fill factor, the current weather, and the particular PV cell type in use. It is commonly calculated to be around 0.85 for poly-crystalline PV modules. But in real-world applications, this constant is frequently dynamically changed by regular PV scans that are carried out every few minutes. After that, up until the next computing cycle, the system makes use of this revised estimate. The control flowchart hence closely mimics the open-circuit voltage method. It is important to remember that this method has similar benefits and drawbacks to the open-circuit voltage control technique. It's crucial to emphasize the practical applications of this tracking method in addition to its core ideas. The system can adapt to shifting weather

conditions, the impacts of shadowing, and the aging of PV cells by continually monitoring the PV current at MPP and altering the proportional constant K_1 in real-time, so maximizing energy yield. On the other hand, the requirement for frequent PV scans may result in increased computing burden and possible responsiveness problems. Additionally, this strategy is susceptible to variations in fill factor and might not always be appropriate for all PV system configurations, just like the open-circuit voltage strategy (Karami et al., 2017).

$$I_{MPP} = K_1 * I_{sc} \dots \dots \dots 2.14$$

K_1 Varies between 0.78 to 0.92 (Alghuwainem, 1994).

2.5.1.9 Adaptive Reference Voltage (ARV)

This method, which is comparable to the CV method, also takes the local climate into account. In addition to the voltage, additional sensors are employed to measure the temperature and solar radiation. Here, the solar radiation is divided into several divisions for a specific temperature, and the equivalent reference voltage is recorded in an offline table. The corresponding proportional integral controller used, compensates the error between the PV voltage and the reference voltage to generate a duty cycle used to control the converter (Bollipo et al., 2020). This method is capable of maintaining its efficiency even under varying solar radiation. This is shown in the work done in (Lasheen et al., 2017).

2.5.1.10 Incremental Conductance (InC)

This is yet another common technique for monitoring maximum PV system power. The method uses the PV modules' voltage and current to determine the MPP. This technique can track MPP in a variety of atmospheric situations. The essential equations underlying this approach are described in depth in (Subudhi et al., 2013b). Despite

being more difficult to implement than P&O, this method is made simpler by the development of DSPs (Digital Signal Processors) (Liu et al., 2008a) (Jately et al., 2021).

2.5.1.11 Look-Up Table Based (LTB) Method

This method successfully synchronizes the array's operational state to maximize its output at the peak power point. It accomplishes this by carefully comparing the solar array's voltage and current values as they are now measured with a vast database of previously recorded data. This vast database includes many system setups that are adjusted to various insolation and temperature conditions. Additionally, it features precisely compiled maximum power points that are specially designed for different solar photovoltaic (PV) arrays. By using this technique, we guarantee that the array continually performs at its peak level, producing the highest amount of power production under a variety of environmental circumstances. This methodology offers helpful information for system optimization and performance monitoring in addition to aligning the operating point of the array with the maximum power point. With a variety of data available, we may adjust system settings to accommodate altering environmental circumstances, improving energy generation efficiency and ensuring the solar PV systems' long-term viability. We are able to make wise judgments, maintain optimal system performance, and maximize the energy harvest from solar arrays under a variety of conditions thanks to our ongoing data-driven strategy (J.-A. Jiang et al., 2005). The method's major flaw is the requirement for bulk storage memory. As tracking accuracy rises, there are more operating circumstances, which calls for more data storage. Due to the tracking scheme's array-specificity, implementation is challenging, and saving and archiving all potential system states is inconvenient. The method's major flaw is the requirement for bulk storage memory. As tracking accuracy rises, there are more operating circumstances, which calls for more data storage. Due

to the tracking scheme's array-specificity, implementation is challenging, and saving and archiving all potential system states is inconvenient (Verma et al., 2016).

2.5.2 Intelligent MPPT control techniques

These approaches accomplish MPPT using soft computing techniques. These methods are more sophisticated since their algorithms make use of machine learning.

2.5.2.1 Artificial Neural Network (ANN)

A soft computing technique called the Artificial Neural Network (ANN) is inspired by the way our brain functions. These machine learning-capable computer models are represented as interconnected neurons in order to produce a network that resembles a biological neural network (artificial nodes). Throughout the training process, connection weights are adjusted to achieve the ideal fit, which is reference voltage comparable to MPP (Verma et al., 2016)(Messalti et al., 2017). As seen in Figure 2.9, it has three levels: input, hidden, and output layers. One can use PV module parameters like V_{oc} and I_{sc} , atmospheric data like temperature and irradiance, or a combination of the two as input variables. Using the hidden layer method, the output reflects the duty cycle signal that instructs the converter to follow the MPP. The weight W_{ij} is applied to the connection between nodes i and j . Node-to-node linkages are weighted in the neural network technique based on a training process in which PV parameters are evaluated and recorded over months or years to determine the appropriate weight for each node. The disadvantage of this strategy is that because the neural network must be specifically trained for the PV module being used, it cannot be modified to operate on numerous types at simultaneously. Additionally, the parameters of the PV panel change with time, requiring regular neural network training to accurately follow the MPP (Karami et al., 2017). More research work to ensure that an algorithm trained on one PV system can be used on other system to track MPP is needed to make this method globally useful.

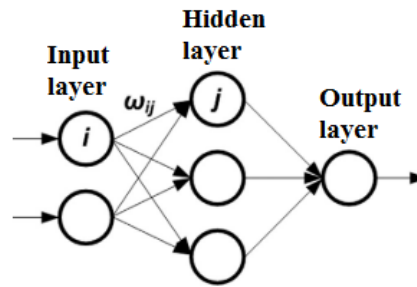


Figure 2.9: Layers of Artificial Neural Network (ANN)

2.5.2.2 Fuzzy Logic Controller (FLC)

Fuzzy logic is a collection of multiple-valued logic, in contrast to binary logic, which only has two states: true or false. The concept of partial truth is introduced by the fuzzy logic variable range of zero to one, where the variable value can either be totally true or completely false. Fuzzy logic is a collection of multiple-valued logic, in contrast to binary logic, which only has two states: true or false. The concept of partial truth is introduced by the fuzzy logic variable range of zero to one, where the variable value can either be totally true or completely false (Verma et al., 2016). Because they continue to track the MPP despite incorrect inputs, fuzzy computation trackers are considered intelligent. Since fuzzy controllers generally function through three important stages: fuzzification, rule base lookup tables, and defuzzification; they do not necessarily rely on mathematical models. The membership function used in the initial modeling stage converts the numerical input variables into linguistic variables using the five unique fuzzy levels NB (negative large), NS (negative small), ZE (zero), PS (positive small), and PB (positive big). The ability of fuzzy computation trackers to intelligently continue pursuing the Maximum Power Point (MPP) despite defective or incorrect inputs is one of its most striking traits. By achieving this intelligent behavior without the need for a traditional mathematical model, fuzzy control systems are further demonstrated to be robust and adaptable. The use of these fuzzy levels (NB, NS, ZE,

PS, and PB) also improves the controller's capacity to recognize subtleties in input data, further enhancing performance. Fuzzy controllers are therefore effective in situations where mathematical models may be difficult to construct or impossible, and they guarantee accurate control and tracking of crucial operational points. The equations (2.15 and 2.16) by Ngan and Tan can be used to derive the input parameters of an MPPT fuzzy logic controller, which are typically an error E and a change in error ΔE (Ngan & Tan, 2011).

$$E(i) = \frac{P_{pv}(i) - P_{pv}(i-1)}{V_{pv}(i) - V_{pv}(i-1)} \dots \dots \dots 2.15$$

$$\Delta E(i) = E(i) - E(i - 1) \dots \dots \dots 2.16$$

Table 2.4 shows the output of the fuzzy controller, which is represented by ΔD (change in duty-cycle) of the power converter. After calculating E and ΔE and converting them to linguistic variables. At the defuzzification stage, the linguistic output variable of the fuzzy logic controller is converted to a numerical variable, producing an analog signal that powers the power converter to the MPP. The MPPT fuzzy logic controller performs brilliantly in a variety of environmental conditions. But its success depends on choosing the right error computation and creating the rule base table (Karami et al., 2017)(Bendib et al., 2015a; X. Li et al., 2019). There is no requirement for mathematical modeling while using this approach for MPPT. Additionally, when less oscillations are seen, the stability of the system surrounding the MPP is improved. However, this strategy makes it challenging to fine-tune the control rules, scaling factor, and membership function. To maximize the application of this approach in MPPT development, more study is needed in these areas.

Table 2.4: Fuzzy Logic Rule Table

Change in Error (ΔE) →	NB	NS	ZE	PS	PB
Error (E) ↓					
NB	ZE	ZE	NB	NB	NB
NS	ZE	ZE	NS	NS	NS
ZE	NS	ZE	ZE	ZE	PS
PS	PS	PS	PS	ZE	ZE
PB	PB	PB	PB	ZE	ZE

2.5.2.3 Sliding Mode Control (SMC)

For nonlinear systems, the sliding mode control technique is employed. For MPPT, this control technique is used in two modes of operation: approaching mode and sliding mode. At MPP, the change in power with respect to voltage or current is equal to zero as shown in equation (2.18) (Kihal et al., 2019; Verma et al., 2016).

$$P = VI = I^2R \dots\dots\dots 2.17$$

$\frac{dP}{dI} = 0$ which implies:

$$2R + I \frac{dR}{dI} = \sigma = 0 \dots\dots\dots 2.18$$

Where σ is the sliding surface (Kim et al., 2006), I is the current, the power is P, V is the voltage, and R is the resistance. The duty ratio δ which is then used to control the converter in the system to track the MPP is updated based on the value of σ . $\Delta\delta$ is the change in duty ratio, δ_i is the duty ratio after the i^{th} iteration while $\delta(i + 1)$ is the updated duty cycle after the $(i + 1)^{th}$ iteration given by equation (2.19).

$$\delta(i + 1) = \begin{cases} \delta_i + \Delta\delta & \text{for } \sigma > 0 \\ \delta_i - \Delta\delta & \text{for } \sigma < 0 \end{cases} \dots\dots\dots 2.19$$

This technique's MPPTs can precisely track the maximum power due to its very effective mathematical model. Its drawback is that the selection of the sliding surface has a significant impact on how well the tracking performs.

2.5.2.4 Fibonacci Series Based (FSB) Method

Tracking the MPP throughout the full search region lengthens processing times and raises serious issues with data storage. This FSB tracking method effectively addresses the issue by shortening the search period by limiting the range of operation. This complex iterative algorithm first refines its search before scanning the range in search of the optimal position. In order to identify which direction the change should be made, it employs two roughly equivalent locations between V_{\min} and V_{\max} in that it alters its operating range using the prior iteration values. This technique is comparable to a divide-and-conquer tactic (Miyatake et al., 2004; Ramaprabha et al., 2012; Zhang et al., 2019). The iterative sequence which is used to fast-track the MPP is given in equation (2.20) below (Bollipo et al., 2020).

$$R_{(n+2)} = R_{(n+1)} + R_n, (n = 1,2,3, \dots \text{ and } R_1 = R_2 = 1) \dots \dots \dots 2.20$$

Where R represent the points which are used on the PV curve to track the MPP.

It however requires complex calculations to track the MPP. This is a setback to this method which needs some adjustments.

2.5.2.5 Gauss Newton Technique (GNT)

The Gauss-Newton approach (Xiao et al., 2007), as compared to other mathematical computing algorithms, which uses a root-finding approach, has the fastest tracking speed. Its algorithm uses the first and second derivatives of the change in power to calculate the direction and quantity of iterations necessary to solve the governing equation (Bollipo et al., 2020; Subudhi et al., 2013b). Due to the advanced level of mathematical modeling, it has a complex construction, which is a drawback. Through additional research in this area, this intricacy can be made simple.

2.5.3 Optimization techniques

The pursuit for a best solution is needed in several areas in engineering and science. The process of altering a device's inputs or attributes using a mathematical method in order to get the best minimal or maximum output is known as optimization. For any system to be optimized, one needs to have the objective function or cost function or fitness function which is the input to the optimization process, and the result is the system's fitness function. The main tool required to solve complex problems is optimization. Five classifications can be used to categorize optimization techniques. One method of optimizing a system is to use the trial-and-error approach. Here, the procedures have an impact on the result without being aware of the limitations that are in charge of generating the result. Another method is using the cost function for optimization which is expressed mathematically. Also, optimization can be one dimensional where only one variable is contained in the optimization process. In case of many variables, multi-dimensional technique is necessary. The method of optimization becomes challenging as the number of variables increase. While static optimization is time independent, dynamic optimization depends on time. Finding the optimum solution to the static problem is challenging, but the addition of the time component makes tackling dynamic problems even more complex. While continuous variables have an unlimited number of possible values, discrete variable optimization only has a finite number of possible values. Variables frequently have boundaries or restrictions. Unconstrained optimization permits the variable to take any value, whereas constrained optimization adds variable equalities and inequalities into the cost function. Through the transformation of variables, a constrained optimization problem can be transformed into an unconstrained problem.

In their original form, many optimization algorithms have been devised. Finding the global maxima or minima of the objective function, also known as the global optima, is the aim of global optimization. To identify good parameters or designs to be used, one needs to make use of optimization algorithms. The most commonly used optimization algorithms are the metaheuristic optimizations techniques. This is a set of algorithms and problem-solving techniques which are used to find suitable solutions to complicated optimization problems. These methods are especially useful for solving issues where computing an exact solution is difficult because of the magnitude, complexity, or abundance of potential solutions. Because of their ability to solving complex problems, engineering optimization problems can be solved using metaheuristics techniques. Although this optimality is not always possible to obtain, optimization algorithms are the tools and approaches used to solve optimization problems. The fact that uncertainty is virtually always present in real-world systems further complicates this quest for optimality. Therefore, in engineering and industry, we strive for optimal design (X.-S. Yang & Deb, 2014).

2.5.3.1 Particle Swarm Optimization (PSO)

This method is regarded as the most effective tool among the several MPPT algorithms because of its quick computing speed, straightforward concept, simple application, high accuracy, and capacity for nonlinear problem optimization. As a result, a multiple MPP under partial shading solution that is satisfactory in comparison to prior methods can be discovered. PSO's core idea is influenced by how huddled birds or schooling fish behave (S. Kumar et al., 2019). PSO requires specific particles to form a swarm of roving wasps across the search space in order to identify the optimum answer. Each particle tries to change its traveling velocity based on its previous flying experiences.

The swarm velocity and position can be obtain using equations (2.21 and 2.22) respectively.

$$C_i^{(k+1)} = wC_i^k + m_1r_1P_{best(i)} + m_2r_2g_{best} \dots\dots\dots 2.21$$

$$S_i^{(k+1)} = S_i^k + C_i^{(k+1)} \dots\dots\dots 2.22$$

Where $C_i^{(k+1)}$ is the velocity of i^{th} swarm for iteration $(k + 1)$, w is the learning factor, m_1, m_2 are position constants, r_1, r_2 are random numbers ranging from 0 to 1, g_{best} is best position for the swarm of particles, and $S_i^{(k+1)}$ is the position of i^{th} swarm for iteration $(k + 1)$ (Ishaque et al., 2012; Khare & Rangnekar, 2013; Miyatake et al., 2011).

The identification of a specific region, known as the solution space, each of which accumulates a possible problem-solving degree, serves as the theoretical basis of PSO. It is anticipated that at the initial stage, a large number of randomly distributed particles in the search area will be preserved in the ideal location (Kaewkamnerdpong & Bentley, 2005). Global ideal positions will be maintained for all vacant roles. The step size for these particles is then altered. The cost function for every particle is then calculated and its results are compared to earlier results. The previous procedures are then repeated until the same results are obtained. PSO uses the converter duty cycle and output power as its objective functions to determine the Global Maximum Power Point (GMPP) of a PV array. When a population that represents the duty cycle is initialized and the associated voltage and current are measured, the power is calculated. The update procedure is repeated if the power rises until the global maximum power is reached. Global ideal positions will be maintained for all vacant roles. The step size for these particles is then altered. The cost function for every particle is then calculated and its

results are compared to earlier results. The previous procedures are then repeated until the same results are obtained. PSO uses the converter duty cycle and output power as its goal functions to determine the Global Maximum Power Point (GMPP) of a PV array. When a population that represents the duty cycle is initialized and the associated voltage and current are measured, the power is calculated. The update procedure is repeated if the power rises until the global maximum power is reached (Mao et al., 2019; Rezk et al., 2017) (Rezk et al., 2019)(Chowdhury & Saha, 2010). Because this method is bio-inspired, it has the capability of tracking the GMPP with a high tracking speed under varying weather and partial shading conditions. This method however has a demerit which is the complex nature of its objective function which depends on the velocity of the particles. Further research on this algorithm should look at the means of simplifying this objective so as to reduce the complexity of the system.

2.5.3.2 Cuckoo Search (CS)

The cuckoo search (CS) approach is a parasitic reproduction strategy that was biologically inspired by cuckoo birds. The cuckoo is a fascinating bird because in addition to making beautiful noises, it reproduces aggressively.

Some species, such as the ani and Guira cuckoos, lay their eggs in communal nests, but they may also take the eggs of other species out of the nests in order to increase the likelihood that their own eggs will hatch (Pavlyukevich, 2007; Wolpert & Macready, 1997; X.-S. Yang & Deb, 2009, 2013, 2014). The obligate brood parasitism is practiced by several species, who lay their eggs in the nests of other host birds (typically other species) (X.-S. Yang & Deb, 2014).

The following three idealized principles can be used to simply describe the common Cuckoo Search. The number of host nests is determined, and the host bird discovers the

cuckoo egg deposited there. Next, the best nests with high-quality eggs will be passed down to the following generations. The number of host nests is determined, and the host bird discovers the cuckoo egg deposited there. Next, the best nests with high-quality eggs will be passed down to the following generations.(X.-S. Yang & Deb, 2013). Each cuckoo lays one egg at a time and deposits it in a randomly selected nest. In this situation, the host bird has two options: either get rid of the egg or simply quit the nest and construct a brand-new one (X.-S. Yang & Deb, 2009).

The levy flight mechanism is used in CS to describe the procedures involved in finding a nest (Pavlyukevich, 2007). A levy flight is essentially a random walk through which the step sizes for levy distributions are generated. Step sizes for CS are bigger than for standard PSO because of the levy flight mechanism. It allows for a convergence that is rapid. The step size gets smaller as the particles get closer to the MPP, until it reaches zero (Mohapatra et al., 2017)(Rezk et al., 2017; X.-S. Yang & Deb, 2014). This method of MPPT is advantageous in that, it has a high convergence speed and efficiency. It also has a lesser number of tuning variables as compared to PSO which gives it a more robust performance. On the other hand, its composite mathematical function which is being used in the algorithm for tracking leaves the method with a disadvantage. Through more research, this complexity can be minimized and this method optimized to give outstanding performance.

2.5.3.3 Artificial Bee Colony (ABC)

The Artificial Bee Colony (ABC) algorithm is a straightforward, bio-inspired technique that only needs a few controllable parameters. Additionally, the algorithm convergence criteria are not dependent on the system's beginning conditions. Swarm-based meta-heuristics are used to solve multidimensional and multimodal optimization problems quickly. The three main categories of artificial bees are workers, observers, and scouts.

A bee who is actively seeking food or using a source of food production is said to be employed; a bee who is waiting in the hive for a decision regarding a food source is said to be an observer (onlooker); and a scout bee is used to conduct a random search for a new food source. The three groups work in concert to find the best solution quickly through communication and cooperation. Maximum power is the ABC algorithm's food source, while duty cycle is its food position. The Artificial Bee Colony (ABC) algorithm is a straightforward, bio-inspired technique that only needs a few controllable parameters. Additionally, the algorithm convergence criteria are not dependent on the system's beginning conditions. Swarm-based meta-heuristics are used to solve multidimensional and multimodal optimization problems quickly. The three main categories of artificial bees are workers, observers, and scouts. A bee that is actively seeking food or using a source of food production is said to be employed; a bee that is waiting in the hive for a decision regarding a food source is said to be an observer (onlooker); and a scout bee is used to conduct a random search for a new food source. The three groups work in concert to find the best solution quickly through communication and cooperation. Maximum power is the ABC algorithm's food source, while duty cycle is its food position (Mohapatra et al., 2017). This method uses very few parameters which is advantageous. However, it has some drawbacks, including complexity, a poor tracking speed, and occasionally, the ability to only track the local MPP rather than the GMPP. Research focus in this area should be on reducing the complexity, improving the tracking speed and ensuring that the GMPP is always tracked at all times.

2.5.3.4 Ant Colony Optimization (ACO)

This probabilistic approach assists in identifying the ideal result based on the ant's foraging behavior. The PSO method has been modified to create this approach. After

measuring the power coming from the PV module and applying it to the converter, it provides the best duty cycle. To reduce the number of local maximum power points on the I-V curve, ACO is utilized in both centralized and distributed type MPPT controllers (Mohapatra et al., 2017). Some advantages of this method are; its convergence is not dependent on the initial sample position which makes the convergence speed faster, it has a simple control strategy, low cost, and is capable of tracking under partial shading conditions. The disadvantage with this method is that the approach used for estimation is complex.

2.5.3.5 Genetic Algorithm (GA)

Darwin's notion of theoretical determination and the influence of the natural part serve as the foundation for GA. GA is intended to extract the most appropriate results from the nonlinearity of the many optimization challenges. Each answer is interpreted as a binary matrix with chromosomal definitions. The population solution raises the quality of these agents, bringing their fitness levels up to date. Due to its slow speed in tracking the MPP, GA is frequently not applied to the MPPT issue right away. As an alternative, GA is used to optimize other global MPP algorithms in order to track the MPP very quickly and accurately. Similar to this, the GA is used to train an ANN to predict the maximum voltage and current at the MPP of the PV array. Additionally, the economic design of PV arrays employing various inverters has been stratified using GA (Rezk et al., 2019).

GA uses different encoding schemes which transform the problem to be solved into chromosomes. The different encoding techniques used are the tree encoding, value encoding, permutation encoding, and binary encoding. Binary encoding is most commonly used in which the data value is converted in to binary strings giving several chromosomes. Permutation encoding on the other hand is best suited for queuing or

ordering problems. Meanwhile in tree encoding, every chromosome is a tree of some objects, commands or functions in programming language and it is best suited for evolving expressions or programs. The processes involved with optimization using GA are explained in (Malhotra et al., 2011).

2.5.3.6 Grey Wolf Optimization (GWO)

The wolf strategy to hunting prey is used in this optimization method (Rezk et al., 2019). Grey wolves typically hunt in three stages, first searching for prey, then encircling prey, and lastly attacking prey. Grey wolves are divided into four levels, with the leader level, also known as alpha (α) wolves, providing the greatest answers to optimization issues. Beta (β) and delta (δ) wolves, respectively, are the names of the second and third better solutions. The last category is known as omega (ω) wolves, and they are thought to be the lowest classification of grey wolves. In actuality, wolf cooperation and effective communication speed up the process of finding the best answer (Q. Li et al., 2017)(Rajkumar et al., 2017)(Cherukuri & Rayapudi, 2017). During MPPT using this method, a search space is created in which the MPP is found. This can be likened to the grey wolfs surrounding an area in which their prey is found. The behaviour of surrounding the prey (tracking the MPP) can be determined using equations (2.23 and 2.24). The alpha (α) wolves are regarded as the best fit (fittest position for the MPP) while beta (β) and delta (δ) wolves are said to have the best solution receptivity. Omega (ω) wolves, however, are thought to be the candidate solution's leftovers (Diab & Rezk, 2019).

$$D = |C \cdot X_p(t) - X(t)| \dots \dots \dots 2.23$$

$$X(t + 1) = X_p(t) - A \cdot (D) \dots \dots \dots 2.24$$

In the above equations, D represent the grey wolves' vector, t is the current position, X_p is the position vector of prey, X is the position vector of grey wolves, A and C are the coefficient vectors which can be calculated using the equations in Mohanty et al. (Mohanty et al., 2015) and Rezk et al. (Rezk et al., 2019). This method is advantageous in that it is more efficient at tracking, has no transient or steady-state oscillations, is more robust, and is faster. It has a number of drawbacks, including a high computational complexity, a huge search space, and a high cost.

2.5.4 Hybrid techniques

2.5.4.1 Adaptive Neuro Fuzzy Inference System (ANFIS)

This hybrid approach makes use of fuzzy logic control methods and artificial neural networks. This approach is quite effective in approximating the GMPP due to the right membership function design. The membership functions are capable of adaptively changing themselves based on the input provided at a given moment, allowing the ANFIS technique to be utilized in PV systems with partial shade situations. In this approach, the FLC is utilized to regulate the non-linear inputs without necessarily requiring any prior system knowledge, while the ANN is used to decrease tracking error and optimize parameters (Abido et al., 2015; Abu-Rub et al., 2012; Al-Majidi et al., 2019; Belhachat & Larbes, 2017; Hassan et al., 2017; Junaid Khan et al., 2020; Kharb et al., 2014; S. Kumar et al., 2020; Mohammed et al., 2016). Because of the complexity of the algorithm used in this method, it is not cost effective for MPPT.

2.5.4.2 Fuzzy Particle Swarm Optimization (FPSO)

The FLC and the PSO are combined in this approach. The tracking efficiency of the controller is increased overall by utilizing these two highly refined strategies. Because of its parameter adjustability and minimal mathematical processing, this hybrid method is highly recommended. Because of this improvement in these two parameters, this

combinational method gives the best membership function distribution. This method has been reported in (Letting et al., 2012; Priyadarshi et al., 2018). It has advantages such as reduced switching losses, avoids the use of proportional integral controllers by self-tuning the membership function which reduces its complexity. It has a disadvantage that while designing the fuzzy rules, some approximations with trial-and-error methods have to be included based on human intelligence. This is a major setback in this method.

2.5.4.3 Grey Wolf Optimization Perturb and Observe (GWO-P&O)

In this hybrid approach, P&O is employed later to enable faster convergence to GMPP while GWO is used in the early stages of MPPT. As a result, the computational cost is reduced and the search space of GWO is also reduced. The whereabouts of the wolves indicate the converter's duty cycle. The need of a PI controller is fully eliminated in the MPPT implementation. The tracking capabilities, convergence speed, and efficiency of this method are all higher than those of the conventional GWO and P&O methods (Mohapatra et al., 2017). The method's disadvantage is that it requires complex mathematical computation.

2.5.4.4 Particle Swarm Optimization Perturb and Observe (PSO-P&O)

At the beginning of the algorithm, PSO is used for global search, and P&O is used at the end. The GMPP is located using the PSO method. GMPP is detected by the hybrid method more quickly than the conventional PSO method (Mohapatra et al., 2017). Additionally, it lessens the output power fluctuations that occur when tracking. On the other hand, it has an expensive hardware implementation, a complex control structure, and poor convergence if the GMPP is outside of the search area. Every time the GMPP departs from the search space, the poor convergence issue needs to be addressed.

2.5.4.5 Hill Climbing Adaptive Neuro Fuzzy Inference System (HC-ANFIS)

The Adaptive Neuro Fuzzy Inference System (ANFIS) and Conventional (HC) methodologies are used in this study's hybrid methodology, which was carefully designed to solve the inherent drawbacks of each individual approach. According to procedures (Lasheen & Abdel-Salam, 2018), this novel MPPT has demonstrated superior speed compared to conventional methods. Figure 2.10, which depicts the various stages involved, offers an informative look into the algorithm's workflow. The ambient temperature (T) and solar radiation (G), which indicate the dynamic conditions affecting the performance of the photovoltaic (PV) system, are the initial input parameters for the ANFIS module. The ANFIS module then determines the duty cycle (D), a crucial factor in MPPT. The HC mechanism activates using the computed duty cycle as input. The HC system expertly calculates the ideal duty ratio using additional data inputs from the PV system, specifically the PV voltage (V_{pv}) and the PV current (I_{pv}). The power converter uses this computed duty ratio as a reference point while it dynamically modifies its operation to efficiently track and optimize the maximum power point (MPP) of the PV system under the current environmental circumstances. In addition to improving tracking speed, this synergistic combination of ANFIS and HC methods also optimizes the overall MPPT performance, ensuring effective energy conversion in photovoltaic systems.

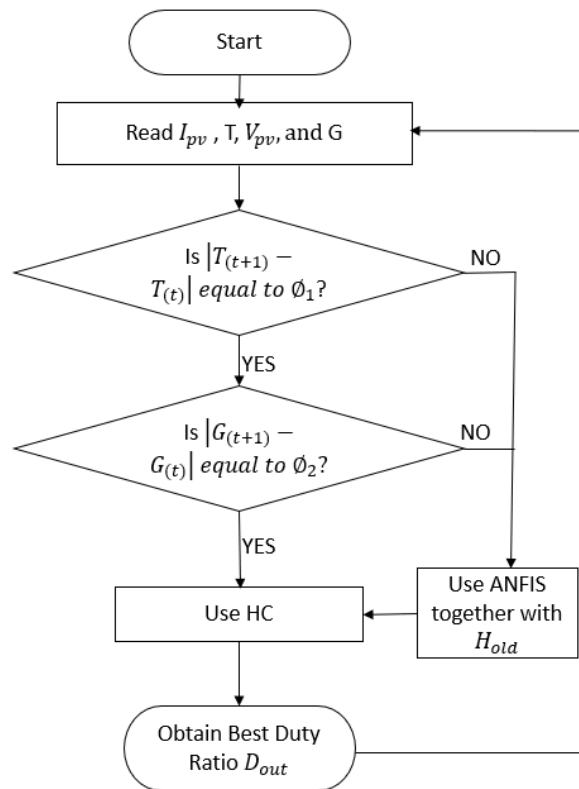


Figure 2.10: Flow diagram of the HC-ANFIS MPPT technique

This method is advantageous because it has a faster tracking rate and doesn't require mathematical modeling. On the other hand, the system has drawbacks due to the complicated design of the membership function and the laborious training of the ANN. The ease of designing membership functions and the introduction of novel training methods for ANNs will encourage widespread adoption of the MPPT technique.

2.6 Summary of related works done on the different MPPT techniques

On the many MPPT methodologies that were previously described, some researchers have done research projects while applying the different methods. Table 2.5 gives a summary of a few of these studies.

Table 2.5: Summary of related works for different MPPT methods

MPPT Method	Reference	Year	Observations
P&O	(Killi & Samanta, 2018)	2018	A P&O algorithm based on voltage sensors was presented. They were able to successfully improve the dynamic and steady-state tracking performance of the PV system at a cheaper cost thanks to their simulation and experiment results.
CV	(Leedy et al., 2012)	2012	They developed a constant voltage algorithm for tracking maximum power point that adapts the reference voltage automatically to account for shifting environmental conditions. Their work was simulated using MATLAB/Simulink, and the simulation and experimental results agreed.
RCC	[73]	2007	Their work focused on a more dependable and energy-efficient digital formulation. The RCC technique was used to create a maximum power point tracker for a solar panel with a tracking efficiency of more than 99 percent and a speedy convergence rate.
HC	(Jately et al., 2021)	2021	On a small-scale experimental prototype, the performance of eight hill-climbing algorithms for two different step sizes was evaluated under both uniform and rapid fluctuations in low irradiance. Their statistical analysis shows that the adaptive HC drift-free MPPT algorithm outperforms traditional HC algorithms in low irradiance situations when applied with the optimal perturbation step-size.
IP&O	(Kamran et al., 2020)	2020	The MPP is included in the 10 percent portion of the power curve's search space that is constrained by this suggested technique, which also begins perturbation and observation inside of that area. In MATLAB/Simulink, the proposed P&O algorithm was examined. The solar tracker made sure that the solar module received steady and maximum irradiation throughout the day as the sun moved across the sky. The steady-state oscillations at the MPP and the response time to changing weather conditions were both slowed down because of the algorithm's constrained search space. With the proposed system, the proposed P&O algorithm was tested, and the results demonstrated that it performed satisfactorily.
IP&O	(A. I. M. Ali & Mohamed, 2022)	2022	For a solar PV system simulation utilizing MATLAB/SIMULINK software, they suggested an improved MPPT technique. Their findings supported the theoretical analysis of the suggested technique, which increases the tracking accuracy of PV systems to 99.7%.
SCC	(Fapi et al., 2021)	2021	In comparison to the traditional fractional SCC technique, they constructed an enhanced MPPT utilizing the SCC approach and gained greater accuracy, lower oscillations, and reduced energy losses.
OCV	(Hmidet et al., 2021)	2021	The suggested method ensures a quick response, fewer oscillations around the MPP, and a system efficiency of 98% due to the extraction of maximum power in their design utilizing the fractional OCV method.
ARV	(Lasheen et al., 2017)	2017	They demonstrated that despite the ARV method's resemblance to the CV method and its ability to retain efficiency despite changes in solar radiation.
InC	(Liu et al., 2008b)	2008	For MPP tracking, a modified variable step InC MPPT algorithm was suggested. To track the maximum power from the PV array, the proposed system may automatically alter the step size. This technique has the potential to simultaneously increase the MPPT's accuracy and speed. Additionally, it is straightforward and quick to apply in DSPs. Their method was tested experimentally with a DSP and verified using simulation results from MATLAB-Simulink. They employed a 0.025-second sample interval. According to their test results, tracking accuracy was 99.2% and response time was 1.5 seconds.

LTB MPPT	(Yue et al., 2021)	2021	In their article, an unique 2-D lookup table-based MPPT system was developed. A 2-D optimal-duty-cycle table is used. They came to the conclusion that the method is deserving of advancement because it outperforms the fixed-step P&O MPPT in terms of power tracking.
ANN	(Yaichi et al., 2014)	2014	They determined that their new way of employing the ANN to track the maximum power point could successfully track the MPP.
FLC	(A. Ali et al., 2014)	2014	The FLC approach outperforms the P&O method in a variety of weather circumstances, according to their comparison of the two methods.
CS	(Rezk et al., 2017)	2017	The PSO, INC, and CS are examined in this paper, and the results demonstrate that the CS outperforms the PSO in conditions of partial shade.
ANFIS	(Mahdi et al., 2020)	2020	When a non-shaded real weather profile was introduced to the system, simulation results utilizing the ANFIS MPPT technique demonstrated the system's capacity to track the MPP under partial shading conditions and respond to changing weather.
	(Al-Majidi et al., 2019)	2019	An ANFIS technique was used in this study based on a sizable amount of data, experimentally trained to prevent high error from training in the system. These numbers were obtained in 2018 through experiments carried out experimentally on a PV array. To evaluate the performance of the proposed ANFIS technique, simulation was performed in MATLAB/Simulink. Using a real measurement test on a partly overcast day, the average effectiveness of the suggested approach under various climatic conditions was computed. The findings demonstrate that, with an efficiency of more than 99.3 percent, the suggested method precisely records the maximum power that is optimal.
FPSO	(Sa-ngawong & Ngamroo, 2015)	2015	They developed a hybrid FPSO system to stabilize the frequency under a variety of loading conditions, and they came to the conclusion that the frequency stability was superior to that achieved when only the FLC is utilized.
GWO-P&O	(Mohanty et al., 2016)	2016	They put out a brand-new hybrid maximum power point tracking (MPPT) approach that blends P&O and GWO methods. GWO handles the earliest stages of MPPT, with the P&O algorithm being used in the last phase to speed up convergence to the global peak. The MPPT avoids the computational expense associated with a GWO-based MPPT method as a result. A faster convergence to the GMPP was desired, hence the hybrid technique was used to minimize the size of the GWO search space. An experimental setup was made in order to put the suggested MPPT technique to the test. It was first built in MATLAB/Simulink. The acquired data showed that the suggested MPPT outperformed both the GWO and PSO-P&O MPPT algorithms in all weather situations.
PSO-P&O	(Avila et al., 2017)	2017	In their research, they tracked the maximum power from a 1.2 MW PV system under partial shadowing conditions using a hybrid PSO-P&O approach. Their findings demonstrated appropriate dynamic and steady-state reactions.
HC-ANFIS	(Lasheen & Abdel-Salam, 2018)	2018	Their findings demonstrated that the maximum voltage could be anticipated and that irradiance and temperature could be measured in real time.

2.7 Criteria for comparing different MPPT techniques

Because MPPT controllers are designed using a variety of technological approaches, their comparison is based on many criteria. In Ahmad et al. (2019), some criteria have been presented for ranking MPPTs. This is shown in Table 2.6.

Table 2.6: Criteria for determining MPPT rankings (R. Ahmad et al., 2019a)

Criterion	Considerations	Ranking
Complexity of Algorithm	Just like P&O	Best
	Needs little correction of the P&O algorithm It's a combination of other methods and P&O	↓
	Makes use of artificial intelligence or bio-inspired algorithm	
	High level of AI	Very complex
Hardware implementation	Uses DC-DC converter with I and V sensor requires modification of DC-DC converter	Best
	For duty cycle modulation of converter, it uses PI/PID controller	↓
	high-tech embedded system is used	Very complex
Tracking Speed	0 ms to 100 ms	Best
	100 ms to a few hundred milliseconds	↓
	From a few hundred milliseconds to seconds	Very slow
Uniform condition Efficiency	97% to $\approx 100\%$	Best
	93% to 96.9%	↓
	<92.9%	Less efficient
Ability to track accurately under partial shading	Tracks global maximum	Best
	Better performance than an MPPT of the same complexity	↓
	Not being able to track GMPP under partial shading	
	Performs better than P&O	Less accurate
	Often caught in the local maximum, similar to P&O	

2.8 Comparative analysis of different MPPT techniques

It's also important to select the best tracker for the job when using MPPT controllers to get the most power out of PV systems. These MPPT controller design strategies are different from one another in a number of ways. Cost, response time, and efficiency

stand out as important considerations to keep in mind when making decisions among the comparison factors of importance. Cost, circuitry, complexity, response time, periodic tuning, sensing parameters, stability, precision, and the partial shading (PS) condition have all been taken into consideration when making the comparison in this work. The comparison is summarized in Table 2.7 below. Additionally, comparing the effectiveness of the various strategies has been done using values from published research, as shown in Figure 2.11.

Table 2.7: Comparison of different MPPT techniques (Karami et al., 2017; Viswambaran et al., 2016)

MPPT Method	Cost	Circuitry (A/D)	Complexity	Response Time	Periodic Tuning	Sensed Parameters	Stability	Accuracy	PS
ANFIS	E	D	High	Fast	Yes	V, I	Stable	Medium	Yes
ANN	E	D	High	Medium	Yes	V, I or G, T	VS	High	Yes
FLC	AF	D	High	Medium	Yes	V, I	VS	High	Yes
GA	AF	D	High	Fast	No	V, I	VS	Medium	Yes
GWO-P&O	AF	D	High	Medium	Yes	V	Stable	High	Yes
HC-ANFIS	AF	D	High	Fast	No	V, I	VS	High	Yes
PSO-P&O	AF	D	High	Fast	Yes	V, I	Stable	Medium	Yes
ACO	AF	D	Low	Fast	Yes	V, I	VS	Medium	Yes
ARV	IE	A/D	Low	Medium	Yes	V, I	NS	Medium	No
CS	VE	D	Low	Fast	No	V, I	VS	High	Yes
CV	IE	A	Low	Slow	Yes	V	NS	Low	No
FPSO	VE	D	Low	Fast	No	V, I	VS	High	Yes
FSB MPPT	AF	D	Low	Very Fast	Yes	V, I	VS	High	Yes
GWO	AF	D	Low	Medium	Yes	V	VS	High	Yes
HC	IE	D	Low	Medium	No	V, I	Stable	Medium	No
LTB MPPT	IE	D	Low	Fast	Yes	G, T or I, T	Memory-based	High	No
OCV	IE	A	Low	Slow	Yes	V	NS	Low	No
P&O	IE	A/D	Low	Slow	No	V, I	NS	Medium	No
RCC	E	A	Low	Fast	Yes	V, I	VS	High	Yes
SCC	IE	A/D	Low	Slow	Yes	I	NS	Medium	No
ABC	E	D	Medium	Fast	No	V, I	VS	Medium	Yes
InC	E	D	Medium	Varies	No	V, I	Stable	Medium	No
IP&O	E	D	Medium	Medium	No	V, I	Stable	High	No
PSO	AF	D	Medium	Fast	Yes	V, I	VS	Medium	Yes
GNT	AF	D	Very High	Fast	No	V, I	Stable	Medium	No
SMC	E	D	Very High	Very fast	No	V, I	VS	Medium	Yes

VS: Very Stable, NS: Not Stable, V: Voltage, I: Current, VE: Very Expensive, E: Expensive, IE: Inexpensive, AF: Affordable, T: Temperature, G: Irradiance, PS: Partial Shading Condition, A: Analog, D: Digital

Due to difficulties in tracking the global MPP, conventional approaches are often not suitable for MPPT in regions with Partial Shading (PS) conditions, as seen by the comparison above. When partial shading occurs, intelligent, hybrid, and optimization approaches are more appropriate for tracking the global MPP. Comparing the conventional procedures to the other three approaches, they are less expensive and less complex. Several efficiency values from various MPPT methods have been published (Bollipo et al., 2020). From the data presented, PSO-P&O have the highest efficiency going up to 100% while the least efficiency of 54.12% was reported with the HC method.

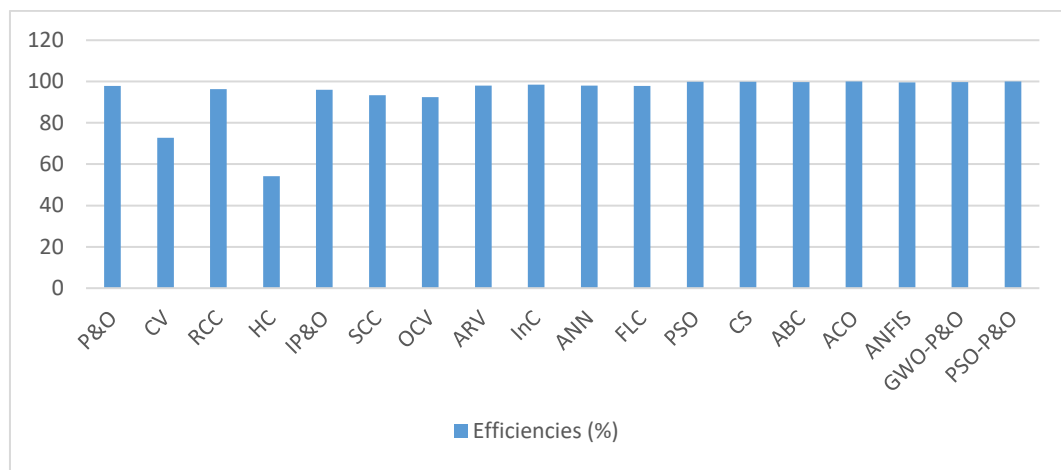


Figure 2.11: Reported efficiencies obtained from different MPPT techniques

2.9 Power Converters Used in PV Systems

Power converters are extensively used in solar PV systems. These converters generally play different roles such as converting a constant DC input voltage to a regulatable voltage, converting AC current to DC current, or enabling bidirectional flow of current to and from battery storage systems (Rashid, 2001).

2.9.1 DC-DC Converters

These are power electronic circuits capable of converting a constant input DC voltage to a regulatable output DC voltage. Some of these converters are buck converters, boost converters, buck-boost converters, and cuk converters.

2.9.1.1 Buck Converter

Here, the conversion is done such that the output voltage from the converter is always smaller than the input voltage. For this reason, the buck converter is also referred to as a step-down converter. The circuit diagram for this power converter is shown in Figure 2.12.

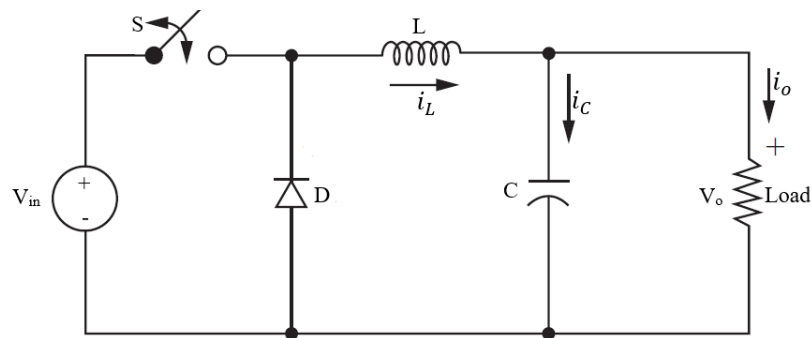


Figure 2.12: Buck converter

From the circuit on Figure 2.12, the relationship between the output voltage (V_o) and the input voltage (V_{in}) for the buck converter is given by equation (2.25) (Daniel W. Hart, 2011; Rashid, 2001).

$$V_o = \alpha V_{in} \dots \dots \dots 2.25$$

Where α is the duty ratio which determines the controllability of the switch. The minimum value of the inductance (L) to maintain a continuous current flow is given by equation (2.26).

$$L_{min} = \frac{(1-\alpha)R}{2f} \dots \dots \dots 2.26$$

Where R is the load resistance in (Ω), f is the switching frequency in (Hz), and L_{\min} is the minimum inductance in (H) with $L > L_{\min}$.

During buck converter design, the current ripple of the inductor is often used as a design criterion. The current ripple for the inductor is given by equation (2.27).

$$\Delta i_L = \frac{(1-\alpha)V_o}{Lf} \dots\dots\dots 2.27$$

Also, to maintain a constant output voltage, a suitable capacitor must be used. The capacitance of this capacitor depends on the output voltage ripple (ΔV_o) given by equation (2.28).

$$\Delta V_o = \frac{(1-\alpha)V_o}{8LCf^2} \dots\dots\dots 2.28$$

The capacitance (C) in Farads (F) of the capacitor is calculated using equation (2.29).

$$C = \frac{(1-\alpha)V_o}{8Lf^2(\Delta V_o)} \dots\dots\dots 2.29$$

2.9.1.2 Boost Converter

This is another type of DC-DC converter that converts a constant input DC voltage to a regulatable output DC voltage whose magnitude is greater than the input. The inductor is often chosen such that the current flow is continuous and the capacitor is chosen to maintain a constant voltage across the load. The circuit diagram for this converter is shown in Figure 2.13.

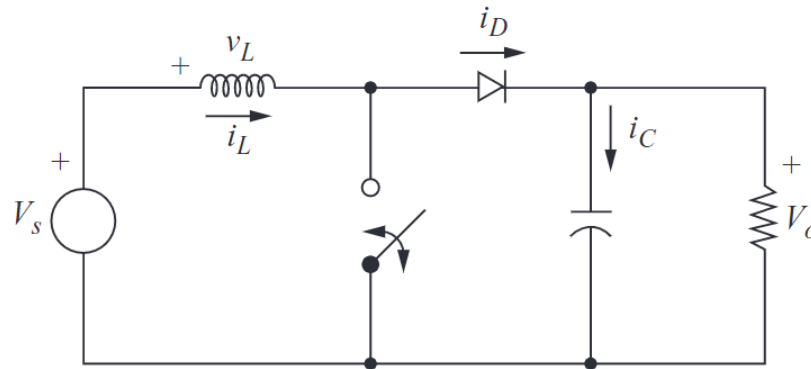


Figure 2.13: Boost converter

The relationship between the input voltage and the output voltage is given by equation (2.30).

$$V_o = \frac{V_s}{1-\alpha} \dots\dots\dots 2.30$$

The minimum inductance for continuous current flow in the boost converter is given by equation (2.31).

$$L_{\min} = \frac{\alpha(1-\alpha)^2 R}{2f} \dots\dots\dots 2.31$$

In the calculation of the inductance, the current ripple of the inductor is often used.

This current ripple is related to the inductance as in equation (2.32).

$$L = \frac{\alpha V_{in}}{\Delta i_L f} \dots\dots\dots 2.32$$

Similar, the output ripple voltage is given by equation (2.33).

$$\Delta V_o = \frac{\alpha V_o}{RCf} \dots\dots\dots 2.33$$

From equation (2.33), the capacitance of the capacitor is calculated as shown in equation (2.34).

$$C = \frac{\alpha V_o}{Rf(\Delta V_o)} \dots\dots\dots 2.34$$

2.9.1.3 Buck-Boost Converter

This converter can either step-up or step down the output voltage when a given input voltage is applied. Because the switch (S) and the diode (D) are not allowed to conduct at the same time, the input voltage cannot be coupled directly to the load. Therefore, the value of the capacitor (C) must be chosen such that a constant voltage is applied to the load during the interval when the switch is open. The circuit diagram for this converter is shown in Figure 2.14 below.

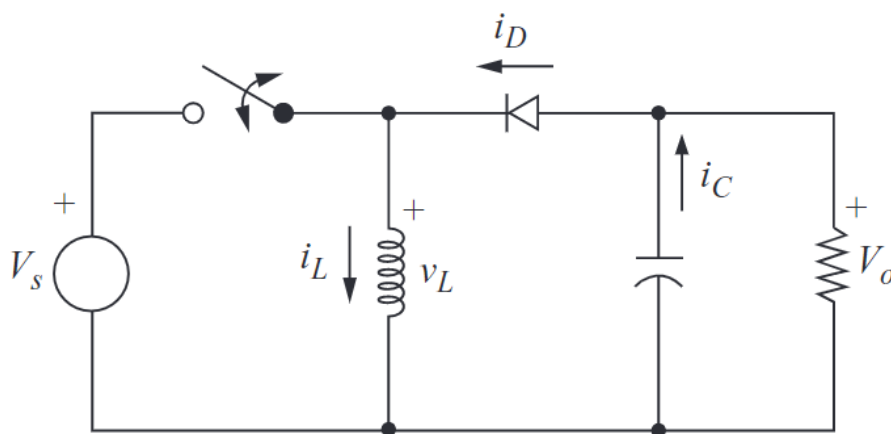


Figure 2.14: Buck-Boost converter

For this converter, the output voltage is related to the input voltage by:

$$V_o = \frac{-\alpha V_s}{1-\alpha} \dots\dots\dots 2.35$$

For specified input and output voltages, the required duty ratio is obtained from:

$$\alpha = \frac{|V_o|}{V_s + |V_o|} \dots\dots\dots 2.36$$

From equation (2.35), we can deduce that the output voltage is greater than the input voltage when $\alpha > 0.5$ (boost mode) and it is smaller than the input voltage when $\alpha < 0.5$ (buck mode).

For continuous current flow, the value of the inductance must be large and the minimum value for this inductance is calculated as in equation (2.37). The output voltage ripple and the value of capacitance to maintain a constant output power can be computed using equations (2.33) and (2.34) respectively.

$$L_{\min} = \frac{(1-\alpha)^2 R}{2f} \dots\dots\dots 2.37$$

2.9.1.4 Cuk Converter

In Figure 2.15, the Cuk switching topology is depicted. There is a polarity reversal on the output, and the amplitude of the output voltage can be either higher or lower than that of the input. To reduce the amount of harmonic content in the dc supply, the input inductor serves as a filter. Energy transfer for the Cuk converter is dependent on the capacitor C1, as opposed to earlier converter topologies where it was linked to the inductor.

These premises form the basis of the analysis: The capacitors C₁ and C₂ are very large and have constant voltages across them, the inductors L₁ and L₂ both have very large inductances, making the currents across them constant, the voltage and current waveforms are periodic, indicating that the circuit is in steady state operation, and the diode and switch are ideal.

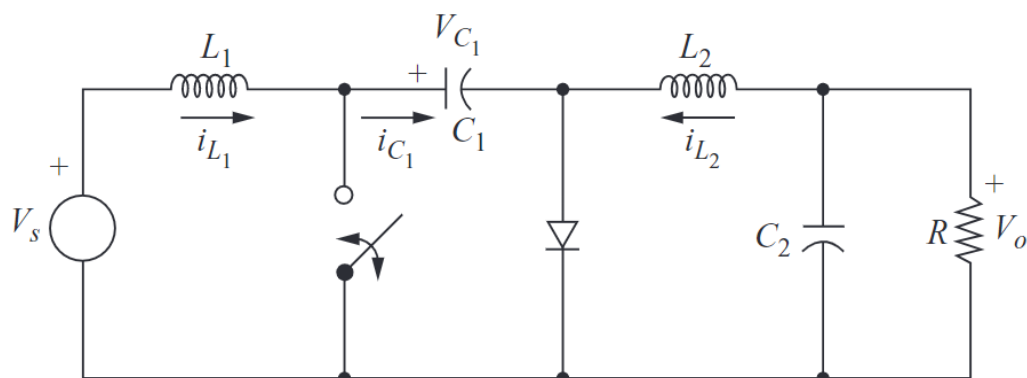


Figure 2.15: Cuk converter

By analysing the circuit in Figure 2.15, the relationship between the currents across the inductors L1 and L2 with the duty ratio is given by equation (2.38).

$$I_{L1} = \frac{\alpha I_{L2}}{1-\alpha} \dots\dots\dots 2.38$$

Furthermore, the output voltage is related to the input voltage as shown in equation (2.39).

$$V_o = \frac{-\alpha V_s}{1-\alpha} \dots\dots\dots 2.39$$

The negative sign in the expression shows that there is a polarity reversal between the input and the output. The ripple output voltage for this converter is calculated using the equation (2.40).

$$\Delta V_o = \frac{(1-\alpha)V_o}{8C_2 L_2 f^2} \dots\dots\dots 2.40$$

The ripple voltage across the capacitor C1 is given by equation (2.41).

$$\Delta V_{C1} = \frac{\alpha V_o}{RC_1 f} \dots\dots\dots 2.42$$

The ripple currents across the inductors L1 and L2 are respectively given by equations (2.43) and (2.44).

$$\Delta i_{L1} = \frac{\alpha V_s}{L_1 f} \dots\dots\dots 2.43$$

$$\Delta i_{L2} = \frac{\alpha V_{in}}{L_2 f} \dots\dots\dots 2.44$$

To maintain a continuous current flow across the inductors L1 and L2, the minimum inductances that must be chosen can be calculated using equations (2.45) and (2.46).

$$L_{1,\min} = \frac{(1-\alpha)^2 R}{2f\alpha} \dots\dots\dots 2.45$$

$$L_{2,\min} = \frac{(1-\alpha)R}{2f} \dots\dots\dots 2.46$$

2.9.2 DC-AC Converters

DC-AC converters or Inverters are electronic devices that convert direct current (DC) into alternating current (AC). They are necessary for many applications that require AC power, including houses, businesses, and electronic equipment. There are various varieties of inverters, such as pure sine wave inverters, which provide high-quality AC power comparable to that of the grid, modified sine wave inverters, which are acceptable for the majority of appliances but are less efficient than pure sine wave inverters, and square wave inverters, which are less prevalent but are best for basic applications. Solar power systems employ inverters to transform DC electricity generated by solar panels into useful AC power. Additionally, they are utilized in UPSs, which offer backup power during power outages (Bellar et al., 1998; Séguier & Labrique, 2012).

2.9.3 AC-DC Converters

In order to change alternating current (AC) into direct current (DC), electrical equipment or circuits called AC-DC converters or rectifiers are employed. They function by allowing current to flow in one direction, thereby changing the AC waveform to create a pulsing DC output. Rectifiers are crucial parts in many applications where a constant DC voltage is necessary, such as power supplies for machinery and electronic equipment (Singh et al., 2003). They are classified as half-wave or full-wave. Half-wave rectifiers produce a pulsing DC output by only allowing one-half (either the positive or negative) of the AC input waveform to pass through. Half-wave rectifiers are easier to construct and less costly as compared to full wave rectifiers. Full-wave Rectifiers on the other hand provide a smoother pulsing DC output.

Compared to half-wave rectifiers, they are more effective. Rectifiers are frequently used in power supply to change the mains (wall outlet) AC voltage into a stable DC voltage suited for electronic appliances and devices (Castro et al., 2003; G. C. R. Kumar & Rao, 2012; Power & Science, n.d.; Séguier & Labrique, 2012; Singh et al., 2003). Additionally, they convert AC voltage to DC voltage needed to charge batteries in battery charging circuits. In addition to that, rectifiers are also employed in motor control systems to drive DC motors, which are frequently utilized in industrial settings, by converting AC power to DC.

These electronic circuits are essential parts of electrical and electronic systems because they enable the conversion of AC power to DC power, which is necessary for numerous tasks like powering industrial operations and electronic gadgets. The type of rectifier selected will rely on the particular needs of the application and the required level of DC output quality (Erickson, 2004).

2.9.4 Bidirectional Converters

A bidirectional converter, often referred to as a bidirectional DC-DC converter, is an electrical component or circuit that can efficiently and controllably convert direct current (DC) power in both the DC to DC and DC to DC directions. These converters are utilized in a variety of applications, but are particularly useful in energy storage, electric car, and renewable energy systems that require the bidirectional flow of energy (Gorji et al., 2019).

These converters have several functions in different electrical applications. They are used in storage systems such as batteries and supercapacitors. In these storage systems, bidirectional converters play a crucial role. During the charging process, energy is

channelled through this converter to charge the battery. When discharging, the energy stored in the battery flows through the converter to the load or to the grid.

Another area where bidirectional converters are used is in EVs (electric vehicles). Bidirectional converters allow for the charging of electric vehicles from an external power source (such as a charging station) as well as the discharge of power from the vehicle's battery to power the electric motor or supply power to external loads. Due to their bidirectional capabilities, EVs can serve as mobile energy storage systems in applications such as vehicle-to-grid (V2G) and vehicle-to-home (V2H) (Onar et al., 2012).

Bidirectional converters are essential for controlling the electrical flow in renewable energy sources, such as solar and wind power. When there is extra energy, they can convert it back to DC for storage in batteries or for feeding into the grid. They can transform the DC electricity produced by solar panels or wind turbines into AC power for use in homes or companies.

Bidirectional converters are used in UPS systems to guarantee a consistent and dependable power supply to key loads during power outages. UPS stands for Uninterruptible Power Supplies. Depending on the situation, they can alternate between rectifier mode (which converts AC grid power to DC for charging the battery) and inverter mode (which converts DC battery power to AC for powering the load) (Govind et al., 2022).

Bidirectional converters are used in microgrid systems to control the energy flow between various distributed energy resources, including solar panels, wind turbines, and energy storage equipment. They allow the grid to run independently or in tandem with the primary grid while maximizing energy usage.

In order to handle sudden changes in power direction and amplitude, bidirectional converters are made to be extremely efficient. They are crucial elements in contemporary energy management and conversion systems because they depend on cutting-edge power electronics and control systems to guarantee the smooth and controlled movement of energy in both directions.

In this work only one application of the bidirectional converter is utilized which is during the charging and discharging process of batteries. The circuit configuration of this converter is shown in Figure 2.16.

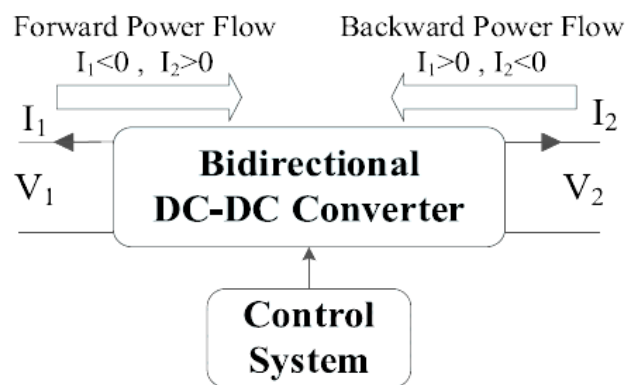


Figure 2.16: Generalized structure for a bidirectional DC-DC converter (Forouzesh et al., 2017)

2.10 Energy Storage Systems

2.10.1 Introduction

As additional producing capacity employs intermittent renewable energy sources, the demand for energy storage in electricity networks is becoming more critical (May et al., 2018). The world's current electrical grid systems, however, are not built to handle the widespread integration of variable energy sources without substantially disrupting the grid. According to general consensus, the grid system can be seriously disrupted if intermittent renewable energy penetration rises to more than 20%. Large-scale electrical energy storage systems can undoubtedly help to improve the grid's

dependability, enable complete integration of sporadic renewable sources, and efficiently control power generation in addition to helping to reduce many of the inefficiencies and defects that are intrinsic to it. Electrical energy storage has further two important benefits. First of all, it separates power generation from the load or electrical consumer, simplifying the management of supply and demand. Furthermore, it makes distributed storage possible for small grids, or microgrids, greatly enhancing grid security and therefore energy security. Therefore, energy storage systems are a potential option for managing independent solar PV systems as well as integrating variable renewable energy sources into grids (Bragard et al., 2010).

2.10.2 Types of Energy Storage Systems

Energy storage systems can be divided into five major categories: mechanical, electrochemical, electrical, chemical, and thermal.

Pumped hydro, flywheel, and compressed air systems are examples of mechanical storage systems. The electromechanical systems use a variety of battery types, including flow batteries, sodium sulphate batteries, lead acid batteries, and lithium-ion batteries. Double layer capacitors and superconducting magnetic energy storage are two of the electrical storage techniques. Fuel cells are a component of chemical storage systems, and thermal storage uses sensible heat storage as its final component. The various classes are displayed in the following Figure 2.17.

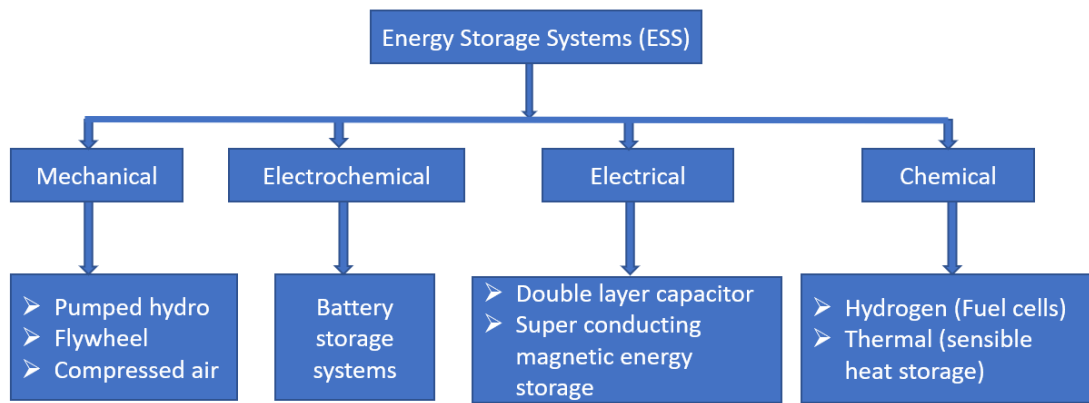


Figure 2.17: Classification of energy storage systems (Asian Development Bank, 2018)

2.10.3 Mechanical storage systems

Mechanical energy storage systems (MESSs) are desirable because they outperform traditional energy storage systems in a number of areas, including cost-effectiveness and long-term viability. This is because these systems use mechanical methods for energy storage. When the involved object is stationary, the energy is stored as potential energy, and when the object is moving, it is stored as kinetic energy. Flywheel energy storage systems (FESS), pumped hydro energy storage (PHES), and compressed air energy storage are the three different forms of MESSs (CAES) (C. K. Das et al., 2018; Mahmoud et al., 2020a).

Pumped Hydro Energy Storage (PHES) is a MESS that has a long-life cycle, is flexible, and requires little maintenance. Pumping system, hydro turbine, and upper reservoir are the three basic components (Guezgouz et al., 2019). The PHES is depicted in Figure 2.18 as an example.

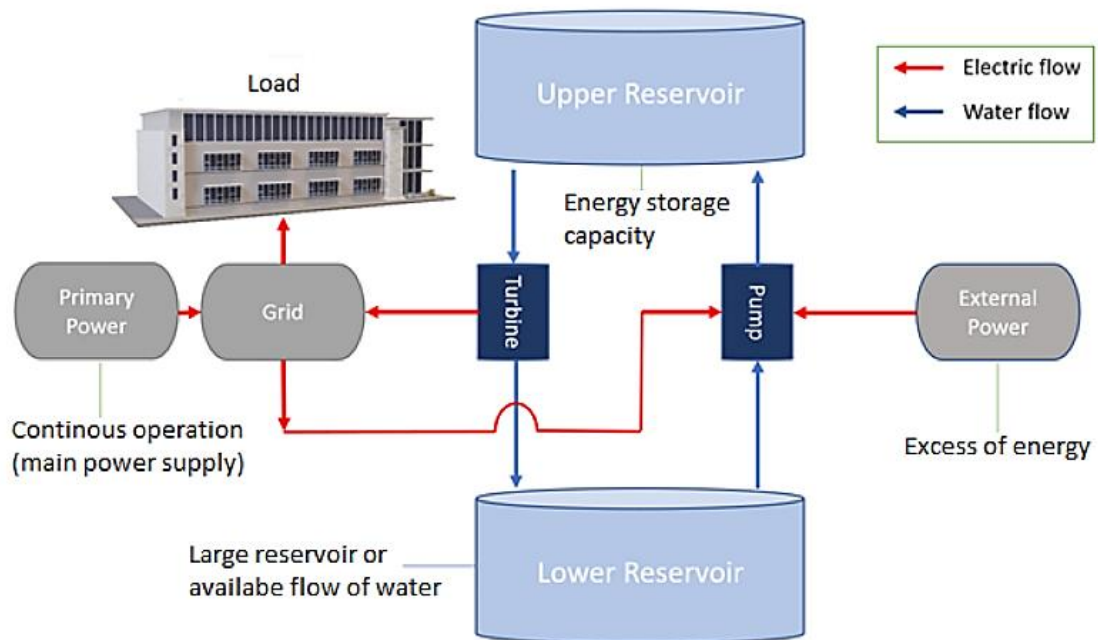


Figure 2.18: Pumped Hydro Storage System (Mahmoud et al., 2020b)

When there is a surplus of electrical energy, water is pumped from the lower reservoir to the upper one by the electric pump, where it can be used again when needed to generate electricity using the generator (Haque & Rahman, 2012). This system is based on the potential gravitational energy, which allows the upper container to offer a positive pressure difference with regard to the lower one, allowing the hydro turbine to generate power. In order to improve the performance of the system for modern PHES, the turbomachines are replaced by a reversible pump-turbine (Javed et al., 2020). The major advantages of this storage system are: high efficiency, low cost/kWh, stability, and long discharge time. It is disadvantageous in that it has a low energy density and occupies a large area during installation.

The second type of MESS is the Flywheel Energy Storage System (FESS) which involves rapidly spinning a rotor (flywheel) and storing the energy as rotational energy in the system (Amiryar & Pullen, 2017). Electrical energy is used to accelerate the rotor, and that energy is subsequently stored as kinetic energy as the flywheel rotates. As a

result of the concept of energy conservation, the flywheel's spinning speed is reduced when this energy is withdrawn from the system by connecting it to a generator for electricity generation. An example of a FESS is shown in Figure 2.19 below.

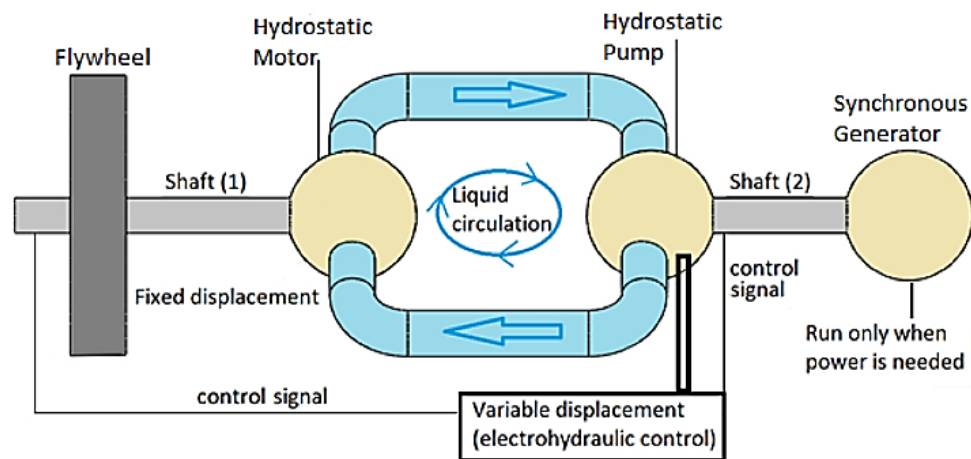


Figure 2.19: Flywheel energy storage system with hydrostatic transmission (Carrillo et al., 2009)

The overall efficiency of a FESS is determined by the design of each component, and one of the key goals is to reduce power transmission losses, which are influenced by the type of bearing used; magnetic bearings were found to be the optimum option (Martin et al., 2016). The FESS can also be connected to three distinct types of electric machines: synchronous machines, induction machines, and switching reluctance machines. Aside from energy storage, flywheels are utilized to extend the life of batteries when used with renewable energy sources due to their intermittent nature (Barelli et al., 2019). In addition to that, FESS has a fast response with considering economic aspects (Aanstoos et al., 2001). The major advantage with this storage system is that it causes no pollution, long life span, and can discharge huge amount of energy in few minutes. On the other hand, it has the disadvantage that it has limited charge/discharge and cannot stand alone with PV systems (Mahmoud et al., 2020b).

The third and final type of MESS is the compressed air energy storage (CAES) system. CAES is based on a straightforward principle. Electrically driven compressors charge the store by converting electric energy into potential energy, or more accurately exergy, of pressured air. The compressed air is kept in any type of compressed air storage volume such as expired well, underground salt caverns, gas chambers, or underground mines and can then be released on demand to generate electricity by expanding the air through an air turbine (Budt et al., 2016). A wide range of CAES concepts exist at various stages of development, each aimed at a distinct application and with its own set of strengths and disadvantages. CAES technologies are classified as diabatic, adiabatic, or isothermal, depending on the idealized process being pursued. Though this technology is still in its early stage of development, it has advantages which are; long discharge time, fast start-up, low cost per kWh, its stable, and has a long service life. However, this storage method also have disadvantages such as low efficiency and the use of natural gas to reheat the air before expansion which leads to carbon dioxide emission (Haisheng et al., 2013; Luo et al., 2014). The energy storage and conversion system block diagram is shown in Figure 2.20 below.

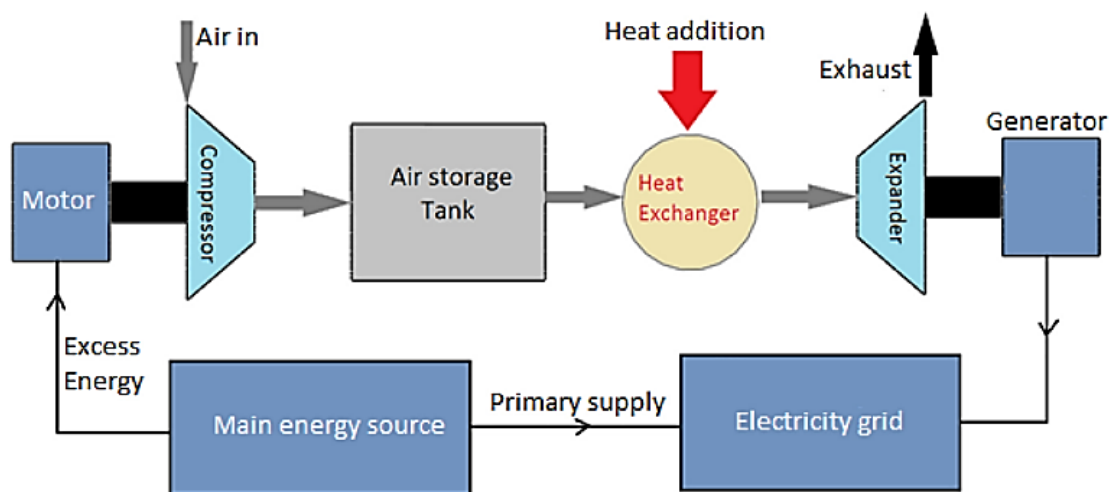


Figure 2.20: CAES system

2.10.4 Electrical storage systems

Electrical energy storage systems can broadly be classified into two namely superconducting magnetic energy storage (SMES) and double layer capacitor (DLC) or supercapacitor. These storage systems are so classified because of their ability to store energy in the presence of electric charge or electromagnetic fields caused by the passage of electric current through these materials. This storage systems are well known for their high-power capabilities but low energy densities. The functional principles of these different types of electrical storage systems are discussed in the proceeding paragraphs.

Supercapacitors are electrochemical capacitors that lie between dielectric capacitors and batteries and can store a lot of energy. Their design architecture is similar to that of batteries, with two electrodes separated by an electrolyte and a separator to prevent the electrodes from shorting. They have extremely high capacitances, ranging from several hundred farads per gram to 1700 F/g, depending on the storage method, electrode material choice, microstructure, and electrolyte. Despite the fact that they hold charge of higher magnitude than dielectric capacitors, their low energy density prevents them from being used as stand-alone storage systems. They can, however, be beneficial in a variety of high-power but low-energy applications (Gür, 2018a). The power density of supercapacitors can go as high as 10kW/kg which is about 2 to 3 times that of batteries. In addition to the high-power density, supercapacitors have a long cycle life of up to 100 000 cycles. On the other hand, they have very low energy density which is less than 5 Wh/kg (Burke, 2007; Gür, 2018b). The schematic diagram of a double layer capacitor is shown in Figure 2.21 below.

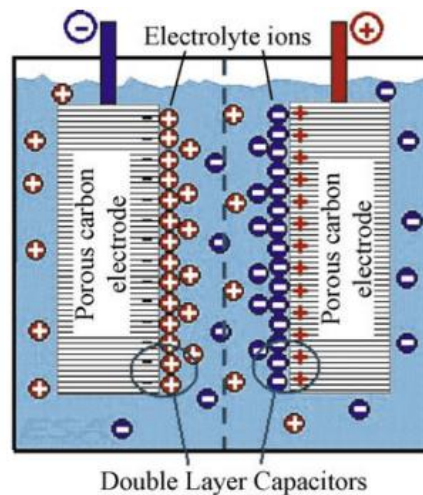


Figure 2.21: Double layer capacitor storage system (H. Chen et al., 2009a)

Another category of electrical energy storage system is the superconducting magnetic energy storage (SMES) system. This is one of the very few direct electric energy storage systems. The magnetic flux density (B) formed by the passage of persistent direct current is stored in a superconducting magnet with shorted input terminals. The current remains constant due to the absence of resistance in the superconductor (Buckles & Hassenzahl, 2000). It stores electric energy as direct electric current flowing via a superconducting inductor (coil) that is circular and allows current to circulate endlessly with nearly no loss. The magnetic field formed by the flow of electric current can also be employed to store energy in SMES. The inductor is immersed in liquid helium housed in a vacuum-insulated cryostat to retain its superconducting condition. The coolant can be liquid helium at 4.2 K or super fluid helium at 1.8 K, and the conductor is usually composed of niobium-titanium (H. Chen et al., 2009b). When the shorted terminals are opened, the stored energy is transmitted to a load in part or all by lowering the coil's current via negative voltage (positive voltage charges the magnet). As a result, the SMES is a current source. Superconducting magnet with supporting structure, cryogenic system (cryostat, vacuum pumps, cryocooler, etc.), power conditioning system (interface between the superconducting magnet and the load or electric grid),

(Haseli, 2018). It generates electricity using external fuel (anode side) and oxidant sources (cathode side). In the presence of an electrolyte, these react. The reactants and reaction products move in and out of the cell in general, but the electrolyte remains in the cell. As long as the flows are maintained, fuel cells can operate nearly indefinitely. A reversible fuel cell is one that can be used to produce electricity and chemical B by consuming chemical A, and then reversed to produce chemical A by consuming electricity and chemical B. Fuel cells differ from batteries in that they need reactants that must be replaced, whereas batteries chemically store electrical energy in a closed system. Furthermore, when a battery is charged or depleted, the electrodes in the battery react and change, but the electrodes in a fuel cell are catalytic and relatively stable (H. Chen et al., 2009b). There are numerous fuel and oxidant combinations that can be used. Hydrogen is used as the fuel and oxygen is used as the oxidant in a hydrogen cell.

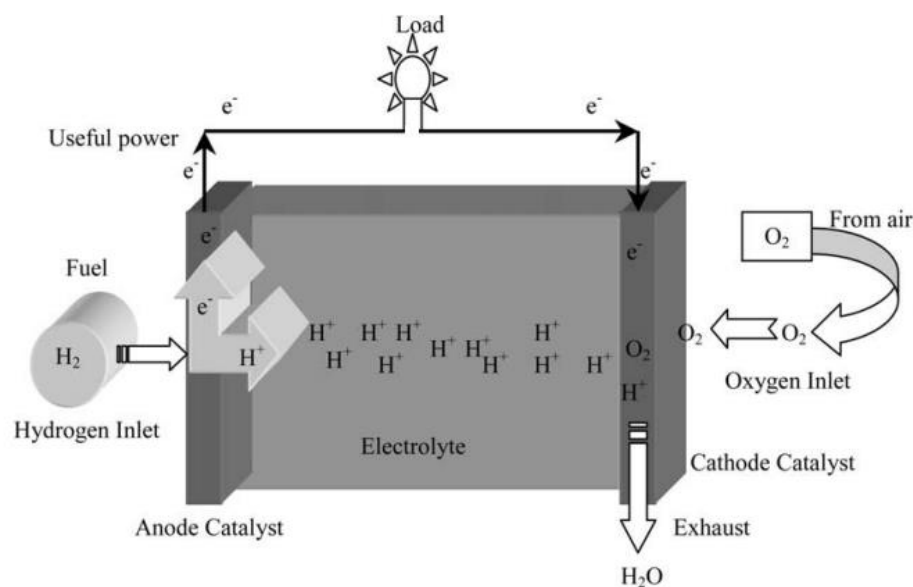


Figure 2.23: Schematic diagram of a fuel cell (Stambouli & Traversa, 2002)

Hydrocarbons, alcohols, and even metals are examples of other fuels. Air, chlorine, and chlorine dioxide are examples of other oxidants. A hydrogen fuel cell for instance produces electricity and water by combining hydrogen and oxygen, as and a reversible

hydrogen fuel cell can produce hydrogen and oxygen using electricity and water (Aardahl & Rassat, 2009). Hydrogen-based energy storage systems are gaining popularity right now, especially because of their ability to integrate with renewable energy sources. An electrolyser unit, which converts electrical energy into hydrogen, a hydrogen storage system, and a hydrogen energy conversion system, which converts the stored chemical energy in hydrogen back to electrical energy, are the fundamental elements. There are also a number of techniques to generate hydrogen directly from thermochemical or photochemical processes using concentrated solar energy, although they are still in the early phases of development (Rahman et al., 2020).

2.10.6 Thermal storage systems

To capture and store energy in the form of heat, thermal energy storage is an essential method. One of the most often used techniques in this area is sensible heat storage (SHS). It entails heating or chilling a solid or liquid medium intended for storage, such as water, sand, molten salts, or rocks. Water stands out as the best option out of these due to its usefulness and adaptability. Since it has so many uses in both the home and industrial sectors, water has actually emerged as the lynchpin of thermal energy storage. Recent years have seen major developments in the use of thermal energy storage, especially with regard to sensible heat storage. This technology is now essential for reducing energy usage and meeting the rising need for sustainable energy solutions. Thermal energy storage systems improve overall energy efficiency by storing extra heat during times of low demand and releasing it when needed. Water has special qualities that make it particularly ideal for this purpose, making it the chosen medium for sensible heat storage. It is a reliable source of heat thanks to its high specific heat capacity, which enables it to absorb and hold significant amounts of thermal energy. Furthermore, water is an appealing option from an economic and practical perspective

due to its abundance, low cost, and ease of handling. Residential heating and cooling systems use thermal energy storage using water in the domestic domain. Homeowners can lessen their dependency on conventional energy sources by storing excess heat produced by renewable energy sources like solar panels or heat pumps for later use. Similar to this, water-based thermal energy storage is essential in industrial settings for a number of activities, including steam generation, chemical reactions, and temperature control in manufacturing facilities (Alva et al., 2018). Underground sensible heat storage (SHS), in both liquid and solid mediums, is widely used in large-scale applications to take advantage of its outstanding benefits. Its affordability, which makes it a financially viable solution for a range of energy storage demands, is one of its main advantages. Additionally, SHS systems provide increased safety because they don't employ harmful materials, reducing threats to the environment and human health. SHS systems take advantage of the storage medium's inherent features as they dynamically interact throughout charging and discharging processes. The system's operating temperature, the amount of storage material used, and the medium's specific heat capacity are the key determinants of how much heat is stored. This delicate interplay guarantees that SHS continues to be a flexible and effective method of regulating thermal energy, offering a long-term solution for a variety of large-scale applications (Sarbu & Sebarchievici, 2018).

These different storage technologies are more appropriate for different power requirements and discharge durations as depicted by Figure 2.24. Power-to-gas (P2G) storage systems are promising technologies for seasonal electricity storage. Supercapacitors on the other hand are only capable of storing energy for a very short period.

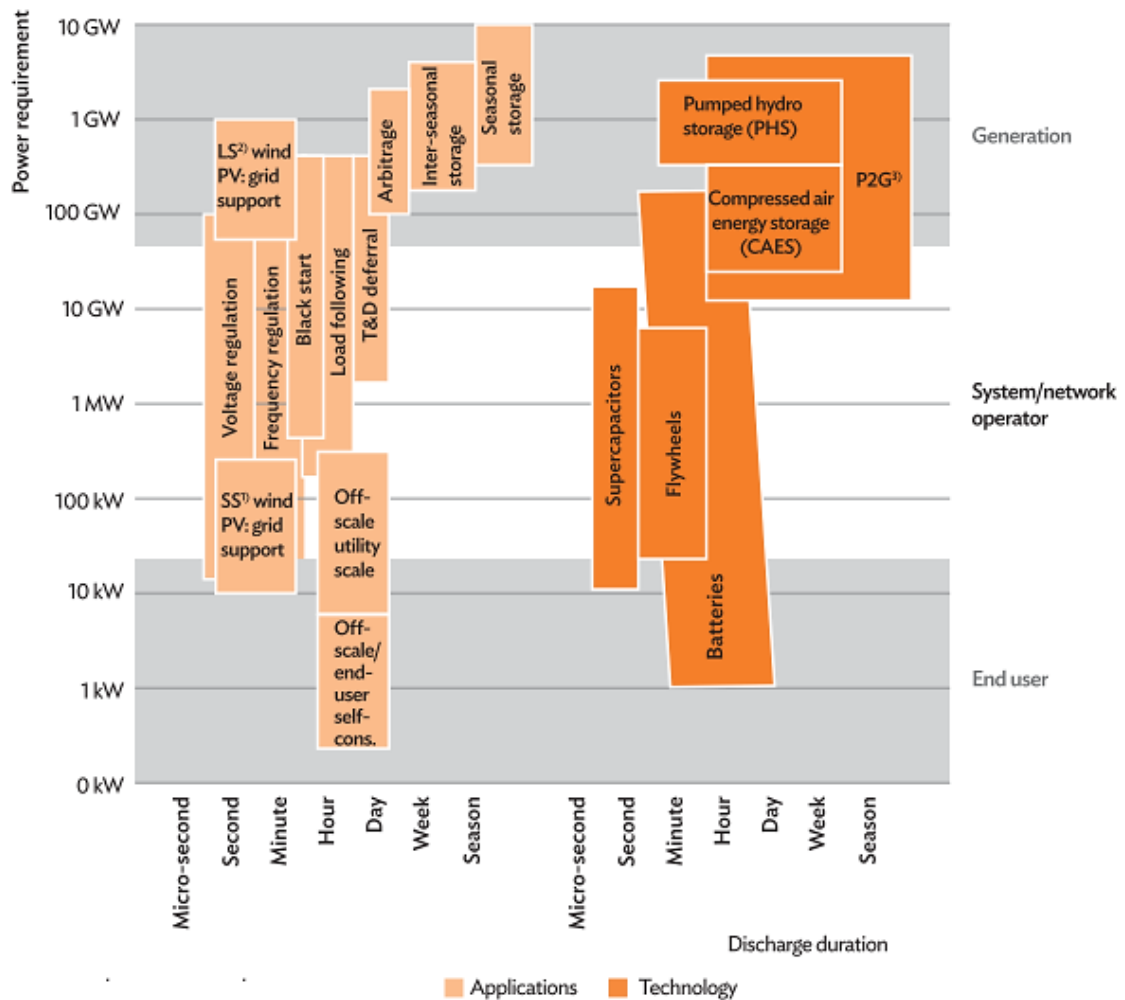


Figure 2.24: Battery technologies for different purposes (Asian Development Bank, 2018).

Electrochemical storage systems will be exploited in this section by describing the different types of battery storage systems.

2.11 Battery Storage systems and types of Batteries

For the grid and other renewable energy systems, batteries have traditionally been the most popular type of energy storage. Grid storage systems involve converting grid electricity to direct current (DC) and storing it in a battery. The grid is then supplied with the retrieved stored energy using the same converter technology (Bose, 2013). In other renewable energy systems like the PV systems, energy is stored directly in the batteries without necessary using a converter. Electrochemical energy storage in

batteries is desirable because it is portable, easy to set up, inexpensive, and provides a virtually instantaneous response to input from the battery as well as output from the network to the battery. Among the several battery chemistries available, lead acid batteries provide a dependable, affordable option that may be customized for various energy storage applications (May et al., 2018; Parker, 2001). There are various battery kinds that might be either primary or secondary batteries that are used for storage. Primary batteries are discharged after usage and cannot be recharged. The majority of primary batteries are known as "dry cells" because they are enclosed in an absorbent (semi-solid) substance. There are various battery kinds that might be either primary or secondary batteries that are used for storage. Primary batteries are discharged after usage and cannot be recharged. The majority of primary batteries are known as "dry cells" because they are enclosed in an absorbent (semi-solid) substance. Examples are 1.5 V alkaline batteries. Secondary batteries, on the other hand, can be electrically recharged to their original precharge state after use by passing current through them. Examples include car and laptop batteries (EU, USAID, 2017). The most commonly used secondary batteries today are the Leads Acid batteries and the Lithium-ion batteries.

2.11.1 Terms used in battery storage systems

Capacity: When a battery is fully charged, its capacity is the total amount of electrical charge that may be extracted from it up until a particular voltage is reached. It is expressed in Ah (Ampere hours). The actual capacity of a battery is dependent on a number of real-world circumstances, including the charging mode, discharge current (a low discharge rate permits greater actual capacity), and operating temperature. A battery's nominal capacity is tested under specific conditions, often 20 ° C. The lead-acid battery's capacity, discharge rate (duration), and temperature are depicted in the

following graph on Figure 2.25 (EU, USAID, 2017). The graph shows that lead acid batteries perform poorly at extremely low temperatures. This means that temperature should be considered before installation of lead acid batteries.

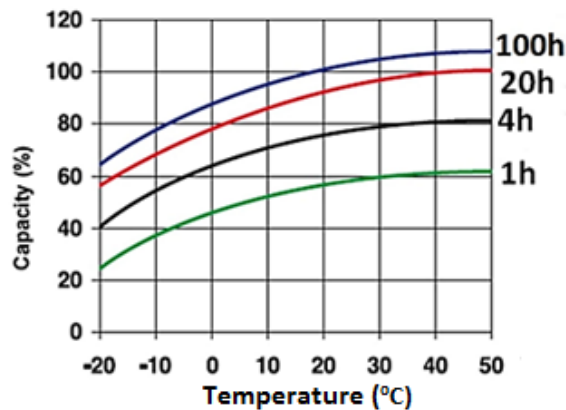


Figure 2.25: Effects of temperature on Lead Acid battery capacity (EU, USAID, 2017)

State of charge (SOC): State of charge is the term used to describe a battery's level of charge. The percentage is provided. The capacity of a battery as compared to its nominal capacity is known as the state of charge. A 100 Ah battery's SOC is 60 percent if it has only been charged up to 60 Ah. By measuring the open circuit voltage on the battery terminals and comparing it to the battery's state of charge chart supplied by the manufacturer, the SOC can be ascertained.

Depth of discharge (DOD): The depth of discharge is the percentage of the battery's capacity that has been discharged relative to its initial charge. The percentage is provided. A battery's DOD is 80 percent, for instance, if it is rated at 200 Ah and only 160 Ah of that capacity has been used.

Life cycle: A cycle is the name given to the process of discharging and recharging. A battery can only be used for a specific number of cycles, which is how battery life is stated in terms of cycle life. The number after which the battery capacity is dropped to 80% of its nominal capacity is often stated by the manufacturer. A battery's cycle life is influenced by its type, quality, and daily discharge rate. The cycle life decreases with

the depth of discharge during a cycle, as seen in Figure 2.26. The battery in solar systems is discharged at night and replenished during the day, therefore a cycle typically lasts one day (EU, USAID, 2017).

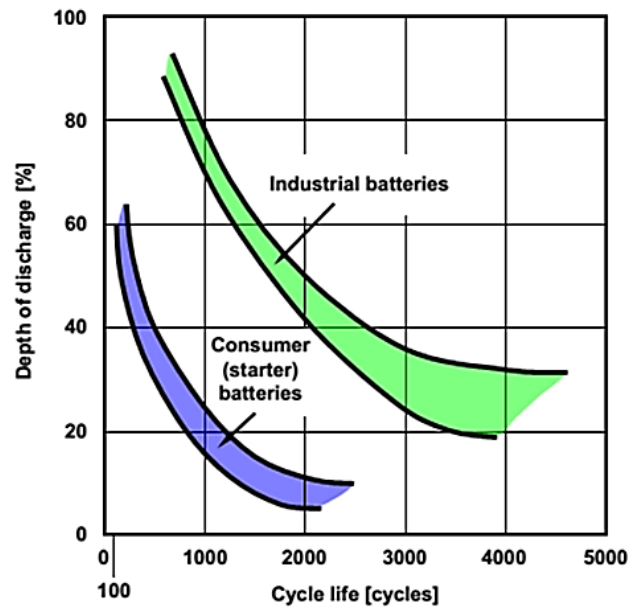


Figure 2.26: Relationship between cycle life and DOD for lead acid batteries (EU, USAID, 2017).

Self-discharge: Lead-acid batteries undergo a process known as self-discharge that causes them to lose energy whether or not they are linked to a load. The battery's self-discharge is influenced by the environment's temperature as well as the battery's kind, age, and condition. This is shown in Figure 2.27.

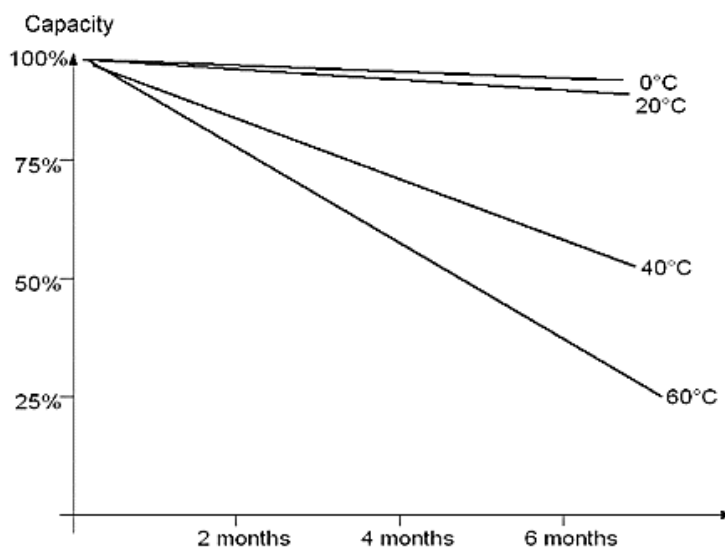


Figure 2.27: Self-discharge rate of lead acid batteries at different temperatures (EU, USAID, 2017).

This shows that at higher temperatures, lead acid batteries have a high self-discharge rate. For instance, a 100% fully charged lead acid battery will self-discharge below 50% over a period of 6 months if stored at a temperature of 60°C.

Float life: The period of time an unused battery will endure while stored and kept in a fully charged state by routine charging is known as the float, or shelf life. The quality of the battery and storage temperature affect the float's longevity. The battery life is significantly shortened by a high storage temperature. For instance, a long-lasting, high-quality gel battery can have a float lifespan of 20 years when maintained at 20 ° C, but at 30 ° C, its lifespan is just 10 years (EU, USAID, 2017). In Table 2.8 are the float lives of PbA batteries at different temperatures.

Table 2.8: Float life of different lead acid batteries at different temperatures

Average operating Temperature (°C)	AGM, deep cycle (years)	Gel, deep cycle (years)	Gel, long life (years)
20	7-10	12	20
30	4	6	10
40	2	3	5

2.12 Types of Secondary Batteries

2.12.1 Lead Acid (PbA) Battery

This is a type of rechargeable battery which is made up of lead-acid, a cheap chemical and is mostly used in energy storage applications in cars and renewable energy installations. Lead-acid batteries employ a diluted sulfuric acid (H_2SO_4) electrolyte, a lead (Pb) negative electrode, and lead dioxide (PbO_2) as the positive electrode (with a specific gravity of about 1.30 and a concentration of about 40 percent). When a battery discharges, the sulfuric acid dissolves into water and the positive and negative electrodes produce lead sulphate ($PbSO_4$). In the event that the battery is charged, the opposite result happens (HIOKI, 2020). There are basically two main types of lead-acid batteries namely sealed lead acid (SLA) batteries and the flooded battery (EU, USAID, 2017).

The SLA battery can also be subdivided into valve regulated lead acid (VRLA) and absorbent glass mat (AGM) (Ogunniyi & Pienaar, 2017). These batteries also find applications in other systems such as uninterruptible power supplies (UPS), emergency lighting, power backup for cellular repeater towers, internet hubs, banks, hospitals, airports, and others.

They are advantageous in that they are simple to manufacture, low cost per watt-hour high specific power, capable of high discharge currents with ability to supply high surge currents (RAND, 2018), and good performance at low and high temperatures (BATTERY-University, 2021a). PbA batteries, on the other hand, have low specific energy, a poor weight-to-energy ratio, a sluggish charging rate, a requirement for storage in a charged state to prevent sulfation, a limited cycle life since repetitive deep-cycling shortens battery life, and negative environmental effects. PbA batteries, on the

other hand, have low specific energy, a poor weight-to-energy ratio, a sluggish charging rate, a requirement for storage in a charged state to prevent sulfation, a limited cycle life since repetitive deep-cycling shortens battery life, and negative environmental effects (EHS, n.d.), (Ci et al., 2016; Crompton, 1996; May et al., 2018). Figure 2.28 shows the image of a lead acid battery.



Figure 2.28: Image a Lead Acid Battery (May et al., 2018; RS Components, 2021).

i) Charge efficiency in lead acid batteries

Not all of the ampere hours (Ah) that travel from the charger to the battery are utilized for charging. The battery's state of charge has a significant impact on charging efficiency. The charging efficiency is almost 100 percent up to a SOC of 70 percent. As a result, it is impossible to provide a precise number for charging efficiency because it greatly relies on the operating mode and the type of charger. The charging efficiency often falls between 70 and 95 percent (EU, USAID, 2017).

ii) Lead acid batteries in operation

Gassing: There is a minor gas formation in the battery if the charging procedure has brought the battery up to 80% of its capacity. This occurs as a result of lead peroxide (PbO) remaining after the majority of the sulfuric acid has been taken off the electrodes. Smaller levels of charging current are needed to complete the charging process because the battery is almost fully charged. The water molecules are next divided into oxygen

and hydrogen by the remaining power, which allows a gas to escape from the battery. This gas leaks into the atmosphere when the batteries are flooded. The battery should be positioned in a well-ventilated area since the combination of hydrogen and oxygen is highly combustible. Gas persists inside VRLA batteries under low pressure where it interacts with other gases to form water. High charging voltages can cause too much gas to be created, in which case a valve allows the gas to escape into the environment. As no battery water may be supplied to make up for the water loss, the leakage of gas from VRLA batteries must be prevented. Gassing results in electrolyte loss, which raises the acid content, loss of electrode material because some of the electrode material outgasses, and a potential short circuit because of electrode particles that detonate and fall to the bottom of the cell (HIOKI, 2020; Ribeiro et al., 2001). The electrolyte is also mixed when a flooded battery is gassed, which has positive effects on battery maintenance. Numerous chargers have the ability to conduct a balancing program. This procedure significantly raises the charging voltage in order to initiate gassing for around one hour. A flooded battery's suggested equalization voltage is in the range of 2.6 volts per cell at 20 °C (Parker, 2001).

Sulfation: Large lead sulphate crystals growing on the electrodes cause sulfation (as opposed to tiny crystals which can be easily broken down when charged). These substantial crystals obstruct the electrode pores, raising the internal resistance of the battery. As a result, the surface area where chemical reactions occur in the battery is reduced. Extreme sulfation will eventually render the battery useless. Sulfation typically happens when a battery is discharged for an excessively long time, the electrolyte level is extremely low as a result of gassing and evaporation, or the battery will never be fully charged. The actions listed below must be done to avoid sulfation. Charge the battery all the way as soon as you can. As lead sulfate is more soluble with

a lower acid density, raise the cell's acid content. Don't discharge the battery too much. Make flooded batteries equal (but never VRLA types as this will result in water loss that cannot be refilled) (EU, USAID, 2017).

iii) Battery storage and maintenance

The following guidelines can be used for Lead Acid battery storage. This battery should not be stored in a discharged state. Charge the batteries regularly to avoid sulfation. The battery should be stored at low temperatures, as high temperatures increase self-discharge. In terms of battery maintenance, Lead Acid battery terminals should be regularly cleaned to avoid short circuits or surface leaks. Also, the connections should regularly be checked to make sure they are tight.

2.12.2 Lithium-ion (Li-ion) batteries

Lithium-ion batteries have become widely used in energy storage systems (S. Yang et al., 2019). They can intercalate lithium ions reversibly in positive electrode materials made of lithium compounds, and they can accommodate lithium in the solid state in negative electrode materials made of carbon or graphite (May et al., 2018). They are the most widely adopted energy storage system in the world. They are used as a backup power for load leveling, frequency and voltage regulation, to stabilize power supply and to help integrate renewable energy (*WORLD BANK GROUP: KOREA'S ENERGY STORAGE SYSTEM DEVELOPMENT* :, 2020). The most energy-dense battery chemistries are Li-ion batteries, which are also regarded as secure. To increase battery life, no planned cycling or memory is needed. Li-ion batteries are rapidly being used for electric mobility and are found in electronic equipment including cameras, calculators, laptop computers, and mobile phones. Lithium cobalt oxide (LiCoO_2), lithium manganese oxide (LiMn_2O_4), lithium nickel manganese cobalt oxide (LiNiMnCoO_2), lithium iron phosphate (LiFePO_4), and lithium titanate are some of the

numerous types of Li-ion batteries that are available ($\text{Li}_4\text{Ti}_5\text{O}_{12}$) (Asian Development Bank, 2018; BATTERY-University, 2021a). Compared to PbA batteries, Li-Ion batteries are more expensive than PbA batteries.

i) Lithium cobalt oxide (LiCoO_2)

A cobalt oxide cathode and a graphite carbon anode make up this battery. The cathode is composed of layers. Lithium ions go from the anode to the cathode during discharge, and they move in the opposite direction during charging. These batteries' short lifespans, poor thermal stability, and constrained load capacities are their main drawbacks.

ii) Lithium manganese oxide (LiMn_2O_4)

The materials research bulletin reported the first study on manganese spinel-infused lithium-ion batteries in 1983. This architecture allows for the formation of a three-dimensional spinel structure, which enhances ion flow on the electrode and lowers internal resistance while enhancing current handling. High thermal stability and improved safety are additional benefits of the spinel structure; nonetheless, cycle and calendar lifespan are constrained although not to the same extent as PbA batteries, and they are still not as economical as PbA batteries (Manthiram et al., 2017).

iii) Lithium nickel manganese cobalt oxide (LiNiMnCoO_2)

One of the most effective Li-ion systems uses nickel, manganese, and cobalt as the cathode. These systems can be modified to function as energy cells or power cells, similar to lithium-manganese (Asian Development Bank, 2018; BATTERY-University, 2021a).

iv) Lithium iron phosphate (LiFePO₄)

Phosphate was first used as a cathode material for rechargeable lithium batteries in 1996 by researchers from the University of Texas and other institutions. Low resistance and strong electrochemical performance are characteristics of lithium phosphate. The primary advantages of this battery are its high current rating, lengthy cycle life, outstanding thermal stability, and increased safety (Ling et al., 2021).

v) Lithium titanate (Li₄Ti₅O₁₂)

In the anode of a conventional lithium-ion battery, lithium titanate takes the role of graphite and crystallizes into a spinel structure. Lithium manganese oxide may be used as the cathode. With a nominal cell voltage of 2.40 V, quick charging capabilities, and a high discharge current of 10 C, or 10 times the specified capacity, lithium titanate is a battery material. It is claimed that the cycle count is higher than that of a typical Li-ion. Safe and with good low-temperature discharge properties is lithium titanate (Mauger & Julien, 2017). The image of a Li-ion battery are shown in Figure 2.29.



Figure 2.29: Image of a Li-ion Battery (Lithium-Ion Battery, n.d.; May et al., 2018)

Li-ion batteries typically have benefits and drawbacks. Li-ion batteries have several benefits, including high specific energy and high load capacities with power cells, long cycle and extended shelf life, high capacity, low internal resistance, good coulombic efficiency, simple charge algorithm, and comparatively quick charge times. To prevent thermal runaway when under stress, degradation at high temperatures and while stored

at high voltage, and the inability of a rapid charge at subfreezing temperatures ($<0^{\circ}\text{C}$, $<32^{\circ}\text{F}$), they need protection circuitry (Sandhya et al., 2014).

2.12.3 Nickel cadmium (NiCd) batteries

Due to their resilience in the face of mechanical and electrical stress, these batteries are frequently utilized in industrial applications. They have been utilized as energy storage for utilities, however they are rather pricey (May et al., 2018), (Ogunniyi & Pienaar, 2017). These batteries have a high cycle count with correct maintenance, can be charged extremely quickly with little stress, operate well under load, can be stored discharged, function well in low temperatures, have the lowest cost per cycle, and are available in a variety of sizes and performance options (May et al., 2018).

Its drawbacks include memory effect, periodic full discharge requirements, poor specific energy compared to newer systems, and the ability to be revived. Because cadmium is a dangerous metal that cannot be disposed of in landfills, it has a low cell voltage of 1.20 V and takes a lot of cells to reach a high voltage (Asian Development Bank, 2018; BATTERY-University, 2021a).

2.12.4 Nickel-metal hydride (NiMH) batteries

These batteries are not employed in battery energy storage systems since they are more expensive than NiCd batteries (May et al., 2018). The sealed NiCd battery's tried-and-true positive electrode chemistry is combined with the energy-storing abilities of metal alloys created for cutting-edge hydrogen energy storage concepts to create the NiMH battery. These batteries work better than conventional rechargeable batteries and have less voltage depression and higher capacity. Currently, they are widely used in high-end portable electronics, where run time and other battery performance factors play a significant role in purchasing decisions. They are advantageous in that they have a high

energy density, which translates into long run times or a reduction in the space needed for the battery, simplify integration into products currently using nickel-cadmium batteries due to the many design similarities between the two chemistries, and provide superior service over other primary battery types at extremely low-temperature operation (-20°C). Their drawbacks include short service life, which means that after 200–300 deep cycles, performance begins to decline, especially at high load currents. Although a NiMH battery is capable of generating high discharge currents, repetitive discharge with high load currents shortens the battery's cycle life. Shallow, rather than deep, discharge cycles are preferred. The best outcomes are obtained with load currents between 0.2 and 0.5 C-rate. Because NiMH produces more heat during charging and needs a longer charge time than NiCd, they need a more complicated charge algorithm. They have a significant self-discharge because NiMH batteries self-discharge roughly 50% more than NiCd batteries (Amanor-Boadu et al., 2018; Smith et al., 2016; Xing et al., 2011) (Hesse et al., 2017).

2.12.5 Sodium Sulfur (NaS) Batteries

This particular molten metal battery is made of sulfur and sodium. It is made of low-cost materials and has a high energy density, high charge and discharge efficiency (89 percent to 92 percent), and a long cycle life. Such cells are typically utilized for large-scale non-mobile applications like power grid energy storage due to their high operating temperatures of 300°C – 350°C (to maintain the electrodes in liquid state and obtain good ionic conductivity in the electrolyte, which is a solid ceramic substance). The electrolyte is beta-alumina ($\beta\text{-Al}_2\text{O}_3$), which at the operating temperature conducts sodium ions. When discharged, sodium and sulfur combine to create sodium polysulfide (Sudworth & Tiley, 1985a). They are favourable due to their high cycle life, good energy and power density, liquid electrodes, low-cost potential, flexible operation

as they can operate under a variety of settings (rate, depth of discharge, temperature), and high energy efficiency. Although they have these benefits, they also have some drawbacks, such as the need to operate above 300°C, the highly reactive nature of metallic sodium (a material used in construction), which ignites when exposed to water, and the additional cost of building the enclosing structure to prevent leakage. They also have strict operation and maintenance requirements (Jones, 1977; Sudworth & Tiley, 1985b).

2.12.6 Flow batteries

This is an electrical storage device that is a blend between a conventional battery and a fuel cell. Liquid electrolyte of metallic salts is pumped through a core that consists of a positive and negative electrode, separated by a membrane. The ion exchange that occurs between the cathode and anode generates electricity (BATTERY-University, 2021b). Vanadium ions or other chemical elements are employed in an oxidation-reduction reaction to charge and discharge these batteries. They offer several great qualities, including a long lifespan with nearly no electrode and electrolyte degradation, high safety because to their lack of combustible elements, and the ability to operate at room temperature. They also have some potential for utility energy storage.

Although different chemistries are employed in flow batteries, all of them have energy-producing cells with remote storage of active materials, making it feasible to create batteries with very large capacity (Ogunniyi & Pienaar, 2017). In vanadium redox batteries (VRBs), distinct valence states of vanadium sulphate solution are circulated through cells with carbon felt electrodes and are separated by an ion selective membrane. On discharge, V^{2+} becomes V^{3+} at the negative electrode and V^{5+} becomes V^{4+} at the positive electrode. The quantity of the vanadium sulfate solution, and consequently the battery's capacity, is not constrained because it is kept in tanks. Reverse reactions take

place during recharge, and the materials are renewed. Although the batteries' claimed lifespan is very lengthy, in reality they are complicated and expensive to make. Due to the size of the battery that is anticipated, only a few demonstrator systems have been deployed thus far, and VRB batteries are only suited for utility energy storage (May et al., 2018).

Zinc bromine (ZnBr_2) battery is another type of flow battery. The cell reaction is for Zn to react with Br_2 to form zinc bromide (May et al., 2018).

As an organic complexing agent in aqueous solution, Br_2 is injected into the cells' carbon electrodes and microporous plastic separator. Although Br_2 is held in tanks and metallic Zn is deposited on charge, the Zn electrode places a restriction on the capacity for any particular design. The predicted life is shorter, but the costs are lower than VRB batteries. It's important to manage bromine leakage because it can be dangerous. Compared to other flow batteries, Zn- Br_2 batteries have only sometimes been employed in utility applications. Other flow battery types exist, such as those made of iron and chromium, although they have not been widely utilized (BATTERY-University, 2021b).

The benefits of flow batteries are as follows: Long service life because redox flow batteries can withstand an indefinite number of charge and discharge cycles without degrading, with a system endurance duration of 20 to 25 years. The electrolytes can also be utilized temporarily. Additionally, the batteries are adaptable. Redox flow batteries enable flexible design since the output and capacity of a battery can be created independently of one another. Additionally, the batteries enable cost-effective power generation by allowing a single system to handle both short and long periods of output variance. Furthermore, flow batteries are extremely safe because they may function at

standard temperatures and are made of non-combustible or flame-resistant materials. The likelihood of a battery fire is really slim. Additionally, flow batteries have a few drawbacks, including the following: complexity due to the need for auxiliary containment vessels, pumps, sensors, flow management, and power control. Additionally, they minimal energy density When compared to other types of batteries, flow batteries often have lower energy densities (BATTERY-University, 2021b), (May et al., 2018).

2.13 Summary of Different Battery Characteristics

Table 2.9 below gives a summary of the different battery technologies in terms of energy density, round trip efficiency, life span, cost, and eco-friendliness. The low cost of PbA batteries as compared to other battery technologies have made them to be widely used in energy system (Anuphapparadorn et al., 2014; Podder & Khan, 2016). This has made it a battery of choice in most low-income countries as compared to Li-ion batteries (Keshan et al., 2016). The cost of flow batteries is also low and promising though the battery is not widely used as compared to PbA batteries since the technology is still under development.

Table 2.9: Summary of battery characteristics (Asian Development Bank, 2018; Korea Battery Industry Association 2017 “Energy Storage System Technology and Business Model,” 2017).

Battery type	Energy Density (kW/kg)	Round Trip Efficiency (%)	Life Span (years)	Cost (\$/kWh)
Li-ion	150-250	95	10-15	400-700
Na-S	125-150	75-85	10-15	500-650
Flow	60-80	70-75	20-25	100-300
Ni-Cd	40-60	60-80	5-10	315-490
PbA	30-50	60-70	3-6	150-200

Figure 2.30 below shows the specific energy in watts hour and specific power in watts that can be stored by different battery technologies per kilogram.

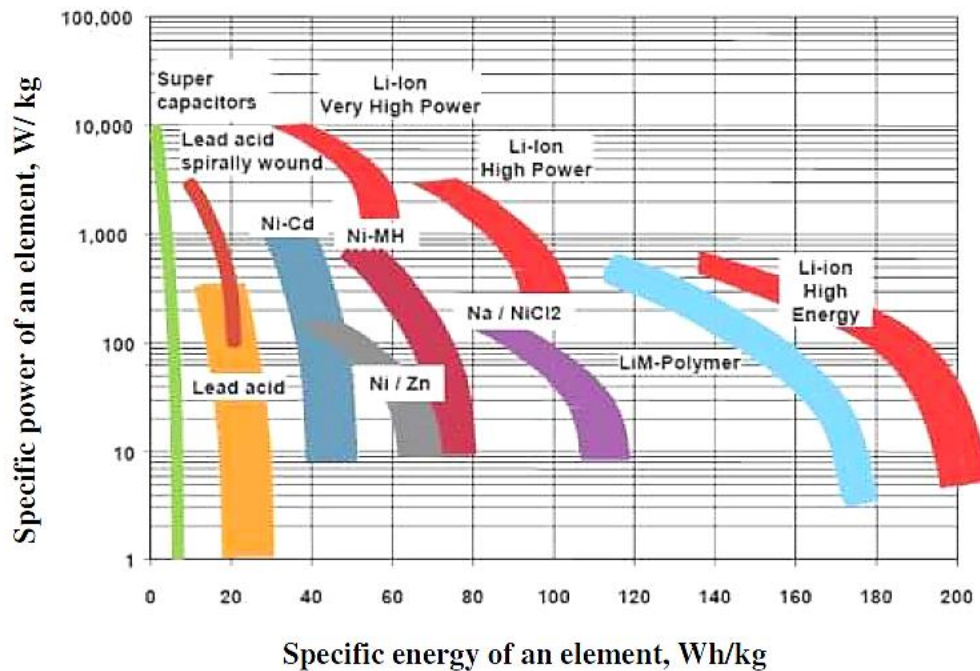


Figure 2.30: Comparison of different battery storage technologies by source (An Li, 2015).

From Table 2.2 and Figure 2.30, it can be seen that lead acid batteries are among the batteries with the smallest energy density and life cycle. Therefore, it is imperative to properly manage these batteries when used for storage in energy systems.

2.14 Battery States and Their Effects on Lead Acid Batteries

The operational effectiveness, safety, dependability, and economics of battery-powered energy systems, such as renewable energy systems, depend heavily on battery management. High-performance battery management systems cannot be produced by a simple, black-box simulation of batteries that measures simply voltage, current, and surface temperature due to intricate electrochemical dynamics and multi-physics coupling. A crucial enabling technology for enhanced battery management is the ability to estimate and monitor essential internal conditions with accuracy and reliability.

Effective charging, temperature, and health management of batteries requires a thorough understanding of the many battery states, including State of Charge (SOC), State of Energy (SOE), State of Health (SOH), State of Power (SOP), State of Temperature (SOT), and State of Safety (SOS) (Hu et al., 2019).

2.14.1 State of Charge (SOC)

State of Charge (SOC) is one of the critical factors which is often taken into consideration in most Battery Management Systems (BMSs). It is the available capacity (Q_a) expressed as a percentage of the nominal capacity (Q_n) of a battery. The nominal capacity of a battery is the maximum amount of charge that can be stored in the battery. The formula used to express the SOC of a battery is given by equation (2.47) below (Hannan et al., 2017).

$$SOC(t) = SOC(t_0) - \int_{t_0}^t \frac{I(t) \cdot \eta}{Q_n} dt \dots \dots \dots 2.47$$

Where SOC(t) is the SOC value at the time (t), SOC(t_0) is the SOC at the initial time (t_0), η is the coulombic efficiency that reflects the ratio of the fully discharged energy to the charged energy required to recover the original capacity of the battery.

Accurate SOC data is necessary for BMSs since it shows how much energy is still available in a battery during operation. Such state information is used for the battery itself to give a prior information for charging/discharging techniques, ensuring battery operations under safe and reliable conditions. In a lab setting, the reference values of SOC are often produced through a carefully regulated coulomb counting approach that accumulates the charge transferred after knowing the initial SOC value (Chang, 2013). However, it is challenging to directly measure the battery SOC in practical applications due to the intricate electrochemical reactions and strong coupling properties. As a result, precisely predicting the SOC in real time becomes a crucial feature in BMSs,

which in turn attracts a lot of research attention. Different methods have been used for SOC estimation. Some the methods are Open-Circuit Voltage (OCV) method, the coulomb counting method, and the Kalman filter method.

2.14.1.1 Open-Circuit Voltage Method

Open-Circuit Voltage (OCV) Method: The OCV method estimates SOC by relating the battery's open-circuit voltage to its state of charge. It involves constructing a lookup table or mathematical model that correlates the battery's terminal voltage with its SOC. The OCV method is relatively simple, low-cost, and suitable for many battery chemistries. However, its accuracy may be affected by various factors such as temperature, aging, and load dynamics (Chang, 2013; A. K. M. A. Habib & Hasan, 2023; Hannan et al., 2017; Hu et al., 2019; Maharjan et al., 2009; Morstyn et al., 2016; Xie et al., 2018).

2.14.1.2 Coulomb Counting

Coulomb counting estimates SOC based on the principle of charge conservation. It measures the current flowing into or out of the battery and integrates it over time to determine the SOC. This method is commonly used in portable electronics where the battery operates under constant current or voltage conditions. However, it is susceptible to errors caused by measurement inaccuracies, variations in battery efficiency, and parasitic losses (Chang, 2013).

2.14.1.3 Model-Based Methods

Model-based methods employ mathematical models of the battery's electrochemical behavior to estimate SOC. These models can be based on electrical circuit models, equivalent circuit models (ECM), or electrochemical models such as the Doyle-Fuller-Newman model. Model-based approaches consider various battery parameters,

including internal resistance, polarization, and diffusion dynamics. They can provide accurate SOC estimates but require knowledge of battery characteristics and complex algorithms, making them computationally intensive (Chang, 2013).

2.14.1.4 Kalman Filtering (KF)

Kalman filtering combines measurements from different sensors, such as voltage, current, and temperature, with a mathematical model to estimate SOC. It utilizes a recursive algorithm that incorporates system dynamics, noise characteristics, and measurement uncertainties. Kalman filtering is widely used due to its ability to handle non-linearities, uncertainties, and time-varying conditions. It can provide accurate SOC estimates but requires accurate system modelling and knowledge of noise characteristics (Chang, 2013).

2.14.1.5 Extended Kalman Filtering (EKF)

Extended Kalman Filtering is an extension of the Kalman filter that considers non-linearities in the battery model. It incorporates a battery model with non-linear state equations into the estimation process. EKF iteratively linearizes the non-linear model, updating the SOC estimate based on the current measurement. EKF can provide accurate SOC estimates for batteries with complex dynamics and non-linear characteristics (Chang, 2013).

2.14.1.6 Artificial Intelligence (AI) Techniques

AI-based methods, such as neural networks, support vector machines, and fuzzy logic, have been increasingly employed for SOC estimation. These techniques utilize historical data and training algorithms to establish a relationship between battery inputs (current, voltage, temperature) and SOC. AI-based methods can capture complex battery behavior and adapt to varying operating conditions. However, they require

substantial training data, computational resources, and careful model selection to achieve accurate SOC estimation.

2.14.2 State of Health (SOH)

Battery state of health (SOH) estimation is crucial for assessing the overall condition and remaining useful life of a battery. SOH provides insights into a battery's capacity degradation, impedance changes, and other performance parameters. Accurate SOH estimation helps optimize battery usage, plan maintenance schedules, and avoid unexpected failures. Several methods and techniques have been developed for battery SOH estimation.

2.14.2.1 Capacity-Based Methods

Capacity-based methods estimate SOH by comparing the actual capacity of a battery to its initial capacity. This approach involves periodically measuring the battery's charge and discharge capacity and tracking its degradation over time. The ratio of current capacity to initial capacity provides an estimation of SOH. However, capacity-based methods require full charge and discharge cycles, which can be time-consuming and may not capture the complete degradation behaviour.

2.14.2.2 Coulomb Counting

Coulomb counting, mentioned earlier in the SOC estimation section, can also be utilized for SOH estimation. By tracking the charge and discharge cycles and comparing the coulombic efficiency, which is the ratio of discharged capacity to charged capacity, one can estimate the degradation and changes in the battery's internal resistance. A decrease in coulombic efficiency over time indicates a decline in SOH (Hu et al., 2019).

2.14.2.3 Impedance Spectroscopy

Impedance spectroscopy measures the complex impedance of a battery at different frequencies to determine its internal resistance, polarization, and diffusion behaviour. By analysing the impedance spectra over time, changes in battery impedance can be correlated with SOH. However, impedance spectroscopy requires specialized equipment and can be time-consuming, limiting its application in real-time monitoring.

2.14.2.4 Voltage-Based Methods

Voltage-based methods estimate SOH by analysing the battery's terminal voltage under different operating conditions. By establishing voltage profiles at various states of charge and discharge, changes in voltage characteristics can be correlated with battery degradation. This approach is relatively simple and can provide insights into SOH, but it may not capture the complete degradation behaviour and can be influenced by external factors like temperature and load dynamics (Hu et al., 2019).

2.14.2.5 Model-Based Methods

Model-based methods utilize mathematical models of battery behaviour to estimate SOH. These models can be based on equivalent circuit models, electrochemical models, or physics-based models. By comparing the simulated responses of the model with actual measurements, changes in SOH can be estimated. Model-based approaches can provide accurate SOH estimation but require detailed knowledge of the battery's electrochemical behaviour and accurate parameterization of the model.

2.14.2.6 Machine Learning and Data-Driven Approaches

Machine learning techniques, such as neural networks, support vector machines, and decision trees, can be employed to estimate SOH. These approaches utilize historical data, including battery performance and environmental parameters, to establish a

relationship between input variables and SOH. By training a model on the available data, it can predict the SOH of a battery. However, these methods require significant amounts of training data and may not capture complex degradation mechanisms.

2.14.2.7 Aging Models and Estimation Algorithms

Aging models, such as the calendar aging or cycle aging models, are used to simulate the degradation processes in batteries. These models consider factors such as temperature, cycling conditions, and aging mechanisms to estimate SOH. Estimation algorithms, such as particle filters or adaptive filtering, can then be applied to update the SOH estimate based on measured data. These methods can provide accurate and dynamic SOH estimation but require accurate modelling of the aging mechanisms.

2.14.3 State of Temperature (SOT)

Battery state of temperature (SOT) refers to the measurement and monitoring of the temperature of a battery. Temperature plays a critical role in the performance, safety, and lifespan of batteries. Monitoring and controlling the SOT is essential for optimizing battery operation, preventing overheating or excessive cooling, and ensuring safe and efficient battery management.

The temperature of a battery can affect various aspects of its behaviour and performance, including capacity, internal resistance, self-discharge rate, cycle life, and chemical reactions within the battery. Therefore, accurate and real-time monitoring of the SOT is crucial for maintaining battery health and maximizing its performance.

The amount of storage capacity that a battery can hold depends on temperature. Capacity loss can occur in both high and low severe temperatures. Additionally, a battery's internal resistance rises at extremely cold temperatures and falls at extreme hot conditions. Voltage drops, decreased efficiency, and power loss can all be caused

by elevated internal resistance. Furthermore, higher temperatures cause a faster loss of energy while the battery is not in use due to an increase in battery self-discharge rates.

More significantly, a battery's cycle life is impacted by temperature. Low temperatures can increase a battery's lifespan whereas high temperatures can shorten it by accelerating deterioration. Specific battery chemistries have optimal temperature ranges.

2.15 Software tools used for HRES designs

Some of the most commonly used software tools for HRES design are HOMER, MATLAB, iHOGA and RETScreen, (Cuesta et al., 2020; Kaur, 2017; Sinha & Chandel, 2014).

2.15.1 HOMER

HOMER is an acronym which means Hybrid Optimization Model for Electric Renewables. It is the most widely used and freely available with premium payable packages. It is user friendly as compared to other commercial software. The software is used for optimization, sensitivity analysis and quick feasibility of hybrid systems and microgrid systems. It functions based on input parameters given by the user and was developed by the National Renewable Energy Laboratory (NREL) USA since 1993 (Sinha & Chandel, 2014). HOMER generates outputs like optimal sizing, net present cost, cost of energy, capital cost, capacity shortage, excess energy generation, renewable energy fraction, and Fuel Consumption from inputs like load demand, renewable energy resources (solar radiation, wind speed, water flow rate, biomass), component details with cost, constraints, and system control. The majority of HRES research has utilized HOMER. (Gebrehiwot et al., 2019) A hybrid model is developed by Gebrehiwot et al. (2019) to electrify a remote Ethiopian community. Utilizing the Hybrid Optimization

of Multiple Electric Renewables (HOMER) model, they evaluated the available primary data, created a load profile, and arrived at the best system at the lowest possible cost for the community. They also conducted a sensitivity analysis to assess how changes in the wind speed, solar radiation, and fuel price might affect the configuration of the ideal system. They concluded that a solar photovoltaic (PV), wind turbine, diesel generator and battery backup was the best option to electrify the village from an economic perspective to supply the peak demand of the village which was 19.6 kW. The results also showed that the energy generation cost was 0.207 \$/kWh, net present cost (NPC) of \$ 82 734 with a carbon dioxide emission reduction of 37.3 tons a year. The system configuration is shown on Figure 2.31 below.

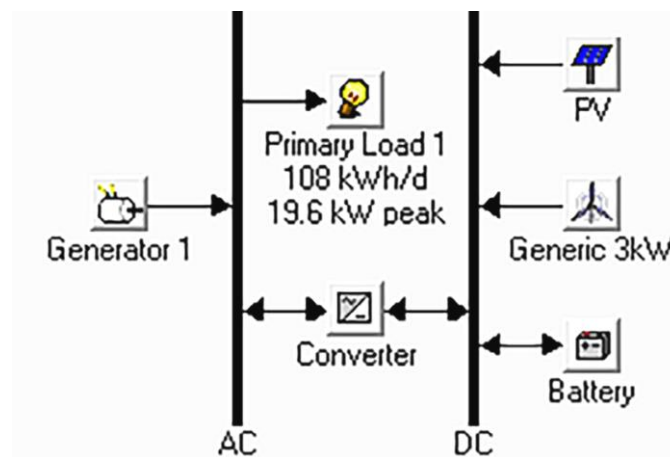


Figure 2.31: Proposed HRES for Golbo II village in Ethiopia (Gebrehiwot et al., 2019)

Murugaperumal et al. (2020) used HOMER to optimize a PV-wind-bio generator HRES to supply a remote rural district of Korkadu in India. The forecasted loads for the district included agricultural, commercial, residential and industrial. They proposed a dispatched strategy which saw the contribution of solar power to be 86.8%, bio generator 0.5% and wind 12.7% to meet the load demand with 6.8% of battery bank losses and 1.78% of converter losses. The different available load patterns for the

village were calculated using the short-term load forecasting technique. Optimal techno-economic simulation results showed that the NPC of the system is Rs 1.2 million while the COE is 13.71 Rs/kWh compared to other dispatched strategies. Also, a suitable reduction in greenhouse gas emissions was observed, indicating 0.196 kg/year of carbon dioxide (CO₂), 0.25 kg/year of carbon monoxide (CO) and 0.291 kg/year of nitrous oxide (NO) (Murugaperumal et al., 2020).

Ramesh and Saini (2020) studied the effects of using lead acid (LA) batteries, lithium-ion (Li-Ion) batteries and diesel generators with and without scheduling on the performance of a standalone HRES for a remote area in Kamataka, India. They found a 35% drop in NPC and cost of energy for the proposed HRES when Li-Ion batteries are used as compared to their lead acid counterparts. They also found that a saving in NPC and COE of \$155,977 and 0.027 \$/kWh respectively could be made when diesel generators are scheduled. Their investigation also saw the effect of running the system without the diesel generator. Here, they concluded that the system was most feasible without the diesel generator and the most optimized HRES was the PV/micro-hydro/Li-Ion battery, giving a NPC of \$467,644 and COE of 0.106 \$/kWh (Ramesh & Saini, 2020).

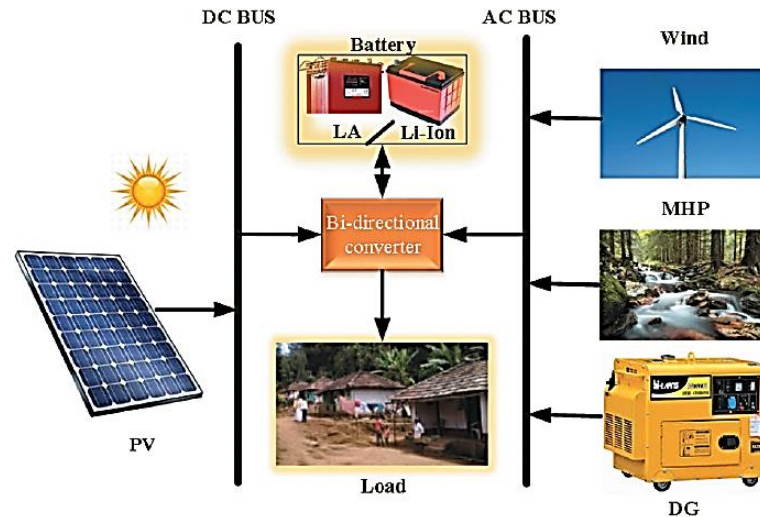


Figure 2.32: Configuration of the proposed HRES used (Ramesh & Saini, 2020)

Aziz et al. (2018) in order to power a remote rural town in Iraq, they investigated the technological, financial, and environmental viability of using a PV-diesel-battery hybrid energy system. Using a multi-input module, they evaluated the optimization and the sensitivity analysis using HOMER software.

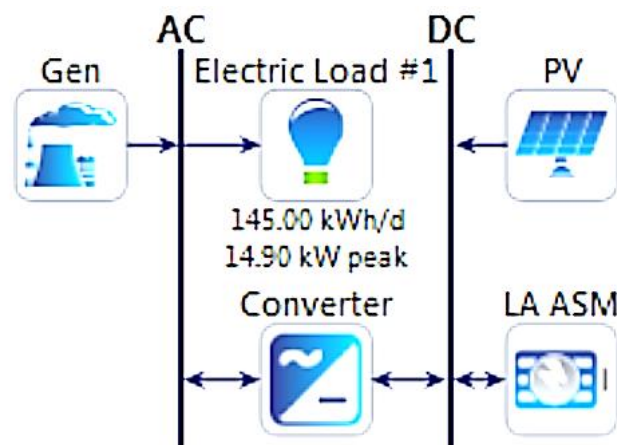


Figure 2.33: Setup of the PV-diesel-battery HES (Aziz et al., 2018)

The performance of the system during the course of the project was taken into account, along with the impact of component deterioration, load growth, and fuel price variations. The findings show that the most practical and cost-effective setup includes

a diesel generator with a 20 kW capacity, 15 batteries, and a 6 kW power converter, with an NPC of \$ 162703. Furthermore, the system performance is significantly impacted by the multi-year input changes, and the batteries degrade by 24.2% towards the end of their lifespan. Additionally, over the course of the project, PV output is decreased by 10% while diesel production is increased by 25.6%, resulting in a 23.1% rise in CO₂ emissions. The system's economic performance suffers as a result of the PV and batteries being highly sensitive to changes in ambient temperature, which causes the annual output energy of the batteries to increase from 5496 kWh to 5871 kWh while decreasing their lifespan from 26.5 months to 23.5 months and the annual PV production from 18268 kWh to 17332 kWh.

Khavari et al. (2016) assessed the viability of a HRES for the electrification of remote area in Binalood, Iran. They used HOMER to assess the techno-economic benefits of using the system and their results show that the wind-diesel-battery storage hybrid system was the most efficient to supply the load of this locality with a total cost of \$1,130,941 for 1000 kWh/d and 142 kW power peak (Khavari et al., 2016).

A techno-economic and environmental analysis of various hybrid systems to provide energy to a typical rural Iraqi community was provided by Aziz et al. (2019). Since the multi-year module hasn't been covered in the literature yet, they employed HOMER software to optimize the systems. The research revealed that the PV-hydro-diesel-battery HRES, which also had acceptable technical and environmental performance standards, was the most cost-effective alternative with an NPC of \$113201. Over the course of the project's 20-year lifespan, the production of PV electricity is reduced by 9.1% while the production of diesel electricity, CO₂ emissions, and served load are increased, respectively, by 90.8%, 91.7%, and 8.8%. The NPC for the multi-year module increased by 22.5% as compared to the single-year module. Additionally, the

sensitivity analysis of a few little-discussed variables, such as water pipe losses, generator minimum load, battery roundtrip efficiency, battery set point state of charge, capacity shortage, and PV capital cost multiplier and multi-year, revealed that changes in these variables significantly affect the system's power flow and economic analysis. On Figure 2.34 below, the hybrid model applied in this work is depicted.

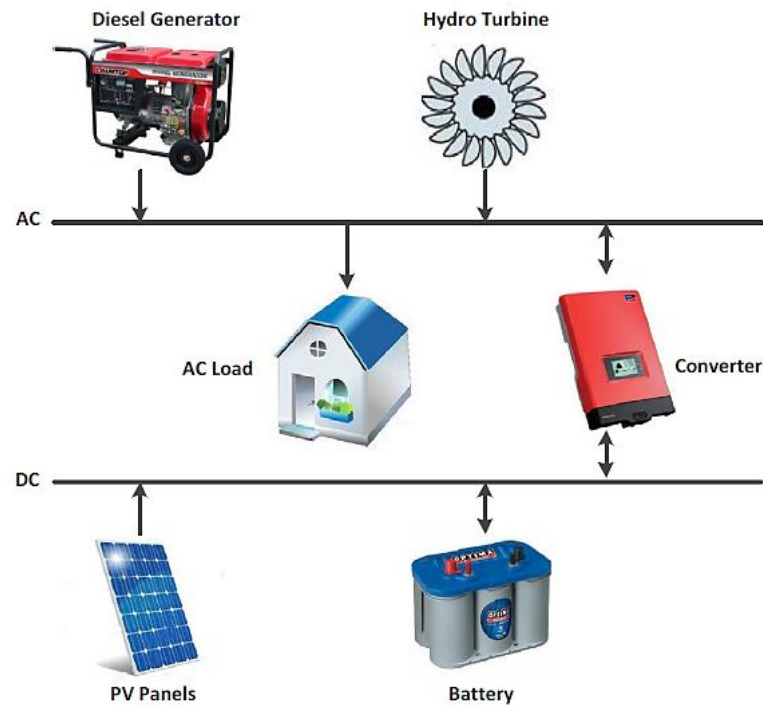


Figure 2.34: PV-hydro-diesel-battery HRES (Aziz et al., 2019)

Bagheri et al. (2018) presented a novel systematic framework to identify optimal hybrid renewable solutions for urban areas at neighborhood scales, Figure 2.35.

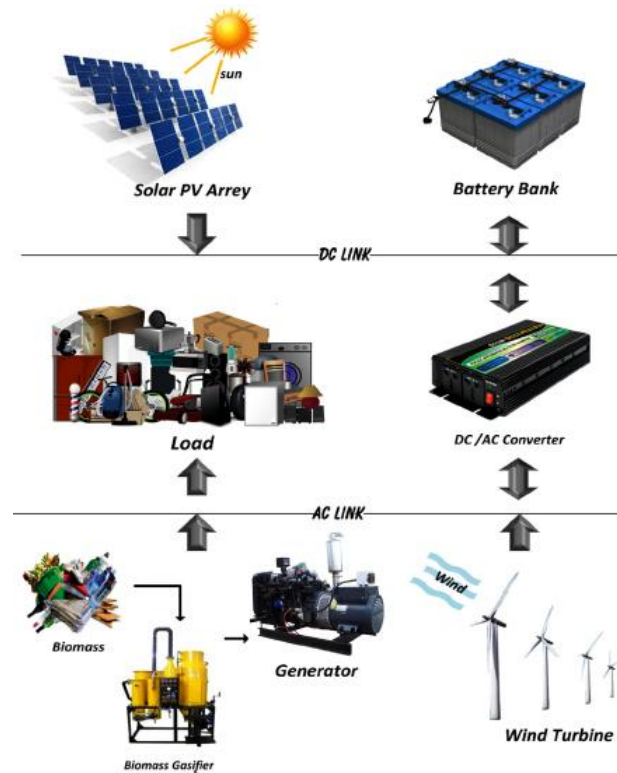


Figure 2.35: HRES for the area (Bagheri et al., 2018)

In particular, they examined the role of economies of scale in the techno-economic feasibility and environmental performance of hybrid renewable energy systems. They demonstrated this by assessing the impact of the economies of scale (at the neighborhood scales of 1/500, 1/250, and 1/100 of the city's electrical load) on the life-cycle costs of optimal hybrid HRESs for Vancouver, Canada. Their results indicated that the total NPC of the optimized systems were 59, 116 and 290 million USD, while the leveled costs of electricity (COE) for the three studied scales were almost identical that is 0.300–0.307 USD/kW h. They compared the proposed scenarios regarding gross atmospheric emissions, land requirements and economic performance and found that the mid-scale 1/250 with 6.3MW of solar PV and 3MW gasifier with waste input of about 117 t/day was preferable to the larger 1/100 and smaller 1/500 scale systems. They further recommended that results from the study could help decision-makers in

creating effective policies and mechanisms to advance the integration of HRESs in cities.

Balachander et al. (2020) proposed a refined hybrid electrical power network to supply a single residential electrical load located in Coimbatore, Tamilnadu. They used a PV-Wind-Diesel hybrid system and optimization done with HOMER. The results showed that the lowest NPC and initial COE was 51.20 INR/kWh. The results also indicated that the initial cost of the overall system was high. Greenhouse gas emissions were also significantly high in the optimized system (Balachander et al., 2020).

Bentouba and Bourouis (2016) evaluated the technical and economic feasibility of using a hybrid generation system to satisfy the electricity demand for Timiaouine town, located in the extreme South Western part of Algeria with more than 200 families not connected to the power grid. They optimized the system using HOMER and the optimization results showed that a wind-PV-diesel generator system could supply 100% of the electricity demand with a COE of 0.176 \$/kWh and a reduction in carbon emissions by 593.125 tons/year (Bentouba & Bourouis, 2016).

Cano et al. (2020) analyzed the impact of a HRES composed of PV-batteries-biomass-hydrokinetic turbines in Cuenca-Ecuador. In order to identify novel patterns in the behavior of sources in relation to electric demand, they developed three types of energy dispatch: charge cycle, load following, and combination cycle. The items such as net present cost and cost of energy were assessed for the various types of control, they added, taking into account the different types of biomasses the gasifier utilized. Increasing the minimum state of charge in the batteries was observed to raise system costs according to the sensitivity analyses, but it was also seen to decrease CO₂ emissions and biomass use. However, it was determined that the renewable system was

able to supply the demand without deviating from any standards despite the realization that the fluctuation in component costs effects the system's overall cost (Cano et al., 2020).

S. Das et al. (2020) explored the feasibility of distributed generation with available local renewable resources for a remote village on the Himalayan Mountains of a northeast state of India. They used HOMER simulation and multi-criteria decision-making approach to optimized the decentralized wind-hydro-battery HRES and reported a minimum COE of \$0.63/kWh and CO₂ emissions of 481 kg/year for optimum uninterrupted power supply. The schematic diagram of the system is shown on Figure 2.36.

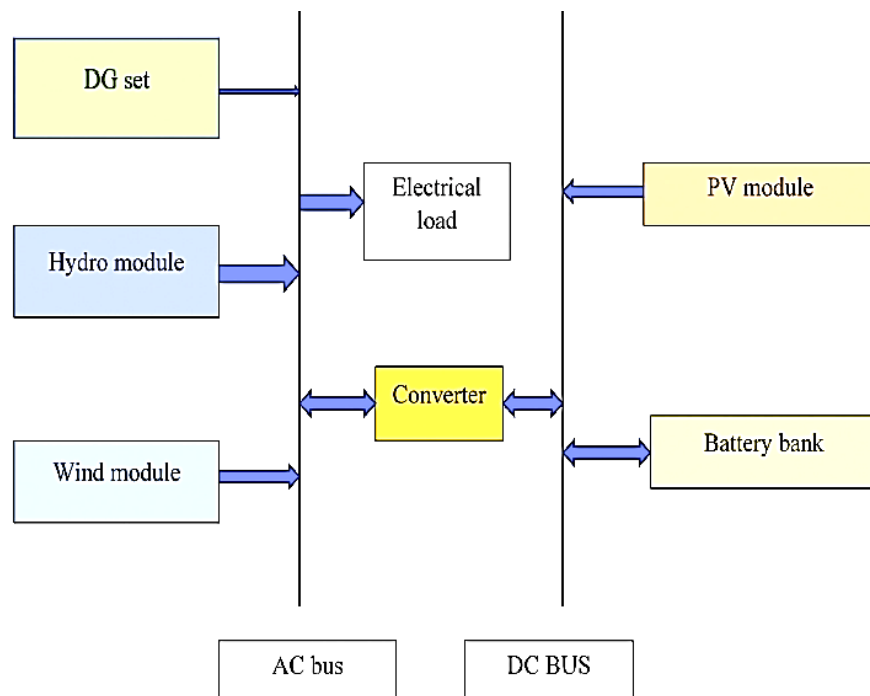


Figure 2.36: Schematic diagram of the hybrid system (S. Das et al., 2020)

Elkadeem et al., (2019) made a comprehensive feasibility analysis of a grid-isolated HRES for electrification of agriculture and irrigation area in Dongola, Sudan. They proposed a systematic and integrative framework combined with techno-economic optimization analysis for adequate planning and design of HRES. The simulation

results using HOMER software indicate that solar-wind-diesel-battery-converter hybrid system is of optimal performance and superiority over the studied cases to serve the load demand of the investigated area. The NPC was seen to be \$24.16 million and leveled COE of 0.387 \$/kWh was recorded. They also achieved a positive return on investment of 39.94% and around 95% reduction in both carbon emissions and fuel consumption compared to the base case.

(Yimen et al., 2018) performed a techno-economic analysis and optimization of a pumped-hydro energy storage based 100%-renewable off-grid HRES for the electrification of Djoundé, a village in Northern Cameroon. They used HOMER software to optimally design the system with 81.8 kW PV array and a 15 kW biogas generator, where they obtained a COE of 0.256 euro/kWh and total NPC of 370,426 euros. The schematic diagram used in this study is presented in Figure 2.37 below.

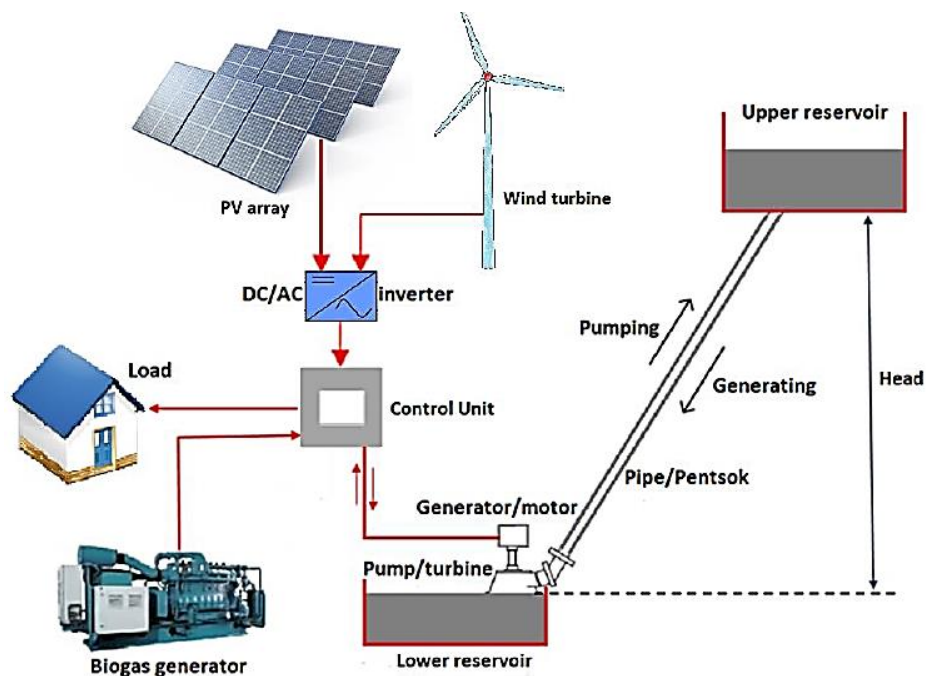


Figure 2.37: HRES schematic diagram (Yimen et al., 2018)

(Kenfack et al., 2009) optimized a microhydro-PV hybrid system for a village in Cameroon using HOMER software and reported encouraging results which could satisfied the load demand of the community optimally. (MUH, 2017) made a comparative assessment of HRESs in Cameroon with optimization done using HOMER software and reported that PV-wind-small hydro-battery HRES was the most feasible system all over the country with a cost of energy of \$0.674/kWh, \$0.677/kWh, \$0.583/kWh for West, Center-South, and Northern parts of Cameroon respectively. (Nfah et al., 2007) modelled a Solar-diesel-battery HRES for the electrification of typical rural households and schools in remote areas of the then Far North Province (Far North Region today) of Cameroon. They discovered that the energy needs of typical rural families in the range of 70-300 kWh/yr may be satisfied by solar-diesel-battery hybrid power systems. Additionally, they discovered that a hybrid solar-diesel-battery power system using a 1440Wp solar array and a 5kW single-phase generator running at a load factor of 70% only needed 136 generator hours per year to provide a normal secondary school with 7 kWh per day. Their findings demonstrated that all of the systems studied had a renewable energy proportion that ranged from 83 to 100 percent. They came to the conclusion that increasing the number of people who have access to electricity in the Far North Province is possible without resorting to grid extensions, adding more thermal power plants to the Northern grid, or expanding the number of independent diesel plants that supply electricity to the province's then remote areas (Far North Region today). (Nfah & Ngundam, 2008) again modelled a wind-diesel-battery hybrid power systems to supply electricity to remote areas of the then Far North Province (Far North Region today) of Cameroon. They again found that the hybrid power system based on a combination of two wind turbines rated 290W and a 5 kW single phase generator operating at a load fraction of 70% required only 106 generator

hours per year to supply 2585 kWh/year or 7 kWh/day to a typical secondary school. They saw that the renewable energy fractions attained in feasible systems were in the range 70–100%. (Nfah et al., 2008) also performed an off-grid simulation study for generation options for remote villages in Cameroon. (Nfah & Ngundam, 2009) made a feasibility study on a pico-hydro and PV hybrid power systems for remote villages in Cameroon with simulations performed using the HOMER software. (Mbaka, 2013) evaluated an optimal photovoltaic hybrid system for remote villages in Far North Cameroon using a recent iterative optimization method based on desired annual number of generator hours and the Net Present Value technique reported that PV hybrid systems are the optimal solutions for the electrification of remote villages in the Far North Region of Cameroon.

Ray et al., (2013) carried out optimization and economic analysis for different combinations of PV, battery and diesel hybrid energy systems in the quest for finding the optimal system to supply reliable power to rural communities in the North-Eastern state of India. Their findings showed that the PV-diesel-battery hybrid power system was the best combination with a COE of 0.118 \$/kWh.

2.15.2 MATLAB

MATLAB means Mathematics Laboratory. It is a sophisticated highly performant software used across many disciplines. It is also used in modelling and simulating HRESs.

Mokhtara et al. (2020) presented a novel approach by optimally designing an off-grid hybrid solar PV-diesel-battery system for the electrification of residential buildings in arid environments with a dwelling in Adrar in Algeria used as a case study. Their approach integrated the demand-supply management (DSM) with particle swarm

optimization. The proposed design was first modelled using MATLAB and optimised by using the total NPC. They validated these results using HOMER software. The system configuration is shown on Figure 2.38 below.

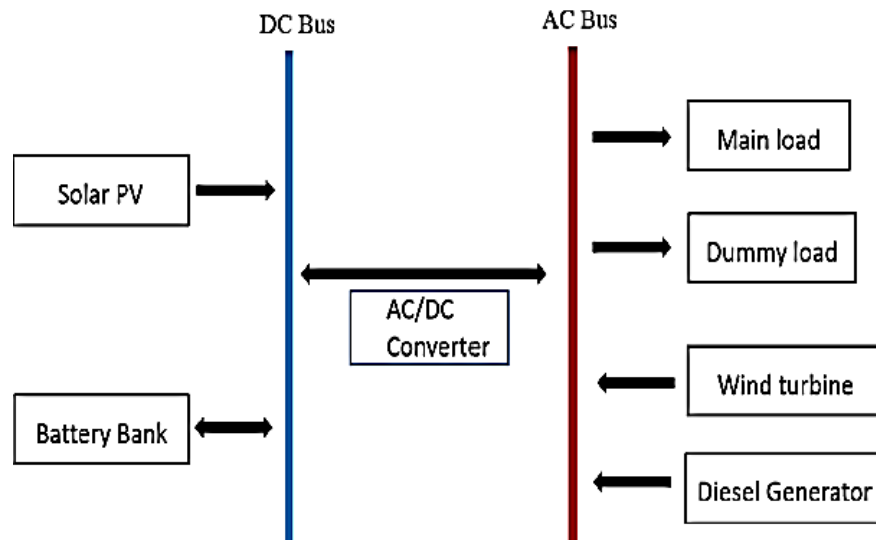


Figure 2.38: Investigated HRES (Mokhtara et al., 2020)

The results showed that total NPC is reduced by 18% and energy demand is reduced by 7% comparatively to when only supply-side management is used. Also, the PV-Li-ion was seen to be the best configuration with total NPC of \$23,427 and cost off energy (COE) 0.23 \$/kWh. In addition to this, energy consumption is reduced by 19% while carbon dioxide emission is reduced by 57%. The optimal configuration with the least COE was obtained using the wind-diesel hybrid system.

(Patel & Singal, 2018) carried out a study on the economic analysis of an integrated renewable energy system (IRES) for rural electrification having scattered settlement. In the study, the IRES model is designed using a hybrid of solar-wind-biomass-biogas energy sources to supply the load demand of Khatisitara village of Gujarat state in India. In their work, they used the distribution losses as a design parameter and the optimization for the NPC is performed using the PSO algorithm in MATLAB

environment and the results validated using the Genetic Algorithm (GA). Their simulation results show that for the study locality, the distribution losses were significant but using the IRES was more feasible than using the grid extension for rural electrification. Their proposed IRES is shown below.

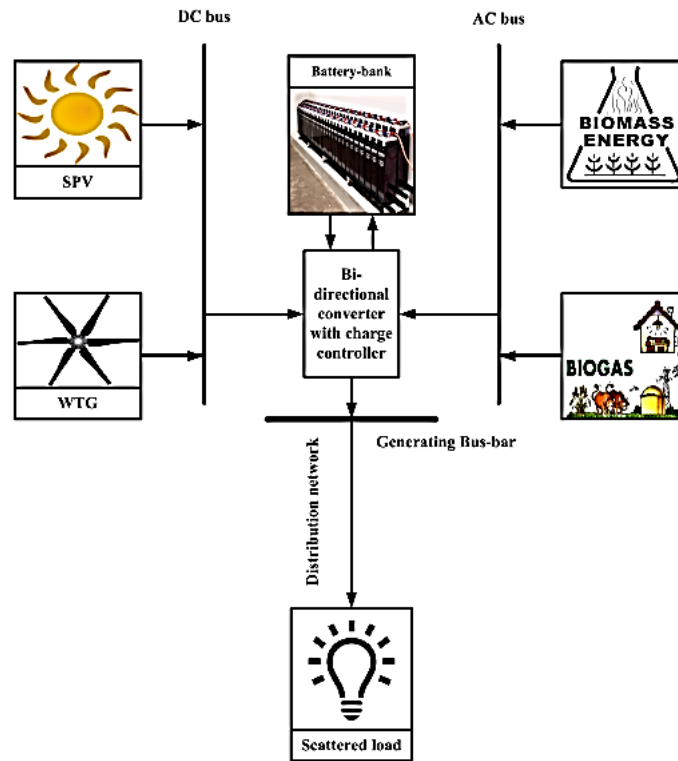


Figure 2.39: Proposed IRES (Patel & Singal, 2018).

Habib et al., (2019) proposed a design optimization methodology power management strategy (PMS) for wind-diesel-battery-converter hybrid renewable energy system (HRES) for a residential load located in a remote rural area in Pakistan. They first investigated the optimal component sizing using the actual meteorological and load profile data for the locality. Using HOMER software, they compared the techno-economic and environmental parameters of several hybrid setups after modeling and analyzing each one. For the developed HRES, a suitable PMS based on the battery's state of charge (SOC) is suggested and implemented in the MATLAB/Simulink program. The goal of this PMS was to keep the battery SOC within a safe range while

maintaining load balancing and maximizing wind output. They also applied model predictive control (MPC) to lower overall harmonic distortion and enhance output voltage profile (THD). In comparison to employing a diesel generator, the wind-battery converter provided a total NPC of \$14,846 and COE of 0.309 \$/kWh, representing a 76.7 percent decrease in both total system cost and energy cost. It also resulted in a 100% reduction in carbon emissions. With a surplus of 30.1 percent energy, the load demand is satisfied. They added that the research could help researchers and system planners create and use HRES more effectively, hence reducing the sharp rise in load demand for both urban and rural areas.

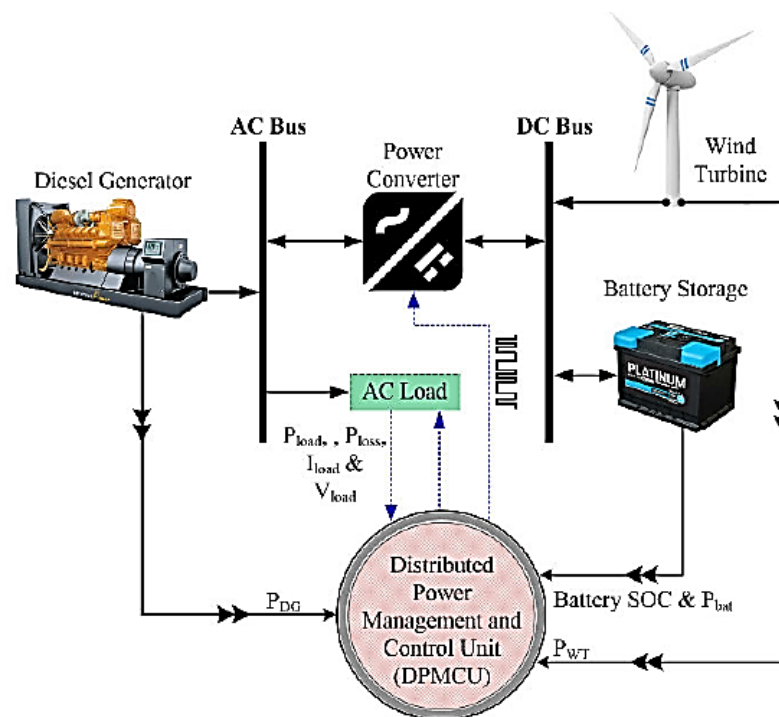


Figure 2.40: HRES proposed diagram (H. U. R. Habib et al., 2019)

(Jagjeevanram, 2020) proposed a hybrid PV-wind-diesel power system with a control scheme to maintain the consumption rate of the diesel generator at a very low level while maximizing the use of the renewable energy sources. The control strategy was simulated in MATLAB's Simulink.

2.15.3 iHOGA

Improved Hybrid Optimization by Genetic Algorithm (iHOGA) is developed by University of Zaragoza, Spain. It is C++ based hybrid optimizer used for optimum sizing of hybrid renewable energy systems. Components included are photovoltaic system, wind turbines, fuel cells, converters, generators, storage devices etc. it uses the mono and multi-objective optimization using genetic algorithm (Kaur, 2017). It takes input data such as constraints, resource data, component data, economic data and gives output information such as multi objective optimization, life cycle emission, probability analysis and buy-sell energy supply analysis (Sinha & Chandel, 2014). Joyti and Daigavane (Fulzele & Daigavane, 2018) used iHOGA to design a hybrid PV-wind-battery system incorporating an inverter. Their work was based on analysing the sensitivity of the system to produce an optimal solution for rural electrification.

2.15.4 RETScreen

RETScreen is another hybrid optimization software, developed at Canmet Energy Diversification Research Laboratory (CEDRL), Natural Resources Canada for evaluating both financial and environmental costs and benefits of different renewable energy technologies for any location in the world. It uses visual basic and C language as working platform (Van Beuzekom et al., 2015). It has two modules, RETScreen 4 and RETScreen Plus. RETScreen 4 is an excel based software used to develop energy efficient models. Input parameters include climate database, Project database, product database, hydrology database (Kaur, 2017; Sinha & Chandel, 2014). (C. Li & Yu, 2016) used RETScreen to design optimal PV-diesel-battery HRESs for households having a peak load of 5.7 kW and a daily energy need of 10.275 kWh in Urumqi area in China. These systems were more economical and cleaner making it the best option for the area.

In addition to the software used are also some control techniques. The most commonly used control techniques as these systems requires sophisticated controls for their optimal performance as the sources of energy are often intermittent are the Particle Swarm Optimization (PSO), Artificial intelligence Technique (AIT), Genetic Algorithm (GA), Simulated Annealing Algorithm (SAA) and the Linear Programming (LP) technique (Zahraee et al., 2016).

In (Cristóbal-Monreal & Dufo-López, 2016), a solar PV-battery-diesel engine hybrid standalone system is analysed and optimised in terms of cost and weight to supply electrical energy to mobile facilities especially in remote rural areas. The genetic algorithms and the multi-objective evolutionary algorithms techniques were used with an applicable example of the method done to a temporary hospital in Central African Republic. The system configuration is shown on Figure 2.41 below.

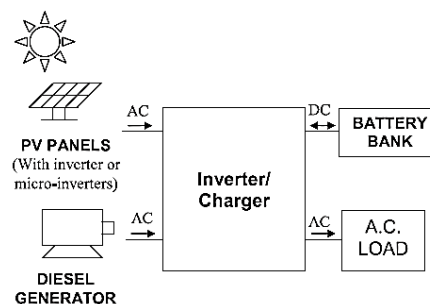


Figure 2.41: Solar PV-battery-diesel generator hybrid standalone system (Cristóbal-Monreal & Dufo-López, 2016).

Mokhtara et al., (2021) presented a methodology for an optimally designed PV-wind-diesel-battery hybrid renewable energy system with the effects of building energy efficiency and the climate diversity on the optimal size of the HRES considered with findings performed. They proceeded by first undertaking a multi-spatial analysis through a common geographical information system tool (ArcGIS 10.2) to come out with the renewable energy potential map for Algeria. They then formulated a multi-

objective problem to minimize COE, maximize system reliability and renewable fraction (RF). From the renewable energy map, seven zones were identified and one location was chosen from each zone making up seven locations.

They found that with low efficiency buildings, PV-wind-diesel-battery is found the best configuration for Adrar and Tindouf, while PV-diesel-battery gives the best results for the other locations. They also found that with highly efficient buildings in Biskra and Tamenrast locations, PV- battery systems produced the best results with 100% penetration of renewable energy and COE of 0.12 \$/kWh. This optimal system with building efficiency considered can be used to reduce the over 40% of energy consumed by buildings worldwide (Landi D, Castorani V, 2019). The system layout is shown on Figure 2.42 below.

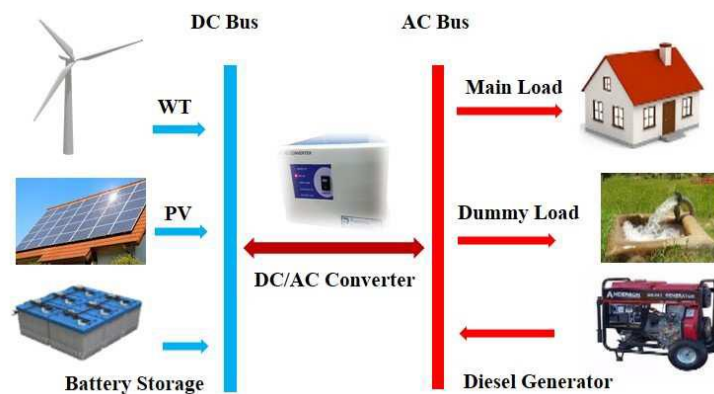


Figure 2.42: PV-wind-diesel-battery HRES (Mokhtara et al., 2021)

Alshammari & Asumadu (2020) used the Harmony Search (HS), Jaya and Particle Swarm Optimization (PSO) algorithms to size an optimum HRES made up of wind-PV-biomass-battery technologies for a small rural community with a goal of having a cost effective, efficient and reliable system capable of satisfying clients' electricity demands. They compared the results from the three algorithms and concluded that the PV-biomass-wind-battery configuration was the least costly and best performant with

a total NPC of \$581,218 and 0.254 \$/kWh COE. The system configuration is shown on the diagram below.

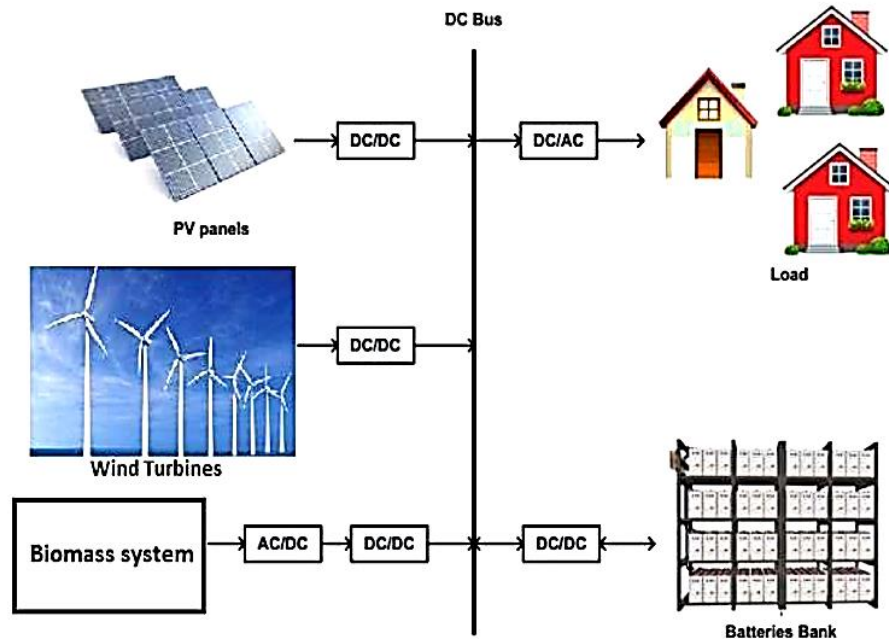


Figure 2.43: PV-wind-biomass-battery HRES (Alshammari & Asumadu, 2020).

In (Corbus & Bergey, 1997), an existing diesel generator was retrofitted to a wind-hybrid diesel system with battery storage to power Costa de Cocos, a small resort located in the state of Quintana Roo, Mexico. The HRES was composed of 15 kW diesel generator, wind turbines with capacity of 7 kW and a battery storage for backup having a capacity of 5 kWh. This HRES was able to supply up to 95 % of the available load in the resort and the rate of fuel consumption was reduced, hence reducing the environmental pollution.

Fazelpour et al (2014a) investigated the feasibility of a standalone hybrid power system to supply a hotel of 125 rooms with an energy consumption of 2 628 000 kWh and a peak demand of 620 kW in Kish Island, Iran. The results of their optimization showed that the wind-diesel-battery storage hybrid system was the most feasible to supply the required load demand of the hotel with five 20 kW wind turbines, one 600 kW diesel

generator and 242.76 kWh battery capacity having a total NPC of \$7,236,000 and a COE of \$0.318/kWh.

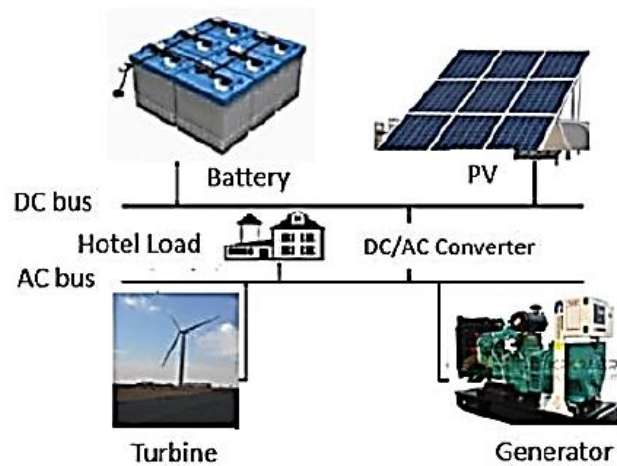


Figure 2.44: Hybrid power system flow diagram (Fazelpour et al., 2014a; Rehman, 2021)

Vai et al. (2020) presented an optimal design of a low-voltage (LV) distribution network for rural electrification using PV and battery storage with a non-electrified village in Cambodia used as a case study. The design was aimed at searching for an optimal topology of a LV distribution system by siting and sizing of a PV and storage over a period of 30 years. The shortest-path algorithm (SPA) and first-fit bin-packing algorithm (FFBPA) were first used to search for the optimal radial topology that minimizes the total length of the distribution line and improves the load balancing. They, further optimized the locations of decentralized BES (DeBES) using a genetic algorithm (GA) to eliminate the under-voltage constraints due to the load consumption. Also, they demonstrated two iterative techniques to size the maximum peak power of PV and the minimum number of DeBES that can be connected to a LV network without violating the voltage and current constraints. A sizing strategy of centralized BES (CeBES) was then developed to avoid power reversal into the medium-voltage (MV)

network. Lastly, a study was done using the Monte Carlo approach to determine the impact of load profile uncertainties on the topology which showed that a $\pm 5\%$ slight variation in the case study does not have an undesirable impact on the system.

(Kazem & Khatib, 2013) in their work presented a method for determining PV array, wind turbine, diesel generator, and battery storage optimal sizes installed in a building integrated system. Their aim was to design a system that will supply reliable electricity in a building at a minimum cost and at a maximum availability of power. They combined climatic factors like temperature, sun energy, and wind speed with mathematical models for the system's individual parts. The findings indicated that the PV array, wind turbine, diesel generator, and battery for a system located in Sohar, Oman, were obtained with optimal size ratios of 0.737, 0.46, 0.22, and 0.17, respectively, which is the daily energy generated by the source to the daily energy requirement. A system with a 30 kWp solar array, an 18 kWp wind farm, and a 5 kVA diesel generator was used as a case study. The system was designed to supply 200 kWh of load demand each day. It was discovered that the solar panel installation, wind farm, and diesel generator generated 36 percent, 55 percent, and 9 percent of the total energy produced, respectively, with a COE of 0.17 dollars per kWh. Additionally, they came to the conclusion that the suggested optimization strategy produced findings that were more accurate than those produced by the HOMER software. They combined climatic factors like temperature, sun energy, and wind speed with mathematical models for the system's individual parts. The findings indicated that the PV array, wind turbine, diesel generator, and battery for a system located in Sohar, Oman, were obtained with optimal size ratios of 0.737, 0.46, 0.22, and 0.17, respectively, which is the daily energy generated by the source to the daily energy requirement. A system with a 30 kWp solar array, an 18 kWp wind farm, and a 5 kVA diesel generator was used as a case study.

The system was designed to supply 200 kWh of load demand each day. It was discovered that the solar panel installation, wind farm, and diesel generator generated 36 percent, 55 percent, and 9 percent of the total energy produced, respectively, with a COE of 0.17 dollars per kWh. Additionally, they came to the conclusion that the suggested optimization strategy produced findings that were more accurate than those produced by the HOMER software.

Ahmad et al., (2018) made a study on the techno-economic feasibility of a grid-tied hybrid microgrid system for local inhabitants of Kallar Kahar near Chakwal city of Punjab province in Pakistan and investigated the potential for electrical power generation via PV-wind-biomass hybrid system. They carried out an assessment of solar energy, wind and biomass resources for grid integration. Their hybrid microgrid system was modeled using the Homer Pro software. After the modelling, optimization and sensitivity analysis was performed to ensure the robustness and cost-effectiveness of the proposed hybrid microgrid system. After due analysis, they concluded that surplus power was supplied to the national grid during low local demand of the load. The system could generate more than 50 MW. The cost of hybrid system for peak load of 73.6 MW was 180.2 million USD and leveled cost of energy was 0.05744 \$/KWh.

Drouilhet, (1999) in his work came up with a control system to overcome the issues faced by designers of wind-diesel-battery hybrid power system dominated by wind penetration in the United States. This control algorithm was used in a wind-diesel-battery hybrid power system installed in a village in Wales, Alaska having installed capacities of 130 kW for wind, 360 kW for diesel and 130 kWh battery storage.

2.16 Conclusion

In this chapter, a literature review to understand: the concepts and techniques used for maximum power point tracking, energy storage systems, hybrid energy systems and some software tools used for the modelling of solar PV systems has been presented. In the proceeding chapter, the methodology adopted to accomplish the specific objectives will be presented.

CHAPTER THREE: METHODOLOGY

3.1 Introduction

This chapter dwells on the methodology that was adopted for the realization of the different objectives. The work had four specific objectives. Firstly, the study site where the work was carried out has been described. This is followed by the method of data collection. Moving forward, the method used to model the system in Homer Pro is explained and the design approach used for the MPPT in MATLAB/Simulink presented. A block diagram of the system is shown below.

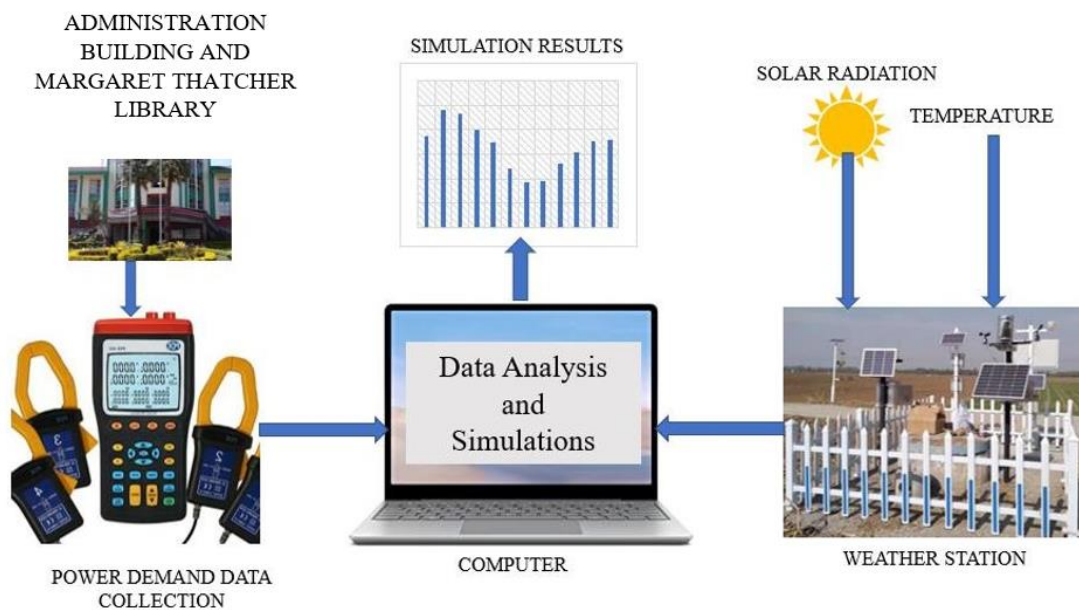


Figure 3.1: System Block Diagram

3.2 Study Site

Moi University is an institution of higher learning in Kenya. Its main campus is located between Latitude 0.286694°N and Longitude 35.294028°E in the town of Eldoret. Figure 3.2 below is a google earth view of the campus. The main source of power supply for the University comes from the grid. Because of this, the University spends huge sums of money for utility bills monthly. In this study, the Administration building

and the Margaret Thatcher Library are used for the power consumption data collection which is used for the design of optimal PV systems to supply the two buildings.

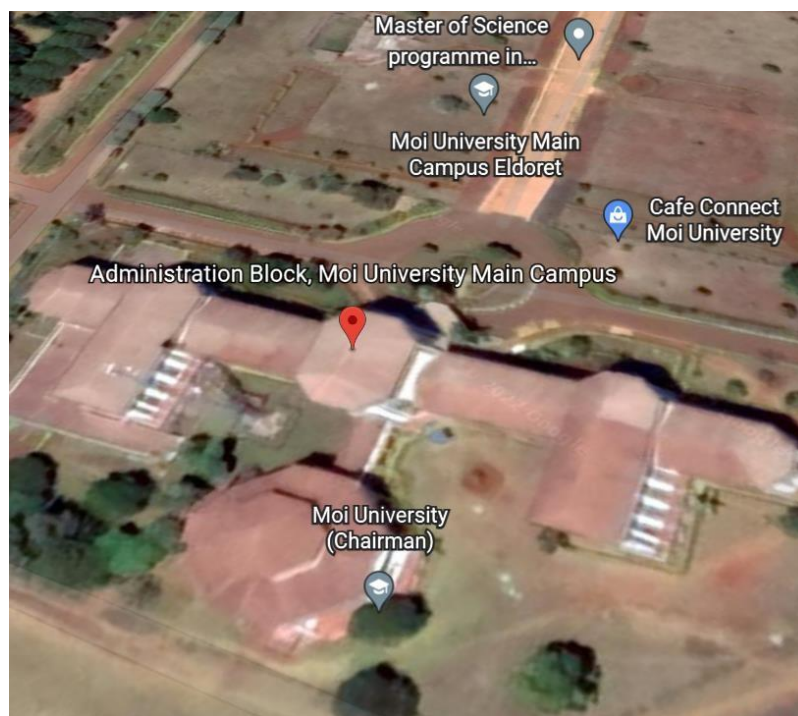


Figure 3.2: View of Moi University Main Campus' Administration Building (Source: Google Earth)

3.3 Data Collection

The power consumption data for the Administration building and Margaret Thatcher Library (represented as LOAD on Figure 3.3) for a period of one month each were logged using the PCE-360 Power Analyser. This was done during the examination period which is the peak month of power consumption. Also, to accompany this, data from an inventory on power consumption for the different appliances in these two buildings (Appendix 1) were used to enable a better appraisal of the logged data. The logging was done for 5 seconds intervals to ensure that detailed information about the power usage was obtained. The temperature and solar radiation data from November 2017 to January 2022 was collected from the meteorological weather station of the

University and these values were compared to those provided by National Aeronautics and Space Administration (NASA) in their database.

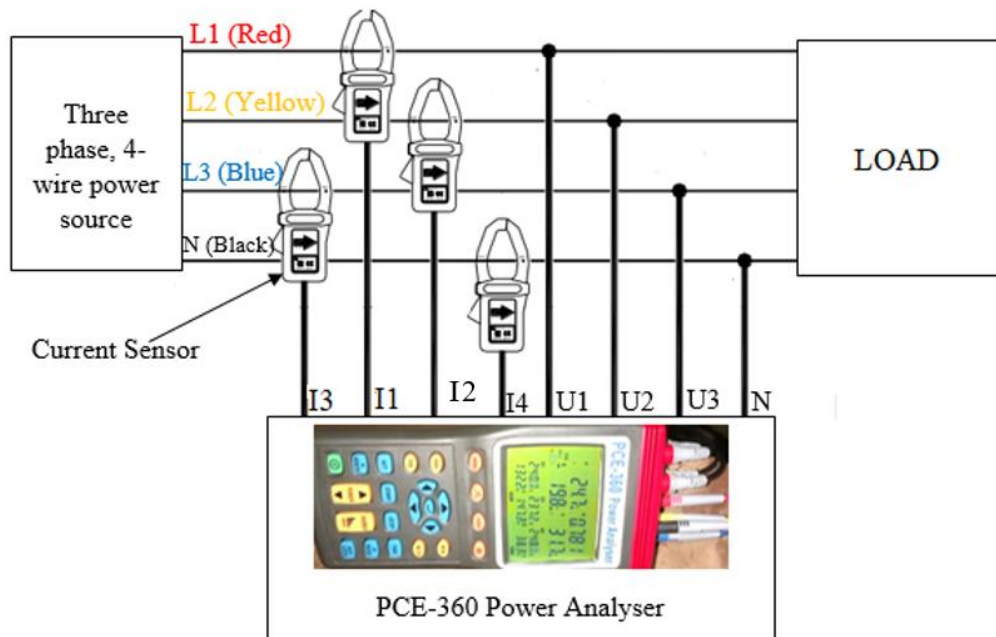


Figure 3.3: Power Consumption Data Collection Using the PCE-360 Power Analyser

From Figure 3.3, L1, L2, L3, and N stands for line 1, line 2, line 3, and neutral respectively. I1 to I4 are the currents while U1 to U3 are the phase voltages.

The Administration building and Margaret Thatcher Library are powered from a three phase four wire system. In order to measure the power consumption for the two buildings, the device was logged as shown on Figure 3.3. The red voltage test lead was connected to line 1 and to U1. This terminal measures the phase voltage for line 1. The yellow voltage test lead was connected to line 2 and to U2. This voltage test lead measures the phase voltage for line 2. The blue voltage test lead was connected to line 3 and to U3. This voltage test lead measures the phase voltage for line 3. The neutral test lead labelled N was connected to the black neutral wire. In addition to the voltage test leads are the current probes labelled I1, I2, I3, and I4. The current probe I1 measures the line current for line one. The current probe I2 measures the line current for line 2.

The current probe I3 measures the line current for line 3, while the current probe I4 measures the neutral current. The meter also measures the power factor of the system and computes the active, reactive, and apparent powers.

More so, while using this device, some precautions need to be followed. The meter is designed to be safely used under temperatures ranging from 0°C to 40°C. The test leads are not allowed to be used if they appear damaged and the maximum input limits to the device must not be exceeded. Some of the quantities the device measures are shown in Table 3.1 below. The range is the maximum value the instrument can measure and should not be exceeded.

Table 3.1: Some quantities measured by the PCE-360 power analyzer

Quantity	Unit	Range	Accuracy
AC Voltage	V	≤ 999.9	$\pm 0.3\%$
AC Current	A	≤ 999.9	$\pm 0.5\%$
Active Power measurement P	kW	≤ 999.9	$\pm 1.0\%$
Apparent Power measurement S	kVA	≤ 999.9	$\pm 1.0\%$
Reactive Power measurement Q	kVAR	≤ 999.9	$\pm 1.0\%$
Power factor	-	$-1 \leq PF \leq 1$	Calculated accuracy is ± 15 digits

3.4 Solar PV-Battery Optimization Using HOMER Pro Software

After collecting the necessary data required, the simulation of the hybrid system was done using the HOMER Pro 3.10.3 software. This software was chosen because it has the capability of performing technical and economic feasibility studies of hybrid energy systems. It also has built-in components which can be readily used to model renewable energy system. In addition to that, HOMER Pro has been extensively used by other researchers as seen in the literature and has proven to be reliable in energy system

modelling. The configuration of the HOMER Pro environment is shown in Figure 3.4. The input information to the software were solar radiation, temperature, power demand, choice of solar module, choice of battery storage, and the cost of all the components used in the system. When this information was input into the software, the simulations were done for different sensitivity cases. The outputs produced after the simulations were the optimization results for the best system to be used with the component sizes, the Net Present Cost (NPC) of the System, Levelised Cost of Energy (LCOE), initial capital cost, and the simple Pay Back Period (PBP).

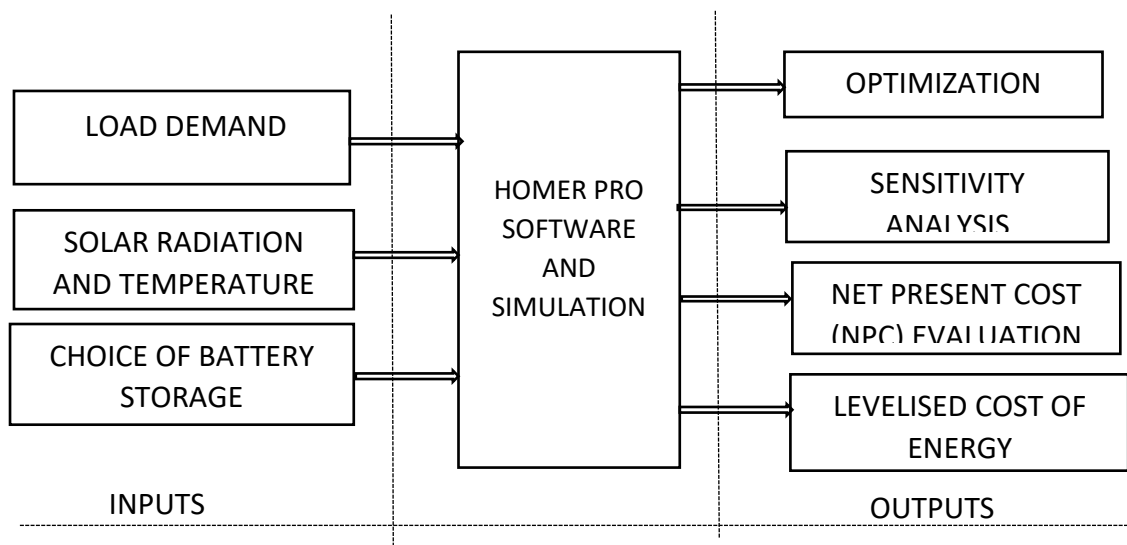


Figure 3.4: Input and Output Parameters Used by HOMER Pro

Sensitivity analysis for the system was done using solar radiation as the main sensitivity variable. This was done to determine the impact of solar radiation on the optimal design of the system. The net present cost and the levelized cost of energy were used for the selection of the optimal system.

The different components which were used in the simulation are specified in the proceeding paragraphs.

3.4.1 Grid

The Administration building and the Margaret Thatcher Library are both powered by the utility grid. For this reason, utility bill costs for a period of one year were used to determine the amount the University is spending annually on electric bills for the two buildings. Knowing this cost, the amount was then used to evaluate the payback period of the proposed solar PV/battery system designed to replace the grid. The choice of completely replacing the grid by the solar PV system was made because solar PV is reliable and clean compared to the utility grid and also, as an academic institution, having a reliable power supply especially in the Margaret Thatcher Library to enable students to study effectively is important. In addition to that, having such a system installed on campus will be a major contribution towards the green campus initiative (Chung et al., 2023). Also, according to the 2019 Energy Act of Kenya, power can be sold back to the grid through net-metering for systems below 1MW at a maximum Fit-in Tariff of Ksh12/kWh (The Energy Act, 2019, 2019). This means that unused energy during the day can be sold to the grid.

3.4.2 Solar PV

In the HOMER Pro environment, the cost, orientation, and performance characteristics of the photovoltaic (PV) array can be entered. Also, the effect of temperature on the power production from the PV module is specified. Added to this page is the area where the capital cost, replacement cost, and the operation and maintenance (O&M) costs are specified. The capital cost is the initial purchase price, the replacement cost is the cost of replacing the PV system at the end of its lifetime, and the O&M cost is the annual cost of operating and maintaining the PV system. When these costs were being specified, all the costs associated with the PV system were considered which were the cost for PV panels, wiring, installation, mounting hardware, and the tracking system.

Furthermore, the cost of the PV system was considered to vary linearly with the PV size.

The SunPower E20-327 monocrystalline solar module with a peak power of 327W was chosen for the simulation. This module has an efficiency of 20.4%. It was selected because of its high conversion efficiency and its high rated power per module which will limit the installation space to be occupied by the overall system. The characteristics of this module are shown in Table 3.2. Given that the power output (P_{out}) of a PV module is often affected by aging, temperature, and solar radiation, the equation (3.1) can be used to calculate P_{out} (Adaramola et al., 2014)(Murugaperumal & Ajay D Vimal Raj, 2019).

$$P_{out} = P_{pv} f_{pv} \left(\frac{G_T}{G_{T,STC}} \right) [1 + \alpha_p (T_C - T_{C,STC})] \dots \dots \dots 3.1$$

In equation (3.1), P_{pv} is the rated power of the PV module under Standard Test Conditions (STC), f_{pv} is the derating factor of the PV module (%) which was 88% for this simulation, G_T is the solar radiation incident on the PV module (W/m^2), $G_{T,STC}$ is the incident radiation at STC ($1000 W/m^2$), α_p is the power temperature coefficient ($\%/^{\circ}C$) which was $-0.38 \%/^{\circ}C$, T_C is the PV cell temperature ($^{\circ}C$) which was $45^{\circ}C$ for this simulation, $T_{C,STC}$ is the PV cell temperature at STC ($25^{\circ}C$).

3.4.3 Battery Storage

Just like PV modules, the HOMER Pro storage page allows for the selection of appropriate battery to use from a variety of different battery technologies. Also, the cost of batteries including capital cost, O&M cost, and replacement cost are added here.

In this work, lead acid batteries were chosen. This is because it is the battery of choice that is mostly used in solar PV systems especially in sub-Saharan Africa due to its low

cost as compared to other battery technologies such as lithium ion (Anuphapparadorn et al., 2014). The summary for the selected battery is shown in Table 3.2.

3.4.4 Inverter

Since solar PV systems produce electricity in DC form and not AC, an inverter is needed to convert DC to AC to enable the AC loads to be powered and also to permit power fit-in to the grid. In this work, the 120kW MTP-4110F 3 phase hybrid inverter was selected with characteristics tabulated in Table 3.2.

3.4.5 Charge controller

Because the system was to be simulated with a battery storage system, the SOLARCON SCM-360400 charge controller was chosen. The role of a charge controller in a PV system is to regulate the charge and discharge cycles of the batteries. It protects the batteries from either overcharging or over discharging. The electrical parameters can be seen in Table 3.2.

Table 3.2: Choice of Components for the PV system

Components	Type	Parameters	Values and Units
Solar Module	SunPower E20-327	Rated power	327Wp
		Rated voltage (Vmpp)	54.7V
		Rated current (Impp)	5.98A
		Short circuit current (Isc)	6.46A
		Open circuit voltage (Voc)	64.9V
		Dimension	1.558x1.046m
		Efficiency	20.4%
		Battery	Lead acid Trojan SAGM 12 205
Capacity	219Ah		
Roundtrip efficiency	85%		
Maximum charging current	41A		
Maximum discharge current	300A		
Inverter	MTP-4110F,3phase hybrid.		
		AC input frequency	50/60Hz \pm 3Hz
		AC output frequency	50/60Hz \pm 0.01%
		AC output voltage	380/400/415V(L-L), 220/230/240V(L-N)
		Efficiency	96%
		Charge Controller	SOLARCON SCM-360400
Maximum current	400A		
Vmp of PV	255-330Vdc		
Output DC voltage	360V		
Efficiency	98%		

The schematic diagram including all the components which were used for simulation in HOMER Pro is shown in Figure 3.5.

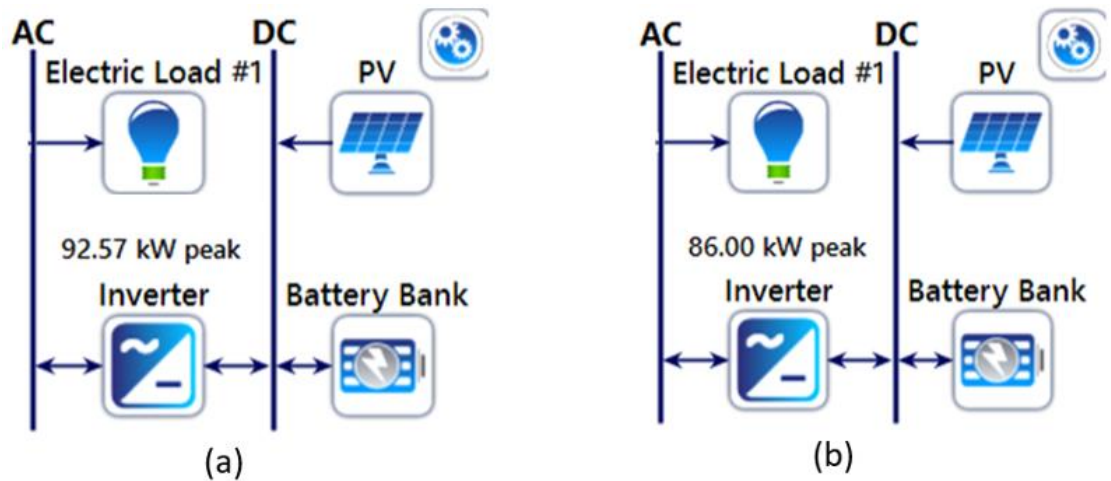


Figure 3.5: Schematic Diagram Designed with HOMER Pro for Simulation: (a) Margaret Thatcher Library and (b) Administration Building

3.4.6 Economic parameters

According to the Central Bank of Kenya, the current discount rate is 7.5% and the inflation rate is estimated to remain at an average of 7.1% in 2022 (Central Bank of Kenya, 2022). In this simulation, 12% was used for both discount and inflation rates to consider worst case scenarios.

The main economic matrices used in evaluating the economic feasibility of the project were the Net Present Cost (NPC) and the Levelized Cost of Energy (LCOE). The total NPC is the present value of all the cost incurred by the system over its lifetime (which include capital costs, replacement costs, O&M costs, fuel costs, emissions penalties, and the costs of buying power from the grid) minus the present value of all revenue earned over the lifetime (which include salvage value and grid sales revenue). HOMER calculates the LCOE using equation (3.2) (Adaramola et al., 2017).

$$LCOE = \frac{C_a - C_b H_s}{E_s} \dots \dots \dots 3.2$$

Where C_a is the total annualized cost of the system (Ksh/Year), C_b is the boiler marginal cost (Ksh/kWh), H_s is the total thermal load served (kWh/year) and for PV systems that do not serve any thermal loads, H_s is zero. E_s is the total electrical load served (kWh/year). C_a is calculated in HOMER using equation (3.3) (Rohani & Nour, 2014)(Eze et al., 2022).

$$C_a = CRF \cdot C_{NPC} \dots\dots\dots 3.3$$

$$CRF = \frac{i(1+i)^n}{(1+i)^n - 1} \dots\dots\dots 3.4$$

Where C_{NPC} is the total NPC, i is the annual real discount rate (%), n is the number of years (project lifetime), CRF is the capital recovery factor. The real discount rate i is calculated in HOMER using equation (3.5).

$$i = \frac{r-f}{1+f} \dots\dots\dots 3.5$$

Where r is the nominal discount rate which is the rate at which money can be borrowed and f is the inflation rate.

3.5 MPPT Technique Used

The Perturbed and Observe (P&O) MPPT techniques was used to harvest maximum power from the PV system. This method was chosen because of its less complex computational ability, making the tracking system cost effective as compared to other tracking methods. In addition to that, a PID controller which was tuned using Genetic Algorithms (GA) was incorporated to the system to reduce the settling time and minimize the oscillations around the maximum power point. The flow chart for the MPPT technique is shown in Figure 3.6.

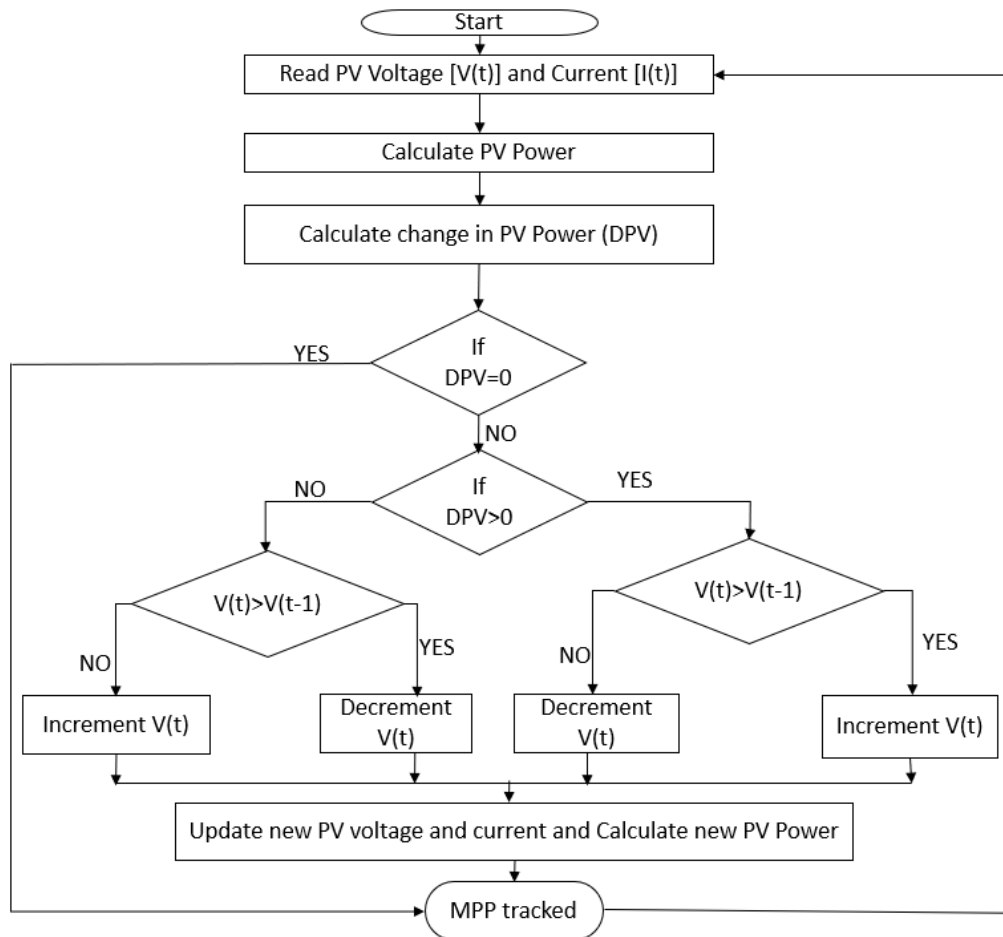


Figure 3.6: Flow chart of the P&O method (Bollipo et al., 2020)

As depicted by the flow chart of Figure 3.6, the tracking of the maximum power point is done as follows. Firstly, the system measures the PV voltage at a given instant $[V(t)]$ and the PV current at a given instant $[I(t)]$. The PV power at that instant is then calculated by multiplying the PV voltage and the PV current. This calculated power is then compared with the actual PV power that was supposed to be generated based on the available solar radiation. If the change in power is zero, it means the measured power is the actual maximum power generated. This will cause the control algorithm to end and goes back to measure the PV voltage and current.

If the measured PV power is different from zero and positive, the control algorithm then compares the measured PV voltage $V(t)$ to its previous value $V(t-1)$. If the measured

PV voltage is greater than its previous value, then the algorithm increments $V(t)$. If the measured PV voltage is less than its previous value, then the algorithm decrements $V(t)$.

On the other hand, if the change in power is less than zero, the control algorithm then compares the measured PV voltage $V(t)$ to its previous value $V(t-1)$. If the measured PV voltage is greater than its previous value, then the algorithm decrements $V(t)$. If the measured PV voltage is less than its previous value, then the algorithm increments $V(t)$.

This process is repeated until the maximum power point is tracked.

3.6 Tuning of the PID controllers Using Genetic Algorithms

In the tuning of the PID controllers in the system to fine the optimal controller gains for effective MPPT and optimal charging and discharging of the battery, we used Genetic Algorithms (GA). Effectively charging and discharging of batteries enable them to last longer and harvesting more power from the sun improves the overall system efficiency. The step-by-step GA approach used in finding the optimal controller gains is explained below as shown in Figure 3.7.

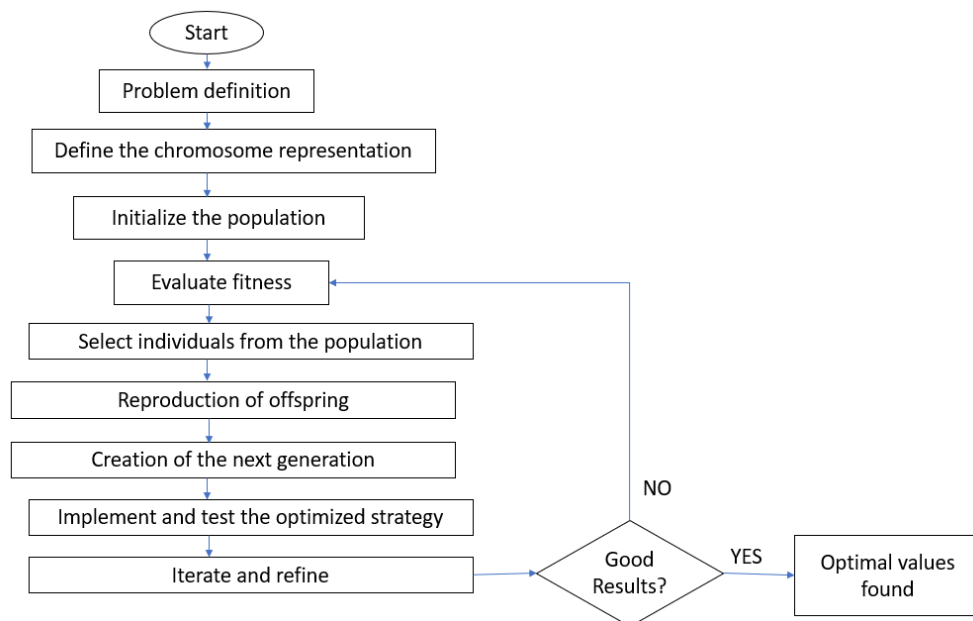


Figure 3.7: Flowchart for optimization using GA

Firstly, the problem was defined which was to optimize the controller gains K_p (proportional gain), K_I (integral gain), and K_d (derivative gain).

The objective function which was used is the Integral Absolute Error (IAE) between the input solar PV voltage (V) and the reference voltage (V_{ref}). This objective function (e) is shown in equation (3.6) (Hassan et al., 2019). This is because the output voltage from the PV module is the main functional parameter to determine the duty cycle at which the boost converter is switched.

$$\text{minimize } e = \int_0^t |V - V_{ref}| dt \dots \dots \dots 3.6$$

The minimum value of the error signal was obtained at all times which was used to generate the pulse width modulation signal to control the boost converter for maximum power point tracking.

The algorithm begins with an initial random population which was 100 for this optimization. The algorithm then creates a sequence of new populations. At each step, the algorithm uses the individuals in the current generation to create the next population. To create the new population, the algorithm performs the following steps: scores each member of the current population by computing its fitness value. These values are called the raw fitness scores. Scales the raw fitness scores to convert them into a more usable range of values. These scaled values are called expectation values. Selects members from the population called parents and the selection method used in this work is the Roulette Wheel which uses the fitness values of the population to select the parents. Some of the individuals in the current population that have lower fitness are chosen as elite. These elite individuals are passed to the next population. The parents then produce offsprings either by making random changes to a single parent known as mutation or by combining the vector entries of a pair of parents which is crossover and,

in this case, the uniform crossover was used because it randomly selects chromosomes from both parents to produce offsprings. Once the offsprings are produced, the current population is replaced with the offsprings to form the next generation. The algorithm stops when one of the stopping criteria is met which in this case was the maximum number of generations which was 25.

3.7 Modelling of the Solar/Battery Hybrid System in MATLAB

The solar/battery system was modelled using SIMULINK in MATLAB. This is because the Simulink library in MATLAB contains built-in blocks of solar modules, controllers, and other function blocks which can be configured to meet system requirements. In addition to that, MATLAB/ Simulink has also been used for similar research as seen in the literature to perform energy system modelling and to model MPPT controllers. The configuration of the system is as shown.

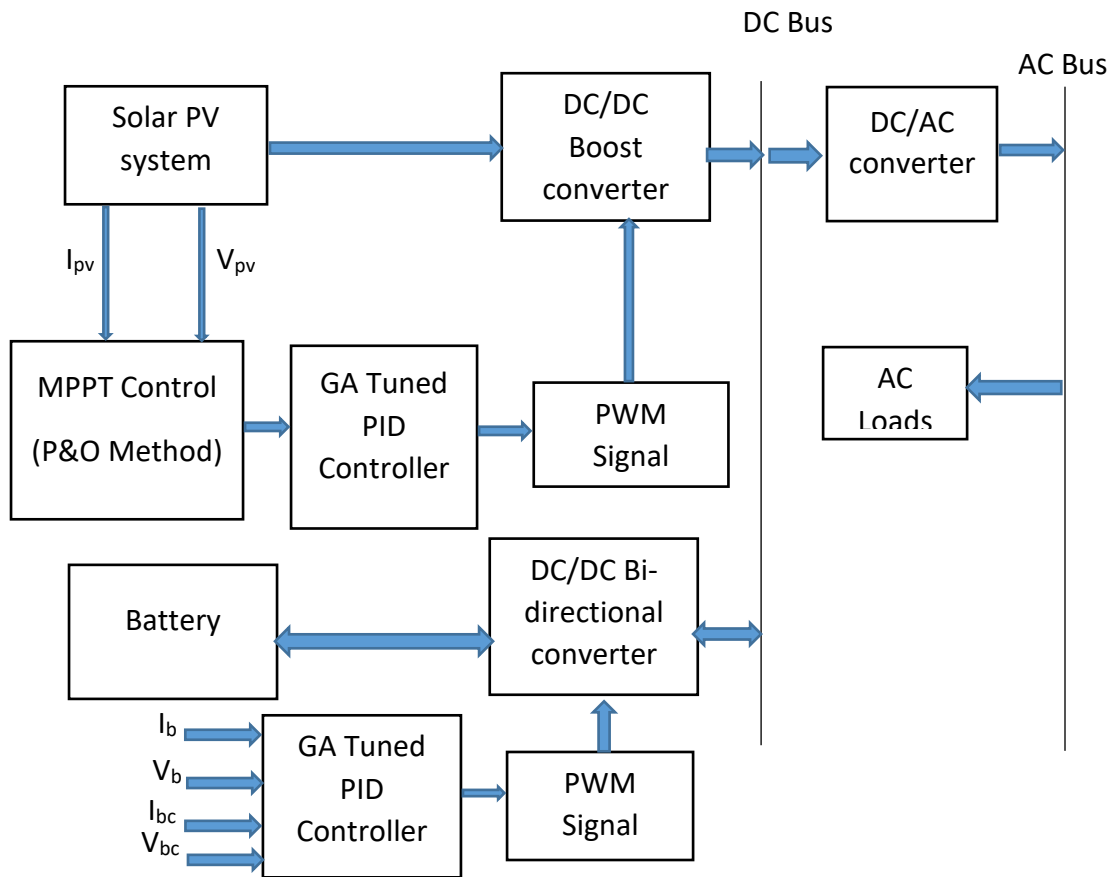


Figure 3.8: MATLAB simulation block diagram

I_{pv} is the PV current, V_{pv} is the PV voltage, I_b is the battery current, V_b is the battery voltage, I_{bc} is the battery charging current, V_{bc} is the battery charging voltage.

To perform the MPPT, a boost converter was used to control the output voltage from the PV module. Also, a bidirectional converter was used for the charging and discharging processes of the battery. The MATLAB/Simulink model for MPPT is shown in Figure 3.9. The Simulink models for the power inverter and the battery system are respectively shown in Appendix F and Appendix G. The MATLAB Function block contains the P&O algorithm used for the MPPT. The main parameters of interest used are the PV voltage and the PV current. These two parameters are used to compute the available power of the PV system which is then compared with the actual PV power

that was supposed to be generated for a given solar radiation value. If the calculated value of power is not equal to the expected power to be generated by the system, the tracking algorithm begins. The algorithm performs the tracking using the PV voltage. Based on the difference between the measured voltage and the reference voltage (considered to be the open circuit voltage of the PV system), an error signal is generated. This error signal is optimized by the GA to ensure that the minimum possible error is sent to the PID controller. This controller then generates an appropriate pulse width modulation (PWM) signal which drives the boost converter to track the maximum available power. The tracking process is repeated until the MPP for the PV system is found.

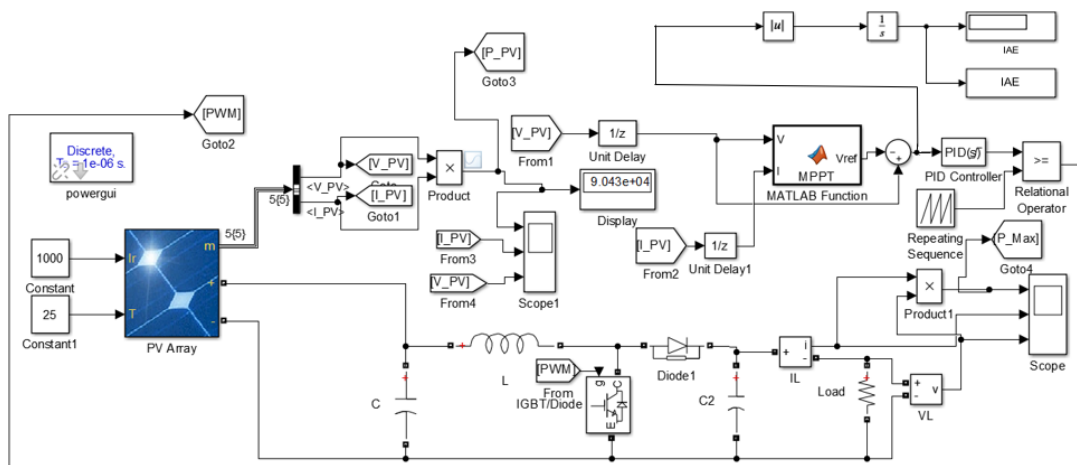


Figure 3.9: MATLAB/Simulink model for MPPT control strategy

3.8 Conclusion

In this chapter, the different methods used for data collection and design of the system have been presented in detail. The software tools selected for the simulation of the system have also been presented. In addition to that, the GA methodology adopted for the tuning of the controllers for MPPT and battery charging/discharging has been explained. The results will then be presented and discussed in the proceeding chapter.

CHAPTER FOUR: RESULTS AND DISCUSSION

This chapter presents and discusses the results obtained. It has been done following the specific objectives which were outlined in Chapter 1. The results and discussion have been combined in the same chapter to ease the flow of information as each result is presented and discussed immediately. Firstly, the results on the solar radiation, temperature, and power consumption are presented and discussed. This is followed by the results for the system model in Homer Pro, the results of the MPPT, and the results of the charge and discharge of the batteries.

4.1 Daily Solar Radiation

The average monthly observed solar radiation on the horizontal surface at Moi University main campus in Eldoret is shown on Figure 4.1. The maximum solar radiation of 5.7 kWh/m²/day occurred in the month of February while the lowest solar radiation of 4.03 kWh/m²/day occurred in the month of July with the average annual solar radiation of 4.93 kWh/m²/day at this site, which is approximately 5 hours of daily sunshine. This is a good capacity to be exploited for solar PV energy generation. Also, the site-specific data and the data collected from the National Aeronautics and Space Administration (NASA) database are plotted. From these two data sets, the month with the highest radiation remains February (6.71 kWh/m²/day as per NASA data) and the lowest month remains July (5.10 kWh/m²/day as per NASA data). In addition to that, the annual average solar radiation for this site according to NASA is 5.90 kWh/m²/day. The two annual averages differ from each other by 0.97 kWh/m²/day. This difference is because the data provided by NASA covers a very large geographic area as opposed to the data which was measured on site. The clearness index on the other hand is a measure of how bright or cloudy the sky is. It varies between zero and one with zero meaning a completely cloudy sky and one meaning a perfectly sunny day. It should be

noted that, site specific data is always advantageous to be used when dealing with solar PV installations.

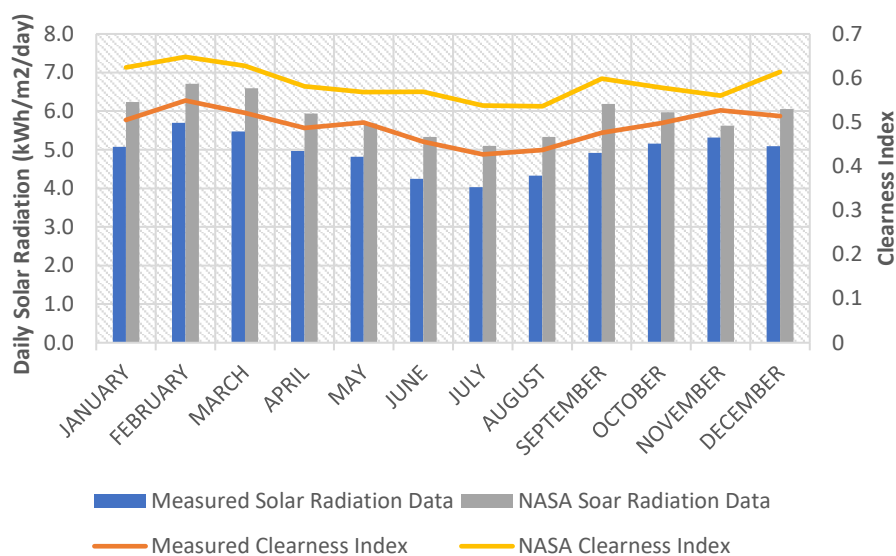


Figure 4.1: Solar radiation

4.2 Daily Temperature Variation

The average monthly temperatures were analyzed and the results showed that the hottest month is February with an average monthly temperature of 18°C while the coldest month is July with an average monthly temperature of 15°C as shown in Figure 4.2. This means that solar panels installed within this site will perform much better as external cooling systems will not be needed for cooling of the solar panels. Cooling of solar panels is often needed because temperature has an effect on the output power of solar modules. For the solar panel that was selected for the simulations, the operating temperature is 45°C and the power temperature coefficient is -0.38 %/°C. This power temperature coefficient is calculated based on the industry standard test conditions used to characterize solar panels which is 25°C. For every degree rise in temperature above 25°C, the solar panels output will drop by that specified power temperature value. In this work, because the temperature collected on site showed that the temperatures will barely go above 25°C, the simulations were done using the industry standard value.

Furthermore, the temperature collected on site was compared with the National Aeronautics and Space Administration (NASA) data. The results showed a slight variation of about 3°C. This is because the temperature found on the NASA database for a particular location covers a broader area. This is why it is always important to collect site specific data when designing solar PV systems.

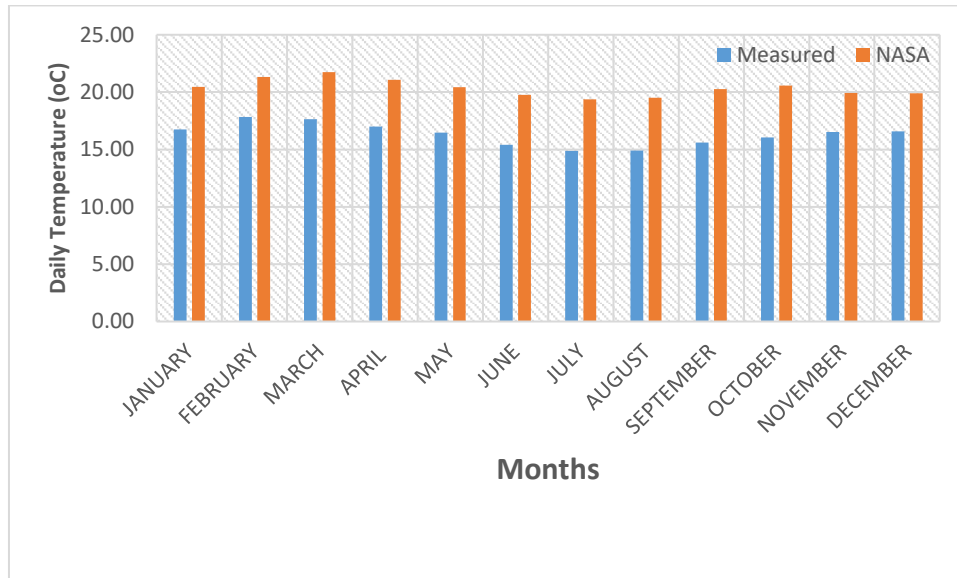


Figure 4.2: Average monthly temperature variation in the study site

4.3 Load Profile for the Administrative Building

The average peak and base loads demand for the Administrative building were respectively 64kW and 30kW. The average consumption during weekdays (Mondays to Fridays) was 41kW while the average consumptions on Saturdays and Sundays were 28kW and 25kW respectively. The overall average weekly load was 37kW. Also, because the load varies randomly during the day, random variability constants of 4% for day-to-day and 4% time-step were used for simulations because the loads does not vary much each day as could be seen from the data collected for different days. Due to these variability constants, the peak load increased to 86 kW as determined by the HOMER software. Furthermore, during weekends, the power demand for this building

is low with a peak value of 31 kW on Saturday as shown on Figure 4.3. This means that most of the energy generated during the day on Saturdays and Sundays will be sold to the grid.

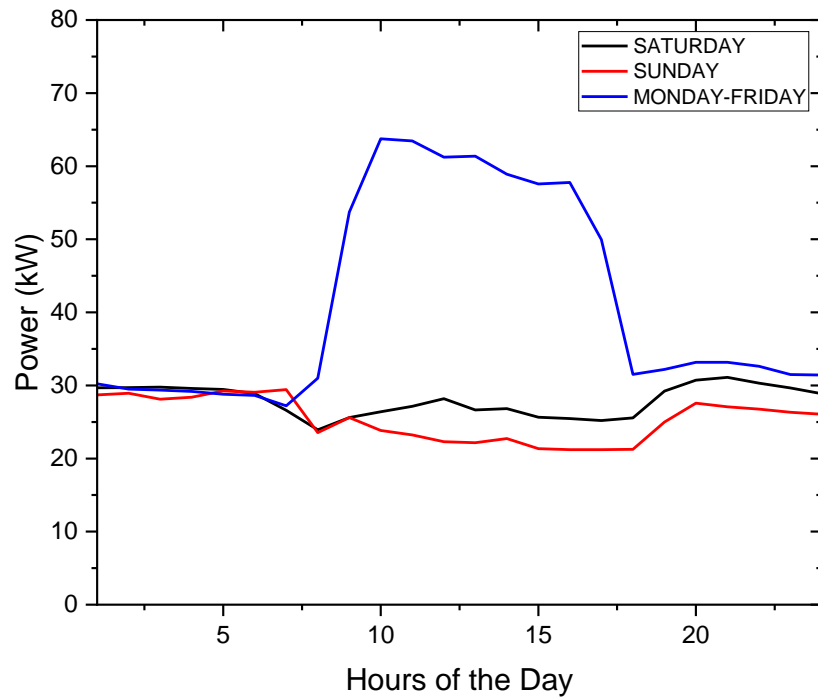


Figure 4.3: Load Profile for the Administration Block

4.4 Load profile for the Margaret Thatcher Library

The results depicted on Figure 4.4 shows that the power consumption in the library is higher than that of the Administration block on weekdays and on weekends.

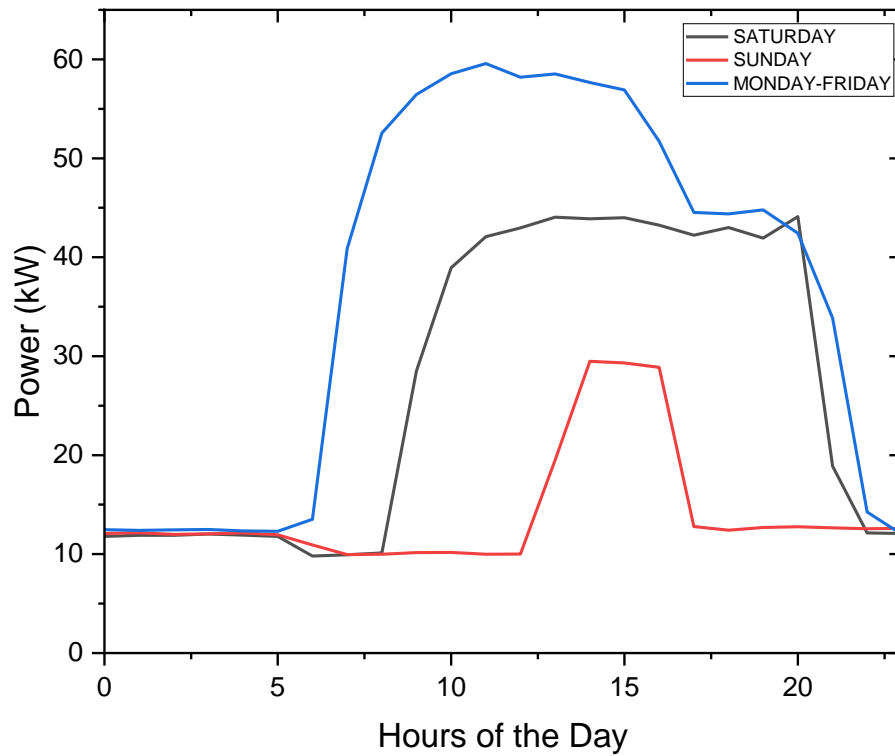


Figure 4.4: Load Demand Profile for Library

A combination of factors relating to working hours and user activity account for the excessive power consumption that was found in the library on weekdays from 7 am to 9 pm. This is the time when the library usually welcomes visitors. As a result, the library is open from 7 am to 9 pm, during which time lighting, computers, and other electrical devices are used to serve users and support their activities. Users, such as students, researchers, and staff members, are most active during this time period. They use lighting, plug-in electronic gadgets, and use computers as they read, study, research, and engage in other academic tasks. The combined effect of these activities results in higher power demand.

Furthermore, the annual load variation from the HOMER Pro simulation is shown in Figure 4.5. From the results, it shows that throughout the year, high power demand occurs during the day.

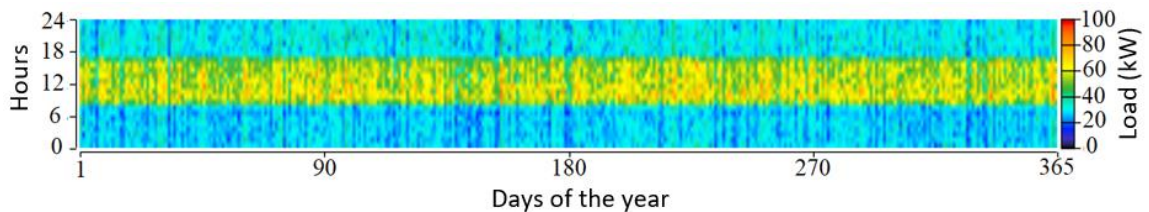


Figure 4.5: Yearly load profile for the Margaret Thatcher Library

4.5 Results for the simulation of a solar PV/Battery system using HOMER Pro

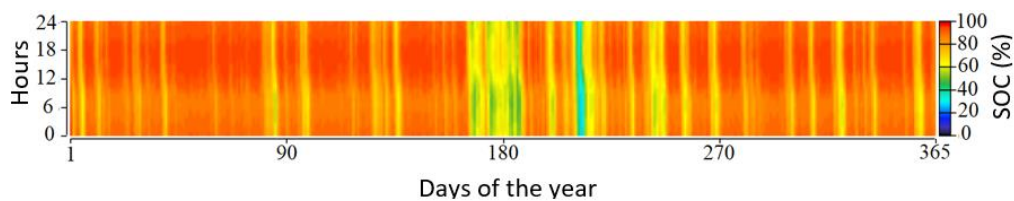


Figure 4.6: Battery State of Charge for the Margaret Thatcher Library

Figure 4.6 shows the charging spectrum for the batteries. From the figure, it shows that the batteries will always be charged between 80% to 100% for a greater part of the year. This means energy will always be available for use during hours of no sunlight. Also, the battery bank size was computed using the maximum energy consumption to ensure that the batteries are not drained during peak loads.

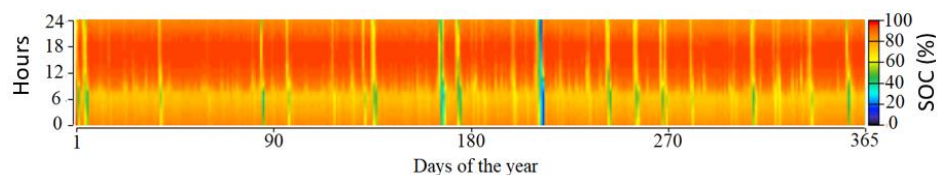


Figure 4.7: Battery state of charge for the Administration building

Similarly, the battery state of charge for the Administration building is shown in Figure 4.7. It shows that the solar PV system is providing enough energy to charge the batteries throughout the year. This is good as storage is an essential element in solar PV standalone systems. This shows that the loads will always be powered even during days with poor solar radiations.

Table 4.1 below gives a technical summary for the simulated solar PV/battery system.

Table 4.1: Technical summary of the solar PV/Battery system

SN	Parameter	Margaret Thatcher Library PV System	Administration building PV System	Total
1	Annual energy consumption	395,263 kWh	371,520 kWh	766,783 kWh
2	Average monthly energy consumption	32,938 kWh	30,960 kWh	63,898 kWh
3	Average daily energy consumption	1,098 kWh	1,032 kWh	2,130 kWh
4	Scaled Average daily peak demand	93 kW	86 kW	179 kW
5	System size	100 kW	90 kW	190 Kw
6	Power per PV module	327 W	327 W	-
7	Number of PV modules	306	276	582
8	Battery capacity	4,575 Ah	4,300 Ah	8,875 Ah

From the HOMER Pro simulations, the annual energy consumption for the Margaret Thatcher Library and the Administration building were respectively 395,263 kWh and 371,520 kWh, giving a total energy consumption of 766, 783 kWh. The average monthly energy consumptions were 32,938 kWh and 30,960 kWh while the average daily energy consumptions were 1,098 kWh and 1,032 kWh respectively for the two buildings.

In Table 4.2, the cost for installing and running the Solar PV/battery system is presented. This gives a total net present cost of 59,000,000 Ksh and a total replacement cost of 33,000,000 Ksh. The replacement cost is less than the net present cost because the life time of the system was 25 years which coincides with the life time of the solar PV modules. This means much replacement will be done for the batteries as they have a relatively short life span. Also, the total cost of the system gave 92,000,000 Ksh meanwhile the University spends 16,412,016 Ksh on utility bills for the two buildings annually. This means that the amount spent on installing the PV system can be recovered in 6 years using the simple Pay Back Period (PBP). Therefore, the system is economically beneficial for the University and it is strongly recommended to be implemented to save on annual utility bills.

Table 4.2: Economic summary of the solar PV/Battery systems

SN	Parameter	Margaret Thatcher Library PV System	Administration building PV System	Total
1	Capital expenditure	32,000,000 Ksh	27,000,000 Ksh	59,000,000 Ksh
3	Replacement cost	20,000,000 Ksh	13,000,000 Ksh	33,000,000 Ksh
3	Annual cost of energy from Utility bills	8,815,980 Ksh	7,596,036 Ksh	16,412,016 Ksh
4	Pay Back Period	6 years	6 years	-

4.6 Fitness Curves for the Tuning of the PID controllers Using Genetic Algorithms

Figures 4.8 and 4.9 respectively show the fitness curves for the tuning of the PID controllers, which are controlling the MPPT tracking process and the battery charging and discharging processes. Since the main objective for the optimization was to tune the PID controllers and obtain optimal proportional, integral and derivative gains which will give the smallest possible errors, the best fitness for the MPPT PID controller gave 86.5×10^{-4} while that for the battery charging PID controller gave 10.8×10^{-4} .

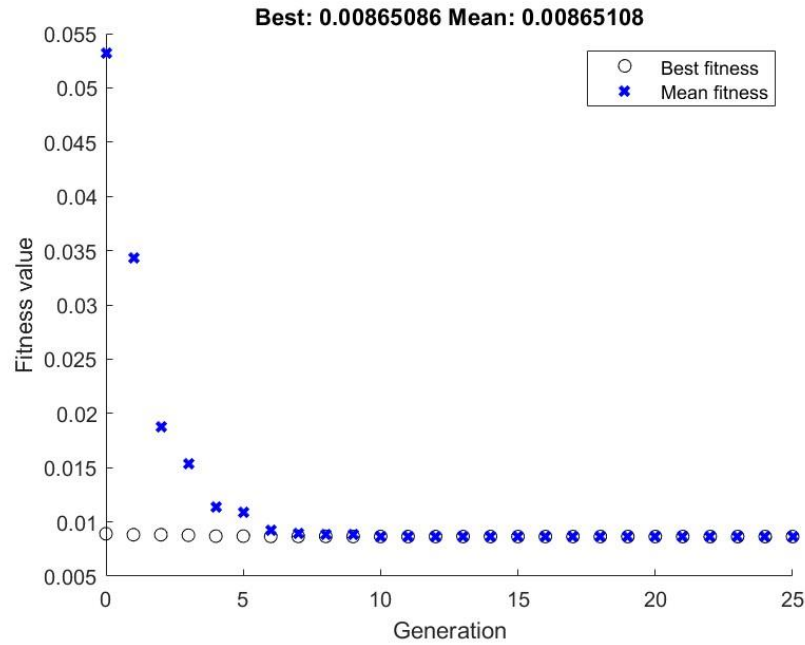


Figure 4.8: Fitness curve for MPPT PID controller

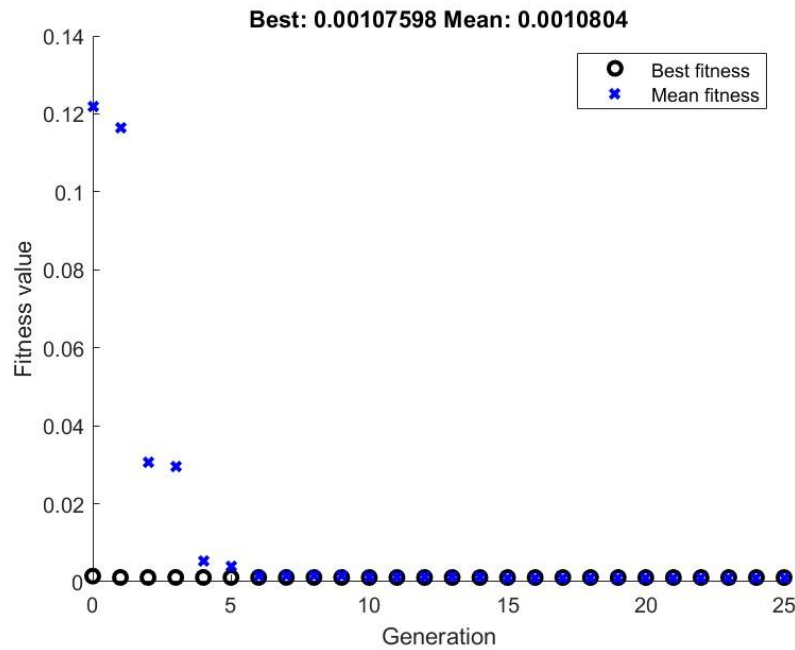


Figure 4.9: Fitness curve for Batter charging/Discharging PID controller

4.6 Results for the MPPT Tracking using MATLAB/Simulink

To evaluate the performance of the maximum power point tracking control strategy, the solar PV system incorporating the tracking algorithm was simulated in MATLAB/Simulink. The solar radiation was varied while maintaining the temperature

at 25°C. From the simulations, a settling time of 0.025 seconds was obtained. This time is smaller compared to that obtained by (Kolluru et al., 2018). The results are shown in Figure 4.10. Also, to test the effectiveness of the tracking system, the Ropp test was used as shown in Appendix H.

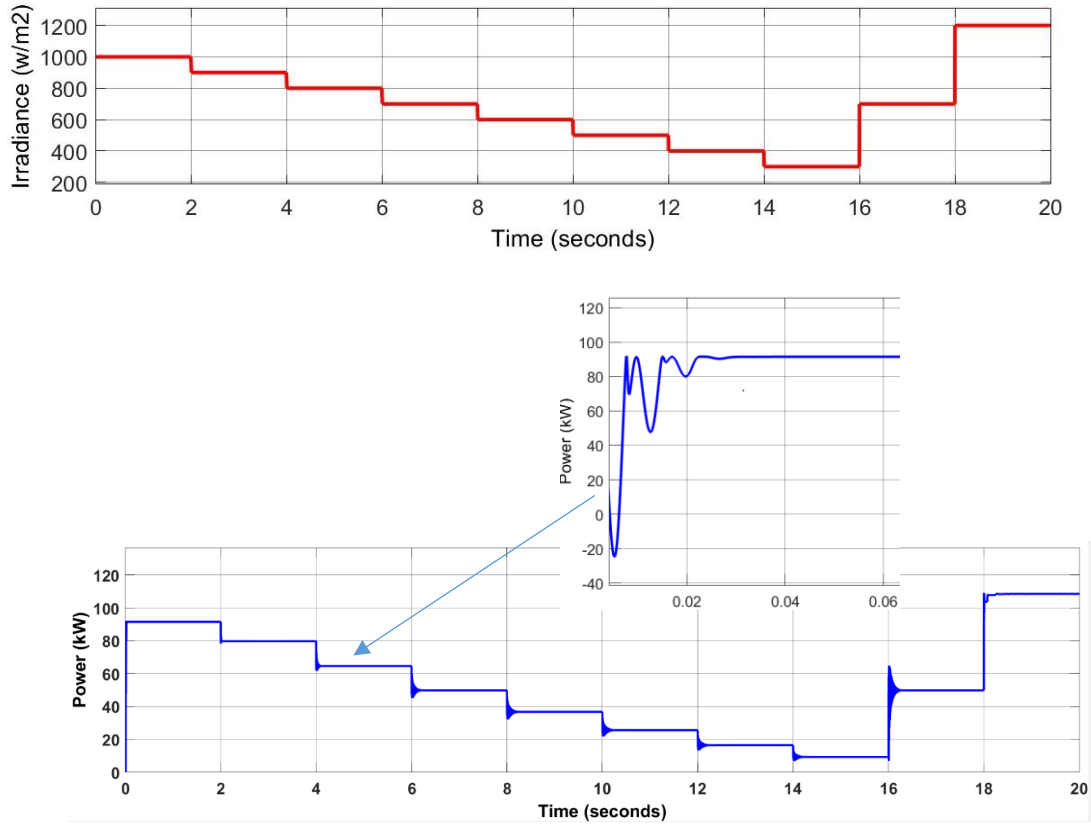


Figure 4.10: Tracking of Maximum Power Point

4.7 Results for the Optimization of the solar system performance and the battery charging/ discharging

The maximum power point tracking system was to determine its impact on the overall efficiency of the solar PV system. The output power was measured with and without the maximum power point tracker. The efficiency was calculated using the EN5030 European standard for converter efficiencies as shown in equation (4.1).

$$\eta = \frac{PV \text{ Power output measured}}{\text{Actual power the PV module could have produced}} \times 100 \dots\dots\dots 4.1$$

From the calculation, a tracking efficiency of 99.5% was obtained when the tracking control strategy was used as compared to 97.2% which was obtained without the tracking system. This means that while the Maximum power point tracking algorithm was implemented, the output power from the solar PV system increased compared to when no tracking algorithm was implemented. Figure 4.11 shows the output power of the solar PV system with and without the solar tracking system.

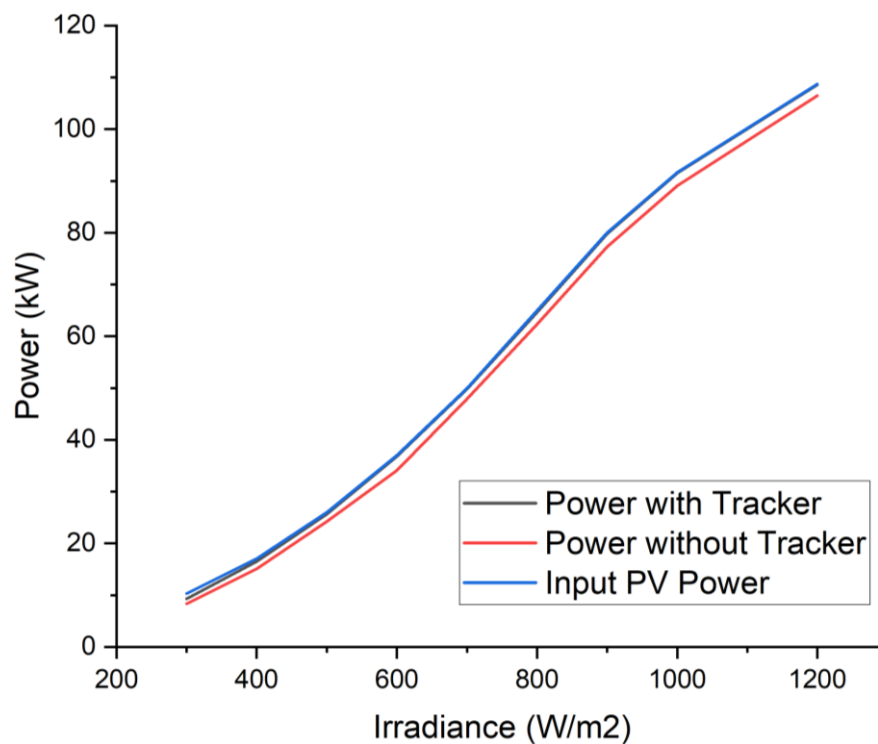


Figure 4.11: Power output of the solar PV system with and without the Maximum Power Point Tracker

These results show that the efficiency of solar PV systems can significantly be improved by making use of MPPT systems. These results are achieved because of the appropriate tuning of the PID controllers to have their optimal control gains using genetic algorithms.

In addition to the increased efficiency of the Solar PV system, the battery state of charge was also controlled such that the minimum stage of charge was 30%. This is because

the cycle life of batteries is limited by the number of charge and discharge cycles of the battery. Because lead acid batteries which were used in this work have a short cycle life, monitoring of the SOC is therefore important to enhance the overall cycle life of the battery. Figure 4.12 below shows the charging and discharging of the batteries. Initially, the battery state of charge (SOC) was considered to be 100%. The battery was then discharged to 30% and back to 100% as set by the controller.

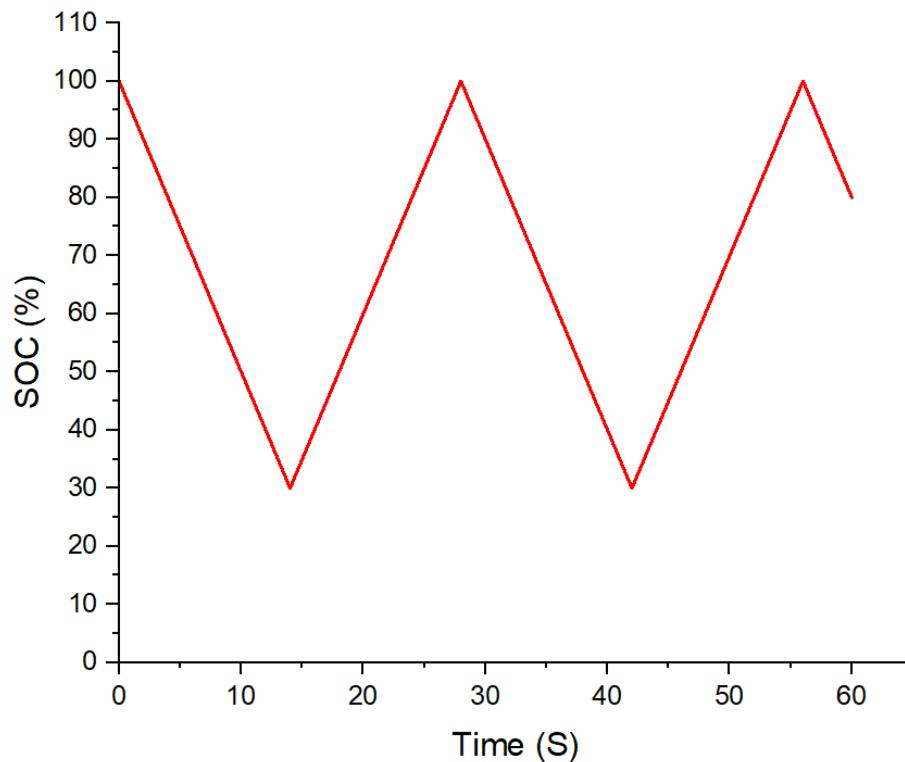


Figure 4.12: Battery State of Charge (SOC) Control

4.9 Output Three Phase Voltage Waveforms from The Inverter

From the simulations, the three phase voltages from the power inverter (Simulink model shown in Appendix F) as shown on Figure 4.13 were pure sine wave with a line voltage of 415 V as expected given that it is the nominal 3 phase voltage from the utility grid. This makes the inverter suitable for use even with sensitive loads.

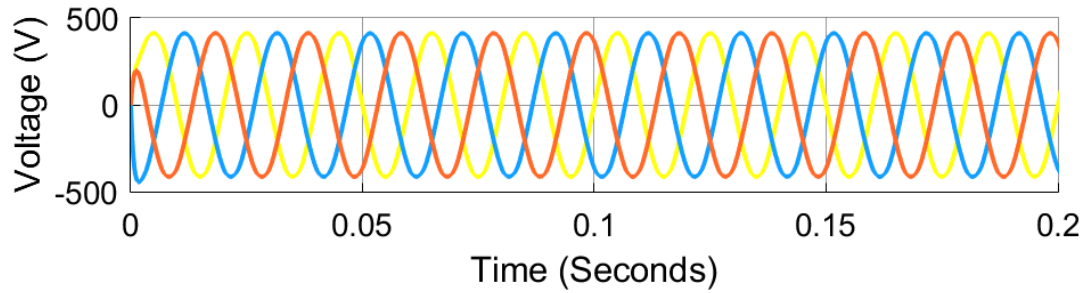


Figure 4.13: Three phase voltage waveforms from the inverter

4.10 Conclusion for Chapter 4

This chapter presents the results obtained from the simulations. It also discusses the research findings. Among the results are the power consumption for the two buildings which is the major achievement for the first objective, the HOMER simulation results which solves the second objective, the MATLAB/Simulink results for the MPPT and battery charging which solves the third objective, and the results for the tuning of the controllers using genetic algorithms enabling proper MPPT to optimize the PV system, and hence addressing the fourth objective.

CHAPTER FIVE: CONCLUSION, RECOMMENDATIONS, AND FUTURE PERSPECTIVES

5.1 Conclusion

Solar photovoltaic energy which is a promising clean energy source to facilitate energy access and decarbonize the ecosystem by replacing conventional fossil fuel-based power plants, requires more research to improve its efficiency. For this reason, the main objective of this research was to model and simulate a solar/battery hybrid energy system with a Maximum Power Point Tracking (MPPT) control strategy and to optimize the battery charging/discharging cycle life. The specific objectives were to: analyze the daily energy consumption within Moi University Administration building and Margaret Thatcher Library; model and simulate a solar/battery hybrid system using HOMER Pro; design and simulate a Maximum Power Point Tracking (MPPT) control strategy using MATLAB/Simulink; and optimize the solar system performance and the battery charging/discharging cycle life using Genetic Algorithms (GA).

To address the first specific objective of the work which was to analyze the daily energy consumption within Moi University Administration building and Margaret Thatcher Library, data was collected on site and the results showed that more energy is consumed by the Margaret Thatcher Library compared to the Administration Library between 6:00 PM and 9:00 PM. This is justified by the fact that during this period, students are studying in the library while little or no work is done within the Administration building.

In the second specific objective which was to model and simulate a solar/battery hybrid system using HOMER Pro, the solar PV/battery system for the two buildings was simulated using HOMER Pro. The results showed a system with an optimal solar PV

size of 90 kW to power the Administration Building and 100 kW to power the Margaret Thatcher Library. Also, the two systems had a short payback period, optimal power supply, and appropriate charging of the storage batteries which should be used to provide energy to the Administration building and the Margaret Thatcher Library.

In the third specific objective which was to design and simulate a Maximum Power Point Tracking (MPPT) control strategy using MATLAB/Simulink, a maximum power point tracker was designed and simulated using the Simulink library in MATLAB version 2022b. A tracking system having a settling time of 0.025 seconds and a tracking efficiency of 99.5% was obtained. This settling time was found to be shorter than that obtained from literature.

To optimize the solar system performance and the battery charging/discharging cycle life using Genetic Algorithms (GA) which was the last specific objective, the PID controller parameters in both the tracking system and the charging/discharging system for batteries were tune using GA. With this, optimal controller gains for the two systems were obtained. These optimal parameters were then used which contributed to the short settling time and higher tracking efficiency obtained for the solar PV system. This also enabled proper control for the charging and discharging processes for the batteries.

Conclusively, this study has addressed successfully the challenges linked with energy harvesting from solar photovoltaic systems for a reliable and continuous power supply, with a focus on the Administration building and Margaret Thatcher Library at Moi University. This study has shown that it is possible to maximize solar energy utilization while effectively managing energy storage by using a solar/battery hybrid energy system with a sophisticated Maximum Power Point Tracking (MPPT) control strategy and the optimization of battery charging/discharging cycles using Genetic Algorithms

(GA). Accurate system design and performance evaluation have been made possible by the use of on-site solar radiation and temperature data, as well as rigorous simulation methodologies using HOMER Pro and MATLAB/Simulink software tools. The outcomes show the economic viability of such hybrid systems by revealing the potential for significant cost savings and short payback periods. Additionally, the system's total efficiency has increased thanks to the integration of PID control and GA optimization, ensuring the batteries' prolonged cycle life. This research ultimately offers important insights that will help academic and other commercial institutions move toward more sustainable energy solutions as solar energy adoption and management tactics develop.

5.2 Recommendations

Hybrid solar system adoption is advised for Moi University and similar institutions based on the research's findings. These systems should include integrated Maximum Power Point Tracking (MPPT) control mechanisms. These systems can more efficiently harness solar energy, improve energy sustainability, and do so while spending less money on maintenance.

Academic institutions and other organizations should give priority to investments in renewable energy infrastructure in order to ease the energy transition in sub-Saharan Africa. This includes setting up solar power systems with improved designs to efficiently satisfy energy demands.

Given the significance of energy storage in solar systems, it is urged to conduct more research on cutting-edge battery technologies that have longer cycle lives and are more affordable. This will enhance overall system performance and assist in addressing the constraints of the available battery options.

It is important to continuously track data on solar radiation, temperature, and energy consumption trends to ensure the best possible performance of solar energy systems. Real-time maintenance and system changes will be possible.

Governments and organizations should aggressively support public awareness campaigns about the advantages of adopting solar energy. Also, public awareness and policy support is much needed. The energy transition can also be accelerated by supportive policies like incentives and subsidies for renewable energy projects.

5.3 Contributions

This study contributes to the area of solar energy adoption in academic institutions which is a good pathway towards having green campuses.

In the domain of control engineering, the study contributes by using an alternative method for tuning PID controllers by adopting metaheuristic genetic algorithm optimization technique, instead of the conventional approaches.

This work also contributes in the area of maximum power point tracking in PV systems by using a cost-effective and less complex approach to solve the problem of high settling time during maximum power point tracking.

In the area of energy storage, the study contributes in energy management in battery storage systems by continuously monitoring and keeping the battery state of charge within acceptable bounds to enhance battery life.

In addition, the work contributes in the area of data-driven design by using site specific data for the design of solar PV systems.

This work through its advocacy for renewable energy adoption aligns with sustainability goals and contributes to the reduction of greenhouse gas emissions, hence the fight against climate change and a more environmentally friendly energy landscape.

The research also contributes in the area of renewable energy system modelling through the use of software and simulations.

5.4 Further Research

To address the drawbacks of conventional batteries and further improve energy system efficiency, future research can examine the integration of other energy storage technologies, such as supercapacitors or sophisticated flywheel systems.

Researching the viability of microgrid systems on educational institutions or in other small, localized locations can be a worthwhile course of action in order to build self-sustaining energy ecosystems, this would include integrating several renewable energy sources, such as solar, wind, and possibly biomass.

As a result of how climate change affects solar energy production, future research may concentrate on creating technology and adaptive strategies to lessen the influence of shifting weather patterns on solar energy output.

Future research on predictive maintenance and energy optimization in solar systems may benefit from the application of artificial intelligence and machine learning techniques.

REFERENCES

- Aanstoos, T. A., Kajs, J. P., Brinkman, W. G., Liu, H. P., Ouroua, A., Hayes, R. J., Hearn, C., Sarjeant, J., & Gill, H. (2001). High voltage stator for a flywheel energy storage system. *IEEE Transactions on Magnetics*, 37(1), 242–247.
- Aardahl, C. L., & Rassat, S. D. (2009). Overview of systems considerations for on-board chemical hydrogen storage. *International Journal of Hydrogen Energy*, 34(16), 6676–6683.
- Abido, M. A., Khalid, M. S., & Worku, M. Y. (2015). An efficient ANFIS-based PI controller for maximum power point tracking of PV systems. *Arabian Journal for Science and Engineering*, 40(9), 2641–2651.
- Abu-Rub, H., Iqbal, A., & Ahmed, S. M. (2012). Adaptive neuro-fuzzy inference system-based maximum power point tracking of solar PV modules for fast varying solar radiations. *International Journal of Sustainable Energy*, 31(6), 383–398.
- Adaramola, M. S., Agelin-Chaab, M., & Paul, S. S. (2014). Analysis of hybrid energy systems for application in southern Ghana. *Energy Conversion and Management*, 88(2014), 284–295. <https://doi.org/10.1016/j.enconman.2014.08.029>
- Adaramola, M. S., Quansah, D. A., Agelin-Chaab, M., & Paul, S. S. (2017). Multipurpose renewable energy resources based hybrid energy system for remote community in northern Ghana. *Sustainable Energy Technologies and Assessments*, 22, 161–170. <https://doi.org/10.1016/j.seta.2017.02.011>
- Ahmad, J., Imran, M., Khalid, A., Iqbal, W., Ashraf, S. R., Adnan, M., Ali, S. F., & Khokhar, K. S. (2018). Techno economic analysis of a wind-photovoltaic-biomass hybrid renewable energy system for rural electrification: A case study of Kallar Kahar. *Energy*, 148, 208–234. <https://doi.org/10.1016/j.energy.2018.01.133>
- Ahmad, R., Murtaza, A. F., & Ahmed, H. (2019a). Power tracking techniques for efficient operation of photovoltaic array in solar applications – A review. *Renewable and Sustainable Energy Reviews*, 101, 82–102. <https://doi.org/10.1016/j.rser.2018.10.015>
- Ahmad, R., Murtaza, A. F., & Ahmed, H. (2019b). Power tracking techniques for efficient operation of photovoltaic array in solar applications – A review. *Renewable and Sustainable Energy Reviews*, 101, 82–102. <https://doi.org/10.1016/j.rser.2018.10.015>
- Alex, Z. (2005). Design of an Optimised PV System for a Remote Himalayan Village. ANZSES.
- Alghuwainem, S. M. (1994). Matching of a dc motor to a photovoltaic generator using a step-up converter with a current-locked loop. *IEEE Transactions on Energy Conversion*, 9(1), 192–198.

- Ali, A., Hasan, A. N., & Marwala, T. (2014). Perturb and observe based on fuzzy logic controller maximum power point tracking (MPPT). *2014 International Conference on Renewable Energy Research and Application (ICRERA)*, 406–411.
- Ali, A. I. M., & Mohamed, H. R. A. (2022). Improved P&O MPPT algorithm with efficient open-circuit voltage estimation for two-stage grid-integrated PV system under realistic solar radiation. *International Journal of Electrical Power & Energy Systems*, 137, 107805.
- Alik, R., Jusoh, A., & Sutikno, T. (2015). A review on perturb and observe maximum power point tracking in photovoltaic system. *TELKOMNIKA (Telecommunication Computing Electronics and Control)*, 13(3), 745–751.
- Al-Majidi, S. D., Abbod, M. F., & Al-Raweshidy, H. S. (2019). Design of an efficient maximum power point tracker based on ANFIS using an experimental photovoltaic system data. *Electronics*, 8(8), 858.
- Alshammari, N., & Asumadu, J. (2020). Optimum unit sizing of hybrid renewable energy system utilizing harmony search, Jaya and particle swarm optimization algorithms. *Sustainable Cities and Society*, 60(March), 102255. <https://doi.org/10.1016/j.scs.2020.102255>
- Alva, G., Lin, Y., & Fang, G. (2018). An overview of thermal energy storage systems. *Energy*, 144, 341–378.
- Amanor-Boadu, J. M., Guiseppi-Elie, A., & Sánchez-Sinencio, E. (2018). The impact of pulse charging parameters on the life cycle of lithium-ion polymer batteries. *Energies*, 11(8), 1–15. <https://doi.org/10.3390/en11082162>
- Amiriyar, M. E., & Pullen, K. R. (2017). A review of flywheel energy storage system technologies and their applications. *Applied Sciences*, 7(3), 286.
- An Li. (2015). *Analyse expérimentale et modélisation d ' éléments de batterie et de leurs assemblages : application aux véhicules électriques et hybrides*. L'UNIVERSITE CLAUDE BERNARD LYON 1.
- Anuphaphradorn, S., Sukchai, S., Sirisamphanwong, C., & Ketjoy, N. (2014). Comparison the economic analysis of the battery between lithium-ion and lead-acid in PV stand-alone application. *Energy Procedia*, 56, 352–358. <https://doi.org/10.1016/j.egypro.2014.07.167>
- Asian Development Bank. (2018). *Handbook on Battery Energy Storage System* (Issue December).
- Avila, E., Pozo, N., Pozo, M., Salazar, G., & Domínguez, X. (2017). Improved particle swarm optimization based MPPT for PV systems under Partial Shading Conditions. *2017 IEEE Southern Power Electronics Conference (SPEC)*, 1–6.

- Aziz, A. S., bin Tajuddin, M. F. N., bin Adzman, M. R., & Ramli, M. A. M. (2018). Feasibility analysis of PV/diesel/battery hybrid energy system using multi-year module. *International Journal of Renewable Energy Research*, 8(4), 1980–1993.
- Aziz, A. S., Tajuddin, M. F. N., Adzman, M. R., Azmi, A., & Ramli, M. A. M. (2019). Optimization and sensitivity analysis of standalone hybrid energy systems for rural electrification: A case study of Iraq. *Renewable Energy*, 138, 775–792. <https://doi.org/10.1016/j.renene.2019.02.004>
- Bagher, A. M., Vahid, M. M. A., & Mohsen, M. (2015). Types of solar cells and application. *American Journal of Optics and Photonics*, 3(5), 94–113.
- Bagheri, M., Shirzadi, N., Bazdar, E., & Kennedy, C. A. (2018). Optimal planning of hybrid renewable energy infrastructure for urban sustainability: Green Vancouver. *Renewable and Sustainable Energy Reviews*, 95(July), 254–264. <https://doi.org/10.1016/j.rser.2018.07.037>
- Balachander, K., Suresh Kumar, G., Mathankumar, M., Manjunathan, A., & Chinnapparaj, S. (2020). Optimization in design of hybrid electric power network using HOMER. *Materials Today: Proceedings*, xxxx. <https://doi.org/10.1016/j.matpr.2020.08.318>
- Barelli, L., Bidini, G., Bonucci, F., Castellini, L., Fratini, A., Gallorini, F., & Zuccari, A. (2019). Flywheel hybridization to improve battery life in energy storage systems coupled to RES plants. *Energy*, 173, 937–950.
- BATTERY-University. (2021a). *BU-201: How does the Lead Acid Battery Work?* https://batteryuniversity.com/learn/article/lead_based_batteries
- BATTERY-University. (2021b). *How does the flow battery work?* https://batteryuniversity.com/learn/article/bu_210b_flow_battery
- Behl, R. K., Chhibar, R. N., Jain, S., Bahl, V. P., & Bassam, N. El. (2012). Renewable energy sources and their applications. *Proceedings of the International Conference on Renewable Energy for Institutes and Communities in Urban and Rural Settings*, 27–29.
- Belhachat, F., & Larbes, C. (2017). Global maximum power point tracking based on ANFIS approach for PV array configurations under partial shading conditions. *Renewable and Sustainable Energy Reviews*, 77, 875–889.
- Bellar, M. D., Wu, T.-S., Tchamdjou, A., Mahdavi, J., & Ehsani, M. (1998). A review of soft-switched DC-AC converters. *IEEE Transactions on Industry Applications*, 34(4), 847–860.
- Bendib, B., Belmili, H., & Krim, F. (2015a). A survey of the most used MPPT methods: Conventional and advanced algorithms applied for photovoltaic systems. *Renewable and Sustainable Energy Reviews*, 45, 637–648. <https://doi.org/10.1016/j.rser.2015.02.009>

- Bendib, B., Belmili, H., & Krim, F. (2015b). A survey of the most used MPPT methods: Conventional and advanced algorithms applied for photovoltaic systems. *Renewable and Sustainable Energy Reviews*, 45, 637–648. <https://doi.org/10.1016/j.rser.2015.02.009>
- Bentouba, S., & Bourouis, M. (2016). Feasibility study of a wind-photovoltaic hybrid power generation system for a remote area in the extreme south of Algeria. *Applied Thermal Engineering*, 99, 713–719. <https://doi.org/10.1016/j.applthermaleng.2015.12.014>
- Bhandari, B., Lee, K. T., Lee, C. S., Song, C. K., Maskey, R. K., & Ahn, S. H. (2014). A novel off-grid hybrid power system comprised of solar photovoltaic, wind, and hydro energy sources. *Applied Energy*, 133, 236–242. <https://doi.org/10.1016/j.apenergy.2014.07.033>
- Bollipo, R. B., Mikkili, S., & Bonthagorla, P. K. (2020). Hybrid, Optimization, Intelligent and Classical PV MPPT Techniques : Review. *CSEE Journal of Power and Energy Systems*, 5(1). <https://doi.org/10.17775/CSEEJ PES.2019.02720>
- Bose, B. K. (2010). Global warming: Energy, environmental pollution, and the impact of power electronics. *IEEE Industrial Electronics Magazine*, 4(1), 6–17. <https://doi.org/10.1109/MIE.2010.935860>
- Bose, B. K. (2013). Global energy scenario and impact of power electronics in 21st century. *IEEE Transactions on Industrial Electronics*, 60(7), 2638–2651. <https://doi.org/10.1109/TIE.2012.2203771>
- Bounechba, H., Bouzid, A., Nabti, K., & Benalla, H. (2014). Comparison of Perturb & Observe and Fuzzy Logic in Maximum Power Point Tracker for PV Systems. *Energy Procedia*, 50, 677–684. <https://doi.org/10.1016/j.egypro.2014.06.083>
- Bragard, M., Soltau, N., Thomas, S., & De Doncker, R. W. (2010). The balance of renewable sources and user demands in grids: Power electronics for modular battery energy storage systems. *IEEE Transactions on Power Electronics*, 25(12), 3049–3056. <https://doi.org/10.1109/TPEL.2010.2085455>
- Buckles, W., & Hassenzahl, W. V. (2000). Superconducting magnetic energy storage. *IEEE Power Engineering Review*, 20(5), 16–20.
- Budt, M., Wolf, D., Span, R., & Yan, J. (2016). A review on compressed air energy storage: Basic principles, past milestones and recent developments. *Applied Energy*, 170, 250–268.
- Burke, A. (2007). R&D considerations for the performance and application of electrochemical capacitors. *Electrochimica Acta*, 53(3), 1083–1091.
- Cano, A., Arévalo, P., & Jurado, F. (2020). Energy analysis and techno-economic assessment of a hybrid PV/HKT/BAT system using biomass gasifier: Cuenca-Ecuador case study. *Energy*, 202. <https://doi.org/10.1016/j.energy.2020.117727>

- Carrillo, C., Feijóo, A., & Cidrás, J. (2009). Comparative study of flywheel systems in an isolated wind plant. *Renewable Energy*, 34(3), 890–898.
- Castro, A. De, Zumel, P., García, O., Riesgo, T., Uceda, J., & Member, S. (2003). *Concurrent and Simple Digital Controller of an AC/DC Converter With Power Factor Correction Based on an FPGA*. 18(1), 334–343.
- Central Bank of Kenya. (2022). <https://www.centralbank.go.ke/>
- Chang, W.-Y. (2013). The state of charge estimating methods for battery: A review. *International Scholarly Research Notices*, 2013.
- Chauhan, A., & Saini, R. P. (2014). A review on Integrated Renewable Energy System based power generation for stand-alone applications: Configurations, storage options, sizing methodologies and control. *Renewable and Sustainable Energy Reviews*, 38, 99–120.
- Chen, H., Cong, T. N., Yang, W., Tan, C., Li, Y., & Ding, Y. (2009a). Progress in electrical energy storage system: A critical review. *Progress in Natural Science*, 19(3), 291–312.
- Chen, H., Cong, T. N., Yang, W., Tan, C., Li, Y., & Ding, Y. (2009b). Progress in electrical energy storage system: A critical review. *Progress in Natural Science*, 19(3), 291–312.
- Chen, P.-C., Chen, P.-Y., Liu, Y.-H., Chen, J.-H., & Luo, Y.-F. (2015). A comparative study on maximum power point tracking techniques for photovoltaic generation systems operating under fast changing environments. *Solar Energy*, 119, 261–276.
- Cherukuri, S. K., & Rayapudi, S. R. (2017). Enhanced grey wolf optimizer based MPPT algorithm of PV system under partial shaded condition. *International Journal of Renewable Energy Development*, 6(3), 203.
- Chowdhury, S. R., & Saha, H. (2010). Maximum power point tracking of partially shaded solar photovoltaic arrays. *Solar Energy Materials and Solar Cells*, 94(9), 1441–1447.
- Chung, J., Sukumaran, S., Hlebnikov, A., & Volkova, A. (2023). Design and Development of a Conceptual Solar Energy Laboratory for District Heating Applications. *Solar*, 3(3), 504–521.
- Ci, S., Lin, N., & Wu, D. (2016). Reconfigurable Battery Techniques and Systems: A Survey. *IEEE Access*, 4, 1175–1189. <https://doi.org/10.1109/ACCESS.2016.2545338>
- Corbus, D., & Bergey, M. (1997). *Costa de Cocos 11-kW wind-diesel hybrid system*. National Renewable Energy Lab., Golden, CO (United States).

- Cristóbal-Monreal, I. R., & Dufo-López, R. (2016). Optimisation of photovoltaic-diesel-battery stand-alone systems minimising system weight. *Energy Conversion and Management*, 119, 279–288. <https://doi.org/10.1016/j.enconman.2016.04.050>
- Crompton, T. R. (1996). Battery reference book. In *Fuel and Energy Abstracts* (Third Edit, Vol. 37, Issue 3). Newnes. [https://doi.org/10.1016/0140-6701\(96\)88678-4](https://doi.org/10.1016/0140-6701(96)88678-4)
- Cuesta, M. A., Castillo-Calzadilla, T., & Borges, C. E. (2020). A critical analysis on hybrid renewable energy modeling tools: An emerging opportunity to include social indicators to optimise systems in small communities. *Renewable and Sustainable Energy Reviews*, 122(December 2019), 109691. <https://doi.org/10.1016/j.rser.2019.109691>
- da Rocha, M. V., Sampaio, L. P., & da Silva, S. A. O. (2020). Comparative analysis of MPPT algorithms based on Bat algorithm for PV systems under partial shading condition. *Sustainable Energy Technologies and Assessments*, 40, 100761. <https://doi.org/https://doi.org/10.1016/j.seta.2020.100761>
- Daniel W. Hart. (2011). *Power Electronics*. McGraw-Hill.
- Das, C. K., Bass, O., Kothapalli, G., Mahmoud, T. S., & Habibi, D. (2018). Overview of energy storage systems in distribution networks: Placement, sizing, operation, and power quality. *Renewable and Sustainable Energy Reviews*, 91(November 2016), 1205–1230. <https://doi.org/10.1016/j.rser.2018.03.068>
- Das, S., Ray, A., & De, S. (2020). Optimum combination of renewable resources to meet local power demand in distributed generation: A case study for a remote place of India. *Energy*, 209, 118473. <https://doi.org/10.1016/j.energy.2020.118473>
- De Brito, M. A. G., Galotto, L., Sampaio, L. P., De Azevedo Melo, G., & Canesin, C. A. (2013). Evaluation of the main MPPT techniques for photovoltaic applications. *IEEE Transactions on Industrial Electronics*, 60(3), 1156–1167. <https://doi.org/10.1109/TIE.2012.2198036>
- Diab, A. A. Z., & Rezk, H. (2019). Optimal sizing and placement of capacitors in radial distribution systems based on grey wolf, dragonfly and moth-flame optimization algorithms. *Iranian Journal of Science and Technology, Transactions of Electrical Engineering*, 43(1), 77–96.
- Drouilhet, S. M. (1999). Power Flow Management in a High Penetration Wind-Diesel Hybrid Power System with Short-Term Energy Storage. *Windpower '99, July*, 1–10.
- EHS. (n.d.). *Lead acid batteries-Environmental Health and Safety*. Concordia University; Concordia University. https://www.concordia.ca/content/dam/concordia/services/safety/docs/EHS-DOC-146_LeadAcidBatteries.pdf

- Elgendy, M. A., Zahawi, B., & Atkinson, D. J. (2010). Comparison of Directly Connected and Constant Voltage Vontrolled Photovoltaic Pumping Systems. *IEEE Transactions on Sustainable Energy*, 1(3), 184–192. <https://doi.org/10.1109/TSTE.2010.2052936>
- Elgendy, M. A., Zahawi, B., & Atkinson, D. J. (2012). Assessment of Perturb and Observe MPPT Algorithm Implementation Techniques for PV Pumping Applications. *IEEE Transactions on Sustainable Energy*, 3(1), 21–33.
- Elkadeem, M. R., Wang, S., Sharshir, S. W., & Atia, E. G. (2019). Feasibility analysis and techno-economic design of grid-isolated hybrid renewable energy system for electrification of agriculture and irrigation area: A case study in Dongola, Sudan. *Energy Conversion and Management*, 196(August), 1453–1478. <https://doi.org/10.1016/j.enconman.2019.06.085>
- Eltawil, M. A., & Zhao, Z. (2013). MPPT techniques for photovoltaic applications. *Renewable and Sustainable Energy Reviews*, 25, 793–813. <https://doi.org/10.1016/j.rser.2013.05.022>
- Eteiba, M. B., Shenawy, E. T. El, Shazly, J. H., & Hafez, A. Z. (2013). A Photovoltaic (Cell , Module , Array) Simulation and Monitoring Model using MATLAB ® / GUI Interface. *International Journal of Computer Applications*, 69(6), 14–28.
- EU, USAID, G. (2017). *Mini-Grid Design (Second)*. GIZ and NESP.
- Eze, F., Ogola, J., Kivindu, R., Egbo, M., & Obi, C. (2022). Technical and economic feasibility assessment of hybrid renewable energy system at Kenyan institutional building: A case study. *Sustainable Energy Technologies and Assessments*, 51(December 2021), 101939. <https://doi.org/10.1016/j.seta.2021.101939>
- Fapi, C. B. N., Wira, P., Kamta, M., Tchakounté, H., & Colicchio, B. (2021). Simulation and dSPACE Hardware Implementation of an Improved Fractional Short-Circuit Current MPPT Algorithm for Photovoltaic System. *Applied Solar Energy*, 57(2), 93–106.
- Fathabadi, H. (2016). Novel high accurate sensorless dual-axis solar tracking system controlled by maximum power point tracking unit of photovoltaic systems. *Applied Energy*, 173, 448–459.
- Fazelpour, F., Soltani, N., & Rosen, M. A. (2014a). Feasibility of satisfying electrical energy needs with hybrid systems for a medium-size hotel on Kish Island, Iran. *Energy*, 73, 856–865. <https://doi.org/10.1016/j.energy.2014.06.097>
- Fazelpour, F., Soltani, N., & Rosen, M. A. (2014b). Feasibility of satisfying electrical energy needs with hybrid systems for a medium-size hotel on Kish Island, Iran. *Energy*, 73, 856–865. <https://doi.org/10.1016/j.energy.2014.06.097>
- Forouzesh, M., Siwakoti, Y. P., Gorji, S. A., Blaabjerg, F., & Lehman, B. (2017). Step-up DC–DC converters: a comprehensive review of voltage-boosting techniques, topologies, and applications. *IEEE Transactions on Power Electronics*, 32(12), 9143–9178.

- Fulzele, J. B., & Daigavane, M. B. (2018). Design and Optimization of Hybrid PV-Wind Renewable Energy System. *Materials Today: Proceedings*, 5(1), 810–818. <https://doi.org/10.1016/j.matpr.2017.11.151>
- Gebrehiwot, K., Mondal, M. A. H., Ringler, C., & Gebremeskel, A. G. (2019). Optimization and cost-benefit assessment of hybrid power systems for off-grid rural electrification in Ethiopia. *Energy*, 177, 234–246. <https://doi.org/10.1016/j.energy.2019.04.095>
- Giallanza, A., Porretto, M., Puma, G. L., & Marannano, G. (2018). A sizing approach for stand-alone hybrid photovoltaic-wind-battery systems: A Sicilian case study. *Journal of Cleaner Production*, 199, 817–830. <https://doi.org/10.1016/j.jclepro.2018.07.223>
- Gorji, S. A., Sahebi, H. G., Ektesabi, M., & Rad, A. B. (2019). Topologies and control schemes of bidirectional DC–DC power converters: An overview. *IEEE Access*, 7, 117997–118019.
- Govind, A., Rajitha, A. R., & Rajalakshmy, S. (2022). A Review of High-Gain Bidirectional DC-DC converter with reduced ripple current. *2022 Third International Conference on Intelligent Computing Instrumentation and Control Technologies (ICICICT)*, 211–216.
- Guezgouz, M., Jurasz, J., Bekkouche, B., Ma, T., Javed, M. S., & Kies, A. (2019). Optimal hybrid pumped hydro-battery storage scheme for off-grid renewable energy systems. *Energy Conversion and Management*, 199, 112046.
- Gür, T. M. (2018a). Review of electrical energy storage technologies, materials and systems: challenges and prospects for large-scale grid storage. *Energy & Environmental Science*, 11(10), 2696–2767.
- Gür, T. M. (2018b). Review of electrical energy storage technologies, materials and systems: challenges and prospects for large-scale grid storage. *Energy & Environmental Science*, 11(10), 2696–2767.
- Habib, A. K. M. A., & Hasan, M. K. (2023). Lithium-ion battery state-of-charge balancing circuit using single resonant converter for electric vehicle applications. *Journal of Energy Storage*, 61, 106727.
- Habib, H. U. R., Wang, S., Elkadeem, M. R., & Elmorshedy, M. F. (2019). Design Optimization and Model Predictive Control of a Standalone Hybrid Renewable Energy System: A Case Study on a Small Residential Load in Pakistan. *IEEE Access*, 7, 117369–117390. <https://doi.org/10.1109/ACCESS.2019.2936789>
- Hafez, A. Z., Yousef, A. M., & Harag, N. M. (2018). Solar tracking systems: Technologies and trackers drive types – A review. *Renewable and Sustainable Energy Reviews*, 91(March), 754–782. <https://doi.org/10.1016/j.rser.2018.03.094>
- Haisheng, C., Jinchao, L. I. U., Huan, G. U. O., Yujie, X. U., & Chunqing, T. A. N. (2013). Technical principle of compressed air energy storage system. *Energy Storage Science and Technology*, 2(2), 146.

- Hannan, M. A., Lipu, M. S. H., Hussain, A., & Mohamed, A. (2017). A review of lithium-ion battery state of charge estimation and management system in electric vehicle applications: Challenges and recommendations. *Renewable and Sustainable Energy Reviews*, 78, 834–854.
- Haque, A., & Rahman, M. A. (2012). Study of a solar PV-powered mini-grid pumped hydroelectric storage & its comparison with battery storage. *2012 7th International Conference on Electrical and Computer Engineering*, 626–629.
- Haseli, Y. (2018). Maximum conversion efficiency of hydrogen fuel cells. *International Journal of Hydrogen Energy*, 43(18), 9015–9021.
- Hassan, S. Z., Li, H., Kamal, T., Arifoğlu, U., Mumtaz, S., & Khan, L. (2017). Neuro-Fuzzy wavelet based adaptive MPPT algorithm for photovoltaic systems. *Energies*, 10(3), 394.
- Hesse, H. C., Schimpe, M., Kucevic, D., & Jossen, A. (2017). Lithium-ion battery storage for the grid - A review of stationary battery storage system design tailored for applications in modern power grids. In *Energies* (Vol. 10, Issue 12). <https://doi.org/10.3390/en10122107>
- HIOKI. (2020). *Lead-acid Battery Handbook*.
- Hmidet, A., Subramaniam, U., Elavarasan, R. M., Raju, K., Diaz, M., Das, N., Mehmood, K., Karthick, A., Muhibbullah, M., & Boubaker, O. (2021). Design of Efficient Off-Grid Solar Photovoltaic Water Pumping System Based on Improved Fractional Open Circuit Voltage MPPT Technique. *International Journal of Photoenergy*, 2021.
- Ho, B. M. T., Chung, S.-H., & Hui, S. Y. R. (2004). An integrated inverter with maximum power tracking for grid-connected PV systems. *Nineteenth Annual IEEE Applied Power Electronics Conference and Exposition, 2004. APEC'04.*, 3, 1559–1565.
- Hohm, D. P., & Ropp, M. E. (2003). Comparative study of maximum power point tracking algorithms. *Progress in Photovoltaics: Research and Applications*, 11(1), 47–62. <https://doi.org/doi.org/10.1002/pip.459>
- Hong, T., Jeong, K., Ban, C., Oh, J., Koo, C., Kim, J., & Lee, M. (2016). A preliminary study on the 2-axis hybrid solar tracking method for the smart photovoltaic blind. *Energy Procedia*, 88, 484–490.
- Hu, X., Feng, F., Liu, K., Zhang, L., Xie, J., & Liu, B. (2019). State estimation for advanced battery management : Key challenges and future trends. *Renewable and Sustainable Energy Reviews*, 114(April), 109334. <https://doi.org/10.1016/j.rser.2019.109334>
- IEA, UN, IRENA, WORLD_BANK, & WHO. (2023). *Tracking SDG7: The Energy Progress Report 2022*. https://trackingsdg7.esmap.org/data/files/download-documents/2021_tracking_sdg7_chapter_6_outlook_for_sdg7.pdf

- Ishaque, K., Salam, Z., Shamsudin, A., & Amjad, M. (2012). A direct control based maximum power point tracking method for photovoltaic system under partial shading conditions using particle swarm optimization algorithm. *Applied Energy*, 99, 414–422.
- Jagjeevanram K, R. M. (2020). Control of PV-Wind-Diesel Hybrid System with BESS for Optimal Operation. *International Journal of Progressive Research in Science and Engineering*, 1(4), 199–203. <https://journals.grdpublications.com/index.php/ijprse/article/view/131/128>
- Jalal, D., & Mehdi, N. (2021). Optimization Methods of MPPT Parameters for PV Systems: Review, Classification, and Comparison. *Journal of Modern Power Systems and Clean Energy*, 9(2), 225–236.
- Jately, V., Azzopardi, B., Joshi, J., V, B. V., & Sharma, A. (2021). Experimental Analysis of hill-climbing MPPT algorithms under low irradiance levels. *Renewable and Sustainable Energy Reviews*, 150, 111467. <https://doi.org/10.1016/j.rser.2021.111467>
- Javed, M. S., Ma, T., Jurasz, J., & Amin, M. Y. (2020). Solar and wind power generation systems with pumped hydro storage: Review and future perspectives. *Renewable Energy*, 148, 176–192.
- Jayalalitha, S., & Kavya, M. (2020). Developments in Perturb and Observe Algorithm for Maximum Power Point Tracking in Photo Voltaic Panel: A Review. *Archives of Computational Methods in Engineering*. <https://doi.org/10.1007/s11831-020-09461-x>
- Jiang, J., Su, Y., Kuo, K., Wang, C., Liao, M., Wang, J., Huang, C., Chou, C., Lee, C., & Shieh, J. (2016). On a hybrid MPPT control scheme to improve energy harvesting performance of traditional two-stage inverters used in photovoltaic systems. *Renewable and Sustainable Energy Reviews*. <https://doi.org/10.1016/j.rser.2016.09.112>
- Jiang, J.-A., Huang, T.-L., Hsiao, Y.-T., & Chen, C.-H. (2005). Maximum power tracking for photovoltaic power systems. *Journal of Applied Science and Engineering*, 8(2), 147–153.
- Jones, I. W. (1977). Recent advances in the development of sodium-sulphur batteries for load levelling and motive power applications. *International Symposium on Solid Ionic and Ionic-Electronic Conductors*, 681–688.
- Junaid Khan, M., Mathew, L., & Yadav, A. K. (2020). Novel Applications of Soft Computing Techniques for Comparative Analysis of Maximum Power Point Tracking in Solar Photo-Voltaic System Under Perturb Conditions. In *Soft Computing in Condition Monitoring and Diagnostics of Electrical and Mechanical Systems* (pp. 363–385). Springer.
- Kaewkamnerdpong, B., & Bentley, P. J. (2005). Perceptive particle swarm optimisation: an investigation. *Proceedings 2005 IEEE Swarm Intelligence Symposium, 2005. SIS 2005.*, 169–176.

- Kamran, M., Mudassar, M., Fazal, M. R., Asghar, M. U., Bilal, M., & Asghar, R. (2020). Implementation of improved Perturb & Observe MPPT technique with confined search space for standalone photovoltaic system. *Journal of King Saud University-Engineering Sciences*, 32(7), 432–441.
- Karami, N., Moubayed, N., & Outbib, R. (2017). General review and classification of different MPPT Techniques. *Renewable and Sustainable Energy Reviews*, 68(September 2016), 1–18. <https://doi.org/10.1016/j.rser.2016.09.132>
- Kaur, D. (2017). *Renewable Energy Sources : -A Review*. 1–4.
- Kazem, H. A., & Khatib, T. (2013). A novel numerical algorithm for optimal sizing of a photovoltaic/wind/ diesel generator/battery microgrid using loss of load probability index. *International Journal of Photoenergy*, 2013(April). <https://doi.org/10.1155/2013/718596>
- Kenfack, J., Pascal, F., Tamo, T., & Mayer, D. (2009). *Microhydro-PV-hybrid system : Sizing a small hydro-PV-hybrid system for rural electrification in developing countries*. 34, 2259–2263. <https://doi.org/10.1016/j.renene.2008.12.038>
- Keshan, H., Thornburg, J., & Ustun, T. S. (2016). Comparison of Lead-Acid and Lithium Ion Batteries for Stationary Storage in Off-Grid Energy Systems. *4th IET Clean Energy and Technology Conference (CEAT 2016)*, 1–7. <https://doi.org/10.1049/cp.2016.1287>
- Kharb, R. K., Ansari, M. F., & Shimi, S. L. (2014). Design and implementation of ANFIS based MPPT scheme with open loop boost converter for solar PV module. *International Journal of Advanced Research in Electrical, Electronics and Instrumentation Engineering*, 3(1), 6517–6524.
- Khare, A., & Rangnekar, S. (2013). A review of particle swarm optimization and its applications in solar photovoltaic system. *Applied Soft Computing*, 13(5), 2997–3006.
- Khavari, A. H., Abdul-Malek, Z., Moradi, M., Tavalaei, J., Abdolazadeh Anbaran, S., & Wooi, C. L. (2016). An Economic Assessment of Hybrid Renewable Energy for a Remote Area Electrification in Iran. *Applied Mechanics and Materials*, 818(December), 151–155. <https://doi.org/10.4028/www.scientific.net/amm.818.151>
- Kihal, A., Krim, F., Laib, A., Talbi, B., & Afghoul, H. (2019). An improved MPPT scheme employing adaptive integral derivative sliding mode control for photovoltaic systems under fast irradiation changes. *ISA Transactions*, 87, 297–306.
- Killi, M., & Samanta, S. (2018). Voltage-sensor-based MPPT for stand-alone PV systems through voltage reference control. *IEEE Journal of Emerging and Selected Topics in Power Electronics*, 7(2), 1399–1407.

- Kim, I.-S., Kim, M.-B., & Youn, M.-J. (2006). New maximum power point tracker using sliding-mode observer for estimation of solar array current in the grid-connected photovoltaic system. *IEEE Transactions on Industrial Electronics*, 53(4), 1027–1035.
- Kimball, J. W., & Krein, P. T. (2007). Digital ripple correlation control for photovoltaic applications. *2007 IEEE Power Electronics Specialists Conference*, 1690–1694.
- Kolluru, V. R., Narne, R., & Patjoshi, R. K. (2018). *Implementation of a novel P & O MPPT controller for photovoltaic system at standard test conditions*. January.
- Korea Battery Industry Association 2017 “Energy storage system technology and business model.” (2017).
- Kumar, G. C. R., & Rao, M. R. C. (2012). AC / DC Converter with Active Power Factor Correction Applied to DC Motor Drive. *International Journal of Engineering Research and Development*, 1(11), 58–66.
- Kumar, S., Kaur, T., Arora, M. K., & Upadhyay, S. (2019). Resource estimation and sizing optimization of PV/micro hydro-based hybrid energy system in rural area of Western Himalayan Himachal Pradesh in India. *Energy Sources, Part A: Recovery, Utilization and Environmental Effects*, 41(22), 2795–2807. <https://doi.org/10.1080/15567036.2019.1576075>
- Kumar, S., Sharma, S., Kurian, C. P., Varghese, M., & George, A. M. (2020). Adaptive Neuro-fuzzy Control of Solar-Powered Building Integrated with Daylight-Artificial Light System. *2020 IEEE International Conference on Power Electronics, Smart Grid and Renewable Energy (PESGRE2020)*, 1–6.
- Landi D, Castorani V, G. M. (2019). Interactive energetic, environmental and economic analysis of renewable hybrid energy system. *Int J Interact Des Manuf*. <https://doi.org/https://doi.org/10.1007/s12008-019-00554-x>.
- Lasheen, M., & Abdel-Salam, M. (2018). Maximum power point tracking using Hill Climbing and ANFIS techniques for PV applications: A review and a novel hybrid approach. *Energy Conversion and Management*, 171, 1002–1019.
- Lasheen, M., Rahman, A. K. A., Abdel-Salam, M., & Ookawara, S. (2017). Adaptive reference voltage-based MPPT technique for PV applications. *IET Renewable Power Generation*, 11(5), 715–722. <https://doi.org/10.1049/iet-rpg.2016.0749>
- Leedy, A. W., Guo, L., & Aganah, K. A. (2012). A constant voltage MPPT method for a solar powered boost converter with DC motor load. *2012 Proceedings of IEEE Southeastcon*, 1–6.
- Letting, L. K., Munda, J. L., & Hamam, Y. (2012). Optimization of a fuzzy logic controller for PV grid inverter control using S-function based PSO. *Solar Energy*, 86(6), 1689–1700.

- Li, C., & Yu, W. (2016). Techno-economic comparative analysis of off-grid hybrid photovoltaic/diesel/battery and photovoltaic/battery power systems for a household in Urumqi, China. *Journal of Cleaner Production*, *124*, 258–265. <https://doi.org/10.1016/j.jclepro.2016.03.002>
- Li, Q., Chen, H., Huang, H., Zhao, X., Cai, Z., Tong, C., Liu, W., & Tian, X. (2017). An enhanced grey wolf optimization based feature selection wrapped kernel extreme learning machine for medical diagnosis. *Computational and Mathematical Methods in Medicine*, 2017.
- Li, X., Wen, H., Hu, Y., & Jiang, L. (2019). A novel beta parameter based fuzzy-logic controller for photovoltaic MPPT application. *Renewable Energy*, *130*, 416–427.
- Ling, J., Karuppiah, C., Krishnan, S. G., Reddy, M. V, Mison, I. I., Ab Rahim, M. H., Yang, C.-C., & Jose, R. (2021). Phosphate polyanion materials as high-voltage lithium-ion battery cathode: a review. *Energy & Fuels*, *35*(13), 10428–10450.
- Lithium-ion Battery*. (n.d.). Retrieved June 1, 2021, from https://www.google.com/search?q=images+of+lithium-ion+batteries&rlz=1C1CHBD_enCM762CM762&sxsrf=ALeKk00LZl_Qarw-pGoVSmxwzZ4o1ltJEQ:1622555818912&tbm=isch&source=iu&ictx=1&fir=T6b-wnikVAKcwM%252CMn0Ngkxkzaa_PM%252C_&vet=1&usg=AI4_-kQzrCFqSBXIqBrs_tPVtO3d5n6
- Liu, F., Duan, S., Liu, F., Liu, B., & Kang, Y. (2008a). A Variable Step Size INC MPPT Method for PV Systems. *IEEE Transactions on Industrial Electronics*, *55*(7), 2622–2628. <https://doi.org/10.1109/TIE.2008.920550>
- Liu, F., Duan, S., Liu, F., Liu, B., & Kang, Y. (2008b). A Variable Step Size INC MPPT Method for PV Systems. *IEEE Transactions on Industrial Electronics*, *55*(7), 2622–2628. <https://doi.org/10.1109/TIE.2008.920550>
- Ludin, N. A., Affandi, N. A. A., Purvis-Roberts, K., Ahmad, A., Ibrahim, M. A., Sopian, K., & Jusoh, S. (2021). Environmental impact and levelised cost of energy analysis of solar photovoltaic systems in selected asia pacific region: A cradle-to-grave approach. *Sustainability (Switzerland)*, *13*(1), 1–21. <https://doi.org/10.3390/su13010396>
- Luo, X., Wang, J., Dooner, M., Clarke, J., & Krupke, C. (2014). Overview of current development in compressed air energy storage technology. *Energy Procedia*, *62*, 603–611.
- Maharjan, L., Member, S., Inoue, S., & Akagi, H. (2009). *State-of-Charge (SOC) - Balancing Control of a Battery Energy Storage System Based on a Cascade PWM Converter*. *24*(6), 1628–1636.
- Mahdi, A. S., Mahamad, A. K., Saon, S., Tuwoso, T., Elmunsyah, H., & Mudjanarko, S. W. (2020). Maximum power point tracking using perturb and observe, fuzzy logic and ANFIS. *SN Applied Sciences*, *2*(1), 1–9.

- Mahmoud, M., Ramadan, M., Olabi, A.-G., Pullen, K., & Naher, S. (2020a). A review of mechanical energy storage systems combined with wind and solar applications. *Energy Conversion and Management*, 210, 112670.
- Mahmoud, M., Ramadan, M., Olabi, A.-G., Pullen, K., & Naher, S. (2020b). A review of mechanical energy storage systems combined with wind and solar applications. *Energy Conversion and Management*, 210, 112670.
- Malhotra, R., Singh, N., & Singh, Y. (2011). Genetic algorithms: Concepts, design for optimization of process controllers. *Computer and Information Science*, 4(2), 39.
- Manthiram, A., Yu, X., & Wang, S. (2017). Lithium battery chemistries enabled by solid-state electrolytes. *Nature Reviews Materials*, 2(4), 1–16.
- Mao, M., Cui, L., Zhang, Q., Guo, K., Zhou, L., & Huang, H. (2020). Classification and summarization of solar photovoltaic MPPT techniques: A review based on traditional and intelligent control strategies. *Energy Reports*, 6, 1312–1327. <https://doi.org/10.1016/j.egy.2020.05.013>
- Mao, M., Zhou, L., Yang, Z., Zhang, Q., Zheng, C., Xie, B., & Wan, Y. (2019). A hybrid intelligent GMPPT algorithm for partial shading PV system. *Control Engineering Practice*, 83, 108–115.
- Martin, J. E., Rohwer, L. E. S., & Stupak Jr, J. (2016). Elastic magnetic composites for energy storage flywheels. *Composites Part B: Engineering*, 97, 141–149.
- Mauger, A., & Julien, C. M. (2017). Critical review on lithium-ion batteries: are they safe? Sustainable? *Ionics*, 23(8), 1933–1947.
- May, G. J., Davidson, A., & Monahov, B. (2018). Lead batteries for utility energy storage : A review. *Journal of Energy Storage*, 15, 145–157. <https://doi.org/10.1016/j.est.2017.11.008>
- Mbaka, E. (2013). Evaluation of optimal photovoltaic hybrid systems for remote villages in Far North Cameroon. *Renewable Energy*, 51, 482–488. <https://doi.org/10.1016/j.renene.2012.09.035>
- Messalti, S., Harrag, A., & Loukriz, A. (2017). A new variable step size neural networks MPPT controller: Review, simulation and hardware implementation. *Renewable and Sustainable Energy Reviews*, 68(August 2015), 221–233. <https://doi.org/10.1016/j.rser.2016.09.131>
- Miyatake, M., Inada, T., Hiratsuka, I., Zhao, H., Otsuka, H., & Nakano, M. (2004). Control characteristics of a fibonacci-search-based maximum power point tracker when a photovoltaic array is partially shaded. *The 4th International Power Electronics and Motion Control Conference, 2004. IPEMC 2004.*, 2, 816–821.
- Miyatake, M., Veerachary, M., Toriumi, F., Fujii, N., & Ko, H. (2011). Maximum power point tracking of multiple photovoltaic arrays: A PSO approach. *IEEE Transactions on Aerospace and Electronic Systems*, 47(1), 367–380.

- Mohamed, Z., & Elbarbary, S. (2021). *Review of maximum power point tracking algorithms of PV system*. <https://doi.org/10.1108/FEBE-03-2021-0019>
- Mohammed, S. S., Devaraj, D., & Ahamed, T. P. I. (2016). Maximum power point tracking system for stand alone solar PV power system using Adaptive Neuro-Fuzzy Inference System. *2016 Biennial International Conference on Power and Energy Systems: Towards Sustainable Energy (PESTSE)*, 1–4.
- Mohanty, S., Subudhi, B., & Ray, P. K. (2015). A new MPPT design using grey wolf optimization technique for photovoltaic system under partial shading conditions. *IEEE Transactions on Sustainable Energy*, 7(1), 181–188.
- Mohanty, S., Subudhi, B., & Ray, P. K. (2016). A grey wolf-assisted perturb & observe MPPT algorithm for a PV system. *IEEE Transactions on Energy Conversion*, 32(1), 340–347.
- Mohapatra, A., Nayak, B., Das, P., & Mohanty, K. B. (2017). A review on MPPT techniques of PV system under partial shading condition. *Renewable and Sustainable Energy Reviews*, 80(May), 854–867. <https://doi.org/10.1016/j.rser.2017.05.083>
- Mokhtara, C., Negrou, B., Bouferrouk, A., Yao, Y., Settou, N., & Ramadan, M. (2020). Integrated supply–demand energy management for optimal design of off-grid hybrid renewable energy systems for residential electrification in arid climates. *Energy Conversion and Management*, 221(April), 113192. <https://doi.org/10.1016/j.enconman.2020.113192>
- Mokhtara, C., Negrou, B., Settou, N., Settou, B., & Samy, M. M. (2021). Design optimization of off-grid Hybrid Renewable Energy Systems considering the effects of building energy performance and climate change: Case study of Algeria. *Energy*, 219, 119605. <https://doi.org/10.1016/j.energy.2020.119605>
- Morstyn, T., Momayyezani, M., Hredzak, B., & Agelidis, V. G. (2016). Distributed Control for State-of-Charge Balancing Between the Modules of a Reconfigurable Battery Energy Storage System. *IEEE Transactions on Power Electronics*, 31(11), 7986–7995. <https://doi.org/10.1109/TPEL.2015.2513777>
- Motahhir, S., Hammoumi, A. El, & Ghzizal, A. El. (2019). The Most Used MPPT Algorithms : Review and the Suitable Low-cost Embedded Board. *Journal of Cleaner Production*. <https://doi.org/10.1016/j.jclepro.2019.118983>
- Mousa, H. H. H., Youssef, A.-R., & Mohamed, E. E. M. (2021). State of the art perturb and observe MPPT algorithms based wind energy conversion systems: A technology review. *International Journal of Electrical Power & Energy Systems*, 126, 106598. <https://doi.org/10.1016/j.ijepes.2020.106598>
- MUH, E. (2017). *A Comparative Assessment Of Hybrid Renewable Energy Systems For Sustainable Rural Electrification In Cameroon*. Pan African University.
- Mukherjee, P., & Rao, V. V. (2019). Design and development of high temperature superconducting magnetic energy storage for power applications-A review. *Physica C: Superconductivity and Its Applications*, 563, 67–73.

- Murphy, F., & McDonnell, K. (2017). *A Feasibility Assessment of Photovoltaic Power Systems in Ireland; a Case Study for the Dublin Region*. 1–14. <https://doi.org/10.3390/su9020302>
- Murugaperumal, K., & Ajay D Vimal Raj, P. (2019). Feasibility design and techno-economic analysis of hybrid renewable energy system for rural electrification. *Solar Energy*, 188(February), 1068–1083. <https://doi.org/10.1016/j.solener.2019.07.008>
- Murugaperumal, K., Srinivasn, S., & Satya Prasad, G. R. K. D. (2020). Optimum design of hybrid renewable energy system through load forecasting and different operating strategies for rural electrification. *Sustainable Energy Technologies and Assessments*, 37(November 2018), 100613. <https://doi.org/10.1016/j.seta.2019.100613>
- Naveen, R., Revankar, P. P., & Rajanna, S. (2020). Integration of renewable energy systems for optimal energy needs-a review. *International Journal of Renewable Energy Research*, 10(2), 727–742.
- Nfah, E. M., & Ngundam, J. M. (2008). *Modelling of wind / Diesel / battery hybrid power systems for far North Cameroon*. 49, 1295–1301. <https://doi.org/10.1016/j.enconman.2008.01.007>
- Nfah, E. M., & Ngundam, J. M. (2009). Feasibility of pico-hydro and photovoltaic hybrid power systems for remote villages in Cameroon. *Renewable Energy*, 34(6), 1445–1450. <https://doi.org/10.1016/j.renene.2008.10.019>
- Nfah, E. M., Ngundam, J. M., & Tchinda, R. (2007). *Modelling of solar / diesel / battery hybrid power systems for far-north Cameroon*. 32, 832–844. <https://doi.org/10.1016/j.renene.2006.03.010>
- Nfah, E. M., Ngundam, J. M., Vandenberg, M., & Schmid, J. (2008). *Simulation of off-grid generation options for remote villages in Cameroon*. 33, 1064–1072. <https://doi.org/10.1016/j.renene.2007.05.045>
- Ngan, M. S., & Tan, C. W. (2011). A study of maximum power point tracking algorithms for stand-alone Photovoltaic Systems. *2011 IEEE Applied Power Electronics Colloquium (IAPEC)*, 22–27. <https://doi.org/10.1109/IAPEC.2011.5779863>
- Noh, H.-J., Lee, D.-Y., & Hyun, D.-S. (2002). An improved MPPT converter with current compensation method for small scaled PV-applications. *IEEE 2002 28th Annual Conference of the Industrial Electronics Society. IECON 02*, 2, 1113–1118.
- Odou, O. D. T., Bhandari, R., & Adamou, R. (2020). Hybrid off-grid renewable power system for sustainable rural electrification in Benin. *Renewable Energy*, 145, 1266–1279. <https://doi.org/10.1016/j.renene.2019.06.032>

- Ogunniyi, E. O., & Pienaar, H. C. V. Z. (2017). Overview of battery energy storage system advancement for renewable (photovoltaic) energy applications. *Proceedings of the 25th Conference on the Domestic Use of Energy, DUE 2017, October*, 233–239. <https://doi.org/10.23919/DUE.2017.7931849>
- Onar, O. C., Kobayashi, J., Erb, D. C., & Khaligh, A. (2012). A bidirectional high-power-quality grid interface with a novel bidirectional noninverted buck–boost converter for PHEVs. *IEEE Transactions on Vehicular Technology*, 61(5), 2018–2032.
- Pandey, A., & Srivastava, S. (2019). Perturb & Observe MPPT Technique used for PV System Under different Environmental Conditions. *International Research Journal of Engineering and Technology*, 6(4), 2829–2835.
- Park, J., Kim, H., Cho, Y., & Shin, C. (2014). *Simple Modeling and Simulation of Photovoltaic Panels Using Matlab / Simulink Modeling of Photovoltaic Module*. 73(Fgcn), 147–155.
- Parker, C. D. (2001). Lead-acid battery energy-storage systems for electricity supply networks. *Journal of Power Sources*, 100(1–2), 18–28. [https://doi.org/10.1016/S0378-7753\(01\)00880-1](https://doi.org/10.1016/S0378-7753(01)00880-1)
- Patel, A. M., & Singal, S. K. (2018). Economic analysis of integrated renewable energy system for electrification of remote rural area having scattered population. *International Journal of Renewable Energy Research*, 8(1), 523–539.
- Pavlyukevich, I. (2007). Lévy flights, non-local search and simulated annealing. *Journal of Computational Physics*, 226(2), 1830–1844.
- Podder, S., & Khan, Md. Z. R. (2016). Comparison of Lead acid and Li-ion Battery in Solar Home System of Bangladesh. *2016 5th International Conference on Informatics, Electronics and Vision (ICIEV)*, 434–438.
- Power, F., & Science, C. (n.d.). *Flyboost Power Factor Correction Cell and Its Applications in Single-Stage AC-DC Converters*. 2(1), 1375–1380.
- Prasad, A. K., Singh, R. P., & Kafatos, M. (2006). *Influence of coal based thermal power plants on aerosol optical properties in the Indo-Gangetic basin*. 33(March), 3–6. <https://doi.org/10.1029/2005GL023801>
- Priyadarshi, N., Padmanaban, S., Bhaskar, M. S., Blaabjerg, F., & Sharma, A. (2018). Fuzzy SVPWM-based inverter control realisation of grid integrated photovoltaic-wind system with fuzzy particle swarm optimisation maximum power point tracking algorithm for a grid-connected PV/wind power generation system: Hardware implementation. *IET Electric Power Applications*, 12(7), 962–971.
- Rahman, M. M., Oni, A. O., Gemechu, E., & Kumar, A. (2020). Assessment of energy storage technologies: A review. *Energy Conversion and Management*, 223, 113295.

- Rajkumar, M. V., Mahakumar, M., Manojkumar, M., Hemaraj, M., & Kumaravel, E. (2017). A new DC-DC converter topology with grey wolf MPPT algorithm for photovoltaic system. *International Journal of Emerging Technologies in Engineering Research (IJETER)*, 5(4), 54–59.
- Ram, J. P., Rajasekar, N., & Miyatake, M. (2017). Design and overview of maximum power point tracking techniques in wind and solar photovoltaic systems: A review. *Renewable and Sustainable Energy Reviews*, 73, 1138–1159. <https://doi.org/10.1016/j.rser.2017.02.009>
- Ramaprabha, R., Balaji, M., & Mathur, B. L. (2012). Maximum power point tracking of partially shaded solar PV system using modified Fibonacci search method with fuzzy controller. *International Journal of Electrical Power & Energy Systems*, 43(1), 754–765.
- Ramesh, M., & Saini, R. P. (2020). Effect of different batteries and diesel generator on the performance of a stand-alone hybrid renewable energy system. *Energy Sources, Part A: Recovery, Utilization and Environmental Effects*, 00(00), 1–23. <https://doi.org/10.1080/15567036.2020.1763520>
- RAND, D. (2018). Secondary Batteries - Lead- Acid Systems. *Encyclopedia of Electrochemical Power Sources*, 550–575. <https://doi.org/10.1016/B978-044452745-5.00136-2>
- Rashid, M. H. (2001). Power Electronics Handbook. In *Power Electronics Handbook*. Academic Press . <https://doi.org/10.1016/c2016-0-00847-1>
- Ray, S., Chakraborty, A. K., & Debnath, D. (2013). Development of a cost-optimized hybrid off-grid power system for a model site in north-eastern India involving photovoltaic arrays, diesel generators and battery storage. *International Journal of ChemTech Research*, 5(2), 771–779.
- Rehman, S. (2021). Hybrid power systems – Sizes, efficiencies, and economics. *Energy Exploration and Exploitation*, 39(1), 3–43. <https://doi.org/10.1177/0144598720965022>
- Rezk, H., Al-oran, M., Gomaa, M. R., Tolba, M. A., Fathy, A., Ali, M., Olabi, A. G., El-sayed, A. H. M., Addawaser, W., Sattam, P., Abdulaziz, B., & Arabia, S. (2019). A novel statistical performance evaluation of most modern optimization- based global MPPT techniques for partially shaded PV system. *Renewable and Sustainable Energy Reviews*, 115(October 2018), 109372. <https://doi.org/10.1016/j.rser.2019.109372>
- Rezk, H., & Eltamaly, A. M. (2015). A comprehensive comparison of different MPPT techniques for photovoltaic systems. *Solar Energy*, 112, 1–11. <https://doi.org/10.1016/j.solener.2014.11.010>
- Rezk, H., Fathy, A., & Abdelaziz, A. Y. (2017). A comparison of different global MPPT techniques based on meta-heuristic algorithms for photovoltaic system subjected to partial shading conditions. *Renewable and Sustainable Energy Reviews*, 74(February), 377–386. <https://doi.org/10.1016/j.rser.2017.02.051>

- Ribeiro, P. F., Johnson, B. K., Crow, M. L., Arsoy, A., & Liu, Y. (2001). Energy Storage systems for Advances Power Applications. *Proceedings of the IEEE*, 89(12), 1744–1756. <https://doi.org/10.1109/5.975900>
- Rizzo, R., & Piegari, L. (2010). Adaptive perturb and observe algorithm for photovoltaic maximum power point tracking. *IET Renewable Power Generation*, 4(4), 317–328. <https://doi.org/10.1049/iet-rpg.2009.0006>
- Robert W. Erickson, D. M. (2004). *Fundamentals of Power Electronics* (SECOND). KLUWER ACADEMIC PUBLISHERS. https://doi.org/10.1007/978-3-319-11626-6_2
- Rohani, G., & Nour, M. (2014). Techno-economical analysis of stand-alone hybrid renewable power system for Ras Musherib in United Arab Emirates. *Energy*, 64, 828–841.
- RS Components. (2021). *Yuasa NP12-12 Lead Acid Battery - 12V, 12Ah*. <https://africa.rsdelivers.com/product>
- Salas, V., Olias, E., Barrado, A., & Lazaro, A. (2006). Review of the maximum power point tracking algorithms for stand-alone photovoltaic systems. *Solar Energy Materials and Solar Cells*, 90(11), 1555–1578. <https://doi.org/https://doi.org/10.1016/j.solmat.2005.10.023>
- Salman, S., Ai, X., & Wu, Z. (2018). Design of a P-&O algorithm based MPPT charge controller for a stand-alone 200W PV system. *Protection and Control of Modern Power Systems*, 3(1), 1–8. <https://doi.org/10.1186/s41601-018-0099-8>
- Sandhya, C. P., John, B., & Gouri, C. (2014). Lithium titanate as anode material for lithium-ion cells: a review. *Ionics*, 20(5), 601–620.
- Sa-ngawong, N., & Ngamroo, I. (2015). Intelligent photovoltaic farms for robust frequency stabilization in multi-area interconnected power system based on PSO-based optimal Sugeno fuzzy logic control. *Renewable Energy*, 74, 555–567.
- Sarbu, I., & Sebarchievici, C. (2018). A comprehensive review of thermal energy storage. *Sustainability*, 10(1), 191.
- Sarvi, M., & Azadian, A. (2021). A comprehensive review and classified comparison of MPPT algorithms in PV systems. In *Energy Systems* (Issue 0123456789). Springer Berlin Heidelberg. <https://doi.org/10.1007/s12667-021-00427-x>
- Séguier, G., & Labrique, F. (2012). *Power electronic converters: DC-AC conversion*. Springer Science & Business Media.
- Sera, D., Mathe, L., Kerekes, T., Spataru, S. V., & Teodorescu, R. (2013). On the perturb-and-observe and incremental conductance mppt methods for PV systems. *IEEE Journal of Photovoltaics*, 3(3), 1070–1078. <https://doi.org/10.1109/JPHOTOV.2013.2261118>

- Seyedmahmoudian, M., Horan, B., Soon, T. K., Rahmani, R., Than Oo, A. M., Mekhilef, S., & Stojcevski, A. (2016). State of the art artificial intelligence-based MPPT techniques for mitigating partial shading effects on PV systems – A review. *Renewable and Sustainable Energy Reviews*, 64, 435–455. <https://doi.org/https://doi.org/10.1016/j.rser.2016.06.053>
- Sibai, F. N. (2014). Modelling and output power evaluation of series-parallel photovoltaic modules. *International Journal of Advanced Computer Science and Applications*, 5(1).
- Singh, B., Singh, B. N., Chandra, A., Al-Haddad, K., Pandey, A., & Kothari, D. P. (2003). A review of single-phase improved power quality AC-DC converters. *IEEE Transactions on Industrial Electronics*, 50(5), 962–981.
- Sinha, S., & Chandel, S. S. (2014). Review of software tools for hybrid renewable energy systems. *Renewable and Sustainable Energy Reviews*, 32, 192–205. <https://doi.org/10.1016/j.rser.2014.01.035>
- Smith, K., Shi, Y., Wood, E., & Pesaran, A. (2016). Optimizing Battery Usage and Management for Long Life. *Advanced Automotive Battery*.
- Stambouli, A. B., & Traversa, E. (2002). Fuel cells, an alternative to standard sources of energy. *Renewable and Sustainable Energy Reviews*, 6(3), 295–304.
- Subudhi, B., Member, S., & Pradhan, R. (2013a). A Comparative Study on Maximum Power Point Tracking Techniques for Photovoltaic Power Systems. *IEEE Transactions on Sustainable Energy*, 4(1), 89–98. <https://doi.org/10.1109/TSTE.2012.2202294>
- Subudhi, B., Member, S., & Pradhan, R. (2013b). A Comparative Study on Maximum Power Point Tracking Techniques for Photovoltaic Power Systems. *IEEE Transactions on Sustainable Energy*, 4(1), 89–98. <https://doi.org/10.1109/TSTE.2012.2202294>
- Subudhi, B., & Pradhan, R. (2012). A comparative study on maximum power point tracking techniques for photovoltaic power systems. *IEEE Transactions on Sustainable Energy*, 4(1), 89–98.
- Sudworth, J., & Tiley, A. R. (1985a). *Sodium Sulphur Battery*. Springer Science & Business Media.
- Sudworth, J., & Tiley, A. R. (1985b). *Sodium Sulphur Battery*. Springer Science & Business Media.
- Tanaka, H., & Nakatake, Y. (2009). One step azimuth tracking tilted-wick solar still with a vertical flat plate reflector. *Desalination*, 235(1–3), 1–8.
- The Energy Act, 2019, (2019).
- Tixador, P. (2008a). Superconducting magnetic energy storage: Status and perspective. *IEEE/CSC & ESAS European Superconductivity News Forum*, 3.

- Tixador, P. (2008b). Superconducting magnetic energy storage: Status and perspective. *IEEE/CSC & ESAS European Superconductivity News Forum*, 3.
- Twidell, J. (2021). *Renewable energy resources*. Routledge.
- UN. (2015). *Transforming our world: the 2030 agenda for sustainable development*.
- Vai, V., Alvarez-Herault, M. C., Raison, B., & Bun, L. (2020). Optimal Low-voltage Distribution Topology with Integration of PV and Storage for Rural Electrification in Developing Countries: A Case Study of Cambodia. *Journal of Modern Power Systems and Clean Energy*, 8(3), 531–539. <https://doi.org/10.35833/MPCE.2019.000141>
- Van Beuzekom, I., Gibescu, M., & Slootweg, J. G. (2015). A review of multi-energy system planning and optimization tools for sustainable urban development. *2015 IEEE Eindhoven PowerTech, PowerTech 2015*. <https://doi.org/10.1109/PTC.2015.7232360>
- Verma, D., Nema, S., Shandilya, A. M., & Dash, S. K. (2016). Maximum power point tracking (MPPT) techniques: Recapitulation in solar photovoltaic systems. *Renewable and Sustainable Energy Reviews*, 54, 1018–1034. <https://doi.org/10.1016/j.rser.2015.10.068>
- Villalva, M. G., Gazoli, J. R., & Ruppert Filho, E. (2009). Comprehensive approach to modeling and simulation of photovoltaic arrays. *IEEE Transactions on Power Electronics*, 24(5), 1198–1208.
- Viswambaran, V. K., Ghani, A., & Zhou, E. (2016). Modelling and Simulation of Maximum Power Point Tracking Algorithms & Review of MPPT Techniques for PV Applications. *2016 5th International Conference on Electronic Devices, Systems and Applications (ICEDSA)*, 4–7. <https://doi.org/10.1109/ICEDSA.2016.7818506>
- Wang, J., Zhang, J., Cui, Y., & Bi, X. (2016). Design and implementation of PLC-based automatic sun tracking system for parabolic trough solar concentrator. *MATEC Web of Conferences*, 77, 6006.
- Wolpert, D. H., & Macready, W. G. (1997). No free lunch theorems for optimization. *IEEE Transactions on Evolutionary Computation*, 1(1), 67–82.
- WORLD BANK GROUP: KOREA'S ENERGY STORAGE SYSTEM DEVELOPMENT : (2020).
- Xiao, W., Dunford, W. G., Palmer, P. R., & Capel, A. (2007). Application of centered differentiation and steepest descent to maximum power point tracking. *IEEE Transactions on Industrial Electronics*, 54(5), 2539–2549.
- Xie, B., Liu, Y., Ji, Y., & Wang, J. (2018). Two-stage battery energy storage system (BESS) in AC microgrids with balanced state-of-charge and guaranteed small-signal stability. *Energies*, 11(2). <https://doi.org/10.3390/en11020322>

- Xing, Y., Ma, E. W. M., Tsui, K. L., & Pecht, M. (2011). Battery management systems in electric and hybrid vehicles. *Energies*, 4(11), 1840–1857. <https://doi.org/10.3390/en4111840>
- Yadav, I., Maurya, S. K., & Gupta, G. K. (2020). A literature review on industrially accepted MPPT techniques for solar PV system. *International Journal of Electrical and Computer Engineering (IJECE)*, 10(2), 2117–2127. <https://doi.org/10.11591/ijece.v10i2.pp2117-2127>
- Yaichi, M., Fellah, M.-K., & Mammeri, A. (2014). A neural network based MPPT technique controller for photovoltaic pumping system. *International Journal of Power Electronics and Drive Systems*, 4(2), 241.
- Yang, S., Ling, C., Fan, Y., Yang, Y., Tan, X., & Dong, H. (2019). A review of lithium-ion battery thermal management system strategies and the evaluate criteria. *International Journal of Electrochemical Science*, 14(7), 6077–6107. <https://doi.org/10.20964/2019.07.06>
- Yang, X.-S., & Deb, S. (2009). Cuckoo search via Lévy flights. *2009 World Congress on Nature & Biologically Inspired Computing (NaBIC)*, 210–214.
- Yang, X.-S., & Deb, S. (2013). Multiobjective cuckoo search for design optimization. *Computers & Operations Research*, 40(6), 1616–1624.
- Yang, X.-S., & Deb, S. (2014). Cuckoo search: recent advances and applications. *Neural Computing and Applications*, 24, 169–174.
- Yimen, N., Hamandjoda, O., Meva'a, L., Ndzana, B., & Nganhou, J. (2018). Analyzing of a photovoltaic/wind/biogas/pumped-hydro off-grid hybrid system for rural electrification in Sub-Saharan Africa - Case study of Djoundé in Northern Cameroon. *Energies*, 11(10). <https://doi.org/10.3390/en11102644>
- Yue, X., Geng, D., Chen, Q., Zheng, Y., Gao, G., & Xu, L. (2021). 2-D lookup table based MPPT: Another choice of improving the generating capacity of a wave power system. *Renewable Energy*, 179, 625–640.
- Zahraee, S. M., Khalaji Assadi, M., & Saidur, R. (2016). Application of Artificial Intelligence Methods for Hybrid Energy System Optimization. *Renewable and Sustainable Energy Reviews*, 66, 617–630. <https://doi.org/10.1016/j.rser.2016.08.028>
- Zainudin, H. N. (2010). Comparison Study of Maximum Power Point Tracker Techniques for PV Systems. *Proceedings of the 14th International Middle East Power Systems Conference (MEPCON'10), Cairo University, Egypt, December 19-21, 1*, 750–755.
- Zhang, J.-H., Wei, X.-Y., Hu, L., & Ma, J.-G. (2019). A MPPT method based on improved fibonacci search photovoltaic array. *Tehnički Vjesnik*, 26(1), 163–170.

APPENDICES

Appendix A: Solar radiation Data for Moi University

MONTHS	2018	2019	2020	2021	AV.	Measured data	Measured clearness index	NASA data	NASA clearness index
JANUARY	4450	5805	4823	5230	5077	5.077	0.505	6.24	0.624
FEBRUARY	5895	6221	5889	4797	5701	5.701	0.549	6.71	0.648
MARCH	4497	6253	5383	5770	5476	5.476	0.521	6.59	0.628
APRIL	4183	5566	4837	5271	4964	4.964	0.487	5.94	0.581
MAY	4784	5135	4821	4525	4816	4.816	0.499	5.68	0.568
JUNE	4163	3669	4255	4899	4247	4.247	0.456	5.33	0.569
JULY	4432	4311	3637	3730	4028	4.028	0.427	5.1	0.538
AUGUST	4432	4578	4228	4080	4330	4.330	0.437	5.33	0.536
SEPTEMBER	5754	4859	4524	4523	4915	4.915	0.476	6.19	0.599
OCTOBER	5403	5477	4600	5146	5157	5.157	0.498	5.97	0.578
NOVEMBER	5762	5268	5085	5153	5317	5.317	0.527	5.62	0.56
DECEMBER	5397	4508	5638	4823	5092	5.092	0.514	6.05	0.614

Appendix B: Temperature Data for Moi University

Months	2018	2019	2020	2021	Measured Average	NASA
JANUARY	16	17	17	17	17	20
FEBRUARY	18	19	17	17	18	21
MARCH	16	19	17	18	18	22
APRIL	15	19	17	17	17	21
MAY	16	18	16	16	16	20
JUNE	15	16	15	16	15	20
JULY	15	15	15	15	15	19
AUGUST	15	15	15	15	15	20
SEPTEMBER	16	15	15	16	16	20
OCTOBER	16	16	16	16	16	21
NOVEMBER	17	16	16	17	17	20
DECEMBER	17	16	17	17	17	20

Appendix C: Power Demand data for Administration building

HOURS	MON P (kW)	TUE P (kW)	WED P (kW)	THUR P (kW)	FRI P (kW)	SAT P (kW)	SUN P (kW)
0	26	32	33	30	31	30	29
1	26	30	31	31	30	30	29
2	26	30	30	31	30	30	28
3	26	30	29	31	30	30	28
4	25	29	29	31	30	29	29
5	25	29	28	30	30	29	29
6	26	27	27	27	28	27	29
7	26	32	33	33	31	24	24
8	50	56	54	54	54	26	26
9	66	65	65	65	59	26	24
10	65	63	64	65	61	27	23
11	63	60	63	61	59	28	22
12	63	62	65	60	57	27	22
13	60	62	62	58	52	27	23
14	59	61	60	58	49	26	21
15	59	62	62	57	49	25	21
16	53	55	51	51	39	25	21
17	33	35	32	32	26	26	21
18	33	31	34	31	33	29	25
19	33	33	34	34	32	31	28
20	34	33	33	34	32	31	27
21	33	34	33	33	31	30	27
22	32	32	32	32	29	30	26
23	32	34	31	31	29	29	26

Appendix D: Power Demand data for Margaret Thatcher Library

HOURS	MON P(KW)	TUE P(KW)	WED P(KW)	THUR P(KW)	FRI P(KW)	SAT P(KW)	SUN P(KW)
0	13	13	12	13	12	12	12
1	13	13	12	12	12	12	12
2	13	13	12	13	12	12	12
3	13	13	12	13	12	12	12
4	12	13	12	12	12	12	12
5	12	12	12	12	12	12	12
6	11	12	12	11	21	10	11
7	43	44	37	33	48	10	10
8	52	51	50	55	54	10	10
9	57	55	56	58	57	29	10
10	58	56	61	60	58	39	10
11	57	57	61	60	62	42	10
12	58	56	60	58	59	43	10
13	60	56	60	58	58	44	20
14	59	55	60	58	56	44	29
15	57	57	61	56	54	44	29
16	52	51	54	51	51	43	29
17	44	45	45	44	45	42	13
18	44	45	44	45	44	43	12
19	43	45	44	48	44	42	13
20	45	46	29	47	44	44	13
21	46	46	12	46	20	19	13
22	16	16	12	15	12	12	13
23	13	12	11	12	12	12	13

**Appendix E: Loads and Energy Consumption Inventory for Administration
Building and Margaret Thatcher Library**

ADMINISTRATION BLOCK

Area	Lamp Type	Rating (W)	Quantity	Total Power (kW)	Daily Runni ng Hours	Total Energy Consumption (kWh)
PABX	4ft	36	8	0.288	9	2.592
Washroom	4ft	36	4	0.144	8	1.152
ADM 20	4ft	36	10	0.36	8	2.88
Chief Accountant	4ft	36	24	0.864	8	6.912
Personal Claim	4ft	36	12	0.432	8	3.456
Expenditure	4ft	36	8	0.288	8	2.304
Examination	4ft	36	12	0.432	8	3.456
Vote Book	4ft	36	12	0.432	8	3.456
Finance Officer	4ft	36	42	1.512	8	12.096
Washroom	4ft	36	1	0.036	8	0.288
Kitchen	2ft	18	1	0.018	8	0.144
Budgetary Control	4ft	36	12	0.432	8	3.456
Room 9	4ft	36	8	0.288	8	2.304
Room 11	4ft	36	8	0.288	8	2.304
Room 6,7,4,2	4ft	36	22	0.792	8	6.336

Salary	4ft	36	24	0.864	8	6.912
Room 11	4ft	36	8	0.288	8	2.304
Room 30	4ft	36	8	0.288	8	2.304
Room 31	4ft	36	8	0.288	10	2.88
Customer Care Office	4ft	36	2	0.072	8	0.576
ADM 33	4ft	36	16	0.576	10	5.76
ADM 34	4ft	36	16	0.576	8	4.608
ADM 35	4ft	36	16	0.576	8	4.608
ADM 36	4ft	36	16	0.576	8	4.608
ADM 39/41	4ft	36	16	0.576	8	4.608
ADM 42	4ft	36	4	0.144	8	1.152
Kitchen	5ft	58	1	0.058	8	0.464
ADM 44	4ft	36	14	0.504	8	4.032
Procurement	4ft	36	28	1.008	8	8.064
Procurement 1	4ft	36	8	0.288	8	2.304
Senior Procurement	4ft	36	14	0.504	8	4.032
Procurement Corridor	4ft	36	22	0.792	8	6.336
QA1	4ft	36	8	0.288	8	2.304
QA2	4ft	36	7	0.252	8	2.016
QA3	4ft	36	7	0.252	8	2.016
QA4	4ft	36	4	0.144	8	1.152

QA5	4ft	36	2	0.072	8	0.576
Room 9	4ft	36	6	0.216	8	1.728
Assistant Procurement Officer	4ft	36	4	0.144	8	1.152
Room 6(Central Services)	4ft	36	4	0.144	8	1.152
Procurement Office 2	4ft	36	4	0.144	8	1.152
Legal Offices	4ft	36	20	0.72	8	5.76
ADM 47	4ft	36	8	0.288	8	2.304
Letting Corridor	4ft	36	28	1.008	8	8.064
Righting Corridor	4ft	36	28	1.008	8	8.064
Security Desk	4ft	36	17	0.612	8	4.896
	2ft	18	2	0.036	8	0.288
Stairs to 1st Floor	2ft	18	6	0.108	8	0.864
Stairs	2ft	18	3	0.054	24	1.296
Corridor (Next to DVC Student Affairs)	4ft	36	11	0.396	24	9.504
Corridor	4ft	36	22	0.792	4	3.168
Recruitment Room 128	4ft	36	10	0.36	24	8.64
ICT Server Room	4ft	36	8	0.288	24	6.912
Registrar Admin ADM 121	4ft	36	4	0.144	8	1.152
ADM 119	4ft	36	4	0.144	8	1.152
ADM 111	4ft	36	8	0.288	8	2.304
Reception Office 1	4ft	36	8	0.288	8	2.304
Reception Office 2	4ft	36	8	0.288	8	2.304
Registrar Rm 112 Reception	4ft	36	8	0.288	8	2.304
Office	4ft	36	8	0.288	8	2.304
Rm 106 Reception	4ft	36	8	0.288	8	2.304
Office 1	4ft	36	8	0.288	8	2.304
Office 2	4ft	36	8	0.288	8	2.304
ADM 105 Reception	4ft	36	8	0.288	8	2.304
Office 1	4ft	36	8	0.288	8	2.304

Rm 103 Front Office	4ft	36	4	0.144	8	1.152
Office 1	4ft	36	8	0.288	8	2.304
Machine Room ADM 102	4ft	36	8	0.288	8	2.304
Central Corridor	5ft	58	16	0.928	24	22.272
Corridor to South Wing	4ft	36	12	0.432	24	10.368
CERM-ESA	2ft	18	1	0.018	8	0.144
Reception	4ft	36	1	0.036	24	0.864
Project Leader	4ft	36	1	0.036	8	0.288
Project Coordinator	4ft	36	1	0.036	24	0.864
Auditorium	4ft	36	20	0.72	8	5.76
Control Room	4ft	36	1	0.036	8	0.288
Lounge	4ft	36	2	0.072	8	0.576
Resource Center	4ft	36	3	0.108	8	0.864
Gents	CFL	11	2	0.022	24	0.528
Ladies	CFL	11	2	0.022	24	0.528
	4ft	36	1	0.036	24	0.864
Wing 2 Corridor	4ft	36	27	0.972	24	23.328
Alumni Office Secretariat	4ft	36	8	0.288	8	2.304
ADM 134				0		0
ADM 133				0		0
ADM 135				0		0
Deputy Registrar	4ft	36	8	0.288	8	2.304
Assistant Registrar Reception			8	0	8	0
Office 1	4ft	36	8	0.288	8	2.304
Office 2	4ft	36	8	0.288	8	2.304
Alumni Office ADM 135	4ft	36	8	0.288	8	2.304
Rm 141	4ft	36	8	0.288	8	2.304
Office	4ft	36	8	0.288	8	2.304
Rm 139	4ft	36	8	0.288	8	2.304
ADM 142 Front Office	4ft	36	8	0.288	8	2.304

Office 2	4ft	36	8	0.288	8	2.304
Office 1	4ft	36	8	0.288	8	2.304
Deputy Registrar				0		0
ADM 143				0		0
Kitchen	2ft	18	1	0.018	8	0.144
Peace and Reconciliation				0		0
Rm 146				0		0
Rm 147	4ft	36	110	3.96	8	31.68
Admission Registry Rm 149	4ft	36	18	0.648	8	5.184
Deputy Registrar Rm 150	4ft	36	8	0.288	4	1.152
ADM 154	4ft	36	12	0.432	8	3.456
ADM 153 Reception	4ft	36	8	0.288	8	2.304
Office 1	4ft	36	12	0.432	8	3.456
Office 2	4ft	36	8	0.288	8	2.304
Ladies	4ft	36	2	0.072	24	1.728
Gents	4ft	36	2	0.072	24	1.728
V C'S Waiting Room	4ft	36	4	0.144	12	1.728
Reception	4ft	36	12	0.432	12	5.184
VC Office	4ft	36	16	0.576	12	6.912
Toilet	CFL	11	2	0.022	12	0.264
Kitchen	2ft	18	1	0.018	8	0.144
Boardroom	4ft	36	12	0.432	12	5.184
Corridor	4ft	36	16	0.576	24	13.824
DVC ARE Reception	4ft	36	16	0.576	12	6.912
Office	4ft	36	18	0.648	12	7.776
Washroom	2ft	18	1	0.018	12	0.216
Waiting Room	4ft	36	8	0.288	12	3.456
Assistant Registrar	4ft	36	8	0.288	12	3.456
DVC Finance Reception	4ft	36	8	0.288	12	3.456
Waiting Room	4ft	36	8	0.288	12	3.456
Office	4ft	36	12	0.432	12	5.184
Washroom	4ft	36	4	0.144	12	1.728

Reception 2	4ft	36	8	0.288	12	3.456
DVC Student Affairs Reception	4ft	36	8	0.288	12	3.456
Office	4ft	36	10	0.36	12	4.32
Washroom	2ft	18	1	0.018	12	0.216
Waiting Room	4ft	36	8	0.288	12	3.456
DVC Planning Reception	4ft	36	10	0.36	12	4.32
Office	4ft	36	12	0.432	12	5.184
Washroom	CFL	11	2	0.022	12	0.264
Waiting Room	4ft	36	2	0.072	12	0.864
Examination	4ft	36	8	0.288	12	3.456
Deputy Registrar	4ft	36	8	0.288	4	1.152
Reception	4ft	36	8	0.288	2	0.576
Transcripts Office	4ft	36	8	0.288	2	0.576
Certificate Issue	4ft	36	8	0.288	2	0.576
Secretary Exam	4ft	36	8	0.288	2	0.576
Assistant Registrar	4ft	36	8	0.288	2	0.576
Administrator Exam	4ft	36	8	0.288	2	0.576
Machine Room Front Area	4ft	36	8	0.288	2	0.576
Machine Room 1	4ft	36	4	0.144	2	0.288
Machine Room2	4ft	36	2	0.072	2	0.144
Machine Room 3	4ft	36	4	0.144	2	0.288
Exam Issue Desk	4ft	36	3	0.108	2	0.216
Corridor	4ft	36	9	0.324	12	3.888
Council Office	4ft	36	34	1.224	12	14.688
Stairs	2ft	18	1	0.018	12	0.216
Development Office	4ft	36	10	0.36	12	4.32
Senior QS 1	4ft	36	3	0.108	12	1.296
Secretary Exam	4ft	36	4	0.144	12	1.728
Senate Chambers	2ft	18	72	1.296	12	15.552
	5ft	58	2	0.116	12	1.392
Washroom	4ft	36	2	0.072	24	1.728

Stairs 3rd Floor	4ft	36	2	0.072	12	0.864
Development Corridor	4ft	36	3	0.108	12	1.296
Integrity Office	4ft	36	4	0.144	2	0.288
Development Office 2	4ft	36	4	0.144	12	1.728
Benevolent Office	4ft	36	2	0.072	12	0.864
Fire Officer	4ft	36	1	0.036	12	0.432
Sewerage OfficeR	4ft	36	1	0.036	12	0.432
Corridor to Internal Audit	4ft	36	2	0.072	24	1.728
Stairs to 3rd Floor	4ft	36	18	0.648	24	15.552
Com Tech Office	4ft	36	3	0.108	12	1.296
Computer Room	4ft	36	8	0.288	12	3.456
Corridor	4ft	36	2	0.072	12	0.864
Lecture Room 9	4ft	36	54	1.944	12	23.328
CTO	4ft	36	7	0.252	12	3.024
Resource Clerk Admin	4ft	36	4	0.144	12	1.728
Room 318	4ft	36	2	0.072	12	0.864
Seminar Room 5	4ft	36	18	0.648	12	7.776
Washroom	4ft	36	2	0.072	12	0.864
Cafeteria Walkway	4ft	36	3	0.108	12	1.296
Cafeteria Corridor	4ft	36	2	0.072	24	1.728
Cafeteria	4ft	36	29	1.044	12	12.528
Stairs	4ft	36	1	0.036	24	0.864
Kitchen Eatery	4ft	36	4	0.144	12	1.728
Kitchen Store	4ft	36	2	0.072	4	0.288
Eatery Store Office	4ft	36	1	0.036	8	0.288
Eatery Store	4ft	36	2	0.072	4	0.288
Stairs	2ft	18	2	0.036	24	0.864
General Audit Office	4ft	36	16	0.576	8	4.608
Deputy Chief Auditor	4ft	36	4	0.144	8	1.152
Internal Auditor	4ft	36	4	0.144	8	1.152
Chief Internal Auditor Reception	4ft	36	8	0.288	8	2.304
CIA 1	4ft	36	8	0.288	8	2.304

CIA2	4ft	36	12	0.432	8	3.456
Extension & Outreach	4ft	36	16	0.576	8	4.608
Corridor ADM 248	4ft	36	16	0.576	8	4.608
Weather Station	4ft	36	4	0.144	8	1.152
Corridor	4ft	36	9	0.324	24	7.776
VLIR Reception	4ft	36	4	0.144	8	1.152
Room1	4ft	36	7	0.252	8	2.016
Room 2	4ft	36	7	0.252	8	2.016
Corridor	4ft	36	14	0.504	24	12.096
Office 1	4ft	36	7	0.252	8	2.016
Office 2	4ft	36	4	0.144	8	1.152
IGERD	4ft	36	8	0.288	8	2.304
Director	4ft	36	8	0.288	8	2.304
ADM 254 Reception	4ft	36	7	0.252	8	2.016
Program Coordinator	4ft	36	8	0.288	8	2.304
Meeting Room	4ft	36	8	0.288	8	2.304
Manager	4ft	36	8	0.288	8	2.304
Cloak Room	4ft	36	4	0.144	8	1.152
Ladies	CFL	11	2	0.022	8	0.176
	2ft	18	2	0.036	8	0.288
Gents	CFL	11	3	0.033	8	0.264
	2ft	18	2	0.036	8	0.288
Vlirous	4ft	36	4	0.144	8	1.152
ICT Kitchen	4ft	36	1	0.036	8	0.288
ICT Office 245	4ft	36	8	0.288	8	2.304
ADM 244	4ft	36	8	0.288	8	2.304
ADM 242	4ft	36	8	0.288	8	2.304
ICT Director 241	4ft	36	8	0.288	8	2.304
Reception	4ft	36	8	0.288	8	2.304
Director Office	4ft	36	8	0.288	8	2.304
Directorate of Research 237	4ft	36	8	0.288	8	2.304
Director Research	4ft	36	8	0.288	8	2.304
Research ADM 238	4ft	36	8	0.288	8	2.304

MUHACU ADM 240	4ft	36	8	0.288	8	2.304
Deputy Registrar ADM 234	4ft	36	8	0.288	8	2.304
Reception	4ft	36	8	0.288	8	2.304
Office 1	4ft	36	8	0.288	8	2.304
Office 2	4ft	36	8	0.288	8	2.304
Deputy Registrar ADM 233	4ft	36	8	0.288	8	2.304
Office 1	4ft	36	8	0.288	8	2.304
Office 2	4ft	36	8	0.288	8	2.304
Central Area	4ft	36	4	0.144	24	3.456
Corridor	4ft	36	12	0.432	24	10.368
Office 201	4ft	36	8	0.288	8	2.304
Corridor (Next to VC Office)	4ft	36	6	0.216	8	1.728
Chairman of Council Office	4ft	36	16	0.576	8	4.608
Reception	4ft	36	8	0.288	8	2.304
Meeting Room	4ft	36	8	0.288	8	2.304
Deputy Registrar Council Secretariat	4ft	36	8	0.288	8	2.304
ADM 224	4ft	36	8	0.288	8	2.304
				74.793		749.032

LIBRARY

Area	Lamp Type	Rating (W)	Quantity	Total Power(kW)	Daily Running Hours	Total Energy Consumption
Security Desk	Mercury	250	16	4	24	96
Issue Desk	6ft	72	84	6.048	24	145.152
	CFL	11	10	0.11	24	2.64
Exhibition	6ft	13	128	1.664	24	39.936
			12	0	24	0
Corridor	5ft	58	8	0.464	24	11.136
Audio Visual	5ft	58	10	0.58	8	4.64
Common Staffroom	5ft	58	4	0.232	8	1.856
Acquisitions Cataloguing	6ft	72	24	1.728	8	13.824
Acquisitions Office	4ft	36	15	0.54	8	4.32
General Office	6ft	72	14	1.008	8	8.064
Library Office	6ft	72	20	1.44	8	11.52
ICT Office	6ft	72	6	0.432	8	3.456
Basement Stairs	5ft	58	5	0.29	24	6.96
Basement	5ft	58	3	0.174	24	4.176
Washrooms	2D	6	4	0.024	24	0.576
	2D	28	12	0.336	24	8.064
Basement Corridor	5ft	58	6	0.348	24	8.352
Office 1	5ft	58	3	0.174	8	1.392
Office 2	5ft	58	20	1.16	8	9.28
LB 07	5ft	58	2	0.116	8	0.928
LB 08 Darkroom	5ft	58	3	0.174	0	0
Security Room	5ft	58	4	0.232	8	1.856
LB 05	5ft	58	4	0.232	8	1.856
Kitchen	5ft	58	1	0.058	8	0.464
				21.564		386.448

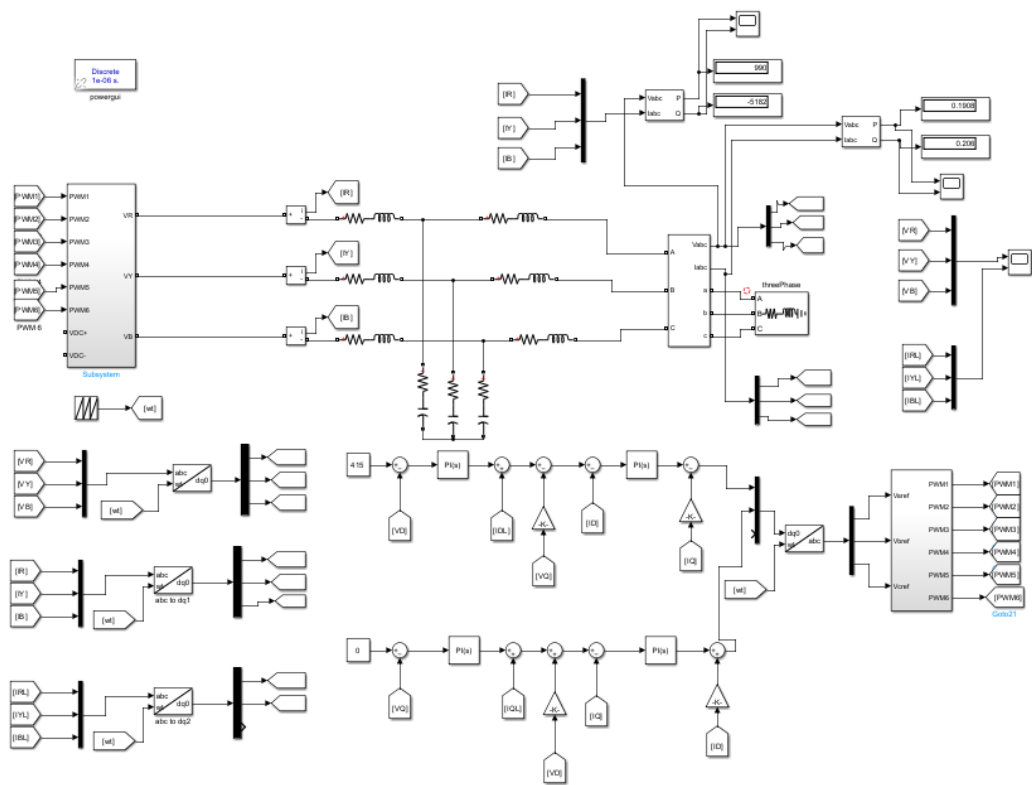
ADMINISTRATION BLOCK

Month	Power Demand (kVA)	Power Consumed (kW)	Power Factor (pf)	Energy Consumed (kWh)			Power Factor Surcharge (KES)	Cost (KES)	Unit Cost (KES/kWh)
				High Rate	Low Rate	Total Energy Consumed			
Feb-18	93	88	0.95	18167	9597	27,764	0	652,034	23.48
Mar-18	97	92	0.95	18004	9307	27,311	0	660,379	24.18
Apr-18									
May-18	93	88	0.95	19157	9576	28,733	0	690,642	24.04
Jun-18	98	93	0.95	17392	9147	26,539	0	574,434	21.64
Jul-18	96	94	0.98	19016	9631	28,647	0	623,109	21.75
Aug-18	99	96	0.97	20740	10840	31,580	0	637,282	20.18
Sep-18	98	96	0.98	19428	11565	30,993	0	620,271	20.01
Oct-18	106	103	0.97	22052	11306	33,358	0	668,665	20.05
Nov-18	96	93	0.97	21056	11230	32,286	0	643,409	19.93
Dec-18	92	89	0.97	16178	12412	28,590	0	580,337	20.30
Jan-19	88	86	0.98	19751	11038	30,789	0	618,980	20.10
Feb-19	93	90	0.97	19082	10662	29,744	0	626,490	21.06

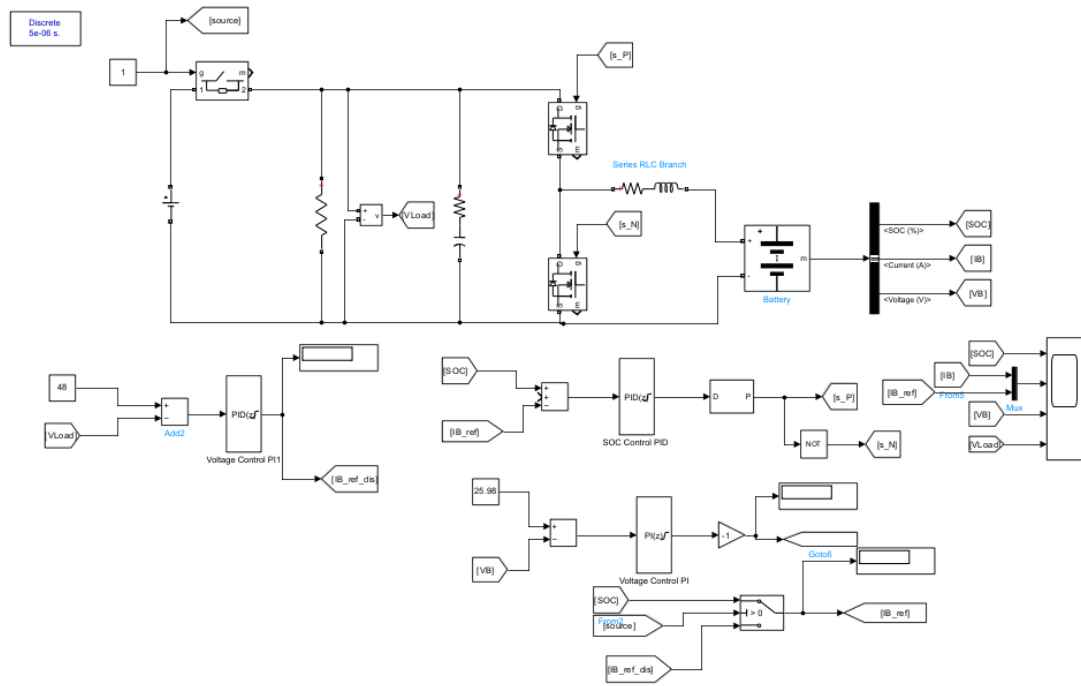
MARGARET THATCHER LIBRARY

Month	Power Demand (kVA)	Power Consumed (kW)	Power Factor (pf)	Energy Consumed (kWh)			Power Factor Surcharge (KES)	Cost (KES)	Unit Cost (KES/kWh)
				High Rate	Low Rate	Total Energy Consumed			
Feb-18	110	87	0.79	22897	6395	29292	94,873.68	797,728	27.23
Mar-18	103	81	0.79	18241	4203	22444	72,718.56	627,080	27.94
Apr-18									
May-18	100	78	0.78	17373	4020	21393	75,089.00	601,362	28.11
Jun-18	102	83	0.81	20927	6012	26939	64,073.96	659,562	24.48
Jul-18	103	90	0.87	24384	6904	31288	14,667.02	691,324	22.10
Aug-18	100	90	0.90	22690	6292	28982	-	595,751	20.56
Sep-18	129	112	0.87	23238	6311	29549	27,118.44	663,488	22.45
Oct-18	140	116	0.83	31585	7830	39415	79,807.28	894,264	22.69
Nov-18	140	110	0.79	32644	8985	41629	82,556.60	930,697	22.36
Dec-18	132	111	0.84	19523	7998	27521	50,531.04	647,058	23.51
Jan-19	133	111	0.83	26647	6880	33527	69,929.44	791,084	23.60
Feb-19	137	113	0.82	29777	8338	38115	89,900.00	916,585	24.05
Total						370,094	721,265.02	8,815,983	24.09
Average	119.0833	98.5	0.83						23.82

Appendix F: Simulink model for the power inverter

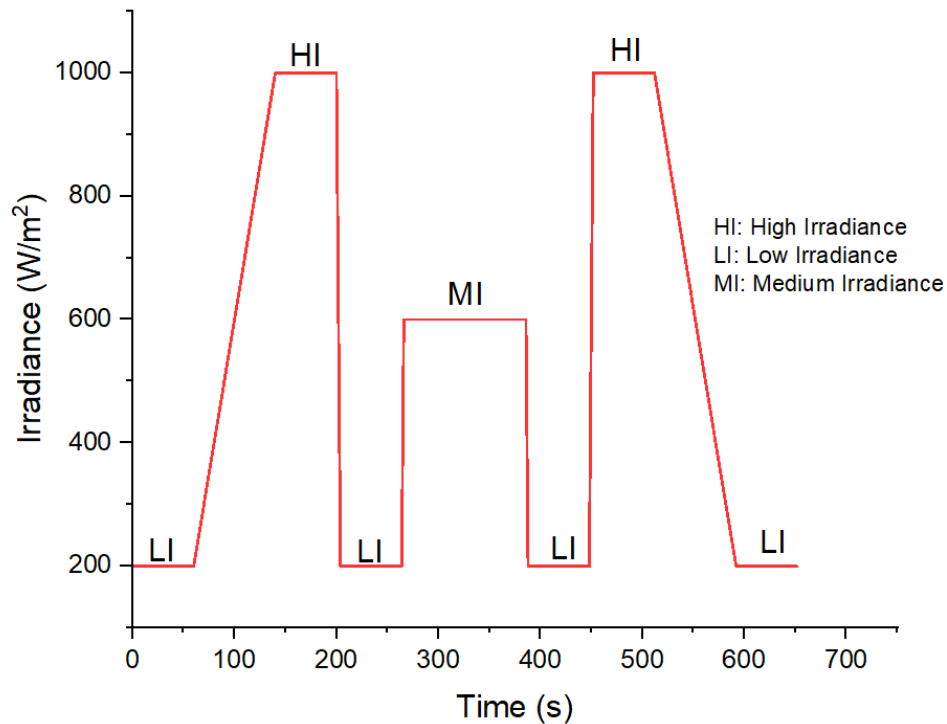


Appendix G: Simulink model for the battery controller



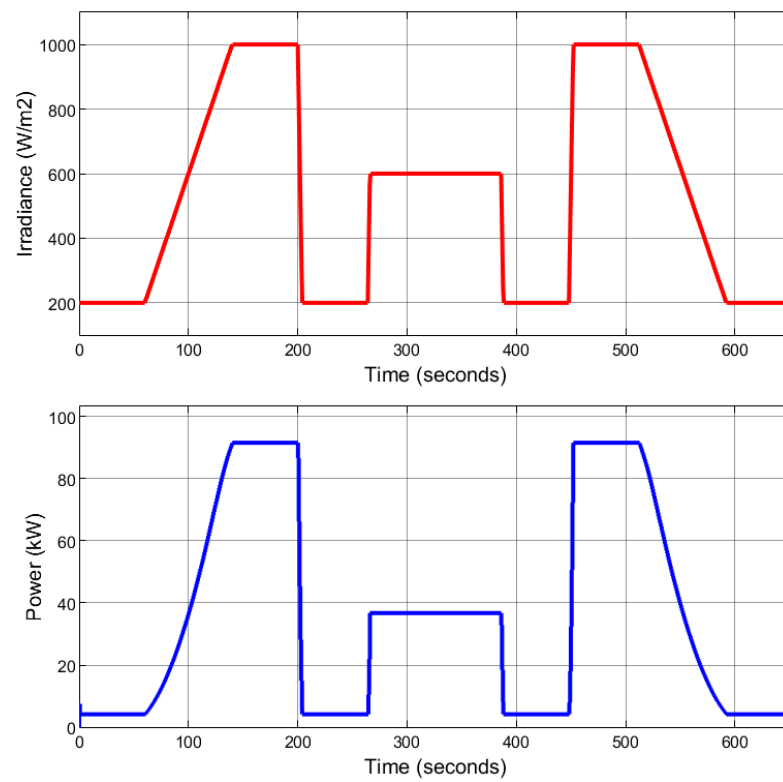
Appendix H: Ropp Test

This standard irradiance profile for testing MPPT controllers was developed by (Ropp et al., 2011). The irradiance profile is divided into static and dynamic sections to account for real world scenarios of irradiance variations.



The test profile begins with an irradiance of 200 W/m² for 60s and slowly ramps up to 1000 W/m² after 80s with a ramp up rate of 10 W/m²/s. The irradiance is then maintained at 1000 W/m² for 60s and then rapidly ramps down to 200 W/m² in 4s with a fast downward ramp rate of -200 W/m²/s. The irradiance stays low at this steady value for 60s before a fast ramp up occurs, taking the irradiance to the medium condition of 600 W/m² in just 2s at a ramp up rate of 200 W/m²/s. This medium irradiance stays steadily for 120s before quickly ramping down to 200 W/m² in 2s at a rate of -200 W/m²/s. From this point, the irradiance remains steadily at 200 W/m² for 60s and then quickly ramps up to 1000 W/m² in 4s, stays constant for 60s and then ramps down slowly to 200 W/m² in 80s.

The figure shows the Ropp irradiance profile and the tracked power using the designed MPPT tracker.



Appendix I: Research Outputs

1. Katche, M. L., Makokha, A. B., Zachary, S. O., & Adaramola, M. S. (2023). *A Comprehensive Review of Maximum Power Point Tracking (MPPT) Techniques Used in Solar PV Systems. Energies, 16(5), 2206.*
2. Katche, M. L., Makokha, A. B., Zachary, S. O., & Adaramola, M. S. (2023). *Solar Photovoltaic Systems: A Technical and Economic Feasibility Design Approach with Homer Pro. International Journal of Advances in Scientific Research and Engineering, 9(11), E-ISSN: 2454-8006. DOI: 10.31695/IJASRE.2023.9.11.2*

Appendix J: Plagiarism Certificate

SR371

ISO 9001:2019 Certified Institution

THESIS WRITING COURSE***PLAGIARISM AWARENESS CERTIFICATE***

This certificate is awarded to

MUSONG LOUIS KATCHE

PHD/ES/5550/21

In recognition for passing the University's plagiarism

Awareness test for Thesis entitled: **MODELLING, SIMULATION AND OPTIMIZATION OF A SOLAR/BATTERY HYBRID RENEWABLE ENERGY SYSTEM WITH MAXIMUM POWER POINT TRACKING CONTROL STRATEGY** with a similarity index of 7% and striving to maintain academic integrity.

Word count: 50607

Awarded by

Prof. Anne Syomwene Kisilu

CERM-ESA Project Leader Date: 8/11/2023